FUNCTIONAL ROLE OF N-MYRISTOYLTRANSFERASE-1 IN PROSTATE CANCER

by

OMAR AWAD S. ALSAIDAN

(Under the Direction of Houjian Cai)

ABSTRACT

Despite numerous strategies for treatment of prostate cancer, there is still shortage in effective approaches of targeting castration resistant prostate cancer (CRPC) and associated mortality. A wide variety of resistance mechanisms has been discovered in CRPC over the last decades. Novel therapeutic targets for CRPC are required. Myristoylation is a co/post-translational protein modification that promote localization of proteins to cellular membranes, thereby maintaining their conformation and molecular functions. A growing body of evidence, including those studies in prostate cancer from our laboratory, has demonstrated that protein myristoylation promotes cancer progression. This dissertation focuses on studies of the role of N-myristoyltransferase 1 (NMT1) in prostate cancer. In the first aim of the study, we determined expression levels and activity of NMT1 and how it impacted growth of the prostate cancer. Our data indicated that NMT1 was highly expressed in prostate cancer cells compared to normal prostate cells. Genetic knockdown of NMT1 inhibited proliferaion of prostate cancer cells through induction of cell cycle arrest. Additionally, we identified a small molecule

inhibitor that suppressed NMT1 activity at low micromolar range. Pharmacological inhibition of NMT1 suppressed growth of prostate tumors *in vivo*. In the second aim of the study, we investigated a regulatory role of NMT1 on AR protein expression and activity in prostate cancer tumorigenesis. We showed that NMT1 expression levels and activity regulated AR protein levels. Inhibiting NMT1 genetically or pharmacologically reduced AR proteins levels, but not at its mRNA levels. A decrease of AR protein levels was coupled with reduction of nuclear AR levels and its transcriptional activity. We further demonstrated that NMT1 regulated AR protein levels through ubiquitination-proteasome pathway. Finally, our results indicated that NMT1 synergized with AR to promote prostate cancer tumorigenesis. Taken together, our study has discovered a novel molecular function of NMT1 in regulation of AR protein levels in prostate cancer, and a therapeutic approach for treatment of CRPC.

INDEX WORDS: Myristoylation; N-myristoyltransferase 1; androgen receptor; LCL204; (*1R,2R*)-D-NMAPPD; Castration resistant prostate cancer

FUNCTIONAL ROLE OF N-MYRISTOYLTRANSFERASE-1 (NMT1) IN PROSTATE CANCER

by

OMAR AWAD S. ALSAIDAN

B.S., College of Pharmacy, King Saud University, Riyadh, Saudi Arabia, 2012

A Dissertation Submitted to the Graduate Faculty of The University of Georgia in Partial Fulfillment of the Requirements for the Degree

DOCTOR OF PHILOSOPHY

ATHENS, GEORGIA

2020

FUNCTIONAL ROLE OF N-MYRISTOYLTRANSFERASE-1 (NMT1) IN PROSTATE CANCER

by

OMAR AWAD S. ALSAIDAN

Major Professor:	Houjian Cai
Committee:	Mandi M. Murph
	James L. Franklin
	Jacek Gaertig

Electronic Version Approved:

Suzanne Barbour
Dean of the Graduate School
The University of Georgia
May 2020

DEDICTATION

I would like to dedicate this dissertation to my beloved parents: Awad and Jamilah for everything that I have and would not achieve anything without their endless love, support and encouragement through my life. To my siblings: Ammar, Hadeel, Aseel, Suliman, and Alwaleed, who always believe in me and support me through the years. Thank you all for everything.

ACKNOWLEDGEMENTS

First and foremost, all Praise is for God (Allah) All Mighty, the One and Only, for His countless blessings and guidance throughout my life.

I would like to thank Dr. Houjian Cai for giving me the opportunity to work in his lab. His amazing support, motivation, and guidance during my doctoral journey helped me to reach this point and earn this degree. I would also like to thank my committee members: Dr. Mandi Murph, Dr. James Franklin, Dr. Jacek Gaertig, and Dr. Shelley Hooks for their valuable suggestions, advice, and comments for my study and research. Thanks to all current and previous lab members in Dr. Cai's lab: Dr. Meng Wu, Dr. Sungjin Kim, Dr. Qianjin Li, Dr. Yongjie Ma, Dr. Sumit Rai, Essilvo Sulejmani, Peter Le, Chenming Ye, Joseph Whitley, Rohit Katti, Junyi Zha, Zixuan Zhen, I couldn't imagine a better lab environment to have called home.

Special thanks to all my friends for their encouragement and support during my stay in Athens, especially Dr. Mohammed Alqinyah, Faris Almutairi, Dr. Sary Alsanea, Dr. Yahya Alhamhoom, Dr. Ali Alshmrani, Ibrahim Asiri, and Mazen Shawosh.

Finally, I would like to thank my sponsor, Aljouf University, The Saudi Arabian Cultural Mission, The Ministry of Higher Education at Saudi Arabia, for financial support through my graduate study.

TABLE OF CONTENTS

LIST OF TABLES

Page

LIST OF FIGURES

Page

CHAPTER 1

INTRODUCTION

Human prostate gland

The prostate is a male exocrine organ located below the bladder and in the front wall of the rectum (2). It is a chestnut-size organ that weighs around 20 grams at puberty and surrounds the beginning of the urethra, which carries urine and semen out of the body through the penis (3, 4). Growth and maturation of the prostate gland depend on testosterone, and it rapidly grows at puberty when testosterone reaches its onset production (6). During ejaculation, the prostate gland plays an essential role in sperm mobility and viability by secreting a milky slightly acidic fluid called prostatic fluid into the urethra (7). Prostatic fluid constitutes up to 30% of semen and contains several ingredients such as zinc, citric acid, and proteolytic enzymes that break-down proteins from seminal vesicles (7).

Anatomically, five major lobes form the human prostate: anterior, posterior, lateral (right and left), and median **(Figure 1.1)** (2). As a non-glandular tissue, the anterior lobe is made up of fibromuscular tissue and lies in the front of the urethra and corresponds to part of the transitional zone (2). The posterior lobe forms the middle part of the lateral lobe and roughly corresponds to the peripheral zone (2). Right and left lateral lobes, which are separated by the urethra, make up the majority of the prostate mass (2). The median lobe is surrounded by ejaculatory ducts and corresponds to the central zone (2). Pathologically, the prostate gland can also be divided into four major zones: 1) Peripheral zone (PZ), 2) Central zone (CZ), 3) Transitional zone (TZ), and 4) Anterior fibromuscular zone (Figure 2) (8, 9). The peripheral zone, where 80% of prostate cancer originates from, contains the majority of prostate glands and constitutes up to 70% of total prostate

volume (8, 10). The central zone constitutes about 20% of the adult prostate gland, and only around 3% of prostate cancer is originated from this zone (8, 11). The transition zone, which alone constitutes 5% of the total volume of the prostate gland, accounts for roughly 15% of prostate cancer and is the site where benign prostatic enlargement develops (8, 12). The anterior zone is the only zone predominately made up of muscle fibers and connective tissue (8, 13).

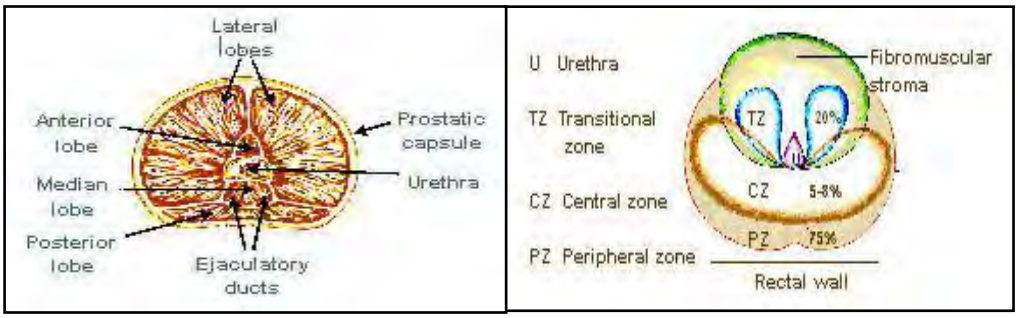

FIGURE 1.1. Prostate gland lobes and zones. Adapted from National Cancer Institute, SEER training modules: https://training.seer.cancer.gov/prostate/anatomy/

Histologically, the prostate tissue is composed of 30% muscular stromal that surrounds 70% of the glandular epithelium (**Figure 1.2**) (14). These two compartments (stroma and epithelial) are surrounded by the prostatic capsule, which plays a significant role in determining the extracapsular extension of the tumor (14). The epithelium compartment contains secretory luminal, basal, intermediate, and neuroendocrine cells (14). Secretory luminal cells, which are characterized by the expression of androgen receptor, cytokeratins K8 (CK8) and K18 (CK18), and specific membrane antigen (PSMA), are columnar tall cells that are important for the secretion of several proteins such as prostatic specific antigen (PSA) and prostatic acid phosphatase (PAP) to the prostatic fluid (14). Basal cells, characterized by the expression of cytokeratins K5 and K14 (CK5 and CK14) and p63, are flattened small cells that form a single layer underneath luminal cells and play a significant role in supporting luminal cell survival and integrity of lumen-urethra ducts (15).

Neuroendocrine cells are distributed among luminal and basal cells (16). Even though the biological function of the neuroendocrine cells is unclear, their secretions support the growth of epithelial cells in the prostate gland (16). The epithelium compartment is surrounded by a stromal cell that consists of the extracellular matrix, fibroblasts, endothelial, and smooth muscle cells (14, 17). Stromal cells support the growth of epithelial cells by epithelial-stromal crosstalk through secreting several paracrine growth factors (14, 17).

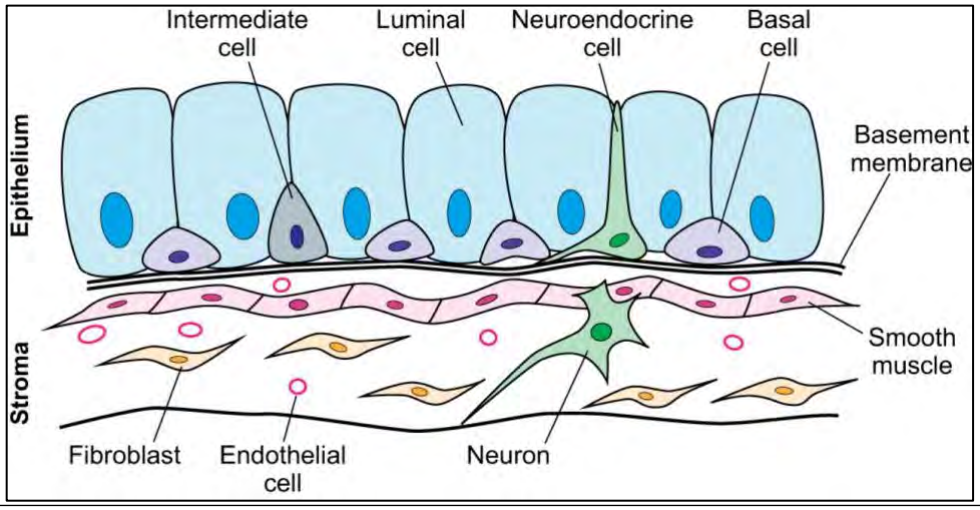

FIGURE 1.2. Structure of prostate gland. Adapted with permission from: Toivanen R, Shen MM. Prostate organogenesis: tissue induction, hormonal regulation and cell type specification. Development. 2017;144(8):1382-1398. (1)

Prostate disorders

There are several disorders of the prostate cancer that are linked to aging (18). An increase in age is correlated with higher rates of prostate disorders. Here, we describe the most common prostate disorders **(Figure 1.3)**:

A- Benign prostatic hyperplasia (BPH): Also called benign enlargement of the prostate (BEP) (19). BPH is characterized by an enlargement of the prostate gland as a result of

an increase in the proliferation and dysregulation of apoptosis of epithelial and stromal cells in the transitional zone of the prostate tissue (19). BPH is very common in men aged 60 years and above (20). This prostate disorder is not a life-threatening disease, and the cause is not fully understood (20). However, several factors have been reported to play a role in the development of BPH, such as an increase in the testosterone levels, amount of food intake, and aging (20). The primary complications of BPH are the pressing or the prostate on the urethra, which makes it painful for patients while urinating, increase the frequency of urination, involuntary urination, urinary tract infection, and bladder outlet obstruction (BOO) (21).

B- Prostatitis: A prostate disorder in which the prostate swells as a result of the inflammation of the prostate gland (22). Usually, prostatitis starts to develop in men at age 50, though men between 18-50 years also can develop the disease (22). Depending on the symptoms, prostatitis can be divided into four types: 1- chronic prostatitis, which accounts for 90% of prostatitis; 2- acute bacterial prostatitis; 3- chronic bacterial prostatitis, both acute and chronic bacterial prostatitis account for less than 10% of prostatitis; 4- asymptomatic inflammatory prostatitis (22). Based on the type of prostatitis, men can develop several symptoms such as dysuria (pain sensation when urinating), nocturia (frequent urination), painful ejaculation, pain in the lower back region, chills, and fever (23). Other than bacteria that cause bacterial prostatitis, the causes of non-bacterial prostatitis are not well identified. However, prostatitis has been linked to stress, pelvic nerve irritation or inflammation, and urinary tract injuries (24, 25). Prostatitis can be treated based on the cause by taking antibiotics, anti-inflammatory, surgery, prostatic massage, or home remedies to ease the pain (26). Inflammation of the

prostate tissue is considered a precursor for prostate cancer (22). Inflammation of the prostate creates a harmful environment attracting several inflammatory mediators and growth factors that cause an imbalance between proliferation and apoptosis of prostate cells resulted in developing lesions in prostate tissue in a process called proliferation inflammatory atrophy (PIA) (27).

C- **Prostate Cancer:** A piece of detailed information about prostate cancer will be provided in the following.

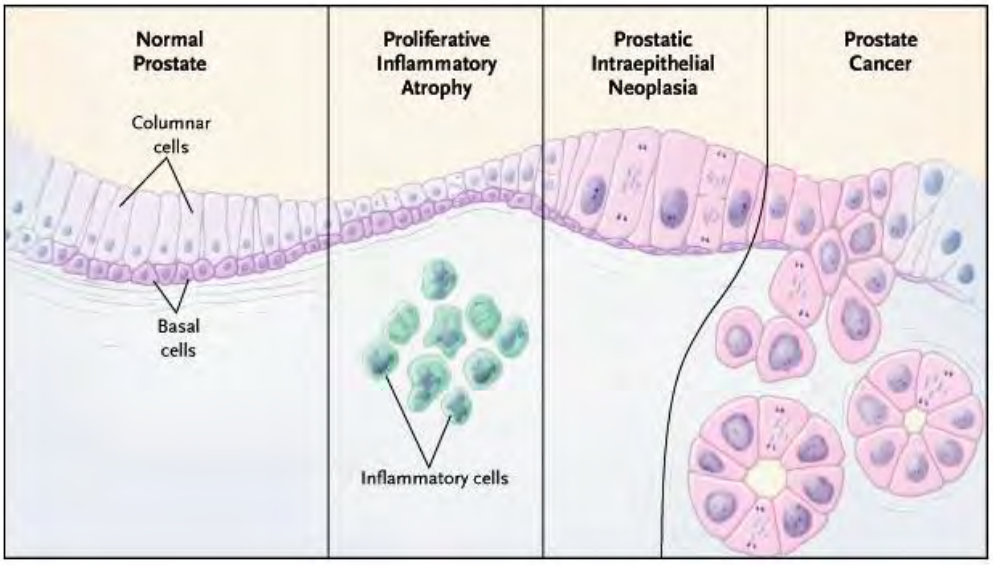

FIGURE 1.3. Prostate disorder stages. Reproduced with permission from Nelson WG, DeMarzo AM, Isaacs WB: Prostate cancer. N Engl J Med 2003;349:366-381, Copyright Massachusetts Medical Society (5).

Prostate Cancer

According to the American Cancer Society, a man will be diagnosed with prostate cancer every 3 minutes, making prostate cancer the most common cancer in American men. An estimated 174,650 newly diagnosed cases were made in 2019, which accounted for 9.9% of all new cancer cases in men during that year. The estimated number of deaths from prostate cancer was 31,620 in 2019, which is 10% of the total estimated deaths from all cancers (28). More than 60% of the

diagnosed cases are in men over 65 years (28). However, prostate cancer can occur in men at age 45 or above, but rarely occurs before age 40 (29). Black men have a 60% higher risk of prostate cancer than white men for unknown reasons (30). Since the early 1990s, there has been a 85% increase in the incidence rate of prostate cancer because of the introducing and using of the prostate-specific antigen (PSA) test (31). Not only has the number of diagnosed prostate cancer increased, but also the detection of tumors at early stages was improved by PSA screening (31). Since prostate cancer grows slowly, not all prostate cancer can develop into the clinically relevant disease before the death of the afflicted. Even though PSA screening led to a sharp increase in diagnosed prostate cancer cases, it helped reduce the mortality rate by 3.5% per year between 2007 and 2011 (32).

Prostate cancer risk factors

Several risk factors have been studied for their correlation to prostate cancer development and progression. Some of these factors are highly correlated to PCs development, such as age, ethnicity/race, and family history (33). Others, such as diet, obesity, environmental factors, and gene mutations, are also linked to PCs development (34). The probability of developing prostate cancer is correlated with age, and that makes it the major risk factor for prostate cancer. Young men aged 30-40 rarely develop prostate cancer (35). However, men with age above 60 account for more than half of prostate cancer cases (35). Family history is another risk factor, with development of prostate cancer twice as likely when having a first-degree relative (father) diagnosed with prostate cancer (36). Recent epidemiological studies show that 10-15% of all prostate cancer cases are diagnosed in patients with a family history (37). Ethnicity has also been shown to play a significant role in prostate cancer development (37). Several studies show that

people with dark skin such as Africans and African Americans are more susceptible to develop prostate cancer and have higher mortality rates compared to other ethnicities (37). On the other hand, Asians and Americans Indian/Alaska have lower rates of prostate cancer incidence (37).

Diet and obesity are other risk factors that have been linked to the development of prostate cancer. A high-fat diet has been shown to contribute to carcinogenesis and the aggressiveness of prostate cancer in several studies (37, 38). The elucidated mechanism of how diet contributes to the development of prostate cancer is inconclusive. Exposure to environmental factors such as cadmium and herbicides has been shown to play a role in the development of prostate cancer, but mechanisms are still unidentified (39). Genetic abnormalities are also associated with an increased risk of prostate cancer, such as men with mutations in BRCA1, BRCA2, and PTEN (40, 41). Additionally, overexpression of mutated HPC1, CAPB, ATM, and HPCX increased susceptibility to prostate cancer (42-45).

Signs and symptoms of prostate cancer

Prostate cancer is a silent disease with no symptoms at the early stages. The disease can go undetected for many years without routine screenings. However, the most common first indication of prostate cancer is blood in the urine (46). Also, the growth of the tumor may cause pressure at the urethra, leading to a painful sensation during urination (47). Several symptoms start to appear in advanced stages of prostate cancer, such as frequent urination at night, weak stream of the urine, dysuria, blood in seminal fluid, difficulty passing urine, inability to empty bladder, and urination interruption (47). However, lower urinary tract symptoms do not mean that the patient has prostate cancer because these symptoms are shared with other prostate conditions such as prostatitis (48). Patients should have more screenings to confirm their diagnosis of prostate cancer.

Screening for prostate cancer

Since prostate cancer is asymptomatic, patients at age 50 and above are recommended to consider prostate cancer tests. Patients who have prostate cancer risk factors should consider prostate cancer screenings before age 50. Two screening tests are available for prostate cancer: prostate-specific antigen (PSA) and digital rectal exams (DRE) (49). PSA was introduced in 1979 as a revolutionary biomarker for prostate cancer (49). PSA is androgen-dependent and secreted into the blood, which makes it an acceptable biomarker (50). Blood PSA levels in the blood of up to 4 ng/ml is considered normal; above four ng/ml indicates an abnormality in the prostate (50). However, the level of PSA can be influenced by other factors such as age, sexual activity, prostate volume, and other prostate diseases such as benign prostate hyperplasia (BPH) (51, 52). However, some prostate cancers have low levels of PSA in the blood (53). Patients with PSA levels above 4 ng/ml are recommended for further analysis, such as a biopsy to confirm prostate cancer (49).

Before introducing PSA, DRE was the only available test for the diagnosis of prostate cancer (49). In DRE, a physician introduces a lubricated, gloved finger rectally to examine abnormalities in prostate size. The outcome of the DRE test depends on the examiner's experience. However, both tests (PSA and DRE) do not diagnose the severity of the disease (49). Further examination by transrectal ultrasound-guided biopsy (TRUS) is performed, and the tissue is graded according to the Gleason Grading system to verify the diagnosis (49). Recently, the Food and Drug Administration (FDA) approved a new prognostic tool for prostate cancer, the measuring of prostate cancer antigen 3 (PCA3) (54). The high expression of PAC3 in the urine of patients with prostate cancer makes it a useful tool for diagnostic testing. PAC3 test is used to decide whether a biopsy is necessary, especially if PSA and DRE were inconclusive.

Grading and staging

The Gleason score system is the primary histological test to determine the aggressiveness of prostate cancer according to the cancer's growth pattern (55). Dr. Donald Gleason introduced the Gleason score system in the 1960s (56). This system has five scores and scales from 1 to 5 (**Figure 1.4**); 1 resembles normal prostate histology, and 5 resembles the loss of prostate tissue histology. The final score is the sum of scores of the most common pattern (primary Gleason score) and the score of the second most common pattern (secondary Gleason score). The final Gleason score ranges from 2-10. Several modifications and updates were applied to the Gleason score system in 2005 and 2014, including the removal of grade 1. Also, since pathologists never assign a score less than 2, the lowest final score is 6. Based on this scoring system, a new grading group system was introduced in 2014. This system was designed to eliminate unnecessary over-treatment of the indolent prostate cancer (55). The new grading system is as follows:

1) Grade group 1: this group is considered low risk; with Gleason Scores $\leq (3 + 3) = 6$ or less; T1-T2a, PSA $\leq$ 10 ng/ml.
2) Grade group 2: this group is considered intermediate risk; with Gleason Scores = (3 + 4) = 7; T2b; PSA 10-20 ng/ml.
3) Grade group 3: this group is considered high intermediate risk; with Gleason Scores = (4 + 3) = 7; T2b; PSA 10-20 ng/ml.
4) Grade group 4: this group is considered high risk; with Gleason Scores = (4 + 4), (5 + 3), (3 + 5) = 8; T2c; PSA $\geq$ 20.
5) Grade group 5: this group is considered high risk; with Gleason Scores = (4 + 5), (5 + 4) = 9 + (5 + 5) = 10; T2c; PSA $\geq$ 20.

Androgen receptor:

Androgen receptor (AR, NR3CA; nuclear receptor subfamily 3, Group C, gene 4) is a nuclear receptor that belongs to a small family of ligand-activated nuclear receptors, Estrogen Receptor-like nuclear receptors. The Estrogen Receptor-like nuclear receptors family accounts for six known nuclear receptors, including estrogen receptor-α (ERα), estrogen receptor-β (ERβ), glucocorticoid receptor (GR), mineralocorticoid receptor (MR), and androgen receptor (AR) (57).

Androgen receptor is a transcription factor that is inactive in the cytoplasm while bound to heat-shock proteins. Androgenic hormones bind to the androgen receptor, causing dissociation of heat-shock protein 90, dimerization, and translocation to the nucleus where it binds to androgen-responsive sequences in the promoter site of target genes and regulates gene expression. The major androgenic hormones that activate androgen receptors are testosterone and dihydrotestosterone (DHT) (57). Testosterone is synthesized in the testis by Leydig cells from cholesterol under the control of the hypothalamus and pituitary gland that releases luteinizing hormone-releasing hormone (LHRH) and luteinizing hormone (LH), respectively. Dihydrotestosterone (DHT) is a more potent form of testosterone and is synthesized by converting testosterone to dihydrotestosterone by 5α-reductase in the prostate (58).

Interaction of androgen and androgen receptor are critical for sexual development through maintaining prostate structure and functions by regulating the expression of a wide range of genes called androgen-responsive genes (ARGs) (57). The well-known ARGs are PSA, TMPRSS2, KLK2, TMEPA1, NOV, and SPKA (57, 59, 60). Additionally, the androgen-responsive genes involved in different cellular functions include cellular metabolites such as acetyl-CoA-carboxylase and HMG-Co-reductase; cellular transport or trafficking such as FK-506 binding-protein (FKBP51) and ANKH; and those involved in cellular proliferation and differentiation such

as Maf and Cdc14B (61-63). The capability of the androgen receptor to control such a wide variety of genes makes it a critical protein in the initiation and development of prostate cancer.

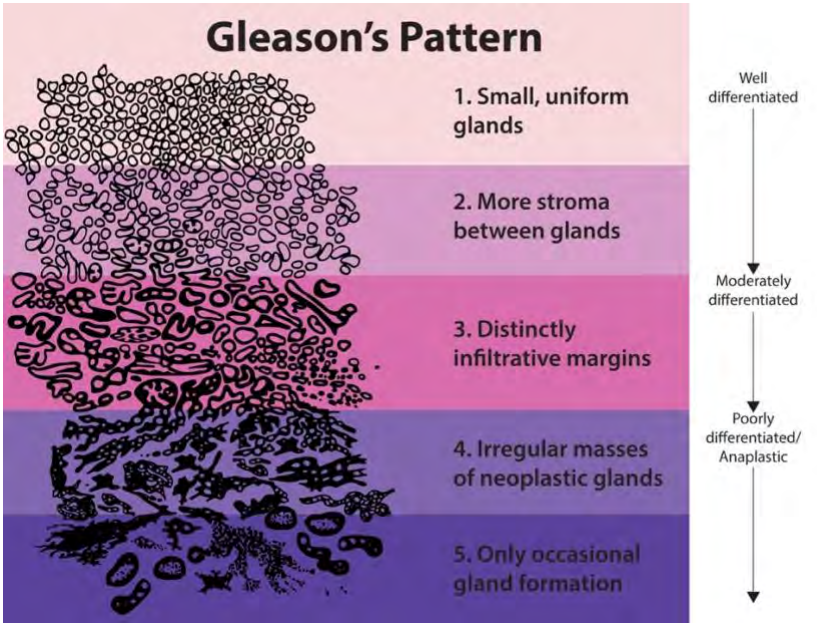

Figure 1.4. Gleason Grading system for prostate cancer. SEER Training Modules, *Prostate Cancer*. U. S. National Institutes of Health, National Cancer Institute. 16, Dec. 2019 <https://training.seer.cancer.gov/prostate/abstract-code-stage/morphology.html>.

AR protein domains:

The AR gene consists of 8 exons with 2757 nucleotides that are located on the X chromosome at Xq11-12. The eight exons of AR encode AR protein (110 kDa) (57). Similar to other steroid hormone nuclear receptors, the androgen receptor protein consists of four major domains: a) N-terminal domain (NTD) (encoded by exon 1); b) DNA binding domain (encoded by exons 2 & 3); c) Hinge region (partially encoded by exon 4); d) Ligand binding domain (LBD) (encoded by exons 4-8) (57). The N-terminal domain is the largest domain of the AR protein and contains activation function-1 (AF1), which is constitutively active and harbors significant transcriptional

activity in a ligand-independent manner. DNA binding domain folds into two zinc-fingers that coordinate direct binding of the AR to the DNA promoter site of the target gene. DBD contains the nuclear localization signal (NLS) where importin-α binds and facilitates the translocation of AR to the nucleus. The Hing region is a flexible region that connects the DBD to the LBD. The LBD is where the ligand binds to AR. The LBD harbors activation function 2 (AF2), which is ligand dependent (57).

AR in prostate cancer

The androgen receptor is considered the primary regulator of prostate cancer. The first to demonstrate the importance of androgen receptor signaling in the progression of prostate cancer was Charles Huggins in 1941 by showing the influence of castration (removal of testes) on the growth of prostate cancer (64). PSA, a downstream gene of AR, is elevated in the most prostate cancer patients, which indicates the activation of AR signaling pathway in patients (65). The attribution of the AR signaling pathway in the initiation of prostate cancer was further demonstrated by studying the activation role of AR on growth pathways. In particular, the fusion of TMPRSS2 with erythroblast transforming specific (ETS) family of transcription factors such as ETS-related gene (ERG) and ETS-translocation variant 1 (ETV1) (66, 67). TMPRSS2-ERG fusion occurs in more than 50% of prostate cancer patients and leads to cell cycle activation (66, 68). First-line treatments of prostate cancer aim to suppress the activity of androgen receptor by Surgical or pharmacological androgen deprivation treatment (ADT), which is effective for most patients, further proving the pivotal role of AR in prostate cancer (69). However, the remission of cancer after patients start ADT does not last long, and the recurrence is inevitable within 2-3 years. At this stage, the cancer is called castration-resistance prostate cancer (CRPC) (70).

AR in castration resistant prostate cancer (CRPC)

Castration resistant prostate cancer is a lethal, incurable stage of prostate cancer in which cancer can grow in the absence of androgen (70). Even though the term CRPC implies that cancer does not rely on androgens and AR for its growth, recent studies have demonstrated that AR is essential for the development of CRPC (70). AR drives the development of CRPC through different resistance mechanisms to ADT:

- **AR gene amplification** is one of the resistance mechanisms for ADT in CRPC. Despite low levels of circulating androgens, prostate cancer cells bypass ADT by overexpressing AR to make it more sensitive to androgens. By this approach, the cells decrease the threshold of AR to androgens and maintain AR signaling in such an environment. Up to 50% of patients with CRPC showed an increase in AR expression (70).
- **Mutation in androgen receptor**: Several point mutations have been found in the AR gene that confers its activity. Up to 30% of CRPC patients have been identified with AR point mutations. The majority of these mutations are located in the ligand-binding domain of AR. The most common mutation is T878A that results in the change of AR affinity and specificity to ligands. A T878A mutation leads to the activation of AR by other hormones such as progesterone and estrogen or by AR antagonists such as bicalutamide and flutamide, which provoke AR transcriptional activity and tumor growth. Furthermore, a T878A mutation results in resistance to the second-generation AR antagonists such as enzalutamide. Moreover, F876L is another point mutation at the LBD of AR that leads to resistance to enzalutamide (70).
- **De novo synthesis of androgen:** CRPC starts the de novo synthesis of androgens as a response to low levels of circulating androgens as a result of ADT. CRPC overexpress

several converting enzymes such as Aldo-keto reductase family 1 member C3 (AKR1C3) that help convert androstenedione and dehydroepiandrosterone into testosterones. Also, CRPC intratumorally over-express CYP17A1that is a key regulator for the testosterone synthesis pathway. Recent studies show that CRPC overexpresses a mutated active form of 3beta-hydroxysteroid dehydrogenase/delta(5)-delta(4)isomerase type I (HSD3β1), which is a key regulator of the dihydrotestosterone synthesis pathway (70).

- **Ligand -independent AR activation:** AR can be activated in the absence of ligand through different signaling pathways. These signaling pathways, including PI3K/Akt/mTOR pathway and tyrosine kinase receptors such as epidermal growth factor (EGF), insulin-like growth factor 1 (IGF-1), and keratinocyte growth factor (KGF), have been recently shown to regulate AR signaling in CRPC. Some of the non-receptor tyrosine kinases such as Src and Ack1 can interact and phosphorylate AR to promote its transcriptional activity. Recently, researchers described the ability of long non-coding RNAs such as PRNCR1, which is overexpressed in CRPC, to interact with AR and induce its transcriptional activity in the absence of AR ligands (70).
- **Androgen receptor variants** is another form of resistance mechanism to escape ADT. CRPC express different AR variants that are androgen-independent and/or constitutively active. Several variants have been identified to be expressed in CRPC, such as AR-V1, AR-V7, and AR-V567es. AR-V7 is the most abundant AR variant expressed in CRPC. AR-V7 lacks a LBD, makeing it resistant to AR antagonists targeting LBD. AR-V7 is constitutively active and located in the nucleus in androgen-independent fashion (70).

Treatment options for prostate cancer

According to the American Urological Association (AUA), there are two major treatment approaches for prostate cancer patients: non-pharmacological and pharmacological approaches (71). The preferred approach depends on several factors such as 1) severity of cancer (localized or metastasized); 2) life expectancy; 3) possible side effects of the approach; and 4) patient medical conditions (72). If the cancer is in its early stage and is confined within the prostate gland, patients usually are recommended to be under active surveillance or watchful waiting (69). Patients who are under active surveillance are recommended to conduct a PSA test every 3 to 6 months. Also, a DRE is recommended once every year and a biopsy within 6 to 12 months, then once every two years. local treatment will occur if the cancer worsens (69).

Local treatments include radiotherapy (RT) or radical prostatectomy (RP). Radiation therapy includes external-beam radiation therapy, brachytherapy, intensity-modulated radiation therapy (IMRT), or proton therapy. Even though radiation therapy is considered a non-invasive procedure, it still has several significant side effects, including frequent urination, impotence, fatigue, and disruption of bowel functions (69). Radical prostatectomy involves the complete removal of the prostate tissue by open surgery, robotic proctectomy, bilateral orchiectomy, or transurethral resection of the prostate (TURP) (73). The major side effect of prostatectomy is incontinence urination and erectile dysfunction (73). After patients receives the non-pharmacological treatment, they are monitored for any increase in PSA levels. However, up to 40 % of patients who removed their prostate by RP and up to 50% of patients who received RT had a recurrence within 10 years (74). At this stage, patients are recommended to begin androgen deprivation therapy (ADT) since the tumor depends on androgen signaling for growth (69).

Androgen deprivation therapy aims to reduce testosterone levels in circulation or block the binding of androgen to the androgen receptor. Currently, luteinizing hormone-releasing hormone (LHRH) agonists such as leuprorelin or goserelin are used to block production and secretion of testosterone (69). Also, gonadotropin-releasing hormone (GnRH) antagonists such as degarelix are another class of ADT, which are more rapid than LHRH agonists in reducing testosterone levels (75). Unlike LHRH agonists and GnRH antagonists, androgen receptor inhibitors such as bicalutamide and flutamide inhibit binding of testosterone (androgen) to the androgen receptor (75). While ADT does not cure cancer, it does slow cancer growth. Eventually, the tumor develops resistance mechanisms to escape the ADT effect and becomes castration-resistance prostate cancer (CRPC) (76). CRPC is usually treated with novel androgen synthesis inhibitors (abiraterone), immunotherapy (sipuleucel-T), or chemotherapy (docetaxel or cabazitaxel) (76). There is an urgent need to develop a novel approach to overcome ADT resistance to improve treatment outcomes for patients with prostate cancer.

References

1. R. Toivanen, M. M. Shen, Prostate organogenesis: tissue induction, hormonal regulation and cell type specification. *Development* **144**, 1382-1398 (2017).
2. L. Aaron, O. E. Franco, S. W. Hayward, Review of Prostate Anatomy and Embryology and the Etiology of Benign Prostatic Hyperplasia. *Urol Clin North Am* **43**, 279-288 (2016).
3. K. Prakash *et al.*, Symptomatic and asymptomatic benign prostatic hyperplasia: molecular differentiation by using microarrays. *Proc Natl Acad Sci U S A* **99**, 7598-7603 (2002).
4. K. H. Leissner, L. E. Tisell, The weight of the human prostate. *Scand J Urol Nephrol* **13**, 137-142 (1979).
5. W. G. Nelson, A. M. De Marzo, W. B. Isaacs, Prostate cancer. *N Engl J Med* **349**, 366-381 (2003).
6. S. J. Xia, X. X. Xu, J. B. Teng, C. X. Xu, X. D. Tang, Characteristic pattern of human prostatic growth with age. *Asian J Androl* **4**, 269-271 (2002).
7. H. Lilja, Structure and function of prostatic- and seminal vesicle-secreted proteins involved in the gelation and liquefaction of human semen. *Scand J Clin Lab Invest Suppl* **191**, 13-20 (1988).
8. J. E. McNeal, The zonal anatomy of the prostate. *Prostate* **2**, 35-49 (1981).
9. I. Laczko, D. L. Hudson, A. Freeman, M. R. Feneley, J. R. Masters, Comparison of the zones of the human prostate with the seminal vesicle: morphology, immunohistochemistry, and cell kinetics. *Prostate* **62**, 260-266 (2005).
10. J. A. Sinnott *et al.*, Molecular differences in transition zone and peripheral zone prostate tumors. *Carcinogenesis* **36**, 632-638 (2015).
11. H. A. Vargas *et al.*, Normal central zone of the prostate and central zone involvement by prostate cancer: clinical and MR imaging implications. *Radiology* **262**, 894-902 (2012).
12. S. Guneyli *et al.*, Magnetic resonance imaging of benign prostatic hyperplasia. *Diagn Interv Radiol* **22**, 215-219 (2016).
13. S. Ishidoya, M. Endoh, H. Nakagawa, S. Saito, Y. Arai, Novel anatomical findings of the prostatic gland and the surrounding capsular structures in the normal prostate. *Tohoku J Exp Med* **212**, 55-62 (2007).
14. J. E. McNeal, Normal histology of the prostate. *Am J Surg Pathol* **12**, 619-633 (1988).
15. J. A. Schalken, G. van Leenders, Cellular and molecular biology of the prostate: stem cell biology. *Urology* **62**, 11-20 (2003).
16. P. A. di Sant'Agnese, Neuroendocrine cells of the prostate and neuroendocrine differentiation in prostatic carcinoma: a review of morphologic aspects. *Urology* **51**, 121-124 (1998).
17. Y. N. Niu, S. J. Xia, Stroma-epithelium crosstalk in prostate cancer. *Asian J Androl* **11**, 28-35 (2009).
18. S. W. Kim, Prostatic disease and sexual dysfunction. *Korean J Urol* **52**, 373-378 (2011).
19. C. G. Roehrborn, Benign prostatic hyperplasia: an overview. *Rev Urol* **7 Suppl 9**, S3-S14 (2005).
20. J. K. Parsons, Benign Prostatic Hyperplasia and Male Lower Urinary Tract Symptoms: Epidemiology and Risk Factors. *Curr Bladder Dysfunct Rep* **5**, 212-218 (2010).

21. E. H. Kim, J. A. Larson, G. L. Andriole, Management of Benign Prostatic Hyperplasia. *Annu Rev Med* **67**, 137-151 (2016).
22. J. C. Nickel, Prostatitis. *Can Urol Assoc J* **5**, 306-315 (2011).
23. J. Rees, M. Abrahams, A. Doble, A. Cooper, G. Prostatitis Expert Reference, Diagnosis and treatment of chronic bacterial prostatitis and chronic prostatitis/chronic pelvic pain syndrome: a consensus guideline. *BJU Int* **116**, 509-525 (2015).
24. G. Paulis, Inflammatory mechanisms and oxidative stress in prostatitis: the possible role of antioxidant therapy. *Res Rep Urol* **10**, 75-87 (2018).
25. H. C. Miller, Stress prostatitis. *Urology* **32**, 507-510 (1988).
26. G. Dickson, Prostatitis--diagnosis and treatment. *Aust Fam Physician* **42**, 216-219 (2013).
27. J. Woenckhaus, I. Fenic, Proliferative inflammatory atrophy: a background lesion of prostate cancer? *Andrologia* **40**, 134-137 (2008).
28. R. L. Siegel, K. D. Miller, A. Jemal, Cancer statistics, 2019. *CA Cancer J Clin* **69**, 7-34 (2019).
29. S. Gupta *et al.*, Prostate Cancer: How Young is too Young? *Curr Urol* **9**, 212-215 (2017).
30. D. Shenoy, S. Packianathan, A. M. Chen, S. Vijayakumar, Do African-American men need separate prostate cancer screening guidelines? *BMC Urol* **16**, 19 (2016).
31. J. Dickinson *et al.*, Trends in prostate cancer incidence and mortality in Canada during the era of prostate-specific antigen screening. *CMAJ Open* **4**, E73-79 (2016).
32. B. T. Howrey, Y. F. Kuo, Y. L. Lin, J. S. Goodwin, The impact of PSA screening on prostate cancer mortality and overdiagnosis of prostate cancer in the United States. *J Gerontol A Biol Sci Med Sci* **68**, 56-61 (2013).
33. M. F. Leitzmann, S. Rohrmann, Risk factors for the onset of prostatic cancer: age, location, and behavioral correlates. *Clin Epidemiol* **4**, 1-11 (2012).
34. P. H. Gann, Risk factors for prostate cancer. *Rev Urol* **4 Suppl 5**, S3-S10 (2002).
35. C. A. Salinas, A. Tsodikov, M. Ishak-Howard, K. A. Cooney, Prostate cancer in young men: an important clinical entity. *Nat Rev Urol* **11**, 317-323 (2014).
36. F. Albright *et al.*, Prostate cancer risk prediction based on complete prostate cancer family history. *Prostate* **75**, 390-398 (2015).
37. P. Rawla, Epidemiology of Prostate Cancer. *World J Oncol* **10**, 63-89 (2019).
38. W. G. Gathirua-Mwangi, J. Zhang, Dietary factors and risk for advanced prostate cancer. *Eur J Cancer Prev* **23**, 96-109 (2014).
39. C. Chen, P. Xun, M. Nishijo, S. Carter, K. He, Cadmium exposure and risk of prostate cancer: a meta-analysis of cohort and case-control studies among the general and occupational populations. *Sci Rep* **6**, 25814 (2016).
40. E. Castro, R. Eeles, The role of BRCA1 and BRCA2 in prostate cancer. *Asian J Androl* **14**, 409-414 (2012).
41. T. Jamaspishvili *et al.*, Clinical implications of PTEN loss in prostate cancer. *Nat Rev Urol* **15**, 222-234 (2018).
42. H. Gronberg *et al.*, Characteristics of prostate cancer in families potentially linked to the hereditary prostate cancer 1 (HPC1) locus. *JAMA* **278**, 1251-1255 (1997).
43. M. W. Datta *et al.*, Perlecan, a candidate gene for the CAPB locus, regulates prostate cancer cell growth via the Sonic Hedgehog pathway. *Mol Cancer* **5**, 9 (2006).
44. H. B. Carter *et al.*, Germline Mutations in ATM and BRCA1/2 Are Associated with Grade Reclassification in Men on Active Surveillance for Prostate Cancer. *Eur Urol* **75**, 743-749 (2019).

45. J. M. Farnham, N. J. Camp, J. Swensen, S. V. Tavtigian, L. A. Albright, Confirmation of the HPCX prostate cancer predisposition locus in large Utah prostate cancer pedigrees. *Hum Genet* **116**, 179-185 (2005).
46. S. J. Bromage, R. D. Napier-Hemy, S. R. Payne, I. Pearce, I. G. McIntyre, The use of prostate-specific antigen testing in men presenting with haematuria. *BJU Int* **98**, 1221-1224; discussion 1224 (2006).
47. S. W. D. Merriel, G. Funston, W. Hamilton, Prostate Cancer in Primary Care. *Adv Ther* **35**, 1285-1294 (2018).
48. R. M. Martin, L. Vatten, D. Gunnell, P. Romundstad, T. I. Nilsen, Lower urinary tract symptoms and risk of prostate cancer: the HUNT 2 Cohort, Norway. *Int J Cancer* **123**, 1924-1928 (2008).
49. J. Eastham, Prostate cancer screening. *Investig Clin Urol* **58**, 217-219 (2017).
50. C. Stephan, H. Rittenhouse, X. Hu, H. Cammann, K. Jung, Prostate-Specific Antigen (PSA) Screening and New Biomarkers for Prostate Cancer (PCa). *EJIFCC* **25**, 55-78 (2014).
51. J. R. Rider *et al.*, Ejaculation Frequency and Risk of Prostate Cancer: Updated Results with an Additional Decade of Follow-up. *Eur Urol* **70**, 974-982 (2016).
52. J. J. Bruno, 2nd, N. A. Armenakas, J. A. Fracchia, Influence of prostate volume and percent free prostate specific antigen on prostate cancer detection in men with a total prostate specific antigen of 2.6 to 10.0 ng/ml. *J Urol* **177**, 1741-1744 (2007).
53. H. B. Carter, Prostate cancers in men with low PSA levels--must we find them? *N Engl J Med* **350**, 2292-2294 (2004).
54. L. Chunhua *et al.*, Clinical Significance of Peripheral Blood PCA3 Gene Expression in Early Diagnosis of Prostate Cancer. *Transl Oncol* **11**, 628-632 (2018).
55. B. L. Braunhut, S. Punnen, O. N. Kryvenko, Updates on Grading and Staging of Prostate Cancer. *Surg Pathol Clin* **11**, 759-774 (2018).
56. R. Montironi *et al.*, Prostate cancer: from Gleason scoring to prognostic grade grouping. *Expert Rev Anticancer Ther* **16**, 433-440 (2016).
57. R. A. Davey, M. Grossmann, Androgen Receptor Structure, Function and Biology: From Bench to Bedside. *Clin Biochem Rev* **37**, 3-15 (2016).
58. S. Slater, R. T. Oliver, Testosterone: its role in development of prostate cancer and potential risk from use as hormone replacement therapy. *Drugs Aging* **17**, 431-439 (2000).
59. L. L. Xu *et al.*, Quantitative expression profile of androgen-regulated genes in prostate cancer cells and identification of prostate-specific genes. *Int J Cancer* **92**, 322-328 (2001).
60. H. Qi *et al.*, Androgens induce expression of SPAK, a STE20/SPS1-related kinase, in LNCaP human prostate cancer cells. *Mol Cell Endocrinol* **182**, 181-192 (2001).
61. J. A. Locke, K. M. Wasan, C. C. Nelson, E. S. Guns, C. G. Leon, Androgen-mediated cholesterol metabolism in LNCaP and PC-3 cell lines is regulated through two different isoforms of acyl-coenzyme A:Cholesterol Acyltransferase (ACAT). *Prostate* **68**, 20-33 (2008).
62. E. Smith *et al.*, Androgen Receptor and Androgen-Responsive Gene FKBP5 Are Independent Prognostic Indicators for Esophageal Adenocarcinoma. *Dig Dis Sci* **61**, 433-443 (2016).
63. P. S. Nelson *et al.*, The program of androgen-responsive genes in neoplastic prostate epithelium. *Proc Natl Acad Sci U S A* **99**, 11890-11895 (2002).

64. C. Huggins, C. V. Hodges, Studies on prostatic cancer: I. The effect of castration, of estrogen and of androgen injection on serum phosphatases in metastatic carcinoma of the prostate. 1941. *J Urol* **168**, 9-12 (2002).
65. B. Bindukumar *et al.*, Prostate-specific antigen modulates the expression of genes involved in prostate tumor growth. *Neoplasia* **7**, 241-252 (2005).
66. S. A. Tomlins *et al.*, Recurrent fusion of TMPRSS2 and ETS transcription factor genes in prostate cancer. *Science* **310**, 644-648 (2005).
67. F. Demichelis, M. A. Rubin, TMPRSS2-ETS fusion prostate cancer: biological and clinical implications. *J Clin Pathol* **60**, 1185-1186 (2007).
68. Z. Wang *et al.*, Significance of the TMPRSS2:ERG gene fusion in prostate cancer. *Mol Med Rep* **16**, 5450-5458 (2017).
69. M. S. Litwin, H. J. Tan, The Diagnosis and Treatment of Prostate Cancer: A Review. *JAMA* **317**, 2532-2542 (2017).
70. T. Karantanos, P. G. Corn, T. C. Thompson, Prostate cancer progression after androgen deprivation therapy: mechanisms of castrate resistance and novel therapeutic approaches. *Oncogene* **32**, 5501-5511 (2013).
71. K. Cotter, B. Konety, M. A. Ordonez, Contemporary Management of Prostate Cancer. *F1000Res* **5** (2016).
72. A. Gasnier, N. Parvizi, Updates on the diagnosis and treatment of prostate cancer. *Br J Radiol* **90**, 20170180 (2017).
73. N. Srivatsa, H. Nagaraja, S. Shweta, S. K. Raghunath, Radical Prostatectomy for Locally Advanced Prostate Cancers-Review of Literature. *Indian J Surg Oncol* **8**, 175-180 (2017).
74. A. Jeffers *et al.*, Predicting Prostate Cancer Recurrence After Radical Prostatectomy. *Prostate* **77**, 291-298 (2017).
75. K. Fujita, N. Nonomura, Role of Androgen Receptor in Prostate Cancer: A Review. *World J Mens Health* **37**, 288-295 (2019).
76. S. J. Kim, S. I. Kim, Current treatment strategies for castration-resistant prostate cancer. *Korean J Urol* **52**, 157-165 (2011).

CHAPTER 2

LITERATURE REVIEW ON PROTEIN MYRISTOYLATION AND N-MYRISTOYLTRANSFERASE

Introduction:

The study of an organism would be simpler and more efficient if the total number of proteins were equal to the total number of genes. The human genome is composed of 20,000 to 25,000 genes, however, the human proteome is more sophisticated, made up of different proteoforms that have been discovered over the past 50 years (1). One key mechanism that drives the complexities of the proteome stem from the variety of co-translational and post-translational modifications. Presently, there are more than 200 different types of post-translational modifications that have been studied (2, 3). These modifications are carried out mostly by enzymes such as ligases, transferases, phosphatases, kinases, and hydrolases (4). Each type of modification allows different proteins to accomplish different functions, such as responding to external and internal stimuli, localization, activation, and degradation of the protein within the cell (4). Most common post-translational modifications include but not limited to acetylation, phosphorylation, methylation, ubiquitination, and lipidation. Recently, protein lipidation gains attention because its emerging roles in cancer. Protein lipidation is the attachment of a lipid to the chain of a protein.

One particular protein lipidation modification, the attachment of myristic acid to the N-terminal glycine, was first described as a blocking group. In 1981, a sequence analysis study was conducted by Shoji and Titani using the Edman degradation method, which identified the sequence of the catalytic subunits of cyclic AMP-dependent protein kinase with a group that

blocked the N-terminal glycine (5). Using gas chromatography mass spectrometry, Carr and Titani found that the unrecognized group was linked to the N-terminal glycine of the cyclic AMP-dependent protein kinase is a myristoyl group. This myristoyl group binds to the N-terminal glycine through an amide linkage (6).

N-Myristoylation:

For several years, tremendous efforts have been made to understand protein lipid modifications, including myristoylation. Protein myristoylation is a post-translational lipid modification in which a C14 saturated fatty acid is irreversibly attached to the N-terminal glycine of a protein through an amide bond. This irreversible modification is facilitated by N-myristoyltransferase (NMT) enzyme (7).

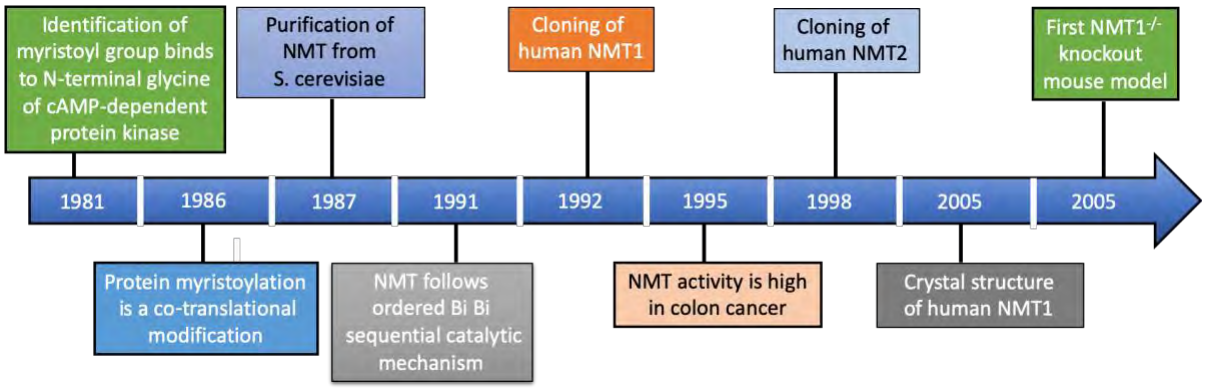

Major events demonstrating important finding for N-myristoyltransferase enzyme

Protein myristoylation modifications can be divided into two categories: a co-translational or a post- translational process, according to when it occurs on the protein (7). In the co-translational process, the initiator methionine on the nascent synthesized polypeptide is removed by methionine aminopeptidase (MetAP), which exposes Gly2 to NMT (7). Post-translational myristoylation may occur for proteins containing an internal glycine residue,

which is revealed by cleavage by caspases, thereby exposing to NMT as a substrate **(Figure 2.1)** (7).

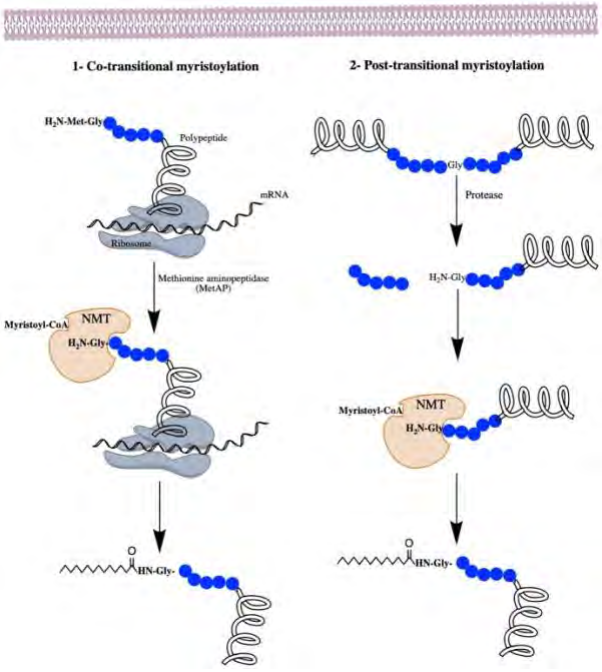

Figure 2.1. Two categorizes of protein myristoylation modification.

The attachment of a myristoyl moiety to a protein is irreversible and has several effects (7). Myristoyl moiety can modulate the affinity of the modified protein to the lipid bilayer membrane to control subcellular localization of the protein and protein-protein interaction (7). For example, myristoylation of Src increases its hydrophobicity and directs it toward the lipid bilayer membrane (8, 9). Also, localization of BID-p15 protein to the mitochondria membrane in the cells is completely controlled by its myristoylation status (10).

Even though the amide bond that forms between the N-terminal glycine of a protein and the myristic acid is irreversible, the attachment of myristoylated protein to the membrane is reversible due to its weak lipophilic nature and the myristoylation switches (7). Myristoylation switches are dynamic processes in which the effect of the myristoyl group can be overcome by

the myristoylated protein itself (11). There are two myristoylation switch mechanisms that have been identified: the myristoylation conformational switch and the myristoylation electrostatic switch (11-13). For the myristoylation conformational switch, the myristoyl group can be sequestered inside a hydrophobic pocket within the protein by inducing a conformational change in that protein (11). This mechanism can be further induced by a ligand, leading to the reveal of the sequestered myristoyl moiety. For example, the binding of calcium to recoverin protein induces a conformational change in the protein, leading to the exposure of the myristoyl moiety to the cytosol, thereby targeting it to the membrane (11). Another mechanism of myristoylation switches depends on a cluster of basic amino acids in the N-terminal of the myristoylated protein called electrostatic myristoylation switches. The highly positive polybasic domain of the protein helps tether the myristoylated protein to the cell membrane. Changes in the net positive charge of the polybasic domain can result in a release of the myristoylated protein from the cell membrane (13). For example, phosphorylation of serine residues in the N-terminal of MARCKS leads to the inability of the polybasic domain to stabilize MARCKS at the membrane (12).

The importance of studying protein myristoylation comes from its critical role in the pathogenesis of several diseases. Several myristoylated proteins such as Src, MARCKS, and heterotrimeric G alpha protein control major intracellular signaling pathways within the cell (14). Alterations of protein-protein interactions or subcellular localization of these proteins by the myristoyl moiety can lead to disruption of the signaling pathways (14). Changes in the myristoylation status of proteins NMT expression levels and activity have been linked to different diseases such as HIV infection (15), Noonan-like syndrome (16), Alzheimer disease (17), and epilepsy (18). In addition, the potential role of NMT in different pathogenic

conditions, such as ischemia-reperfusion and diabetes mellitus, have been demonstrated using animal models (19, 20). Myristoylation of several fungal proteins is critical for their survival. Interestingly, yeast NMT (yNMT) has distinct substrates different from human NMT (hNMT), which could be utilized for developing a selective inhibitor for yNMT (21). Myristoylation of viral proteins, such as Gag and Nef proteins, are essential for viral assembly and survival (22). More importantly, dysregulation of NMT expression and activity has been linked to the progression of cancer [section 4] (15).

N-myristoyltransferase:

NMT belongs to the GCN5-related N-acetyltransferase superfamily (GNAT) (7). The function of this superfamily is characterized by transferring an acyl group from the acetyl-CoA to the acceptor peptide (7). NMT is a unique member of the GNAT family given its wide range of substrates (7). Using algorithm prediction analysis methods, up to 0.5 % of mammalian encoded proteins are substrates for NMT (23). The diversity of substrates makes the enzyme critical in several organisms.

NMT is a ubiquitous protein that can be found in 53 different species. NMT has been identified experimentally or bioinformatically to be expressed in lower eukaryotes including *Dictyostelium discoideum* (24), *Candida albicans* 2 (25), *Cryptococcus neoformans* (26), *Arabidopsis thaliana* (27), *Plasmodium falciparum* (28), Wheat germ (29), and *Saccharomyces cerevisiae* (30). It is also expressed in higher eukaryotes including humans (31), bovines (32), rats (33), and mice (34).

A huge effort has been made to purifiy, characterize, and clone NMT from yeast. Towler *et. al*., was the first to describe NMT enzyme as a membrane bound protein that facilitates the

attachment of the myristic acid to the N-terminal of synthetic octapeptide derived from a known N-myristoylated acyl protein in yeast (30). Further characterization of NMT in yeast revealed only one isoform of NMT in *S. cerevisiae* strain JR15, which showed 65% and 35% activity in the membrane and soluble fractions, respectively (35). By using synthetic peptides and inhibitors, Glaser *et. al.* demonstrated that NMT in murine muscle cells has the same peptide specificity as yNMT (36, 37). In 1987, Gordon *et. al.* purified a 55 kDa monomer NMT protein from *S. cerevisiae*. No other isoforms of NMT were ever found to be expressed in yeast (30). Later, NMT was found to be highly expressed in rat tissue (38) and rat brain (39) with molecular weight of 84 and 50 kDa, respectively. In contrast to what is known about yNMT, Sharma's group demonstrated different molecular weights of NMT in the bovine brain (bNMT) including: 390 kDa, 224 kDa, 190 kDa and 76 kDa (40). A follow up study in 1997 by Glover *et. al*., showed that bovine brain tissue contained a heterogenous mixture of NMT oligomeric complexes (390 and 126 kDa), which assign to multimerization of 60 kDa NMT subunits (41). Unlike bovine brain tissue, only one form of NMT protein (with a molecular mass of 50kDa) was found in bovine spleen, which indicates that the spleen bNMT is a monomeric protein (Table 1) (42).

The hNMT gene was first cloned from a hepatocarcinoma cell line, HepG2, by a functional complementation of yNMTl-181 mutant, a temperature-deficient mutant that cause a myristic acid auxotrophy. hNMT protein, which contains 416 amino acids, shares a 44% sequence similarity to *S. cerevisiae* NMT (43). Later, a single isoform of hNMT was purified from the erythroleukemia (HEL) cell line (44) and murine leukemia cell line (L1210) (45). The purified enzyme shows a 67 kDa molecular mass, which varies from the apparent molecular mass of yNMT (53 kDa) and bNMT (60 kDa) (46). A second genetically distinct NMT (hNMT2)

cDNA was isolated from a human liver library that shares 77% sequence similarity to the previous characterized human NMT (hNMT1). hNMT2 has a molecular mass of 65 kDa (47). Similarly, mouse, bovine and rat tissues express two family members of NMT: mNMT1/2, bNMT1/2 and rNMT1/2 **(Table 2.1)** (33, 34, 48).

Species	Isoforms	Molecular weight (kDa)	Multimerization	Reference
S. Cerevisiae	NMT	55	No	(30)
C. albicans	NMT	53	No	(25)
Drosophila	NMT	46	No	(49)
Rattus norvegicus (Rat)	NMT1 and NMT2	55 and 66	No	(33)
Mus musculus	NMT1 and NMT2	65 and 67	No	(34) (47)
Bos taurus (Bovine)	NMT1 and NMT2	50 and 76	No	(48)
Homo sapiens	NMT1 and NMT2	65 and 67	No	(47)

Table 2.1. Isoforms of N-myristoyltransferase in different species.

A characterization study of hNMT2 shows that it catalyzes myristoylation in a similar fashion to hNMT1, but with different preference (47). For example, both hNMT1 and hNMT2 have a 100% myristoylation rate for a peptide derived from Src kinase (47). Conversely, the myristoylation rate of the peptide derived from cAMP-dependent protein kinase was higher by NMT1 (70%) compared to hNMT2 (50%), and 43% by NMT1 compare to 27% by hNMT2 on the peptide derived from c-abl (47). NMT1 and NMT2 genes differ only at the N-terminus, which contributes to target the enzymes at different sites at the cytoplasm (31). Organisms that

only express a single isoform of NMT, such as *S. cerevisiae* (50) and Drosophila (51), were incapable of surviving without active NMT protein. Furthermore, NMT1-/- knockout mice failed to deliver healthy pups since NMT1-/- knockout is embryonic lethal (34). NMT2 was not able to balance the absence of NMT1, clearly suggesting the substrate specificity of each NMT members (34).

Regulation of N-myristoyltransferase:

The regulation of NMT expression and activity is still not fully understood. It is not clear whether NMT could be regulated by the myristoyl-CoA pool or by the expression of endogenous myristoylated proteins, as has been suggested by several researchers. Also, the mechanisms that induce NMT activity in some diseases is still unknown. However, several miRNAs have been identified in regulation of NMT expression. Recently, Chaunhan R. *et. al.*, using bioinformatics and functional analysis, predicted 35 miRNAs (15 miRNAs target NMT1 and 20 miRNAs target NMT2) that bind and modulate NMT transcription in cancer. Out of the 35 miRNAs, 11 miRNAs have a described role in prostate cancer, such as miR-421, miR-186-5p, miR-497, and miR-1193. Furthermore, 4 miRNAs are linked to colorectal cancer (miR-409-3p, miR-1914-5p, miR-301a-5p, and miR-133a-5p), breast cancer (miR-127-3p, miR-137, miR-187-5p, and miR-411-5p), and liver cancer (miR-520b, miR-15b-5p, miR-199a-5p, and miR-584p). In addition, 3 miRNAs play a crucial role in the progression of esophageal cancer (miR-140-5p, miR-330-3p, and 452-5p), and one miRNA has a defined role in renal cell carcinoma (miR-200a-3p), brain cancer (miR-503-5p), and squamous cell carcinoma (miR-346) (52).

The crosstalk between NMT and its substrates has been identified, and this reciprocal interaction shows some regulatory effect on NMT activity. NMT is phosphorylated by Src family kinase (Fyn and Lyn) at Y100 (53). NMT Y100F mutant shows 98% reduction in its activity compared to the wild type (53). Also, phosphorylation of NMT may play a role in its localization to the plasma membrane, away from newly synthesized proteins from ribosomes, which may affect the myristoylation process (53). NMT interacts with Lyn in a phosphorylation-dependent manner, and this interaction contributes to the movement of NMT to different cellular compartments (53). On the other hand, phosphorylation of NMT by Akt/PKB attenuates NMT activity as described by Sharma *et. al*. (54). The site and significance of NMT phosphorylation by Akt/PKB is still unknown.

Several endogenous proteins controlling the activity of NMT have been identified. From bovine brain tissue, Sharma *et. al.* was the first to demonstrate the inhibitory effect of NMT inhibitor protein 71 (NIP71) on the activity of NMT (55). NIP71 has 44% homology to heat-shock cognate protein 70 (HSC70) (55, 56). The exact mechanism of NIP71 is not known, but it is believed that NIP71 directly interacts with NMT, since it does not possess any protease or thioesterase activity and does not interact with myristoyl-CoA (55). In addition to NIP71, Enolase shows a potent inhibition on NMT with IC_{50} = 0.6 μM *in vitro* (57). The potential of both endogenous proteins to serve as NMT inhibitors has not been evaluated *in vivo*. On the other hand, 45 kDa NMT activator (NAF4) works as an activator for NMT in bovine brain tissue (58). NAF45 was copurified with one form of NMT, but does not have an effect on other forms (58). Incubation of NMT with NAF45 resulted in a 4-fold increase in NMT activity (58).

Other protein in regulation of NMT activity has also been reported in different studies. In human mononuclear phagocytes, tumor necrosis factor alpha (TNF-a) and interferon gamma (INF-g) induce the activity of NMT (59). Also, NMT activity was abolished by retinoic acid and induced by TPA in a human leukemia cell line (HL-60) (60).

N-myristoyltransferases Localization:

NMT localization was first determined by immunocytochemical methods in HeLa cells using an affinity antibody raised against a synthetic peptide based on the sequence of NMT. An even distribution of immunofluorescence staining for NMT was detected across the cytoplasm of HeLa cells, indicating NMT localization to the cytosol (61, 62). The measurement of NMT in different subcellular fractions confirms this finding, where the majority of NMT activity comes from the cytosolic fraction, and only a small portion of the activity was detected in the crude total membrane fraction (63). Sub-cytosolic localization of NMT was further characterized by Glover *et. al.*, in different cancer cell lines such as Hela, CEM, and MOLT4 cells using differential centrifugation methods (64). Full length NMT, 60 kDa, is associated with ribosomal fractions compared to other subcellular fractions. This ribosomal association is essential for NMT function since NMT carries out co-translational modification of *de novo* synthesized polypeptides. The localization of NMT to the ribosome is totally dependent on the k box motif, a poly-lysine region in the N-terminal domain of NMT, which has no catalytic activity of the enzyme (64). However, short forms of NMT1, which lack the N-terminal domain, are diffused through the cytoplasm (64). Of note, NMT is localized to the nucleus in bone marrow mononuclear cells of a tumor-bearing rat (65). The significance of NMT localized at the nucleus is still unknown.

Kinetics of N-myristoyltransferase:

-Mechanism of protein myristoylation:

NMT can specifically transfer myristoyl group from myristoyl-CoA to the N-terminus glycine of intracellular proteins. The characterization of NMT was studied by the interaction between the *S. cerevisiae* NMT and myristoyl-CoA using isoelectric focusing gel shift assay and tryptophan fluorescence quenching experiments. Incubation of NMT with myristoyl-CoA generates an intermediate with a highly resolved pI equal to 6.7. This is compared to the basic intermediate for apo-NMT (pI=8.15). The more acidic intermediate was restored by the addition of a peptide substrate and resulted in a band identical to the NMT alone. This suggests that there is a high affinity interaction between NMT and myristoyl-CoA, and this complex can form in the absence of the peptide substrate. Addition of [14C] myristoyl-CoA to the apo-NMT, followed by proteolytic digestion, denaturing protein electrophoresis, and treatment with hydroxylamine leads to a result that is highly suggestive of a thioester linkage between the NMT and myristoyl-CoA. This linkage is mediated by a serine, cystine, or threonine located between Arg42 to Thr220. The binding of NMT with myristoyl-CoA facilitates the binding of NMT-myr-CoA to the peptide. However, these data are not sufficient to distinguish whether the NMT follows a ping-pong or Bi-Bi (sequential) catalysis mechanism, because the release of CoA may occur before or after the binding of the peptide (66). In 1991, Gordon *et. al.* further characterized the catalytic mechanism of NMT by using a non-hydrolyzable myristoyl-CoA analog. Binding and kinetic studies revealed that the release of the CoA group is tightly controlled by the addition of the peptide. By using the non-hydrolyzable myristoyl-CoA analog (S-(2-oxo)pentadecyl-CoA), the CoA group is retained in the NMT-myristoyl-CoA complex, even after the addition of the peptide, because the linkage between the acyl and

CoA is non-hydrolyzable (67). This clearly demonstrates that the NMT does not follow the ping-pong reaction mechanism in which the second substrate does not bind prior the release of the first product. Further studies were conducted on *S. cerevisiae* NMT to demonstrate the catalytic mechanism of the enzyme. These studies revealed that the CoA is a non-competitive inhibitor for both substrates (peptide and myristoyl-CoA), and myristoylated-peptide is a non-competitive inhibitor for peptide but a competitive inhibitor for myristoyl-CoA (68). This pattern of product binding inhibition can be used to distinguish different catalytic mechanism of the enzyme such as ping-pong and bi-bi mechanisms. From the product binding inhibition, structural, and kinetic studies, the catalytic mechanism order for NMT is following the ordered sequential Bi-Bi mechanism. In addition, the affinity of the peptide is greatly affected by the binding of different acyl-CoAs as a function of the bound fatty acyl-CoA, which suggests that the fatty acyl-CoA binds to NMT before the nascent polypeptide **(Figure 2.2)** (69). In summary, this characterized mechanism suggests that NMT binds to myristoyl-CoA prior to binding and acylating a nascent polypeptide chain that contains the required sequence.

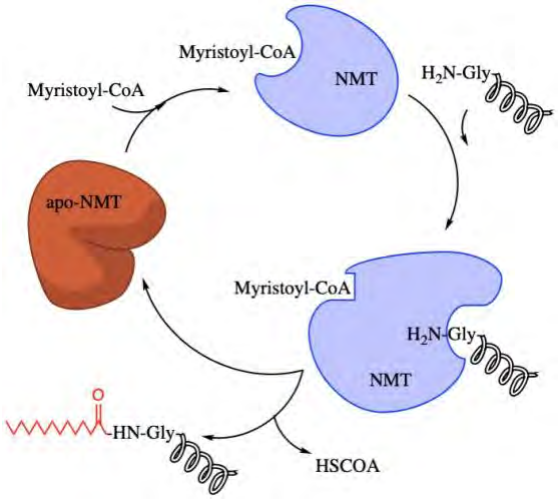

Figure 2.2. Catalytical cycle of N-myristoyltransferase.

-Structure and reaction mechanism of N-myristoyltransferase:

NMT structural analyses helped to identify important protein groups that play a major role in NMT catalytic function. In term of NMT structure, NMT has two binding pockets, one for the binding of myristoyl-CoA (the N-terminal half of NMT) and the other (the C-terminal half) for the binding of peptide substrates (70). Each binding pocket has several amino acid residues that contribute to the binding of the designated substrate (myristoyl-CoA or peptides).

In the myristoyl-CoA binding pocket, myristoyl-CoA binds to NMT with an overall conformation that morphologically like a question mark with four bends. The first bend is generated by the interactions between H38, K39, F40, and W41 of the A helix with the 3' phosphate of CoA. The interactions between N8, C6 of pantetheine with the E105 and Y103 and the hydrogen bond between O5 of pantetheine and the N6 amine of adenine generate the second bend of myristoyl-CoA that push it to the active site. The thioester carbonyl of the myristoyl-CoA forms hydrogen bonds with the backbone of Phe-170 and Leu-171 of NMT, and these interactions form the third bend, which orients the acyl chain toward the alpha carbon. Polarization of the thioester carbonyl is mediated by the oxyanion hole formed by Phe-170 and Leu-171. The fourth bend, which is formed by W41, I168, I187, and Y204 side chains, is positioned at the sixth carbon of the myristoyl-CoA acyl chain and push the acyl chain deeper into the myristoyl-CoA pocket of NMT. Val-194, Ala-202, and Phe-425 (side chains) and Thr-191, Trp-200, and His-201 (main chain) form the floor of the acyl chain binding pocket. Stabilization and release of the CoA thiol, which is formed by the nucleophilic addition-elimination reaction, is facilitated by the second bend, which is created by the CoA conformation that forms a hydrogen bond between the sulfur of the CoA and the N6a of pantetheine (70-72).

The specificity of fatty acids for wheat germ and yNMT was comprehensively studied by the Gordon group. Using a synthetic octapeptide of a well-known NMT substrate, they found that the myristate (C-14 fatty acid) has 100% transfer efficiency from the myristoyl-CoA to the octapeptide substrate, in comparison to 9% and 0% for C-10 and C-16 fatty acyl-CoAs, respectively (29). Oxygen- or sulfur-substituted myristoyl-CoA (12-oxy- and 13-oxy-myristoyl-CoA) shows a comparable affinity similar to the myristoyl-CoA (69). The length of the fatty acyl-CoA is the major determinant of the binding to NMT, rather than its hydrophobicity. As described above, the length of the acyl-CoA is very important since it is forming a part of the peptide binding site.

The structure of the apo-NMT is characterized by a small peptide binding site. A comparison of the crystal structure and stopped-flow fluorescence studies show that the myristoyl-CoA binding site of NMT is in a closed conformation prior to the binding of myristoyl-CoA (73). Binding of myristoyl-CoA to NMT induces a conformational change involving the N-terminal alpha helix and the Ab loop (74). This change in the structure of the protein leads to a more open peptide binding site compared to the apo-enzyme. Also, a ternary complex crystal structure of NMT shows binding to S-(2- oxo)pentadecyl-CoA (a non-hydrolyzable form of myristoyl-CoA) and the N-terminal of the Arf2 protein (GLYASKLS), suggesting that the myristoyl-CoA forms a part of the peptide binding site, since the Gly1 and Leu2 of the peptide interact with the C5 of S-(2- oxo)pentadecyl-CoA (75).

The specificity of NMT for peptide substrates was extensively studied for N-myristoylated proteins in yeast (74), rat (37), and human (76). These studies show that not only the amino-terminal residue, but the first six amino acids (Gly2-aa3-aa4-aa5-aa6-aa7) of myristoylated

proteins have direct contact with NMT and contribute significantly to the recognition and binding of peptides to NMT (36). Physiochemical properties of the first six amino acids of nascent polypeptides can be detected by NMT (30). Studies of over 100 synthetic octapeptides derived from the N-terminus of the catalytic subunit of cAMP-protein dependent kinase reveals a consensus sequence: $G1X_2X_3X_4X_5X_6$ with glycine residues at the N-terminal. Substitution of Gly1 with another amino acid (i.e. Ala) diminishes this interaction, making Gly1 critical for the myristoylation process to take place (30, 77, 78). Also, substitution of a glycine residue with a glycine analog, such as methyl-glycine, resulted in a very poor interaction with NMT (30). The requirement of the N-terminal glycine is consistent with the structural studies of known myristoylated proteins. In addition, mutational substitution of Gly with Ala or Glu for known NMT substrates, such as Src, gag, and MARCKS, produces a non-myristoylated protein (79-81). The second amino acid was found to be directed toward the Ab loop's aromatic side chains of Y103 and F113, and close to V104, F111, E105 of the Ab loop and to F334 of the beta strand of NMT (66). These residues preferred to interact with amino acids containing a hydrophobic side chain, since three potential hydrogen bonds can be formed (70). Uncharged amino acids such as Ala, Asn, Ser, Gln, and Val are allowed at position 2 (30). A charged amino acid at position 2 leads to a non-myristoylated peptide (30). Large hydrophobic residues at this position produce an inhibition feature (30). Unlike position 2, the third amino acid interacts with Y219, Y330, and Y349, and this environment makes it suitable for a broader range of residues with hydrophobic and/or aromatic side chains. The fourth amino acid is surrounded by a large aromatic pocket formed by F111, F234, F334, I347, and V395. For positions 3 and 4, basic, acidic, bulky hydrophobic, and small uncharged amino acids are allowed. NMT binds with high affinity to peptides with uncharged, basic, or acidic residues at

positions 3 and 4. NMT has low affinity for peptides with Pro at position 3, but it is tolerated. The fifth amino acid is located close to H221, G418, and D417. These hydrophobic residues make it a favorable position for Ser with high affinity. Also, small uncharged residues such as Ala, Thr, Cys, Asn, and Gly are allowed at position 5. Bulky hydrophobic, charged, or Pro residues are not favorable at this position. The sixth amino acid is located in between D106, R106, D108, F111, F234 and D417. Position 6 has a broad range of amino acids with less restrictions, except for Pro (30, 74, 75).

N-terminus of NMT plays a major role in substrate specificity. A study was conducted to examine whether the N-terminal of the enzyme contributes to the recognition of peptides. Expressing of two forms of yNMT (full-length or truncated) in *E. coli*, which lacks endogenous NMT, showed some differences in the specificity of the truncated NMT toward some peptides. The ability of the truncated NMT (i.e. lacks the first 39 amino acids of the N-terminus) to add myristate to some of the peptides was dramatically reduced when compared to the full-length NMT. These findings strongly suggest the importance of the N-terminus of NMT in the recognition of peptides, along with the sequence of the peptides themselves (72).

Detection of N-myristoyltransferase activity:

To fully understand an enzyme's function, having an effective and precise assay to detect its activity is crucial. Over the past 30 years, several techniques have been described for measuring NMT activity. The traditional technique was based on using radiolabeled myristoyl-CoA ([3H] myristoyl-CoA). The myristoylated peptides labeled with [H3] myristate are separated from other peptides by HPLC (82). This method was extensively used by several groups for studying the specificity of NMT to numerous octapeptides, but it was not applicable for studying

myristoyl-CoA analogues. Later, Heuckeroth *et. al.* (29)(83) introduced iodine to the octapeptide (GNAAS[125I]YRR) to test the reactivity of NMT to myristoyl-CoA analogues by measuring the radioactive trace of the end product. The synthesis of radiolabeled peptides was a limitation for using this method since these modifications on the peptides may have an effect on the recognition process of these peptides by NMT (84).

In 1991, Sharma's group introduced a new method for measuring NMT activity using phosphocellulose paper which is cheaper, more reliable, and can be used to assay multiple samples in a short time frame compared to the HPLC method (85). In this assay, [3H]-myristoylated labeled peptides bind to a P81 phosphocellulose paper matrix and are separated from non-myristoylated peptides. Then, radioactivity is incorporated and measured by liquid scintillation.

Several modifications have been done to previous methods. For example, instead of using reversed-phase HPLC, Paige *et. al.* used CM-Sepharose ion-exchange chromatography to separate 3H-myristoylated peptide from non-labeled peptides (86). Wagner *et. al.* separated 14C-myristoyl-peptide from non-myristoylated peptide in a one-step procedure using acidic alumina (87). These methods provided a more rapid assay for detecting NMT activity compared to using HPLC alone.

Currently, the process of labeling and identifying myristoylated proteins has been used in cellular levels. For example, non-radioactive molecules such as myristic-azide has been used to label myristoylated proteins. The labeled proteins are then conjugated with a reporter *in vitro* by biorthogonal reactions, such as copper catalyzed azide-alkyne cycloaddition (CuAAC). The enzymatically labeled proteins can be visualized by SDS-PAGE (88-90).

Additional progress was made with recent work from Goncalves *et. al.,* in which an *in vitro* fluorescence-based assay, which is an alternative to radioactive assays, was successfully developed for measuring NMT activity. This fluorogenic assay monitors CoA production, where it reacts to a pro-fluorescent probe, 7-diethylamino-3-(4-maleimido-phenyl)-4-methylcoumarin (CPM) (91), to produce a florescencent signal (92). The fluorescence-based assay can be used to study the kinetics of NMT and for high-throughput screening for inhibitors (92).

Myristoylated proteins:

A large variety of proteins undergo myristoylation modification, including in humans where up to 0.5-1 % of all proteins are myristoylated. This modification ensures proper functioning, subcellular localization, protein-membrane, and protein-protein interactions. **Table 2.2** summarizes myristoylated proteins and the function of the myristoyl moiety.

Myristoylation, NMT, and cancer:

NMT manipulates the function of several proteins, including oncoproteins which are involved in signaling pathways that mediate cell proliferation. Flested *et. al.* was the first to propose NMT as a chemotherapeutic target in 1995 (93). In order to establish NMT as a therapeutic target for cancer, several points need to be addressed: 1) Understand whether cancer is the driver or the result of change in NMT activity, 2) Identify what regulates NMT activity during the pathogenesis of cancer, 3) Determine methods to selectively block protein myristoylation in cancer cells to avoid general toxicity (93).

Sharma's group was the first to demonstrate an increase of NMT activity in early stage colorectal cancer using an azoxymethane-induced rat model (94). Later, high NMT activity was observed in human colorectal cancer (65), breast cancer (95), gallbladder carcinoma (96), brain cancer (97) , and oral squamous cell carcinoma (98). Of note, the distribution of NMT in colon cancer cells is predominantly cytosolic, compared to normal colon cells where NMT is localized to the cell membrane (65). This may indicate a regulatory mechanism of NMT localization in cancer tissue that keeps NMT close to newly synthesized proteins from ribosomes. In a small-scale study, *hNMT1* mRNA was investigated in different cancer tissues. *hNMT1* was found to be up-regulated with 1.8-3.7 fold in colon, breast, ovarian, and lung cancer (99).

Knockdown of NMT using small interfering RNA (siRNA) in ovarian and colorectal adenocarcinomas was the first direct evidence showing that NMT1 can be utilized as a therapeutic target for cancer (31). Knockdown of NMT1, but not NMT2, significantly inhibited the replication of cancer cells (31). Interestingly, ablation of NMT1 and/or NMT2 induced apoptotic cascades and decreased cell survival (31). Moreover, siRNA against NMT1 reduced tumor size *in vivo* (31). However, further investigation about the role of NMT in cancer is still needed to confirm these findings, because the experiments were not tightly controlled and optimized.

Another study investigated the impact of NMT inhibition on cancer progression using a selective NMT inhibitor on breast, colon, and cervical cancer cells. Inhibition of NMT activity in these cells led to G1 cell cycle arrest after 1 day, blocking DNA synthesis and induction of ER stress, followed by sub-G1 arrest (apoptotic) for most of the cells at day seven. This gradual onset of cell toxicity is due to the time needed for the existing myristoylated proteins to be

degraded and depleted. A quantitative analysis of the proteome in response to NMT inhibition in these cells showed 236 up-regulated proteins and 162 down-regulated proteins, all of which were spread across several important cellular processes. Functional grouping of these proteins revealed that NMT inhibition significantly down-regulates proteins that are responsible for controlling chromatin condensation/organization, mitochondrial electron transport, and cell cycle processes. On the other hand, NMT inhibition significantly up-regulates proteins controlling Golgi vesicle transport/targeting, N-linked glycosylation, and ER stress (100).

Myristoylation modification is considered a maturation process for proteins. Several oncoproteins, such as c-Src and Lck kinases, require myristoylation for membrane association and transformation capabilities (8)(101)(102)(103)(104)(105)(106)(107)(108). These kinases have been documented to be up-regulated in several human cancers including colorectal, prostate, and breast cancer (8) (109) (110) (111). In colon cancer, the increased expression level of Src is correlated with the expression level of NMT (112), which may indicate the requirement of the myristoylated oncoprotein for NMT activity to ensure proper acylation and function. Blocking Src myristoylation, whether through a G2A mutant (myristoylation dead mutant) or using an NMT inhibitor, effectively prevented the transformation capability of Src in human colon adenocarcinoma cells (113), clearly showing the role of myristoylation in the progression of colon cancer.

Myristoylation modification can inhibit activity of proteins that involve in apoptosis pathways. A large body of evidence shows the protective effect of the activated Abl kinase against progression of cancer by inducing apoptosis cascades (114) (115) (116) . Myristoylation of Abl has an inhibitory effect on the Abl kinase activity (117, 118). An N-terminal myristoyl group binds to a hydrophobic region in the kinase domain of the Abl, leading to an

autoinhibitory conformational change in the structure of the protein, inhibiting its activity (119). Interestingly, inhibition of the binding of the myristoyl group to the hydrophobic pocket on the kinase domain by a small inhibitor led to activation of the Abl kinase (119). Whether or not inhibiting NMT will have similar effect is still unknown and needs further investigation.

NMT inhibitors:

There has been a huge increase in the number of synthetic NMT inhibitors developed as anti-fungal and anti-viral agents and, to a lesser extent, as anti-cancer agents (120). Most of these agents were developed based on NMT substrates: myristoyl-CoA or peptide substrate. Structurally, NMT enzyme is composed of two binding pockets: myristoyl-CoA and peptide pockets (66). The myristoyl-CoA binding site is highly conserved among species (hNMT vs fungal NMT), however, the peptide binding site is divergent, making it a favorable target site for developing selective inhibitors for fungal NMT to avoid toxicity (121). NMT inhibitors are broadly classified as myristoyl-CoA analogues, myristic acid analogues, peptidomimetics, or synthetic compounds.

-Myristoyl-CoA and myristic acid analogues:

Due to the cooperativity between NMT myristoyl-CoA binding site and Myristoyl-CoA, NMT is very selective for myristoyl-CoA as a lipid source. Based on this rational, several myristoyl-CoA and myristic acid analogues have been developed as inhibitors for NMT and evaluated as anti-viral 109, anti-fungal, and anti-neoplastic agents (120, 122).

The first reported myristic acid analogues used as alternative substrates for NMT were synthesized by replacing a methylene group of the acyl-CoA backbone chain at different positions with oxygen, sulfur, or aromatic groups; such as 12-methoxydodecanoic acid, 10-

propoxydecanoic acid, 5-octyloxypentanoic acid, 11-Phenylundecanoic acid and 11-ethylthioundecanoic acid. These compounds can serve as NMT substrates but show a significant reduction in hydrophobicity. They can also inhibit the replication of human immunodeficiency virus 1 (HIV-1) and Moloney murine leukemia virus (MoMLV) at 10-100 μM, which demonstrates the potential of NMT as a therapeutic target against HIV and MoMLV (123, 124). In addition, 10-propoxydecanoic acid reduces partitioning of 63 kDa N-myristoyl protein and Src kinase to the cell membrane by 90% in BC3H1 fibroblast cells (83, 125).

Paige *et. al*. reported a non-hydrolyzable analogue of myristoyl-CoA, S-(2-oxopentadecyl)-CoA, as NMT inhibitor. S-(2-oxopentadecyl)-CoA blocks the catalytic transfer of the myristoyl moiety to the protein substrate. It is a competitive inhibitor and has been tested against partially purified mouse brain NMT *in vitro*. S-(2-oxopentadecyl)-CoA inhibited NMT activity with nanomolar range (126) and had a cytotoxic effect *in vitro* against human breast and lung cells (127). Even though S-(2-oxopentadecyl)-CoA shows a great inhibitory effect against NMT *in vitro*, it would not be easy for this highly charged compound to pass through cell membranes to inhibit NMT in intact cells. Synthesis of metabolically activated compounds would facilitate the delivery of myristic acid analogues to cells where it can be activated by acyl-CoA synthetase enzyme. 2-substituted myristic acid derivatives, 2-bromomyristic acid, 2-fluoromyristic acid, and 2-hydroxy myristic acid, were synthesized and tested against mouse brain NMT1, showing a weak inhibitory effect *in vitro* (IC50= 100 μM). However, the metabolically-activated 2-substituted myristic acid derivatives, 2-bromomyristoyl-CoA, 2-fluoromyristoyl-CoA, and 2-hydroxy myristoyl-CoA, are potent NMT inhibitors with IC50= 450, 200, and 45 nM, respectively(128).

Glover *et. al.*, reported a number of myristoyl-CoA analogs as competitive inhibitors for bovine brain NMT. The most potent inhibitor was S(2-ketopentadecyl)-CoA which has a thioether linkage rather than thioester. This compound inhibits bovine brain NMT *in vitro* with Ki= 0.11 μM (129).

Various N-myristoyl derivatives have been reported as potent inhibitors for NMT. N-myristoyl-3-(S)-carboxy-1,2,3,4-tetrahydroisoquinoline and N-myristoylamino-2-phenylethanehydrogen-phosphonate (IC50= 0.18 μM and 2 μM, respectively) are cytotoxic agents and inhibit NMT activity of human leukemia cells (HL-60) and mouse lymphocytic leukemia cells (L1210) (130). These compounds inhibit NMT activity with different potencies according to NMT origin (cytosolic or microsomal) (45). For example, N-myristoyl-3-(S)-carboxy-1,2,3,4-tetrahydroisoquinoline inhibited cytosolic NMT at a rate 10-fold greater than microsomal NMT in L1210 cells (45). Other N-myristoyl derivatives, such as N-myristoyl-(S)-phenylalanine and N-myristoyl glycine, show a weak inhibitory effect against L1210 NMT activity with IC50= 200 μM (45).

-Peptidomimic inhibitors:

The peptide binding site is located at the C-terminal of NMT where it has low sequence similarity between different species, such as fungal NMT and hNMT (66). The major differences between the hNMT peptide binding site and *C. albicans* are the replacement of some specific amino acids, such as Ser339, Ala352 and Glu451 in hNMT for Phe339, Ile352 and Leu451 in *C. albicans* NMT (131). In addition, *C. albicans* NMT can recognize some peptides which cannot be recognized by hNMT (131). These differences in the peptide binding site were utilized by researchers to develop specific inhibitors targeting fungal or viral NMT, but not human, in order to eliminate cytotoxicity of these agents (132). A characterization study

of *C. albicans* NMT peptide binding site shows three major elements, all of which are important for the recognition process: the N-terminal amino group of the glycine, the hydroxyl group of Ser5, and the ε- amino group of the Lys6 (133). Based on these findings, substituting the N-terminal glycine of the Arf2b (GLYASKLS-NH2) peptide with L-alanine (ALYASKLS-NH2) led to the first competitive peptidomimic inhibitor (134). This compound showed a 4-fold increase in potency against *C. albicans* compared to hNMT (Ki= 5.8 and 35 μM for *C. albicans* and hNMT, respectively) (134). Different substitution modifications on the N-terminal octapeptide of Arf2b protein were carried out to enhance its selectivity toward *C. albicans,* such as replacing Leu2 and Tyr3 with alanine, which increases its potency by 8-fold (135). Also, substituting the N-terminal amino acid residues at positions 1-4 with an 11-aminoundecanoyl group produced a more potent inhibitor than the starting peptide (ALYASKLS-NH2) (135). These peptidomimetics were a starting point for developing more potent and selective NMT inhibitors by other researchers. In 1995, Devadas *et. al.* reported a dipeptide 2-methylimidazole containing inhibitor (4-[4-(1H-Imidazol-1-yl)butyl]phenylacetyl-Ser-Lys-N-(2-cyclohexylethyl)amide) with IC50= 56 nM and a 250-fold increased selectivity towards *C. albicans* versus hNMT (105,108). Also, several ω-aminoalkyl-substituted Ser-Lys dipeptides of the Arf octapeptide, such as [2-[4-(6-Aminohexyl)phenyl]propionyl]-Ser-Lys-2-cyclohexylethylamide, have been reported as potent inhibitors for human and *C. albicans* NMT *in vitro* (136).

-Synthetic compounds:

A number of thiol alkylators, such as Mannich bases of α,β-unsaturated ketones (137), which contain two sites of thiolation, and 3,5-bis(Benzylidene)-4-piperidone derivatives (138), have been reported as cytotoxic agents. These compounds were tested against Molt 4/C8, CEM T-

lymphocytes, NCI-H460, MCF7, and as well as murine L1210 and P388 cells, and demonstrated a marked cytotoxicity, especially toward leukemia and colon cancer cells (137). Specifically, compound 3a was the most potent cytotoxic agent with IC50= 0.683 and 0.447 μM for colon cancer and leukemia cells, respectively (137). Since the NMT peptide binding site contains a mercapto group at cysteine169 (139), these compounds were proposed to exert their effect through targeting NMT. 3,5-bis(Benzylidene)-4-piperidone derivatives, such as 3,4-dichlorophenylamino, 4-methylphenylamino, 3,4-dichlorophenylamino, and 4-methylphenylamino, inhibited NMT activity with an IC50 range from 50 to 100 μM (138). However, Mannich bases of α,β-unsaturated ketones compounds showed a weak inhibitory effect against NMT *in vitro* with IC50= 0.5, 1.5, 25, 4, and 10 mM, respectively, when assayed using cAMP dependent protein kinase substrate (140). Interestingly, no inhibition effect on NMT activity was observed when these compounds were assayed with pp60Src substrate (137). The difference in the affinities between the substrates (PKA, Src) and NMT enzyme may cause the variation in the inhibitory effect of the compounds.

A medium-throughput screening study starting with 1600 compounds has revealed 32 potential NMT inhibitors (141). These inhibitors are cyclohexyl-octa hydro-pyrrolo [1,2-a]pyrazine (COPP)-based structure derivatives with IC50 values ranging from 6 μM to mM against hNMT1 (141). Among the 32 compounds identified, compound 24 (COPP24), which possesses a 9-ethyl-9H-carbazole-3-ylmethyl group on the purazine nitrogen atom, is the most potent inhibitor with IC50= 6 μM. COPP24 targets the peptide binding site of NMT1 with competitive inhibition. A computational docking study using the yNMT crystal structure demonstrated that COPP24 binds to the peptide binding site of the enzyme. The efficacy of COPP24 as an NMT inhibitor in cells was evaluated using monkey CV-1 cells expressing N-

myristoylated GFP-fused protein. Cells treated with COPP24 redistributed GFP signal from the plasma membrane to the cytosol. COPP24 displays cytotoxic effects against several cancer cells, such as HepG2 (liver), HT29 (colon), MCF7 (breast), A-498 (kidney), and DU145 (prostate) with IC50= 4.4, 3.7, 0.9, 5.8, and 14.8 μM, respectively (141). The high potency and cytotoxicity effect of COPP24 makes it a promising inhibitor for NMT as an anti-cancer agent.

A number of benzofuran derivatives as lead compounds for inhibiting NMT activity were identified by random screening of the Roche chemical libraries. Based on the crystal structure of *C. albicans* NMT and SAR studies, substituting the tert-butyl group in the C4 side chain on the benzofuran ring with (pyridine-3-ylmethyl)amino resulted in developing 3-Methyl-4-{3-[(pyridin-3-ylmethyl)amino] propoxy}benzo- furan-2-carboxylic acid ethyl ester; a potent *C. albicans* NMT inhibitor (IC50= 0.1 μM) and an *in vitro* anti-fungal agent (IC50= 1.6 μM) 117. Due to the short elimination half-life, further optimization was conducted on the C2 side chain of the benzofuran ring. The ester linker at C2 was replaced with a phenyl group via a CH2O linker to increase the stability of the inhibitor. Introducing a 2,4-difluoro or 2,3,4-trifluoro group to the phenylether at the C2 side chain resulted in two stable and potent *C. albicans* NMT inhibitors, {3-[2-(2,4-Difluorophenoxymethyl)-3-methylbenzofuran-4-yloxy]propyl}pyridin-3-ylmethylamine and {3-[2-(2,3,4-Trifluorophenoxymethyl)-3-methylbenzo-furan-4-yloxy]propyl}pyridin-3-ylmethylamine, which demonstrate inhibitory activity (IC50= 0.0075 and 0.0057 μM) against *C. albicans* NMT and anti-fungal agents (IC50= 0.03 and 0.035 μM), respectively. These compounds were very effective as anti-fungal agents *in vivo* when tested in a murine systemic candidiasis model (120).

A virtual screening of a database containing two million compounds, followed by CaNMT screening, led to a weak hit, 2-aminobenzothiazole, as a CaNMT inhibitor (142). Several modifications were performed on the 2-aminobenzothiazole, resulting in a number of 2-aminobenzothiazole derivatives as potent and selective CaNMT inhibitors (143). (1*R*,3*S*)-*N*-{2-[(cyclopeanthylcarbonyl)amino]-benzothiazol-6-yl}-3-[(2-naphthylmethyl) amino] cyclohexane carboxamide (FTR1335) selectively inhibited *C. albicans* NMT with 50% inhibitory concentration at 0.049 nM versus 5400 nM for hNMT. FTR1335 inhibits CaNMT by competing with peptide substrates for the NMT peptide binding site (142).

A number of pyrazole sulfonamide derivatives have been developed based on a lead hit, which was identified by screening a diverse library against *T. brucei* NMT (144). DDD85646 was the most potent pyrazole sulfonamide derivative with a single digit nanomolar IC50= 2 nM and has 200-fold selectivity toward TbNMT versus hNMT (144). DDD85646 has a competitive mode of inhibition, binding to the peptide binding site of the TbNMT as revealed by kinetic characterization and X-ray crystallography (144).

References

1. C. Huttenhower *et al.*, Exploring the human genome with functional maps. *Genome Res* **19**, 1093-1106 (2009).
2. D. Brett, H. Pospisil, J. Valcarcel, J. Reich, P. Bork, Alternative splicing and genome complexity. *Nat Genet* **30**, 29-30 (2002).
3. R. E. Banks *et al.*, Proteomics: new perspectives, new biomedical opportunities. *Lancet* **356**, 1749-1756 (2000).
4. G. Duan, D. Walther, The roles of post-translational modifications in the context of protein interaction networks. *PLoS Comput Biol* **11**, e1004049 (2015).
5. S. Shoji *et al.*, Complete amino acid sequence of the catalytic subunit of bovine cardiac muscle cyclic AMP-dependent protein kinase. *Proc Natl Acad Sci U S A* **78**, 848-851 (1981).
6. S. A. Carr, K. Biemann, S. Shoji, D. C. Parmelee, K. Titani, n-Tetradecanoyl is the NH2-terminal blocking group of the catalytic subunit of cyclic AMP-dependent protein kinase from bovine cardiac muscle. *Proc Natl Acad Sci U S A* **79**, 6128-6131 (1982).
7. J. A. Boutin, Myristoylation. *Cell Signal* **9**, 15-35 (1997).
8. P. Patwardhan, M. D. Resh, Myristoylation and membrane binding regulate c-Src stability and kinase activity. *Mol Cell Biol* **30**, 4094-4107 (2010).
9. S. Kim *et al.*, Blocking Myristoylation of Src Inhibits Its Kinase Activity and Suppresses Prostate Cancer Progression. *Cancer Res* **77**, 6950-6962 (2017).
10. J. Zha, S. Weiler, K. J. Oh, M. C. Wei, S. J. Korsmeyer, Posttranslational N-myristoylation of BID as a molecular switch for targeting mitochondria and apoptosis. *Science* **290**, 1761-1765 (2000).
11. J. B. Ames *et al.*, Molecular mechanics of calcium-myristoyl switches. *Nature* **389**, 198-202 (1997).
12. J. T. Seykora, M. M. Myat, L. A. Allen, J. V. Ravetch, A. Aderem, Molecular determinants of the myristoyl-electrostatic switch of MARCKS. *J Biol Chem* **271**, 18797-18802 (1996).
13. S. McLaughlin, A. Aderem, The myristoyl-electrostatic switch: a modulator of reversible protein-membrane interactions. *Trends Biochem Sci* **20**, 272-276 (1995).
14. N. Hayashi, K. Titani, N-myristoylated proteins, key components in intracellular signal transduction systems enabling rapid and flexible cell responses. *Proc Jpn Acad Ser B Phys Biol Sci* **86**, 494-508 (2010).
15. P. Selvakumar, S. Kumar, J. R. Dimmock, R. K. Sharma, NMT1 (N-myristoyltransferase 1). *Atlas Genet Cytogenet Oncol Haematol* **15**, 570-575 (2011).
16. V. Cordeddu *et al.*, Mutation of SHOC2 promotes aberrant protein N-myristoylation and causes Noonan-like syndrome with loose anagen hair. *Nat Genet* **41**, 1022-1026 (2009).
17. S. M. Stabler, L. L. Ostrowski, S. M. Janicki, M. J. Monteiro, A myristoylated calcium-binding protein that preferentially interacts with the Alzheimer's disease presenilin 2 protein. *J Cell Biol* **145**, 1277-1292 (1999).
18. P. Selvakumar *et al.*, Expression of myristoyltransferase and its interacting proteins in epilepsy. *Biochem Biophys Res Commun* **335**, 1132-1139 (2005).

19. H. Zhao *et al.*, Myristoylated methionine sulfoxide reductase A protects the heart from ischemia-reperfusion injury. *Am J Physiol Heart Circ Physiol* **301**, H1513-1518 (2011).
20. R. K. Sharma, Potential role of N-myristoyltransferase in pathogenic conditions. *Can J Physiol Pharmacol* **82**, 849-859 (2004).
21. D. A. Rudnick, R. L. Johnson, J. I. Gordon, Studies of the catalytic activities and substrate specificities of Saccharomyces cerevisiae myristoyl-coenzyme A: protein N-myristoyltransferase deletion mutants and human/yeast Nmt chimeras in Escherichia coli and S. cerevisiae. *J Biol Chem* **267**, 23852-23861 (1992).
22. H. Li, J. Dou, L. Ding, P. Spearman, Myristoylation is required for human immunodeficiency virus type 1 Gag-Gag multimerization in mammalian cells. *J Virol* **81**, 12899-12910 (2007).
23. S. Maurer-Stroh, B. Eisenhaber, F. Eisenhaber, N-terminal N-myristoylation of proteins: prediction of substrate proteins from amino acid sequence. *J Mol Biol* **317**, 541-557 (2002).
24. F. Hanakam *et al.*, The pH-sensitive actin-binding protein hisactophilin of Dictyostelium exists in two isoforms which both are myristoylated and distributed between plasma membrane and cytoplasm. *J Biol Chem* **270**, 596-602 (1995).
25. R. C. Wiegand *et al.*, The Candida albicans myristoyl-CoA:protein N-myristoyltransferase gene. Isolation and expression in Saccharomyces cerevisiae and Escherichia coli. *J Biol Chem* **267**, 8591-8598 (1992).
26. J. K. Lodge, E. Jackson-Machelski, D. L. Toffaletti, J. R. Perfect, J. I. Gordon, Targeted gene replacement demonstrates that myristoyl-CoA: protein N-myristoyltransferase is essential for viability of Cryptococcus neoformans. *Proc Natl Acad Sci U S A* **91**, 12008-12012 (1994).
27. Q. Qi *et al.*, Molecular cloning, genomic organization, and biochemical characterization of myristoyl-CoA:protein N-myristoyltransferase from Arabidopsis thaliana. *J Biol Chem* **275**, 9673-9683 (2000).
28. R. S. Gunaratne *et al.*, Characterization of N-myristoyltransferase from Plasmodium falciparum. *Biochem J* **348 Pt 2**, 459-463 (2000).
29. R. O. Heuckeroth, D. A. Towler, S. P. Adams, L. Glaser, J. I. Gordon, 11-(Ethylthio)undecanoic acid. A myristic acid analogue of altered hydrophobicity which is functional for peptide N-myristoylation with wheat germ and yeast acyltransferase. *J Biol Chem* **263**, 2127-2133 (1988).
30. D. A. Towler *et al.*, Purification and characterization of yeast myristoyl CoA:protein N-myristoyltransferase. *Proc Natl Acad Sci U S A* **84**, 2708-2712 (1987).
31. C. E. Ducker, J. J. Upson, K. J. French, C. D. Smith, Two N-myristoyltransferase isozymes play unique roles in protein myristoylation, proliferation, and apoptosis. *Mol Cancer Res* **3**, 463-476 (2005).
32. A. Shrivastav *et al.*, Expression and activity of N-myristoyltransferase in lung inflammation of cattle and its role in neutrophil apoptosis. *Vet Res* **41**, 9 (2010).
33. V. Rioux *et al.*, Identification and characterization of recombinant and native rat myristoyl-CoA: protein N-myristoyltransferases. *Mol Cell Biochem* **286**, 161-170 (2006).
34. S. H. Yang *et al.*, N-myristoyltransferase 1 is essential in early mouse development. *J Biol Chem* **280**, 18990-18995 (2005).

35. D. Towler, L. Glaser, Protein fatty acid acylation: enzymatic synthesis of an N-myristoylglycyl peptide. *Proc Natl Acad Sci U S A* **83**, 2812-2816 (1986).
36. D. A. Towler, S. R. Eubanks, D. S. Towery, S. P. Adams, L. Glaser, Amino-terminal processing of proteins by N-myristoylation. Substrate specificity of N-myristoyl transferase. *J Biol Chem* **262**, 1030-1036 (1987).
37. D. A. Towler, J. I. Gordon, S. P. Adams, L. Glaser, The biology and enzymology of eukaryotic protein acylation. *Annu Rev Biochem* **57**, 69-99 (1988).
38. C. J. Glover, C. Goddard, R. L. Felsted, N-myristoylation of p60src. Identification of a myristoyl-CoA:glycylpeptide N-myristoyltransferase in rat tissues. *Biochem J* **250**, 485-491 (1988).
39. R. A. McIlhinney, K. McGlone, Characterisation of a myristoyl CoA:glycylpeptide N-myristoyl transferase activity in rat brain: subcellular and regional distribution. *J Neurochem* **54**, 110-117 (1990).
40. M. J. King, R. K. Sharma, Demonstration of multiple forms of bovine brain myristoyl CoA:protein N-myristoyl transferase. *Mol Cell Biochem* **113**, 77-81 (1992).
41. C. J. Glover, R. L. Felsted, Identification and characterization of multiple forms of bovine brain N-myristoyltransferase. *J Biol Chem* **270**, 23226-23233 (1995).
42. R. V. Raju, J. Kalra, R. K. Sharma, Purification and properties of bovine spleen N-myristoyl-CoA protein:N-myristoyltransferase. *J Biol Chem* **269**, 12080-12083 (1994).
43. R. J. Duronio, S. I. Reed, J. I. Gordon, Mutations of human myristoyl-CoA:protein N-myristoyltransferase cause temperature-sensitive myristic acid auxotrophy in Saccharomyces cerevisiae. *Proc Natl Acad Sci U S A* **89**, 4129-4133 (1992).
44. N. S. Kishore *et al.*, Comparison of the acyl chain specificities of human myristoyl-CoA synthetase and human myristoyl-CoA:protein N-myristoyltransferase. *J Biol Chem* **268**, 4889-4902 (1993).
45. J. A. Boutin *et al.*, Myristoyl-CoA:protein N-myristoyltransferase activity in cancer cells. Purification and characterization of a cytosolic isoform from the murine leukemia cell line L1210. *Eur J Biochem* **214**, 853-867 (1993).
46. J. A. Boutin *et al.*, N-myristoyl-transferase activity in cancer cells. Solubilization, specificity and enzymatic inhibition of a N-myristoyl transferase from L1210 microsomes. *Eur J Biochem* **201**, 257-263 (1991).
47. D. K. Giang, B. F. Cravatt, A second mammalian N-myristoyltransferase. *J Biol Chem* **273**, 6595-6598 (1998).
48. P. Selvakumar, A. Lakshmikuttyamma, R. K. Sharma, Biochemical characterization of bovine brain myristoyl-CoA:protein N-myristoyltransferase type 2. *J Biomed Biotechnol* **2009**, 907614 (2009).
49. M. Ntwasa, M. Egerton, N. J. Gay, Sequence and expression of Drosophila myristoyl-CoA: protein N-myristoyl transferase: evidence for proteolytic processing and membrane localisation. *J Cell Sci* **110 (Pt 2)**, 149-156 (1997).
50. R. J. Duronio, D. A. Towler, R. O. Heuckeroth, J. I. Gordon, Disruption of the yeast N-myristoyl transferase gene causes recessive lethality. *Science* **243**, 796-800 (1989).
51. M. Ntwasa, S. Aapies, D. A. Schiffmann, N. J. Gay, Drosophila embryos lacking N-myristoyltransferase have multiple developmental defects. *Exp Cell Res* **262**, 134-144 (2001).
52. R. Chauhan, D. Datzkiw, S. Varma Shrivastav, A. Shrivastav, In silico identification of microRNAs predicted to regulate N-myristoyltransferase and Methionine

Aminopeptidase 2 functions in cancer and infectious diseases. *PLoS One* **13**, e0194612 (2018).
53. R. V. Rajala *et al.*, Phosphorylation of human N-myristoyltransferase by N-myristoylated SRC family tyrosine kinase members. *Biochem Biophys Res Commun* **288**, 233-239 (2001).
54. A. Shrivastav *et al.*, Overexpression of Akt/PKB modulates N-myristoyltransferase activity in cancer cells. *J Pathol* **218**, 391-398 (2009).
55. M. J. King, R. K. Sharma, Identification, purification and characterization of a membrane-associated N-myristoyltransferase inhibitor protein from bovine brain. *Biochem J* **291 (Pt 2)**, 635-639 (1993).
56. P. Selvakumar *et al.*, N-myristoyltransferase inhibitor protein is homologous to heat shock cognate protein 70. *J Cell Biochem* **92**, 573-578 (2004).
57. A. Shrivastav *et al.*, Potent inhibitor of N-myristoylation: a novel molecular target for cancer. *Cancer Res* **63**, 7975-7978 (2003).
58. M. J. King, R. K. Sharma, Differential activation of bovine brain N-myristoyltransferase(s) by a cytosolic activator. *Biochem Biophys Res Commun* **212**, 580-588 (1995).
59. G. Poli, C. Sorio, G. Berton, Protein myristoylation in human mononclear phagocytes: modulation by interferon-gamma and tumor necrosis factor-alpha. *J Cell Sci* **100 (Pt 4)**, 833-840 (1991).
60. M. Almagor, J. Bar-Tana, Retinoic acid inhibits the myristoylation of a membrane protein in HL-60 cells. *Biochem Biophys Res Commun* **172**, 877-882 (1990).
61. R. A. McIlhinney, K. McGlone, Immunocytochemical characterization and subcellular localization of human myristoyl-CoA: protein N-myristoyltransferase in HeLa cells. *Exp Cell Res* **223**, 348-356 (1996).
62. R. A. McIlhinney, Characterization and cellular localization of human myristoyl-COA: protein N-myristoyltransferase. *Biochem Soc Trans* **23**, 549-553 (1995).
63. L. J. Knoll, M. A. Levy, P. D. Stahl, J. I. Gordon, Analysis of the compartmentalization of myristoyl-CoA:protein N-myristoyltransferase in Saccharomyces cerevisiae. *J Biol Chem* **267**, 5366-5373 (1992).
64. C. J. Glover, K. D. Hartman, R. L. Felsted, Human N-myristoyltransferase amino-terminal domain involved in targeting the enzyme to the ribosomal subcellular fraction. *J Biol Chem* **272**, 28680-28689 (1997).
65. A. Shrivastav, S. Varma, A. Saxena, J. DeCoteau, R. K. Sharma, N-myristoyltransferase: a potential novel diagnostic marker for colon cancer. *J Transl Med* **5**, 58 (2007).
66. D. A. Rudnick *et al.*, Structural and functional studies of Saccharomyces cerevisiae myristoyl-CoA:protein N-myristoyltransferase produced in Escherichia coli. Evidence for an acyl-enzyme intermediate. *J Biol Chem* **265**, 13370-13378 (1990).
67. D. A. Rudnick *et al.*, Kinetic and structural evidence for a sequential ordered Bi Bi mechanism of catalysis by Saccharomyces cerevisiae myristoyl-CoA:protein N-myristoyltransferase. *J Biol Chem* **266**, 9732-9739 (1991).
68. W. J. Rocque, C. A. McWherter, D. C. Wood, J. I. Gordon, A comparative analysis of the kinetic mechanism and peptide substrate specificity of human and Saccharomyces cerevisiae myristoyl-CoA:protein N-myristoyltransferase. *J Biol Chem* **268**, 9964-9971 (1993).

69. R. O. Heuckeroth, L. Glaser, J. I. Gordon, Heteroatom-substituted fatty acid analogs as substrates for N-myristoyltransferase: an approach for studying both the enzymology and function of protein acylation. *Proc Natl Acad Sci U S A* **85**, 8795-8799 (1988).
70. R. S. Bhatnagar *et al.*, Structure of N-myristoyltransferase with bound myristoylCoA and peptide substrate analogs. *Nat Struct Biol* **5**, 1091-1097 (1998).
71. R. S. Bhatnagar, K. Futterer, G. Waksman, J. I. Gordon, The structure of myristoyl-CoA:protein N-myristoyltransferase. *Biochim Biophys Acta* **1441**, 162-172 (1999).
72. J. Wu *et al.*, Crystal structures of Saccharomyces cerevisiae N-myristoyltransferase with bound myristoyl-CoA and inhibitors reveal the functional roles of the N-terminal region. *J Biol Chem* **282**, 22185-22194 (2007).
73. S. A. Weston *et al.*, Crystal structure of the anti-fungal target N-myristoyl transferase. *Nat Struct Biol* **5**, 213-221 (1998).
74. T. A. Farazi, G. Waksman, J. I. Gordon, Structures of Saccharomyces cerevisiae N-myristoyltransferase with bound myristoylCoA and peptide provide insights about substrate recognition and catalysis. *Biochemistry* **40**, 6335-6343 (2001).
75. T. A. Farazi, J. K. Manchester, G. Waksman, J. I. Gordon, Pre-steady-state kinetic studies of Saccharomyces cerevisiae myristoylCoA:protein N-myristoyltransferase mutants identify residues involved in catalysis. *Biochemistry* **40**, 9177-9186 (2001).
76. R. V. Raju, B. A. Magnuson, R. K. Sharma, Mammalian myristoyl CoA: protein N-myristoyltransferase. *Mol Cell Biochem* **149-150**, 191-202 (1995).
77. D. A. Towler *et al.*, Myristoyl CoA:protein N-myristoyltransferase activities from rat liver and yeast possess overlapping yet distinct peptide substrate specificities. *J Biol Chem* **263**, 1784-1790 (1988).
78. R. J. Duronio, D. A. Rudnick, S. P. Adams, D. A. Towler, J. I. Gordon, Analyzing the substrate specificity of Saccharomyces cerevisiae myristoyl-CoA:protein N-myristoyltransferase by co-expressing it with mammalian G protein alpha subunits in Escherichia coli. *J Biol Chem* **266**, 10498-10504 (1991).
79. T. David-Pfeuty, S. Bagrodia, D. Shalloway, Differential localization patterns of myristoylated and nonmyristoylated c-Src proteins in interphase and mitotic c-Src overexpresser cells. *J Cell Sci* **105 (Pt 3)**, 613-628 (1993).
80. J. Dou *et al.*, Characterization of a myristoylated, monomeric HIV Gag protein. *Virology* **387**, 341-352 (2009).
81. S. L. Swierczynski, S. R. Siddhanti, J. S. Tuttle, P. J. Blackshear, Nonmyristoylated MARCKS complements some but not all of the developmental defects associated with MARCKS deficiency in mice. *Dev Biol* **179**, 135-147 (1996).
82. D. Towler, L. Glaser, Acylation of cellular proteins with endogenously synthesized fatty acids. *Biochemistry* **25**, 878-884 (1986).
83. R. O. Heuckeroth *et al.*, Novel fatty acyl substrates for myristoyl-CoA:protein N-myristoyl-transferase. *J Lipid Res* **31**, 1121-1129 (1990).
84. J. A. Boutin, Tyrosine protein kinase assays. *J Chromatogr B Biomed Appl* **684**, 179-199 (1996).
85. M. J. King, R. K. Sharma, N-myristoyl transferase assay using phosphocellulose paper binding. *Anal Biochem* **199**, 149-153 (1991).
86. L. A. Paige, D. R. Chafin, J. M. Cassady, R. L. Geahlen, Detection of myristoyl CoA:protein N-myristoyltransferase activity by ion-exchange chromatography. *Anal Biochem* **181**, 254-258 (1989).

87. A. P. Wagner, J. Retey, Assay of N-myristoyl transferase by selective adsorption of myristoyl-coenzyme A on acidic alumina. *Anal Biochem* **188**, 356-358 (1990).
88. D. D. Martin *et al.*, Rapid detection, discovery, and identification of post-translationally myristoylated proteins during apoptosis using a bio-orthogonal azidomyristate analog. *FASEB J* **22**, 797-806 (2008).
89. R. N. Hannoush, Development of chemical probes for biochemical detection and cellular imaging of myristoylated and palmitoylated proteins. *Curr Protoc Chem Biol* **3**, 15-26 (2011).
90. A. J. Witten *et al.*, Fluorescent imaging of protein myristoylation during cellular differentiation and development. *J Lipid Res* **58**, 2061-2070 (2017).
91. C. C. Chung *et al.*, A fluorescence-based thiol quantification assay for ultra-high-throughput screening for inhibitors of coenzyme A production. *Assay Drug Dev Technol* **6**, 361-374 (2008).
92. V. Goncalves *et al.*, A fluorescence-based assay for N-myristoyltransferase activity. *Anal Biochem* **421**, 342-344 (2012).
93. R. L. Felsted, Glover, Constance J., Hartman, Kathleen, Protein N -Myristoylation as a Chemotherapeutic Target for Cancer. *Journal of the National Cancer Institute* **87**, 571-1573 (1995).
94. B. A. Magnuson, R. V. Raju, T. N. Moyana, R. K. Sharma, Increased N-myristoyltransferase activity observed in rat and human colonic tumors. *J Natl Cancer Inst* **87**, 1630-1635 (1995).
95. R. A. Clegg, P. C. Gordge, W. R. Miller, Expression of enzymes of covalent protein modification during regulated and dysregulated proliferation of mammary epithelial cells: PKA, PKC and NMT. *Adv Enzyme Regul* **39**, 175-203 (1999).
96. R. V. Rajala, J. M. Radhi, R. Kakkar, R. S. Datla, R. K. Sharma, Increased expression of N-myristoyltransferase in gallbladder carcinomas. *Cancer* **88**, 1992-1999 (2000).
97. Y. Lu *et al.*, Expression of N-myristoyltransferase in human brain tumors. *Neurochem Res* **30**, 9-13 (2005).
98. A. Shrivastav *et al.*, Elevated N-myristoyltransferase activity and expression in oral squamous cell carcinoma. *Oncol Rep* **18**, 93-97 (2007).
99. L. B. Chen L, Alcorn J, Yang J., Quantitative Analysis of the Expression of Human N-myristoyltransferase 1 (hNMT-1) in Cancers. *The open Biomarker Journal* **2**, 6–10 (2009).
100. E. Thinon, J. Morales-Sanfrutos, D. J. Mann, E. W. Tate, N-Myristoyltransferase Inhibition Induces ER-Stress, Cell Cycle Arrest, and Apoptosis in Cancer Cells. *ACS Chem Biol* **11**, 2165-2176 (2016).
101. J. Park, A. I. Meisler, C. A. Cartwright, c-Yes tyrosine kinase activity in human colon carcinoma. *Oncogene* **8**, 2627-2635 (1993).
102. J. G. Krueger, E. A. Garber, A. R. Goldberg, H. Hanafusa, Changes in amino-terminal sequences of pp60src lead to decreased membrane association and decreased in vivo tumorigenicity. *Cell* **28**, 889-896 (1982).
103. F. R. Cross, E. A. Garber, D. Pellman, H. Hanafusa, A short sequence in the p60src N terminus is required for p60src myristylation and membrane association and for cell transformation. *Mol Cell Biol* **4**, 1834-1842 (1984).

104. M. P. Kamps, J. E. Buss, B. M. Sefton, Rous sarcoma virus transforming protein lacking myristic acid phosphorylates known polypeptide substrates without inducing transformation. *Cell* **45**, 105-112 (1986).
105. M. Shi, J. C. Cooper, C. L. Yu, A constitutively active Lck kinase promotes cell proliferation and resistance to apoptosis through signal transducer and activator of transcription 5b activation. *Mol Cancer Res* **4**, 39-45 (2006).
106. T. C. Lund *et al.*, The Src-family kinase Lck can induce STAT3 phosphorylation and DNA binding activity. *Cell Signal* **11**, 789-796 (1999).
107. M. B. Majolini, M. Boncristiano, C. T. Baldari, Dysregulation of the protein tyrosine kinase LCK in lymphoproliferative disorders and in other neoplasias. *Leuk Lymphoma* **35**, 245-254 (1999).
108. S. Kim *et al.*, Myristoylation of Src kinase mediates Src-induced and high-fat diet-accelerated prostate tumor progression in mice. *J Biol Chem* **292**, 18422-18433 (2017).
109. M. S. Talamonti, M. S. Roh, S. A. Curley, G. E. Gallick, Increase in activity and level of pp60c-src in progressive stages of human colorectal cancer. *J Clin Invest* **91**, 53-60 (1993).
110. D. K. Luttrell *et al.*, Involvement of pp60c-src with two major signaling pathways in human breast cancer. *Proc Natl Acad Sci U S A* **91**, 83-87 (1994).
111. Z. Guo *et al.*, Regulation of androgen receptor activity by tyrosine phosphorylation. *Cancer Cell* **10**, 309-319 (2006).
112. R. V. Rajala, S. Dehm, X. Bi, K. Bonham, R. K. Sharma, Expression of N-myristoyltransferase inhibitor protein and its relationship to c-Src levels in human colon cancer cell lines. *Biochem Biophys Res Commun* **273**, 1116-1120 (2000).
113. S. Shoji, T. Kurosawa, H. Inoue, T. Funakoshi, Y. Kubota, Human cellular src gene product: identification of the myristoylated pp60c-src and blockage of its myristoyl acylation with N-fatty acyl compounds resulted in the suppression of colony formation. *Biochem Biophys Res Commun* **173**, 894-901 (1990).
114. G. Hamer, I. S. Gademan, H. B. Kal, D. G. de Rooij, Role for c-Abl and p73 in the radiation response of male germ cells. *Oncogene* **20**, 4298-4304 (2001).
115. M. W. Wagner *et al.*, Role of c-Abl kinase in DNA mismatch repair-dependent G2 cell cycle checkpoint arrest responses. *J Biol Chem* **283**, 21382-21393 (2008).
116. T. M. Allington, A. J. Galliher-Beckley, W. P. Schiemann, Activated Abl kinase inhibits oncogenic transforming growth factor-beta signaling and tumorigenesis in mammary tumors. *FASEB J* **23**, 4231-4243 (2009).
117. O. Hantschel *et al.*, A myristoyl/phosphotyrosine switch regulates c-Abl. *Cell* **112**, 845-857 (2003).
118. J. Yang *et al.*, Discovery and characterization of a cell-permeable, small-molecule c-Abl kinase activator that binds to the myristoyl binding site. *Chem Biol* **18**, 177-186 (2011).
119. Y. Choi *et al.*, N-myristoylated c-Abl tyrosine kinase localizes to the endoplasmic reticulum upon binding to an allosteric inhibitor. *J Biol Chem* **284**, 29005-29014 (2009).
120. C. Zhao, S. Ma, Recent advances in the discovery of N-myristoyltransferase inhibitors. *ChemMedChem* **9**, 2425-2437 (2014).
121. D. R. Johnson, R. S. Bhatnagar, L. J. Knoll, J. I. Gordon, Genetic and biochemical studies of protein N-myristoylation. *Annu Rev Biochem* **63**, 869-914 (1994).

122. S. M. Cordo, N. A. Candurra, E. B. Damonte, Myristic acid analogs are inhibitors of Junin virus replication. *Microbes Infect* **1**, 609-614 (1999).
123. M. L. Bryant, R. O. Heuckeroth, J. T. Kimata, L. Ratner, J. I. Gordon, Replication of human immunodeficiency virus 1 and Moloney murine leukemia virus is inhibited by different heteroatom-containing analogs of myristic acid. *Proc Natl Acad Sci U S A* **86**, 8655-8659 (1989).
124. K. Parang *et al.*, In vitro antiviral activities of myristic acid analogs against human immunodeficiency and hepatitis B viruses. *Antiviral Res* **34**, 75-90 (1997).
125. R. O. Heuckeroth, J. I. Gordon, Altered membrane association of p60v-src and a murine 63-kDa N-myristoyl protein after incorporation of an oxygen-substituted analog of myristic acid. *Proc Natl Acad Sci U S A* **86**, 5262-5266 (1989).
126. L. A. Paige, G. Q. Zheng, S. A. DeFrees, J. M. Cassady, R. L. Geahlen, S-(2-oxopentadecyl)-CoA, a nonhydrolyzable analogue of myristoyl-CoA, is a potent inhibitor of myristoyl-CoA:protein N-myristoyltransferase. *J Med Chem* **32**, 1665-1667 (1989).
127. G. Q. Zheng, X. Hu, J. M. Cassady, L. A. Paige, R. L. Geahlen, Synthesis of myristoyl CoA analogues and myristoyl peptides as inhibitors of myristoyl CoA:protein N-myristoyltransferase. *J Pharm Sci* **83**, 233-238 (1994).
128. L. A. Paige, G. Q. Zheng, S. A. DeFrees, J. M. Cassady, R. L. Geahlen, Metabolic activation of 2-substituted derivatives of myristic acid to form potent inhibitors of myristoyl CoA:protein N-myristoyltransferase. *Biochemistry* **29**, 10566-10573 (1990).
129. C. J. Glover, M. R. Tellez, F. S. Guziec, Jr., R. L. Felsted, Synthesis and characterization of inhibitors of myristoyl-CoA:protein N-myristoyltransferase. *Biochem Pharmacol* **41**, 1067-1074 (1991).
130. A. Bielawska *et al.*, (1S,2R)-D-erythro-2-(N-myristoylamino)-1-phenyl-1-propanol as an inhibitor of ceramidase. *J Biol Chem* **271**, 12646-12654 (1996).
131. S. Sogabe *et al.*, Crystal structures of Candida albicans N-myristoyltransferase with two distinct inhibitors. *Chem Biol* **9**, 1119-1128 (2002).
132. A. S. Bell *et al.*, Selective inhibitors of protozoan protein N-myristoyltransferases as starting points for tropical disease medicinal chemistry programs. *PLoS Negl Trop Dis* **6**, e1625 (2012).
133. C. A. McWherter *et al.*, Scanning alanine mutagenesis and de-peptidization of a Candida albicans myristoyl-CoA:protein N-myristoyltransferase octapeptide substrate reveals three elements critical for molecular recognition. *J Biol Chem* **272**, 11874-11880 (1997).
134. B. Devadas *et al.*, Design and synthesis of novel imidazole-substituted dipeptide amides as potent and selective inhibitors of Candida albicans myristoylCoA:protein N-myristoyltransferase and identification of related tripeptide inhibitors with mechanism-based antifungal activity. *J Med Chem* **40**, 2609-2625 (1997).
135. J. A. Sikorski *et al.*, Selective peptidic and peptidomimetic inhibitors of Candida albicans myristoylCoA: protein N-myristoyltransferase: a new approach to antifungal therapy. *Biopolymers* **43**, 43-71 (1997).
136. S. R. Nagarajan *et al.*, Conformationally constrained [p-(omega-aminoalkyl)phenacetyl]-L-seryl-L-lysyl dipeptide amides as potent peptidomimetic inhibitors of Candida albicans and human myristoyl-CoA:protein N-myristoyl transferase. *J Med Chem* **40**, 1422-1438 (1997).

137. U. Das, S. Kumar, J. R. Dimmock, R. K. Sharma, Inhibition of protein N-myristoylation: a therapeutic protocol in developing anticancer agents. *Curr Cancer Drug Targets* **12**, 667-692 (2012).
138. A. Jha *et al.*, E,E,E-1-(4-Arylamino-4-oxo-2-butenoyl)-3,5-bis(arylidene)-4-piperidones: a topographical study of some novel potent cytotoxins. *Bioorg Med Chem* **15**, 5854-5865 (2007).
139. S. M. Peseckis, M. D. Resh, Fatty acyl transfer by human N-myristyl transferase is dependent upon conserved cysteine and histidine residues. *J Biol Chem* **269**, 30888-30892 (1994).
140. J. R. Dimmock *et al.*, Cytotoxic and topographical properties of 6-arylidene-2-dimethylaminomethylcyclohexanone hydrochlorides and related compounds. *J Enzyme Inhib Med Chem* **19**, 1-10 (2004).
141. K. J. French *et al.*, Cyclohexyl-octahydro-pyrrolo[1,2-a]pyrazine-based inhibitors of human N-myristoyltransferase-1. *J Pharmacol Exp Ther* **309**, 340-347 (2004).
142. S. Ebara, H. Naito, K. Nakazawa, F. Ishii, M. Nakamura, FTR1335 is a novel synthetic inhibitor of Candida albicans N-myristoyltransferase with fungicidal activity. *Biol Pharm Bull* **28**, 591-595 (2005).
143. K. Yamazaki *et al.*, Synthesis of potent and selective inhibitors of Candida albicans N-myristoyltransferase based on the benzothiazole structure. *Bioorg Med Chem* **13**, 2509-2522 (2005).
144. J. A. Frearson *et al.*, N-myristoyltransferase inhibitors as new leads to treat sleeping sickness. *Nature* **464**, 728-732 (2010).
145. S. Doll *et al.*, FSP1 is a glutathione-independent ferroptosis suppressor. *Nature* **575**, 693-698 (2019).
146. J. W. Streb, C. M. Kitchen, I. H. Gelman, J. M. Miano, Multiple promoters direct expression of three AKAP12 isoforms with distinct subcellular and tissue distribution profiles. *J Biol Chem* **279**, 56014-56023 (2004).
147. Y. Liu, R. A. Kahn, J. H. Prestegard, Structure and membrane interaction of myristoylated ARF1. *Structure* **17**, 79-87 (2009).
148. H. Gao *et al.*, A Method to Generate and Analyze Modified Myristoylated Proteins. *Chembiochem* **18**, 324-330 (2017).
149. C. A. Langner *et al.*, 4-oxatetradecanoic acid is fungicidal for Cryptococcus neoformans and inhibits replication of human immunodeficiency virus I. *J Biol Chem* **267**, 17159-17169 (1992).
150. M. Franco, P. Chardin, M. Chabre, S. Paris, Myristoylation of ADP-ribosylation factor 1 facilitates nucleotide exchange at physiological Mg2+ levels. *J Biol Chem* **270**, 1337-1341 (1995).
151. J. K. Lodge *et al.*, N-myristoylation of Arf proteins in Candida albicans: an in vivo assay for evaluating antifungal inhibitors of myristoyl-CoA: protein N-myristoyltransferase. *Microbiology* **143 (Pt 2)**, 357-366 (1997).
152. N. Burnaevskiy, T. Peng, L. E. Reddick, H. C. Hang, N. M. Alto, Myristoylome profiling reveals a concerted mechanism of ARF GTPase deacylation by the bacterial protease IpaJ. *Mol Cell* **58**, 110-122 (2015).
153. R. S. Haun, S. C. Tsai, R. Adamik, J. Moss, M. Vaughan, Effect of myristoylation on GTP-dependent binding of ADP-ribosylation factor to Golgi. *J Biol Chem* **268**, 7064-7068 (1993).

154. S. J. Berger, A. C. Claude, P. Melancon, Analysis of recombinant human ADP-ribosylation factors by reversed-phase high-performance liquid chromatography and electrospray mass spectrometry. *Anal Biochem* **264**, 53-65 (1998).
155. D. Padovani, M. Zeghouf, J. A. Traverso, C. Giglione, J. Cherfils, High yield production of myristoylated Arf6 small GTPase by recombinant N-myristoyl transferase. *Small GTPases* **4**, 3-8 (2013).
156. A. S. Caumont, M. C. Galas, N. Vitale, D. Aunis, M. F. Bader, Regulated exocytosis in chromaffin cells. Translocation of ARF6 stimulates a plasma membrane-associated phospholipase D. *J Biol Chem* **273**, 1373-1379 (1998).
157. C. D'Souza-Schorey, P. D. Stahl, Myristoylation is required for the intracellular localization and endocytic function of ARF6. *Exp Cell Res* **221**, 153-159 (1995).
158. H. P. Price, C. Panethymitaki, D. Goulding, D. F. Smith, Functional analysis of TbARL1, an N-myristoylated Golgi protein essential for viability in bloodstream trypanosomes. *J Cell Sci* **118**, 831-841 (2005).
159. A. Takasaki, N. Hayashi, M. Matsubara, E. Yamauchi, H. Taniguchi, Identification of the calmodulin-binding domain of neuron-specific protein kinase C substrate protein CAP-22/NAP-22. Direct involvement of protein myristoylation in calmodulin-target protein interaction. *J Biol Chem* **274**, 11848-11853 (1999).
160. H. Kwon, J. Lee, K. Jeong, D. Jang, Y. Pak, Fatty acylated caveolin-2 is a substrate of insulin receptor tyrosine kinase for insulin receptor substrate-1-directed signaling activation. *Biochim Biophys Acta* **1853**, 1022-1034 (2015).
161. M. Jiang, Y. Gao, T. Yang, X. Zhu, J. Chen, Cyclin Y, a novel membrane-associated cyclin, interacts with PFTK1. *FEBS Lett* **583**, 2171-2178 (2009).
162. M. Darshi *et al.*, ChChd3, an inner mitochondrial membrane protein, is essential for maintaining crista integrity and mitochondrial function. *J Biol Chem* **286**, 2918-2932 (2011).
163. T. Utsumi *et al.*, Identification and characterization of protein N-myristoylation occurring on four human mitochondrial proteins, SAMM50, TOMM40, MIC19, and MIC25. *PLoS One* **13**, e0206355 (2018).
164. C. Yorikawa *et al.*, Human CHMP6, a myristoylated ESCRT-III protein, interacts directly with an ESCRT-II component EAP20 and regulates endosomal cargo sorting. *Biochem J* **387**, 17-26 (2005).
165. M. T. Kennedy, H. Brockman, F. Rusnak, Contributions of myristoylation to calcineurin structure/function. *J Biol Chem* **271**, 26517-26521 (1996).
166. N. Meyer-Schaller *et al.*, The human Dcn1-like protein DCNL3 promotes Cul3 neddylation at membranes. *Proc Natl Acad Sci U S A* **106**, 12365-12370 (2009).
167. E. Beauchamp *et al.*, Myristic acid increases the activity of dihydroceramide Delta4-desaturase 1 through its N-terminal myristoylation. *Biochimie* **89**, 1553-1561 (2007).
168. H. Ezanno *et al.*, Myristic acid increases dihydroceramide Delta4-desaturase 1 (DES1) activity in cultured rat hepatocytes. *Lipids* **47**, 117-128 (2012).
169. L. Fort *et al.*, Fam49/CYRI interacts with Rac1 and locally suppresses protrusions. *Nat Cell Biol* **20**, 1159-1171 (2018).
170. Y. Yoshida *et al.*, Ubiquitination of exposed glycoproteins by SCF(FBXO27) directs damaged lysosomes for autophagy. *Proc Natl Acad Sci U S A* **114**, 8574-8579 (2017).

171. C. Neumann-Giesen *et al.*, Membrane and raft association of reggie-1/flotillin-2: role of myristoylation, palmitoylation and oligomerization and induction of filopodia by overexpression. *Biochem J* **378**, 509-518 (2004).
172. Y. Han *et al.*, Formin-like 1 (FMNL1) is regulated by N-terminal myristoylation and induces polarized membrane blebbing. *J Biol Chem* **284**, 33409-33417 (2009).
173. K. Moriya *et al.*, Protein N-myristoylation is required for cellular morphological changes induced by two formin family proteins, FMNL2 and FMNL3. *Biosci Biotechnol Biochem* **76**, 1201-1209 (2012).
174. Q. Li *et al.*, Pharmacologically targeting the myristoylation of the scaffold protein FRS2alpha inhibits FGF/FGFR-mediated oncogenic signaling and tumor progression. *J Biol Chem* **293**, 6434-6448 (2018).
175. L. Alland, S. M. Peseckis, R. E. Atherton, L. Berthiaume, M. D. Resh, Dual myristylation and palmitylation of Src family member p59fyn affects subcellular localization. *J Biol Chem* **269**, 16701-16705 (1994).
176. H. B. Eberle *et al.*, Identification and characterization of a novel human plant pathogenesis-related protein that localizes to lipid-enriched microdomains in the Golgi complex. *J Cell Sci* **115**, 827-838 (2002).
177. R. Alvarez *et al.*, G protein-membrane interactions I: Galphai1 myristoyl and palmitoyl modifications in protein-lipid interactions and its implications in membrane microdomain localization. *Biochim Biophys Acta* **1851**, 1511-1520 (2015).
178. K. Moriya *et al.*, Identification of dually acylated proteins from complementary DNA resources by cell-free and cellular metabolic labeling. *Anal Biochem* **511**, 1-9 (2016).
179. P. B. Wedegaertner, Characterization of subcellular localization and stability of a splice variant of G alpha i2. *BMC Cell Biol* **3**, 12 (2002).
180. A. Kuo, C. Zhong, W. S. Lane, R. Derynck, Transmembrane transforming growth factor-alpha tethers to the PDZ domain-containing, Golgi membrane-associated protein p59/GRASP55. *EMBO J* **19**, 6427-6439 (2000).
181. S. Kumar, S. Parameswaran, R. K. Sharma, Novel myristoylation of the sperm-specific hexokinase 1 isoform regulates its atypical localization. *Biol Open* **4**, 1679-1687 (2015).
182. M. Kobayashi, K. Takamatsu, S. Saitoh, T. Noguchi, Myristoylation of hippocalcin is linked to its calcium-dependent membrane association properties. *J Biol Chem* **268**, 18898-18904 (1993).
183. S. Nada *et al.*, The novel lipid raft adaptor p18 controls endosome dynamics by anchoring the MEK-ERK pathway to late endosomes. *EMBO J* **28**, 477-489 (2009).
184. K. Moriya *et al.*, Protein N-myristoylation plays a critical role in the endoplasmic reticulum morphological change induced by overexpression of protein Lunapark, an integral membrane protein of the endoplasmic reticulum. *PLoS One* **8**, e78235 (2013).
185. M. Broncel *et al.*, Multifunctional reagents for quantitative proteome-wide analysis of protein modification in human cells and dynamic profiling of protein lipidation during vertebrate development. *Angew Chem Int Ed Engl* **54**, 5948-5951 (2015).
186. J. Pu *et al.*, BORC, a multisubunit complex that regulates lysosome positioning. *Dev Cell* **33**, 176-188 (2015).
187. S. K. Kolluri, C. Balduf, M. Hofmann, M. Gottlicher, Novel target genes of the Ah (dioxin) receptor: transcriptional induction of N-myristoyltransferase 2. *Cancer Res* **61**, 8534-8539 (2001).

188. M. Thelen, A. Rosen, A. C. Nairn, A. Aderem, Regulation by phosphorylation of reversible association of a myristoylated protein kinase C substrate with the plasma membrane. *Nature* **351**, 320-322 (1991).
189. M. Matsubara, K. Titani, H. Taniguchi, N. Hayashi, Direct involvement of protein myristoylation in myristoylated alanine-rich C kinase substrate (MARCKS)-calmodulin interaction. *J Biol Chem* **278**, 48898-48902 (2003).
190. E. Schleiff, A. Schmitz, R. A. McIlhinney, S. Manenti, G. Vergeres, Myristoylation does not modulate the properties of MARCKS-related protein (MRP) in solution. *J Biol Chem* **271**, 26794-26802 (1996).
191. T. Braun, R. A. McIlhinney, G. Vergeres, Myristoylation-dependent N-terminal cleavage of the myristoylated alanine-rich C kinase substrate (MARCKS) by cellular extracts. *Biochimie* **82**, 705-715 (2000).
192. J. M. Lim, J. C. Lim, G. Kim, R. L. Levine, Myristoylated methionine sulfoxide reductase A is a late endosomal protein. *J Biol Chem* **293**, 7355-7366 (2018).
193. T. Chida *et al.*, N-Myristoylation is essential for protein phosphatases PPM1A and PPM1B to dephosphorylate their physiological substrates in cells. *Biochem J* **449**, 741-749 (2013).
194. N. Ali *et al.*, beta-subunit myristoylation functions as an energy sensor by modulating the dynamics of AMP-activated Protein Kinase. *Sci Rep* **6**, 39417 (2016).
195. R. J. Duronio *et al.*, Protein N-myristoylation in Escherichia coli: reconstitution of a eukaryotic protein modification in bacteria. *Proc Natl Acad Sci U S A* **87**, 1506-1510 (1990).
196. E. C. Gaffarogullari *et al.*, A myristoyl/phosphoserine switch controls cAMP-dependent protein kinase association to membranes. *J Mol Biol* **411**, 823-836 (2011).
197. E. Santonico *et al.*, Multiple modification and protein interaction signals drive the Ring finger protein 11 (RNF11) E3 ligase to the endosomal compartment. *Oncogene* **29**, 5604-5618 (2010).
198. J. P. Chapple *et al.*, Mutations in the N-terminus of the X-linked retinitis pigmentosa protein RP2 interfere with the normal targeting of the protein to the plasma membrane. *Hum Mol Genet* **9**, 1919-1926 (2000).
199. J. Babitt *et al.*, Murine SR-BI, a high density lipoprotein receptor that mediates selective lipid uptake, is N-glycosylated and fatty acylated and colocalizes with plasma membrane caveolae. *J Biol Chem* **272**, 13242-13249 (1997).
200. J. E. Buss, B. M. Sefton, Myristic acid, a rare fatty acid, is the lipid attached to the transforming protein of Rous sarcoma virus and its cellular homolog. *J Virol* **53**, 7-12 (1985).
201. S. M. Peseckis, I. Deichaite, M. D. Resh, Iodinated fatty acids as probes for myristate processing and function. Incorporation into pp60v-src. *J Biol Chem* **268**, 5107-5114 (1993).
202. C. Gutierrez-Ford *et al.*, Characterization of tescalcin, a novel EF-hand protein with a single Ca2+-binding site: metal-binding properties, localization in tissues and cells, and effect on calcineurin. *Biochemistry* **42**, 14553-14565 (2003).
203. H. C. Zaun, A. Shrier, J. Orlowski, N-myristoylation and Ca2+ binding of calcineurin B homologous protein CHP3 are required to enhance Na+/H+ exchanger NHE1 half-life and activity at the plasma membrane. *J Biol Chem* **287**, 36883-36895 (2012).

204. F. Uno *et al.*, Myristoylation of the fus1 protein is required for tumor suppression in human lung cancer cells. *Cancer Res* **64**, 2969-2976 (2004).
205. A. K. Najumudeen, M. Kohnke, M. Solman, K. Alexandrov, D. Abankwa, Cellular FRET-Biosensors to Detect Membrane Targeting Inhibitors of N-Myristoylated Proteins. *PLoS One* **8**, e66425 (2013).
206. G. Hoxhaj *et al.*, ZNRF2 is released from membranes by growth factors and, together with ZNRF1, regulates the Na+/K+ATPase. *J Cell Sci* **125**, 4662-4675 (2012).

Table 2.2. List of all experimentally validated myristoylated proteins and the function of the myristoyl moiety.

#	Gene name	Protein name	Detection method	Myristoyl function
1	AIFM2	Apoptosis-inducing factor 2	MYR Predictor, myristoylator, metabolic labeling (myristic alkyne) (145)	Mitochondria localization (145)
2	AKAP12	A-kinase anchor protein 12	MYR Predictor, myristoylator, Fluorescence Microscopy (146)	Localization to ER-derived vesicles (146)
3	ARF1	ADP-ribosylation factor 1	MYR Predictor, myristoylator, NMR (147), metabolic labeling ([3H]myristic acid) (148, 149)	Golgi membrane loclaization (147) and stabilize Arf and GTP interaction (150)
4	ARF3	ADP-ribosylation factor 3	MYR Predictor, myristoylator, change in mobility on SDS-PAGE (151)	Golgi membranes (152), GTP-dependent conformational change (153)
5	ARF4	ADP-ribosylation factor 4	MYR Predictor, myristoylator, HPLC (154)	Protein-protein interaction (152)
6	ARF5	ADP-ribosylation factor 5	MYR Predictor, myristoylator, DEAE chromatography (153)	Golgi membrane (153)
7	ARF6	ADP-ribosylation factor 6	MYR Predictor, myristoylator, Nano ESI-MS (155), [3H]Myristic acid (156)	plasma membrane localization (157), activity (157)
8	ARL1	ADP-ribosylation factor-like protein 1	MYR Predictor, myristoylator, [9,10-3H]Myristic acid (158)	Golgi association (158)
9	BASP1	Brain acid soluble protein 1	MYR Predictor, myristoylator, liquid chromatography/electrospray mass spectrometric analysis (159)	Protein interaction to calmodulin , transcriptional (159)
10	CAV2	Caveolin-2	MYR Predictor, myristoylator, [9,10-3H]Myristic acid (160)	plasma membrane (160)
11	CCNY	Cyclin-Y	MYR Predictor, myristoylator, IF, fractionation (161)	plasma membrane (161)
12	CHCHD3	MICOS complex subunit MIC19	MYR Predictor, myristoylator, Mass spectrometric analysis (162)	Mitochondrial localization (162)

13	CHCHD6	MICOS complex subunit MIC25	MYR Predictor, myristoylator, [9,10-3H]Myristic acid (163)	unknown
14	CHMP6	Charged multivesicular body protein 6	MYR Predictor, myristoylator, [9,10-3H]Myristic acid (164)	interacts physically not only with CHMP4b, but also with EAP20 (164)
15	CHP1	Calcineurin B homologous protein 1	MYR Predictor, myristoylator, [3H]myristic acid (165)	Stability and transport activity of NHE1 at the cell surface (165)
16	DCUN1D3	DCN1-like protein 3	MYR Predictor, myristoylator, azido-myristate (166)	Plasma membrane (166)
17	DEGS1	Sphingolipid delta(4)-desaturase DES1	MYR Predictor, myristoylator, azido-myristate (167)	Mitochondrial Localization (168)
18	FAM49A	Protein FAM49A	MYR Predictor, myristoylator, myristate-azide (169)	plasma membrane (169)
19	FAM49B	Protein FAM49B	MYR Predictor, myristoylator, myristate-azide (169)	plasma membrane (169)
20	FBXO27	F-box only protein 27	MYR Predictor, myristoylator, myristate-azide (170)	ER, Golgi, endosomes, and lysosomes LOCALIZATION (170)
21	FLOT2	Flotillin-2	MYR Predictor, myristoylator ,[3H]myristate (171)	membrane association (171)
22	FMNL1	Formin-like protein 1	MYR Predictor, myristoylator , [3H]myristic acid (172)	membrane localization (172)
23	FMNL2;FMNL3	Formin-like protein 2;Formin-like protein 3	MYR Predictor, myristoylator , [3H]myristic acid (173)	plasma membrane (173)
24	FRS2		MYR Predictor, myristoylator , myristate-azide (174)	plasma membrane (174)
25	FYN	Proto-oncogene tyrosine-protein kinase Fyn	MYR Predictor, myristoylator , [3H]myristic acid (175)	plasma membrane (175)
26	GLIPR2/ GAPR-1	Golgi-associated plant pathogenesis-related protein 1	MYR Predictor, myristoylator , electrospray mass spectrometry (176)	Golgi membranes (176)

27	GNAI1	Guanine nucleotide-binding protein G(i) subunit alpha-1	MYR Predictor, myristoylator , [3H]myristic acid (177) (178)	Golgi apparatus, plasma membrane, β γ interaction (177) (178)
28	GNAI2	Guanine nucleotide-binding protein G(i) subunit alpha-2	MYR Predictor, myristoylator , [3H]myristic acid (179)	plasma membranes (179)
29	GORASP2; p59	Golgi reassembly-stacking protein 2	MYR Predictor, myristoylator , [3H]myristic acid (180)	Golgi membrane (180)
30	HK1	Hexokinase-1	MYR Predictor, myristoylator , myristic acid azide (181)	plasma membrane (181)
31	HPCAL1; HPCA; NCALD	Hippocalcin-like protein 1;Neuron-specific calcium-binding protein hippocalcin;Neurocalcin-delta	MYR Predictor, myristoylator , [3H]myristic acid (182)	plasma membrane (182)
32	LAMTOR1	Ragulator complex protein LAMTOR1	MYR Predictor, myristoylator , Mass spectrometric analysis (183)	lysosomal membrane (183)
33	LNP	Protein lunapark	MYR Predictor, myristoylator , [3H]myristic acid (184)	loclaization to the ER junctions and membrane topology formation (184)
34	LOH12CR1	Loss of heterozygosity 12 chromosomal region 1 protein	MYR Predictor, myristoylator , [3H]-myristic acid (185) (186)	attached to the cytosolic side of the lysosomal membrane (185) (186)
35	LYN	Tyrosine-protein kinase Lyn	MYR Predictor, myristoylator , [3H]-myristic acid (187)	plasma membrane (187)
36	MARCKS	Myristoylated alanine-rich C-kinase substrate	MYR Predictor, myristoylator , 3H-myristate (188)	membrane phospholipids and MARCKS-calmodulin interaction (188, 189)
37	MARCKSL1	MARCKS-like protein 1	MYR Predictor, myristoylator , 3H-myristate (190)	Membrane binding (191) (190)
38	MSRA	Mitochondrial peptide methionine sulfoxide reductase	MYR Predictor, myristoylator , HPLC-mass spectrometry (192)	Protein-protein (STARD3), colocalized with STARD3 at late

				endosomes/lysosomes (192)
39	PPM1A	Protein phosphatase 1A	MYR Predictor, myristoylator , [3H]myristic acid (193)	membrane localization (193)
40	PPM1B	Protein phosphatase 1B	MYR Predictor, myristoylator , [3H]myristic acid (193)	membrane localization (193)
41	PRKAB1	5'-AMP-activated protein kinase subunit beta-1	MYR Predictor, myristoylator , Mass Spectral Analysis (194)	Basal membrane association (194)
42	PRKACA	cAMP-dependent protein kinase catalytic subunit alpha	MYR Predictor, myristoylator , [3H]myristate, ESI mass spectrometry (195)	membrane binding, to provide structural stability (195, 196)
43	PRKACB	cAMP-dependent protein kinase catalytic subunit beta	MYR Predictor, myristoylator , [3H]myristate, ESI mass spectrometry (195)	membrane binding, to provide structural stability (195, 196)
44	RFTN1	Raftlin	MYR Predictor, myristoylator , Fluorescence microscopy (wt/g2a) and 2-hydroxymyristic acid, [(3)H]myristic acid (178)	localization in rafts (178)
45	RNF11	RING finger protein 11	MYR Predictor, myristoylator , [3H]myristic acid (197)	association with the A20 ubiquitin-editing protein complex and , endosomal localization (197)
46	RP2	Protein XRP2	MYR Predictor, myristoylator , Fluorescence microscopy (wt/g2a) (198)	plasma membrane (198)
47	SAMM50	Sorting and assembly machinery component 50 homolog	MYR Predictor, myristoylator , [3H]myristic acid (163)	mitochondrial targeting and protein-protein interaction (163)
48	SCARB1	Scavenger receptor class B member 1	MYR Predictor, myristoylator , [3H]myristic acid (199)	plasma membrane (199)

49	SERINC1	Serine incorporator 1	MYR Predictor, myristoylator , [3H]myristic acid (184)	plasma membrane (184)
50	SRC	Proto-oncogene tyrosine-protein kinase Src	MYR Predictor, myristoylator , 13-[125I]iodotridecanoic acid (200, 201)	membrane binding (201)
51	TESC	Calcineurin B homologous protein 3	MYR Predictor, myristoylator , [3H]myristic acid (202, 203)	conformational change that facilitates its interaction with membranes (202) (203)
52	TUSC2	Tumor suppressor candidate 2	MYR Predictor, myristoylator , SELDI-MS, 14C-myristate (204)	plasma membrane (204)
53	TLDC1	TLD domain-containing protein 1	MYR Predictor, myristoylator , [3H]myristic acid (184)	plasma membrane (184)
54	YES1	Tyrosine-protein kinase Yes	MYR Predictor, myristoylator , NANOclustering and Myristolyation Sensors (NANOMS) (205)	plasma membrane (205)
55	ZNRF2	E3 ubiquitin-protein ligase ZNRF2	MYR Predictor, myristoylator, mass spectrometric analysis (206)	internal membranes and plasma membrane, mediate interactions with the Na+/K+ATPasea1 subunit (206)

CHAPTER 3

Blocking myristoylation of Src inhibits its kinase activity and suppresses prostate cancer progression[#]

[#]Sungjin Kim[*], Omar Awad Alsaidan[*], Octavia Goodwin, Qianjin Li, Essilvo Sulejmani, Zhen Han , Aiping Bai, Thomas Albers, Zanna Beharry, Y. George Zheng, James S. Norris, Zdzislaw M. Szulc, Alicja Bielawska, Iryna Lebedyeva, Scott D. Pegan, Houjian Cai

*****: Co-first author

Abstract:

Protein N-myristoylation enables localization to membranes and helps maintain protein conformation and function. N-myristoyltransferases (NMT) catalyze co- or post-translational myristoylation of Src family kinases and other oncogenic proteins, thereby regulating their function. In this study, we provide genetic and pharmacological evidence that inhibiting the N-myristoyltransferase NMT1 suppresses cell cycle progression, proliferation and malignant growth of prostate cancer cells. Loss of myristoylation abolished the tumorigenic potential of Src and its synergy with androgen receptor in mediating tumor invasion. We identified the myristoyl-CoA analog B13 as a small molecule inhibitor of NMT1 enzymatic activity. B13 exposure blocked Src myristoylation and Src localizaiton to the cytoplasmic membrane, attenuating Src-mediated oncogenic signaling. B13 exerted its antiinvasive and antitumor effects against prostate cancer cells with minimal toxic side-effects in vivo. Structural optimization based on structure-activity relationships enabled the chemical synthesis of LCL204 with enhanced inhibitory potency against NMT1. Collectively, our results offer a preclincal proof of concept for the use of protein myristoylation inhibitors as a strategy to block prostate cancer progression.

Introduction

N-myristoylation is a co/post-translational modification that results in the covalent attachment of the 14-carbon saturated myristic acid to the N-terminus of a target protein (1). N-myristoyltransferase (NMT) catalyzes this transfer of the myristoyl- group of myristoyl-CoA to a glycine in the N-terminus. N-myristoylation is ubiquitously found in eukaryotes, and two mammalian NMT isoforms, NMT1 and NMT2, have been identified that share 77% identity (2). NMTs have been considered as promising targets for the development of antifungal, antiparasitic, and antitumor progression therapeutics (3).

One set of proteins where myristoylation has been observed to play an important role is Src family kinases (SFKs). Myristoylation together with other modifications allow SFKs to attach to the cytoplasmic membrane and mediate their kinase activity and cellular functions (4, 5). SFKs are pleiotropic activators in signal transduction pathways and numerous studies have documented their role as oncogenic driver genes in a variety of cancers (6). SFKs interact with a variety of cellular receptors, and are downstream effectors of G protein-coupled receptors, integrins, and many receptor tyrosine kinases (RTKs) (7, 8). Activation of SFKs also activates a variety of downstream signaling to facilitate tumor growth, angiogenesis, and metastatic invasion (6, 9, 10). Particularly, aberrant expression of Src kinase facilitates the phosphorylation of androgen receptor (AR) and bypasses ligand dependent AR activation in castration resistant prostate cancer (9, 11). Our previous study showed that co-overexpression of Src and AR promotes invasive prostate adenocarcinoma (11, 12).

In vitro studies have indicated that NMT1 regulates Src kinase myristoylation and phosphorylation or kinase activity in COS-1 cells (5) or HT-29 cells (13). Here we further study if genetic and pharmacological inhibitions of NMT1 regulate proliferation of prostate cancer cells

and growth of prostate tumor *in vivo*. We demonstrate that knockdown of NMT1 suppressed proliferation of prostate cancer cells by blocking cell cycle progression and inhibited the myristoylation and tyrosine phosphorylation of Src kinase. The inhibitory effect increased with increasing expression levels of NMT1. Myristoylation was shown to facilitate SFKs-mediated prostate tumorigenesis, and mediate the interaction of Src kinase with AR, with the synergistic effect of promoting prostate tumor progression. Screening a panel of small molecule compounds based on the myristoyl-CoA scaffold identified a compound that blocked the enzymatic activity of NMT1 and myristoylation of Src kinase. The inhibitor suppressed proliferation, migration and invasion of prostate cancer cells and tumor growth with a limited toxicity to normal cells or major organs *in vivo*. The inhibitory activity of this compound was optimized through structurally guided and SAR based methods. Our study provides a novel therapeutic approach for the treatment of prostate cancer by targeting lipidation.

Materials and Methods:

Plasmid constructs

The open reading frames of the Src(WT) and its mutants [(Src(WT/G2A), Src(Y529F), Src(Y529F/G2A), Src(Y529F/S3C/S6C), Src(Y529F/G2A/S3C/S6C), Src(Y529F/K298M)], Fyn(WT) and its mutants [(Fyn(WT/G2A), Fyn(Y528F), Fyn(Y528F/G2A), Fyn(Y528F/C3S/C6S), Fyn(Y528F/G2A/C3S/C6S), Fyn(Y528F/K298M)], and AR genes were cloned into FUCRW or FUCGW lentiviral vectors as described previously (14, 15). Src(Y529F) and Src(Y529F/G2A) were also cloned into the pTK380 vector (16), designated as TRE/Src(Y529F), which expresses the reverse tetracycline-controlled transactivator (rtTA), and is regulated by doxycycline (Dox). To knock down the human Src and NMT1 genes, shRNAs targeting Src and NMT1 were generated using primers listed in Table S1. After the primers were annealed, the inserts were cloned into psiRNA-W [H1.4] vector at the Bbs I site. The shRNAs with the H1 promoter were further sub-cloned into FUCRW and/or FUCGW lentiviral vectors at the Pac I site. To knock down the human Fyn gene, shRNA constructs were purchased from Sigma.

Cell culture

PNT2 cells were purchased from Sigma (Cat#95012613). 293T and prostate cancer cell lines including LNCaP, 22Rv1 DU145, and PC-3 were purchased from American Type Culture Collection (ATCC). The above cell lines were obtained in September 2013 and were defined as passage 1 (the first thawing) when arrived in the lab. SYF1 ($Src^{-/-}Yes^{-/-}Fyn^{-/-}$) mouse fibroblast cell line and LNCaP-abl, and 293T expressing rtTA (293T-rtTA) were gifts from Dr. Jonathan Cooper's lab in August 2008 (17), Dr. Qianben Wang's lab in March 2016 (18), and Dr. Kathrin Plath's lab in May 2008 (12), respectively. Cancer cell lines were cultured in ATCC-recommended medium, and LNCaP-abl was grown in 10% charcoal-stripped fetal calf serum. Cell lines from

ATCC and Sigma had a certificate of mycoplasma-free and authentication when purchased. Other cell lines including SYF1 and LNCaP-abl were tested by the universal mycoplasma detection kit (ATCC Cat# 30-1012K) and determined to be mycoplasma free. PNT2, LNCaP, 22Rv1 DU145, and PC-3 lines were used within no more than 8-10 passages. LNCaP-abl cells were at 62 passages in this study. SYF1 cells and 293T-rtTA cells were used at the passage of less than 35. Loss of Src and Fyn expression in SYF cells was confirmed by Western analysis as indicated in each experiment. The doxycycline induction ability in 293T-rtTA did not show any difference in terms of cell passage number. SYF1 cells transduced with Src/Fyn(WT) or their mutants, or 293T-rtTA transduced with TRE/Src(Y529F) by lentiviral infection (12) were grown in DMEM with 10% FBS (HyClone, Logan, UT). The expression of Src kinase was induced by 1 μg/mL doxycycline. All the cell lines were periodically examined for mycoplasma contamination.

Protein fractionation

The fractionation protocol for the cytosol and the cytoplasmic membrane were as described previously with slight modification (19). Briefly, SYF1 cells expressing Src/Fyn(WT) or its mutants were incubated in DMEM including 2% bovine serum albumin (BSA) for 24 h. After lysing with TNE lysis buffer (50 mM Tris, 150 mM NaCl, 2 mM EDTA pH 7.4, protease inhibitor cocktail, and phosphatase inhibitor cocktails), the protein extracts were homogenized using a 25-gauge needle syringe (15 strokes) and centrifuged at 14,000 rpm for 10 min. The supernatant was collected as the cytosolic (Cyt.) fraction. Pellets were rinsed twice with TNE lysis buffer and re-suspended in TNE lysis buffer which contained 60 mM β-octylglucoside. Samples were incubated on ice for 30 min and centrifuged at 14,000 rpm for 20 min at 4 °C. The supernatants were collected as the total membrane (TM) fraction.

Crystallization of NMT1 and structure determination

Purified NMT1 was dialyzed overnight against a buffer containing 20 mM Tris pH 7.5, 100 mM NaCl, and 1 mM DTT. The enzyme was concentrated to 6.3 mg/mL and incubated at a 1:5 molar ratio with myristoyl CoA. This mixture was filtered with a 0.2 μm filter. NMT1 crystals were obtained through vapor drop diffusion using a 500 μL reservoir with a 4 μL hanging drop containing equal parts of NMT1 and reservoir solution (22.5% PEG 4000, 5 mM $NiCl_2$, 100 mM sodium citrate pH 4.5, and 2.5% glycerol) (20). The crystals were flash frozen in liquid nitrogen using the reservoir solution as a cryoprotectant. The data was collected at the SER-CAT 22ID beamline at 1 Å using a MAR300hs detector. HKL-2000 was used to index, integrate, and scale data sets. Phenix and coot were used for molecular replacement and refinement of the structure.

Detecting the myristoylation of Src kinase by Click chemistry

To evaluate myristoylation of proteins, PNT2, LNCaP, LNCaP-abl, 22Rv1, PC-3, and DU145 cancer cells were grown in the ATCC-recommended medium with myristic acid azide. The protein lysates were extracted using M-PER buffer, and a 40 μL protein lysate aliquot was used for the Click reaction. Myristoyl-proteins were detected by immunoblotting using Streptavidin-HRP.

To detect the effect of NMT1 on expression levels of myristoylated Src protein, PC-3 cells were transduced with shRNA-control or shNMT1. Additionally, to examine the inhibition of B13 on Src myristoylation, PC-3 cells were treated with 0, 1, 15, 30 μM of B13 for 2 h. The shNMT1 transduced or B13-treated cells were cultured in the medium with 60 μM of myristic acid-azide for 24 h. Proteins were extracted with M-PER buffer (Thermo Scientific) containing protease inhibitors and phosphatase inhibitors. Cell lysates were centrifuged at 14,000 rpm for 20 min. The supernatants were incubated with Src antibody for 16 h at 4 °C. Protein A agarose beads were added, and the mixtures were incubated for 1 h at 4 °C. After washing five times with IP lysis buffer, the Click chemistry reaction was accomplished by adding Click reagents according to the

manufacturer's instructions (Life Technologies). In brief, 30 μL of the Click-iT reaction buffer containing 40 μM alkyne-biotin, 10 μL of $CuSO_4$, and 10 μL of additive 1 solution was mixed with the equal volume of immunoprecipitated agarose beads. Then 20 μL of additive 2 solution was added. The myristoyl-Src was further mixed with loading buffer and boiled. The lysate was detected by immunoblotting using Streptavidin-HRP.

To screen the compounds inhibiting the Src myristoylation, SYF1($Src^{-/-}Fyn^{-/-}Yes^{-/-}$) cells were transduced with Src(WT) or Src(G2A) by lentiviral infection. The transduced cells were grown in DMEM with 2% fatty acid free BSA containing 60 μM myristic acid-azide for 24 h after pre-treatment of LCL or GRU compounds for 2 h. To examine Src myristoylation in a dose dependent manner, SYF1+Src(WT) cells were treated at 0, 1, 5, 15, 30 μM of B13 for 2 h, followed by the addition of 60 μM of myristic acid azide. The expression levels of myristoyl-Src (60 kDa) were detected by immunoblotting.

Screening for NMT1 inhibitors and measurement of IC_{50}

For screening of NMT1 inhibitors or the measurement of IC_{50}, the 1X reaction buffer (50 mM HEPES and 0.5 mM EDTA), 140 nM of NMT1 purified enzyme (See the NMT1 purification Section, the enzyme stock was preserved in the buffer containing 1mM EDTA, 250 mM NaCl, and 20 mM Tris pH 8.5), 5 μM of peptide Gly-Ser-Asn-Lys-Ser-Lys-Pro-Lys (derived from the N-terminus of human pp60Src tyrosine kinase), and the inhibitor at 0, 10, 20, 40, 80, 120, 160, or 200 μM respectively were mixed in a 96-well plate. After incubation at 30 °C for 10 min, the reaction was started by adding 1 μM myristoyl coenzyme A (Avanti Polar Lipids). The total volume of the above mixture was set 80 μL/well. After incubation at 30 °C for 60 min, the released coenzyme A was detected by adding 80 μL of 30 μM of 7-diethylamino-3-(4'-maleimidylphenyl)-4-methylcoumarin (CPM) stock solution (Sigma Aldrich) to each well and incubated in the dark

for 12 min. The fluorescence intensity was measured by a Flex Station 3, microplate reader (excitation at 390 nm; emission at 479 nm).

Analysis of mRNA copy number in TCGA database

Expression values were extracted from the cBioPortal for Cancer Genomics (http://www.cbioportal.org/) for the following genes using the Gene Set Query functions: NMT1 and Src. The expression values were then cross-referenced with the data sets from the TCGA Data Portal. The data was then downloaded and aligned to the respective TCGA Sample IDs in order to be used in statistical analysis. Additional data was extracted from the TCGA Provisional Prostate Adenocarcinoma clinical data set (http://www.cbioportal.org/study?id=prad_tcga#clinical), giving more information for each Sample ID such as: Gleason Score, Survival Status, Days to Sample Collection, and Cancer status.

Soft agar colony formation assay

The effect of Src(WT), Src(Y529F), Src(Y529F/G2A), Src(Y529F/S3C/S6C), and Src(Y529F/K298M) on colony formation in SYF1 cells was assessed by soft agar colony formation assay using Cell Transformation Detection Assay Kit (Millipore, Darmstadt, Germany). The assay was performed in six-well plates as follows: 1 mL of 0.8 % agar solution was layered in the bottom of each well followed by 0.5 mL of 0.4 % agar solution as the top layer. A total of 1,500 cells were suspended in 0.4 % top layer agar containing 0.5 mL of DMEM with 10% FBS and plated on top of the bottom layer in the same medium according to the manufacturer's instructions. After 21-28 days of incubation at 37 °C in a 5% CO_2 incubator humidified atmosphere, the number of colonies were counted and photographed under a fluorescence microscope (Carl Zeiss, Germany).

Cell proliferation, invasion, migration assay, and cell cycle analysis

For cell proliferation assays, cells were seeded in 96-well plates at a density of 3000-5000 cells per well and treated with different concentrations of B13. The medium was removed and replaced with 100 μL of fresh culture medium without phenol red. Next, 10 μL of 12 mM MTT (ThermoFisher) was added to each well, and incubated at 37 °C for 4 h. The reaction was stopped using 100 μL of 10% SDS (dissolved in 0.01 M HCl), and incubated at 37 °C for another 4 h. The absorbance was measured at 570 nm (FlexStation 3, Molecular Devices).

For wound-healing assays, $8x10^5$ cells were seeded in a 6-well plate and incubated for 24 h. Once the cells reached 95% confluence, a space was created using a 1 mL pipette tip to scratch wounds across the well. After washing with medium to remove floating cells, fresh medium with a tested compound was added. The scratched space was monitored and imaged daily.

For cell migration assays, cells were cultured to around 80% confluence. After incubation for 24 h in serum free medium, the cells were seeded according to the manufacturer's instructions. The top well contained medium with compound or DMSO, and the receiver well contained 10% FBS. After 48 h incubation, the medium was removed from the insert and washed with PBS, then fixed with 3.7% formaldehyde for 2 min and methanol for 20 min. The fixed cells were washed with PBS, and stained with 0.1% crystal violet at room temperature for 15 min in the dark. After washing with PBS, the non-migrated cells were removed with cotton swabs, and the migrated cells were imaged and counted.

For cell cycle analysis, cells were grown in ATCC-recommended medium. After attaching, the medium was replaced with fresh medium with/without 15 or 30 μM of B13 every 24 h for 3 days. 1×10^6 cells were obtained from the plate, and washed with PBS, then fixed with 70% ethanol for 1 h at 4 °C. After washing with PBS, the fixed cells were stained by FxCycle™ propidium

iodide/RNAse solution (Invitrogen) for 30 minutes in the dark at room temperature. The stained cells were then analyzed by flow cytometry (CyAn ADP Analyzer, 488 nm excitation and 585nm emission).

Prostate regeneration assay and xenograft tumors.

C57BL/6J and CB.17$^{SCID/SCID}$ (SCID) mice were purchased from Taconic (Hudson, NY). For the prostate regeneration assay, primary prostate cells were isolated from 8-12 week-old male C57BL/6J mice, and infected with lentivirus expressing Src/Fyn(WT) or mutants, or co-infected with Src(WT)/Src(G2A) and AR according to the experimental setup. Infected cells (2-3 x 10^5 cells/graft) were combined with urogenital sinus mesenchyme (UGSM) (2-3 x 10^5 cells/graft) together with 25 μL of collagen type I (adjusted to pH 7.0) (12). After overnight incubation, grafts were implanted under the kidney capsule in SCID mice by survival surgery. All animals were sacrificed at 8 weeks after grafts were implanted.

To examine the role of Src or NMT1 in tumor progression, the xenograft tumor model was applied. PC-3 cancer cells transduced with Src-shRNA, NMT1-shRNA or control shRNA by lentiviral infection and were grown in DMEM with 10% FBS. 3x10^5 cells were mixed with 50 μL of collagen type I (pH 7.0) (BD Biosciences) and inoculated subcutaneously in both lateral flank sides of SCID mice. The size of tumors was measured weekly. The host mice were sacrificed, and xenograft tumors were harvested after two months incubation.

For examining the inhibition of B13 on xenograft tumors, PC-3 cells were subcutaneously inoculated in the flank side of SCID mice. Mice carrying xenografts were randomly separated into two groups after 2-3 weeks. B13 was dissolved in the vehicle solution containing 30% kolliphor, 65% saline (0.9% NaCl), and 5% ethanol. Mice were administrated intravenously (i.v) with 200 μL of the drug solution at a concentration of 75 mg/kg body weight or vehicle twice a week for 4-

6 weeks. Body weight and tumor size were measured (length x width) weekly. Xenograft tumors, the liver, lung and kidney were harvested for immunohistochemistry analysis. All animals were maintained according to the surgical and experimental procedures of the protocol A2013 03-008 approved by IACUC at the University of Georgia.

Statistical Analysis: Prism software was used to carry out statistical analyses. The data are presented as mean ± SEM and analyzed using the Student's t test. All t tests were performed at the two-sided 0.05 level for significance. "*": $P<0.05$; "**":$P<0.01$; "N.S.": not significant.

RESULTS

Ablation of N-myristoyltransferase 1 inhibits proliferation of prostate cancer cells.

Protein lipidation including myristoylation is essential for regulation of the structure and function in numerous disease-related proteins (3). N-myristoyltransferase (NMT) catalyzes protein myristoylation, and has been considered a major target to block cancer progression (13, 21). NMT1 was expressed in normal or prostate cancer cells, and mRNA and protein expression levels of NMT1 were significantly elevated in DU145 and PC3 cancer cells (Fig. 3.1A-B). Increased expression of NMT1 correlated with elevated protein myristoylation at ~60 kDa (Fig. 3.1C). To examine if NMT1 regulates the growth of prostate cancer cells, shRNA targeting NMT1 (shNMT1) was generated (Fig. S3.1A-B). Knockdown efficiency was validated in SYF1 ($Src^{-/-}$ $Yes^{-/-}Fyn^{-/-}$) cells expressing Src(WT) by demonstrating a reduction in myristoylated Src kinase using Click chemistry (Fig. S3.1C). While knockdown of NMT1 showed no inhibition on the growth of PNT2 cells (normal cells), it inhibited the proliferation of LNCaP, 22Rv1, DU145, and PC-3 prostate cancer cells (Fig. 3.1D and Fig. S3.1D). In particular, the inhibitory effect on cell proliferation correlated with the expression levels of NMT1 (Fig. 3.1E) and the lack of inhibition of normal cells (PNT2 cells) suggests that NMT1 might serve as a potential inhibition target in prostate tumors without causing major toxicity.

PC-3 cells were selected for xenograft studies since NMT1 expression was highest in this cell line. Knockdown of NMT1 significantly inhibited the growth of PC-3 xenograft tumors leading to a decrease in the size and weight of tumors (Fig. 3.1F-G). Suppression of NMT1 led to cell cycle arrest at the S-phase with a decrease of the cell population at the G2/M phase (Fig. 3.1H), but had no significant effect on cell apoptosis (Fig. 3.1I).

NMT1-Src axis mediates proliferation of prostate cancer cells.

Myristoylation of Src kinase regulates its kinase activity (5). SFKs are important oncogenic driver genes in a variety of cancers including advanced stages of prostate cancer (9, 22). Expression levels of NMT1 and Src kinase were significantly correlated in human tumors (Fig. 3.2A) and expression levels of NMT1 correlated with the active Src kinase [detected by pSrc(Y416) antibody] in prostate cancer cells (Fig. 3.1B). Similar to the effect of shRNA-NMT1 on PC-3 xenografts, the growth of PC-3 cancer cells (Fig. S3.2A-B) and xenografts (Fig. 3.2B) were dependent on expression of Src kinase. Knockdown of another SFK member Fyn kinase led to only mild inhibition of PC-3 and LNCaP cell proliferation (Fig. S3.2C-D). Down-regulation of NMT1 appears to inhibit Src myristoylation (Fig. 3.2C), tyrosine phosphorylation (pSrcY416), and the level of FAK phosphorylation, a downstream target of Src kinase (Fig. 3.2D), highlighting a potential NMT1-Src axis to inhibit tumor growth, particularly in Src-driven tumors.

Single and double knockdown of NMT1 and Src were performed to evaluate the effect on cell proliferation in LNCaP, 22Rv1, and PC-3 cell lines. Single knockdown of Src or NMT1 inhibited proliferation of the three cell lines (Fig. 3.2E) but double knockdown (shSrc and shNMT1) showed no additive effect in LNCaP and 22Rv1 cells. However, double knockdown in PC-3 cells (showing the highest expression of NMT1 and pSrc) showed greater inhibition of proliferation compared to either single knockdown (Fig. 3,2E). These results demonstrate an NMT1-Src axis that plays a role in prostate cancer cell growth.

Loss of N-myristoylation inhibits SFK-induced oncogenic signaling *in vitro* and prostate tumorigenesis *in vivo*.

The tumorigenic potential of the following Src and Fyn kinase mutants were examined *in vitro* and *in vivo*: constitutively active that recapitulates activated Src kinase in tumors [Src(Y529F) or

Fyn(Y528F)], loss of the myristoylation site [Src(Y529F/G2A) or Fyn(Y528F/G2A)], gain [Src(Y529F/S3C/S6C)] or loss [Fyn(Y528F/C3S/C6S)] of two palmitoylation sites, and loss of both myristoylation and palmitoylation sites [Fyn(Y528F/C3S/C6S/G2A)] (Fig. 3.3A and 3.3B). Src(Y529F/G2A), Fyn(Y528F/G2A) and Fyn(Y528F/C3S/C6S/G2A) inhibited phospho-Erk, pFAK expression (Fig. S3.3A and B), and colony formation (Fig. S3.3C and D), suggesting that specifically myristoylation and not palmitoylation is essential for SFKs-mediated oncogenic signaling and transformation *in vitro*.

As previously reported (17), while regenerated tissue derived from Src(Y529F) or Fyn(Y528F/C3S/C6S) infected epithelial cells formed a solid tumor (Fig. 3.3C-D), tissue from Src(Y529F/S3C/S6C) showed normal tubule structure (Fig. 3.3C and E). Src(Y529F)-induced tumors were composed of sheets of poorly differentiated carcinoma cells without glandular structures and with focal sarcomatoid areas (Fig. 3.3C). In contrast, the regenerated tissue derived from Src(Y529F/G2A) showed normal tubule structure (Fig. 3.3E). Additionally, regenerated prostate tissue derived from Fyn(Y528F) and Fyn(Y528F/C3S/C6S) exhibited high grade adenocarcinoma and invasive tumor, respectively (17). The tissues from Fyn(Y528F/C3S/C6S) showed solid tumors with un-differentiated tumorigenic cells. In contrast, tissues from Fyn(Y528F/G2A) or Fyn(Y528F/C3S/C6S/G2A) showed normal glandular tubules (Fig. 3.3D and F). Collectively, these results indicate that myristoylation is essential for SFKs-induced tumorigenesis and loss of myristoylation abolishes tumorigenic potential, suggesting that myristoylation is an important oncogenic target.

Blockade of myristoylation inhibited synergy of Src and AR in prostate tumorigenesis.

Co-expression of c-Src and AR induces activation of Src kinase and leads to invasive prostate tumorigenesis *in vivo* (12). The role of myristoylation in the synergy of Src-AR induced

tumorigenesis was also examined. Prostate primary cells were transduced with AR, Src(WT), Src(G2A), AR+Src(WT), or AR+Src(G2A) by lentiviral infection (Fig. 3.4A). Their expression was visualized in the regenerated tissues by fluorescence imaging of the GFP/RFP markers (Fig. 3.4B). Although the size of regenerated tissue showed no visible difference, the weight of regenerated tissue derived from Src(WT)+AR increased significantly in comparison with Src(WT), Src(G2A), AR, or Src(G2A)+AR (Fig. 4B). As reported previously (12), over-expression of AR or Src(WT) alone did not induce prostate tumorigenesis, and regenerated tissues contained histologically normal prostate tubules (Fig. 3.4C). Regenerated tissues derived from Src(WT)+AR displayed phenotypic features of a poorly differentiated or undifferentiated high grade carcinoma with an invasion of some tumorigenic cells into the neighboring tissues. While normal tubules usually contains a large lumen cavity, tumors from Src(WT)+AR tumors are comprised of tumorigenic cells without cavity. As a result, although regenerated tissues showed no difference in size, the weight of regenerated tissue from Src(WT)+AR group was significantly elevated than those from normal tubules. In contrast, regenerated tissues derived from over-expression of Src(G2A) alone or Src(G2A)+AR showed normal tubule structure (Fig. 3.4C), suggesting that loss of Src kinase myristoylation blocks the synergy of Src(WT) and AR induced tumorigenesis *in vivo*. Since myristoylation was important for Fyn transformation, the synergy of AR and Fyn was examined. However, the results showed no synergistic effect in the regenerated tissues (Fig. S3.4A-B), suggesting differential functions of Src family kinases (17), likely dictated by differential intracellular trafficking pathways (23).

Loss of Src myristoylation interfered with the protein interaction of exogenously expressed Src and endogenous AR in LNCaP (Fig. S3.5A-C) and 22Rv1 prostate cancer cells (Fig. S3.5D-F) in the presence or absence of AR agonist (R1881), and inhibited AR-regulated expression of the PSA,

KLK2, and TMPRSS2 genes (Fig. S3.5G). These results further suggest that myristoylation is a potential therapeutic target for the inhibition of Src kinase function and its mediated tumorigenesis.

Small molecule targeting of NMT1 enzymatic activity.

To identify small molecule compounds that target NMT activity, recombinant NMT1 protein (with an exclusion of the 108 amino acids DNA sequence in the N-terminus) was used (Fig. S3.6A-B). The protein was purified by affinity chromatography (Fig. S3.6C) (20). A fluorescence-based *in vitro* assay was developed (Fig. S3.7A) (24) and the myristoylation process was found to occur by a "Ping-Pong" mechanism (Fig. S3.7B). The detection of Src myristoylation using click chemistry was developed to examine the inhibition of compounds at the cellular level (Fig. S3.8A-B). The assays were used to screen a selected panel of LCL compounds of previously synthesized myristoyl-CoA analogs (Fig. S3.8C and Fig. S3.9). D-NMAPPD, N-[(1R,2R)-2-hydroxy-1-(hydroxymethyl)-2-(4-nitrophenyl)ethyl]-tetradecanamide, also named B13 (or LCL4), was the top hit that inhibited NMT1 activity and Src kinase myristoylation (Fig. 3.5). The IC_{50} of B13 (77.6 μM) was not improved with analogs with longer or shorter N-acyl carbon chains on R1 group such as LCL7 or LCL35 likely due to steric clashes of the longer tails or loss of hydrophobic interactions with shorter tails with the NMT1 protein (Fig. 3.5). Additionally, when the nitro (R2 group) was removed from the *p*-position of the aromatic ring of LCL4 along with the addition of hydroxymethyl (R4 group) such as the compound LCL1, it showed a significant increase in IC_{50} value. However, N,N'-Disubstituted urea as a linker between aromatic ring and aliphatic tail such as LCL17 led to a decrease of the IC_{50} value, which could be due to the planar and non-flexible nature of the –NH-CO-NH- linker (Fig. 3.5).

B13 and its derivative LCL204 compete with the myristoyl-CoA binding site of NMT1.

B13 is structurally similar to myristoyl-CoA as both contain a 14-carbon alkyl tail (Fig. 3.6A). The crystal structure of NMT1 was solved to understand how B13 interacts with NMT1 (Table S3.2). Similar to the reported structure (20), the myristoyl-CoA binding site of NMT1 was identified in our structure and placement of B13 within this site was performed initially by overlaying B13's alkyl tail with that of myristoyl-CoA (Fig. 3.6B). Additionally, orientation of B13 within the active site was driven by the SAR data (Fig. 3.6B and S3.9). Several favorable interactions between B13 and the NMT1 the binding pocket, including the interaction of 1) the aromatic ring with a hydrophobic patch comprised of Tyr180 and Val181; 2) the aliphatic tail with Asn246; 3) potential hydrogen bonds between R2 nitro group and Arg255, between the amide group and Thr282 and the backbone amide of Leu248, and between the R4 hydroxymethyl group and the hydroxyl group of Tyr180 (Fig. 3.6B).

The interactions of B13 and NMT1 described above were used to identify an analog with improved efficacy. Based on the B13-NMT1 model in Fig. 3.6B, the hydroxymethyl group and carbonyl oxygen are competing for hydrogen bonding interactions with NMT1. Therefore, the removal of the carbonyl could potentially enhance binding and thus increase inhibition. Molecular modeling by using Autodock Vina further suggested that the carbonyl group behaved in a more rigid manner than the NO_2 moiety (Fig. 3.6B) and could extend the half-life due to introduction of the stable alkane group. To probe the predictive accuracy of this structural placement and molecular modeling, LCL204 was synthesized (Fig. 3.6A-B) and found to exhibit an order of magnitude enhancement in potency towards NMT1 (IC_{50} = 8.7 μM, Fig. 3.6C). These results suggest a likely path forward for further structure optimization for greater potency in targeting NMT1 activity.

B13 inhibits Src myristoylation, localization at the cytoplasmic membrane, and its mediated oncogenic signaling and transformation.

Src myristoylation is a down-stream target of NMT1. B13 inhibited Src myristoylation of ectopically expressed Src kinase or endogenous Src kinase (Fig. 3.6D-E). Myristoylation is essential for the attachment of Src family kinases at the cytoplasmic membrane. The majority of Src/Fyn proteins were found to localize in the cytosol in the Src(G2A), Src(Y529F/G2A), Fyn(G2A), and Fyn (Y528F/G2A) mutants (Fig. S3.10A-D). Loss of myristoylation inhibited the association of Src kinase with the cellular membrane (Fig. S3.10E). B13 inhibited Src kinase tyrosine phosphorylation [detected by pSrc(Y416)] in association with down-regulation of pFAK and pAkt (Fig. 3.6F), or suppression of *de novo* synthesized Src-induced signaling (Fig. 3.6G). Similarly, the amount of non-phosphorylated Src kinase in the open conformation [detected by non-pSrc(Y527)] at the cytoplasmic membrane, representing the doxycycline induced *de novo* synthesized Src kinase, was reduced after treatment with B13 (Fig. 3.6H). Expression levels of non-phosphorylated Src in the cytoplasmic fraction did not change with B13 treatment most likely because only a small portion of the total cytosol lysate was analyzed due to the limited loading volume available in the gel. Additionally**,** while Src(Y529F) significantly increased colony formation, the transformation was inhibited by B13 (Fig. 3.6I).

B13 inhibits proliferation, migration, and invasion of prostate cancer cells and growth of xenograft tumors.

The ability of B13 to inhibit transformation and proliferation of prostate cancer cells was examined. B13 significantly inhibited proliferation of 22Rv1, PC-3, and DU145 prostate cancer cells, but this effect was less sensitive in LNCaP cells (Fig. 3.7A), which is correlated with the lower expression of NMT1 (Fig.3.1A-B). Cell cycle progression was significantly inhibited in the

tested prostate cancer cells (Fig. 3.7B). The cell cycle inhibition was further confirmed by decreased expression of CDK2 and cyclin D1, increased expression of p27 in PC-3 and DU145 cells, and decreased expression of CDK6 in DU145 cells (Fig. 3.7C). B13 also suppressed invasion of 22Rv1 and migration of PC-3 cancer cells (Fig. 3.7D). However, B13 had a limited effect on PNT2 normal cell proliferation and did not affect the cell cycle in PNT2 cells (Fig. S3.11A-C) or proliferation of 293T cells (Fig. S3.11D).

To examine the specificity of B13 for targeting the NMT1-Src axis, 22Rv1 or PC-3 cells transduced with shRNA-control or shRNA-Src were subjected to the B13 treatment. Single B13 treatment or knockdown of Src showed significant inhibition on proliferation of 22Rv1 and PC-3 cells (Fig. S3.12A-B). PC-3 cells with Src knockdown and B13 treatment showed a combined effect on reducing proliferation (shRNA-Src+B13 versus B13) (Fig. S3.12A). This effect on proliferation was not observed in 22Rv1 cells (shRNA-Src+B13 versus shRNA-Src) (Fig. S3.12B). As PC-3 cells showed the highest and 22Rv1 the lowest expression of NMT1 and pSrc, this data suggests that the NMT1-Src axis sensitizes cells to targeting myristoylation to reduce proliferation.

The effect of B13 in host mice carrying PC-3 xenograft tumors was further examined. B13 significantly inhibited the size and weight of PC-3 xenograft tumors (Fig. 3.7E) with no observed pathological toxicity to the major organs of host SCID mice including the liver, kidney, and lung (Fig. 3.7F), and no significant changes in body (Fig. S3.13A) or organs' weight (Fig. S3.13B). Collectively, B13 exhibited inhibition on the growth of prostate cancer cells, suggesting its potential as an effective agent for the treatment of prostate tumors.

Discussion:

Our study demonstrates that the inhibition of NMT1 genetically or pharmacologically suppresses proliferation of prostate cancer cells and growth of xenograft tumors. The magnitude of the inhibitory effect is positively correlated with the expression levels of NMT1 and pSrc(Y416) in cancer cells. Inhibition of NMT1 suppresses myristoylation and tyrosine phosphorylation of Src kinase *in vitro* and *in vivo*. Targeting myristoylation exhibits dual effects in inhibiting Src-mediated oncogenic activity since both the catalytic domain and scaffold function are essential for SFKs (10). The myristoyl group may participate in protein folding and promote Src kinase to switch to its active conformation leading to phosphorylation at Tyr416 (25). Loss of myristoylation suppresses down-stream signaling including FAK as well as the MAPK signaling pathway (13). Additionally, inhibition of myristoylation blocks the scaffold function of Src kinase, and prevents the protein–protein interaction with AR thus inhibiting androgen independent AR activation. Several studies have reported that high levels of Src kinase dead mutants are still able to enhance FAK catalytic activity (26) and decrease osteoporosis in the $Src^{-/-}$ animal model (27), and promote AR activity in part (12). Inhibition of Src kinase anchoring to the intracellular membrane could change the protein intracellular trafficking path (23). Inhibition of NMT provides an additional pathway to inhibit SFK-mediated oncogenic signaling in comparison with numerous Src kinase inhibitors such as dasatinib that only target the ATP binding site (28). We show that expression of NMT1 is correlated with expression levels of Src kinase in human tumors. Given the fact that the elevation of Src expression and activity has been well documented in advanced prostate cancer (9), targeting the NMT1-Src axis provides a novel approach for inhibiting tumor progression, particularly in Src-driven tumors.

Although numerous NMT inhibitors have been developed as antiviral, antifungal or antiparastic agents (29), only a limited number of inhibitors including COPP24 and "Compound 1" have been reported as anticancer agents (30, 31). NMT activity occurs via the formation of a ternary complex with myristoyl-CoA and glycine at the N-terminus of the target proteins (32). Our study identifies B13 as a novel NMT inhibitor that can be modeled into the myristoyl-CoA binding site in NMT. B13 shows limited effect on normal cells or organs, which may be due to elevated fatty acid metabolism and lipogenesis in cancer cells in comparison with normal cells (33). Elevated expression of fatty acid synthase (FASN) has been well documented in numerous cancers, and targeting FASN shows benefit in inhibiting cancer progression (34). Biosynthesis of acyl-CoAs including myristoyl-CoA is a required step for phospholipid synthesis (35). In concert with aberrant expression of NMT in a variety of cancer cells (3, 21, 36), an increase of myristoyl-CoA production either from exogenous fatty acids or through *de novo* synthesis could further promote protein myristoylation to facilitate the growth of cancer cells (35). In particular, Src expression and/or activity are highly elevated in advanced prostate cancer (9). Further studies are required to determine if the amount of myristoylated Src, which is essential for its kinase activity, is also elevated in advanced prostate cancer. Nevertheless, the differential activity of fatty acid metabolism coupled with an elevation of NMT enzymatic activity might provide a molecular basis to differentiate cancer cells with normal cells. Our study emphasizes the NMT1-Src axis in mediation of the growth of prostate cancer cells. It should be noted that targeting NMT may also lead to inhibition of other NMT downstream proteins in which myristoylation is essential for their function. For example, myristoylation of AMPK is required for its recruitment to the mitochondria for the induction of mitophagy and cell viability (37). The inhibition of B13 on NMT1 activity could potentially block the AMPK recruitment process to inhibit the proliferation of prostate

cancer cells. Regardless, our study has demonstrated that targeting NMT activity provides a promising therapeutic approach for treatment of cancer progression.

It should be noted that B13 could have other inhibitory targets in addition to NMT1. For example, it has been reported that B13 can inhibit acid ceramidase (38, 39). The inhibition suppresses the conversion of ceramide to sphingosine, which leads to an increase of ceramide levels including C_{14}-, C_{16}-, C_{24}-, $C_{24:1}$-ceramides and a decrease of sphingosine (24, 38, 39). The alteration of ceramides and sphingosine triggers the cell apoptosis pathway (40). It remains to be studied if inhibition of NMT activity could also contribute to the alteration of ceramide levels. The biosynthesis of ceramides requires fatty acyl-CoA as substrates, and the accumulation of myristoyl-CoA resulting from the blockade of NMT activity might potentially facilitate ceramide biosynthesis. Therefore, B13 might potentially be a dual inhibitor in targeting both NMT and acid ceramidase.

Further optimization of B13 and development of a drug delivery vehicle may improve the efficacy for cancer treatment. We have illustrated that LCL204, a B13 derivative identified by structure replacement, shows 9-fold decrease in IC_{50} on NMT1 enzymatic activity. Interestingly, LCL204 is also reported as an inhibitor of acid ceramidase with higher inhibitory potential than B13 (38). Further development of LCL204 will rely on its toxicity to normal cells and organs in pre-clinical trials. Additionally, the myristoyl group of B13 confers hydrophobicity to the compound. Using a nanoparticle-based vehicle to deliver the compound might be helpful for the improvement of its efficacy *in vivo* and reduction of adverse side effects in cancer treatment (41).

References

1. Bhatnagar RS, Futterer K, Farazi TA, Korolev S, Murray CL, Jackson-Machelski E, et al. Structure of N-myristoyltransferase with bound myristoylCoA and peptide substrate analogs. Nat Struct Biol. 1998;5:1091-7.
2. Yang SH, Shrivastav A, Kosinski C, Sharma RK, Chen MH, Berthiaume LG, et al. N-myristoyltransferase 1 is essential in early mouse development. The Journal of biological chemistry. 2005;280:18990-5.
3. Felsted RL, Glover CJ, Hartman K. Protein N-myristoylation as a chemotherapeutic target for cancer. J Natl Cancer Inst. 1995;87:1571-3.
4. Resh MD. Myristylation and palmitylation of Src family members: the fats of the matter. Cell. 1994;76:411-3.
5. Patwardhan P, Resh MD. Myristoylation and membrane binding regulate c-Src stability and kinase activity. Molecular and cellular biology. 2010;30:4094-107.
6. Summy JM, Gallick GE. Treatment for advanced tumors: SRC reclaims center stage. Clin Cancer Res. 2006;12:1398-401.
7. Gioeli D. Signal transduction in prostate cancer progression. Clinical science. 2005;108:293-308.
8. Blume-Jensen P, Hunter T. Oncogenic kinase signalling. Nature. 2001;411:355-65.
9. Guo Z, Dai B, Jiang T, Xu K, Xie Y, Kim O, et al. Regulation of androgen receptor activity by tyrosine phosphorylation. Cancer Cell. 2006;10:309-19.
10. Thomas SM, Brugge JS. Cellular functions regulated by Src family kinases. Annu Rev Cell Dev Biol. 1997;13:513-609.
11. Chen Y, Sawyers CL, Scher HI. Targeting the androgen receptor pathway in prostate cancer. Curr Opin Pharmacol. 2008;8:440-8.
12. Cai H, Babic I, Wei X, Huang J, Witte ON. Invasive Prostate Carcinoma Driven by c-Src and Androgen Receptor Synergy. Cancer Res. 2011;71:862-72.
13. Ducker CE, Upson JJ, French KJ, Smith CD. Two N-myristoyltransferase isozymes play unique roles in protein myristoylation, proliferation, and apoptosis. Mol Cancer Res. 2005;3:463-76.
14. Xin L, Teitell MA, Lawson DA, Kwon A, Mellinghoff IK, Witte ON. Progression of prostate cancer by synergy of AKT with genotropic and nongenotropic actions of the androgen receptor. Proc Natl Acad Sci U S A. 2006;103:7789-94.
15. Cai H, Smith DA, Memarzadeh S, Lowell CA, Cooper JA, Witte ON. Differential transformation capacity of Src family kinases during the initiation of prostate cancer. Proceedings of the National Academy of Sciences of the United States of America. 2011;108:6579-84.
16. Haack K, Cockrell AS, Ma H, Israeli D, Ho SN, McCown TJ, et al. Transactivator and structurally optimized inducible lentiviral vectors. Molecular therapy : the journal of the American Society of Gene Therapy. 2004;10:585-96.
17. Cai H, Smith DA, Memarzadeh S, Lowell CA, Cooper JA, Witte ON. Differential transformation capacity of Src family kinases during the initiation of prostate cancer. Proceedings of the National Academy of Sciences of the United States of America. 2011;108:6579-84.
18. Sunkel B, Wu D, Chen Z, Wang CM, Liu X, Ye Z, et al. Integrative analysis identifies targetable CREB1/FoxA1 transcriptional co-regulation as a predictor of prostate cancer recurrence. Nucleic acids research. 2016;44:4105-22.

19. Adam RM, Yang W, Di Vizio D, Mukhopadhyay NK, Steen H. Rapid preparation of nuclei-depleted detergent-resistant membrane fractions suitable for proteomics analysis. BMC Cell Biol. 2008;9:30.
20. Thinon E, Serwa RA, Broncel M, Brannigan JA, Brassat U, Wright MH, et al. Global profiling of co- and post-translationally N-myristoylated proteomes in human cells. Nat Commun. 2014;5:4919.
21. Wright MH, Heal WP, Mann DJ, Tate EW. Protein myristoylation in health and disease. J Chem Biol. 2010;3:19-35.
22. Aleshin A, Finn RS. SRC: a century of science brought to the clinic. Neoplasia. 2010;12:599-607.
23. Sato I, Obata Y, Kasahara K, Nakayama Y, Fukumoto Y, Yamasaki T, et al. Differential trafficking of Src, Lyn, Yes and Fyn is specified by the state of palmitoylation in the SH4 domain. Journal of cell science. 2009;122:965-75.
24. Szulc ZM, Mayroo N, Bai A, Bielawski J, Liu X, Norris JS, et al. Novel analogs of D-e-MAPP and B13. Part 1: synthesis and evaluation as potential anticancer agents. Bioorganic & medicinal chemistry. 2008;16:1015-31.
25. Bagrodia S, Taylor SJ, Shalloway D. Myristylation is required for Tyr-527 dephosphorylation and activation of pp60c-src in mitosis. Mol Cell Biol. 1993;13:1464-70.
26. Cary LA, Klinghoffer RA, Sachsenmaier C, Cooper JA. SRC catalytic but not scaffolding function is needed for integrin-regulated tyrosine phosphorylation, cell migration, and cell spreading. Mol Cell Biol. 2002;22:2427-40.
27. Schwartzberg PL, Xing L, Hoffmann O, Lowell CA, Garrett L, Boyce BF, et al. Rescue of osteoclast function by transgenic expression of kinase-deficient Src in src-/- mutant mice. Genes Dev. 1997;11:2835-44.
28. Araujo JC, Trudel GC, Saad F, Armstrong AJ, Yu EY, Bellmunt J, et al. Docetaxel and dasatinib or placebo in men with metastatic castration-resistant prostate cancer (READY): a randomised, double-blind phase 3 trial. The lancet oncology. 2013;14:1307-16.
29. Zhao C, Ma S. Recent advances in the discovery of N-myristoyltransferase inhibitors. ChemMedChem. 2014;9:2425-37.
30. French KJ, Zhuang Y, Schrecengost RS, Copper JE, Xia Z, Smith CD. Cyclohexyl-octahydro-pyrrolo[1,2-a]pyrazine-based inhibitors of human N-myristoyltransferase-1. J Pharmacol Exp Ther. 2004;309:340-7.
31. Thinon E, Morales-Sanfrutos J, Mann DJ, Tate EW. N-Myristoyltransferase Inhibition Induces ER-Stress, Cell Cycle Arrest, and Apoptosis in Cancer Cells. ACS chemical biology. 2016;11:2165-76.
32. Farazi TA, Waksman G, Gordon JI. The biology and enzymology of protein N-myristoylation. J Biol Chem. 2001;276:39501-4.
33. Menendez JA, Lupu R. Fatty acid synthase and the lipogenic phenotype in cancer pathogenesis. Nat Rev Cancer. 2007;7:763-77.
34. Sounni NE, Cimino J, Blacher S, Primac I, Truong A, Mazzucchelli G, et al. Blocking lipid synthesis overcomes tumor regrowth and metastasis after antiangiogenic therapy withdrawal. Cell Metab. 2014;20:280-94.
35. Grevengoed TJ, Klett EL, Coleman RA. Acyl-CoA metabolism and partitioning. Annu Rev Nutr. 2014;34:1-30.
36. Rajala RV, Radhi JM, Kakkar R, Datla RS, Sharma RK. Increased expression of N-myristoyltransferase in gallbladder carcinomas. Cancer. 2000;88:1992-9.

37. Liang J, Xu ZX, Ding Z, Lu Y, Yu Q, Werle KD, et al. Myristoylation confers noncanonical AMPK functions in autophagy selectivity and mitochondrial surveillance. Nature communications. 2015;6:7926.
38. Bielawska A, Bielawski J, Szulc ZM, Mayroo N, Liu X, Bai A, et al. Novel analogs of D-e-MAPP and B13. Part 2: signature effects on bioactive sphingolipids. Bioorganic & medicinal chemistry. 2008;16:1032-45.
39. Samsel L, Zaidel G, Drumgoole HM, Jelovac D, Drachenberg C, Rhee JG, et al. The ceramide analog, B13, induces apoptosis in prostate cancer cell lines and inhibits tumor growth in prostate cancer xenografts. Prostate. 2004;58:382-93.
40. Ogretmen B, Hannun YA. Biologically active sphingolipids in cancer pathogenesis and treatment. Nat Rev Cancer. 2004;4:604-16.
41. Nagesh PK, Johnson NR, Boya VK, Chowdhury P, Othman SF, Khalilzad-Sharghi V, et al. PSMA targeted docetaxel-loaded superparamagnetic iron oxide nanoparticles for prostate cancer. Colloids Surf B Biointerfaces. 2016;144:8-20.

Figures

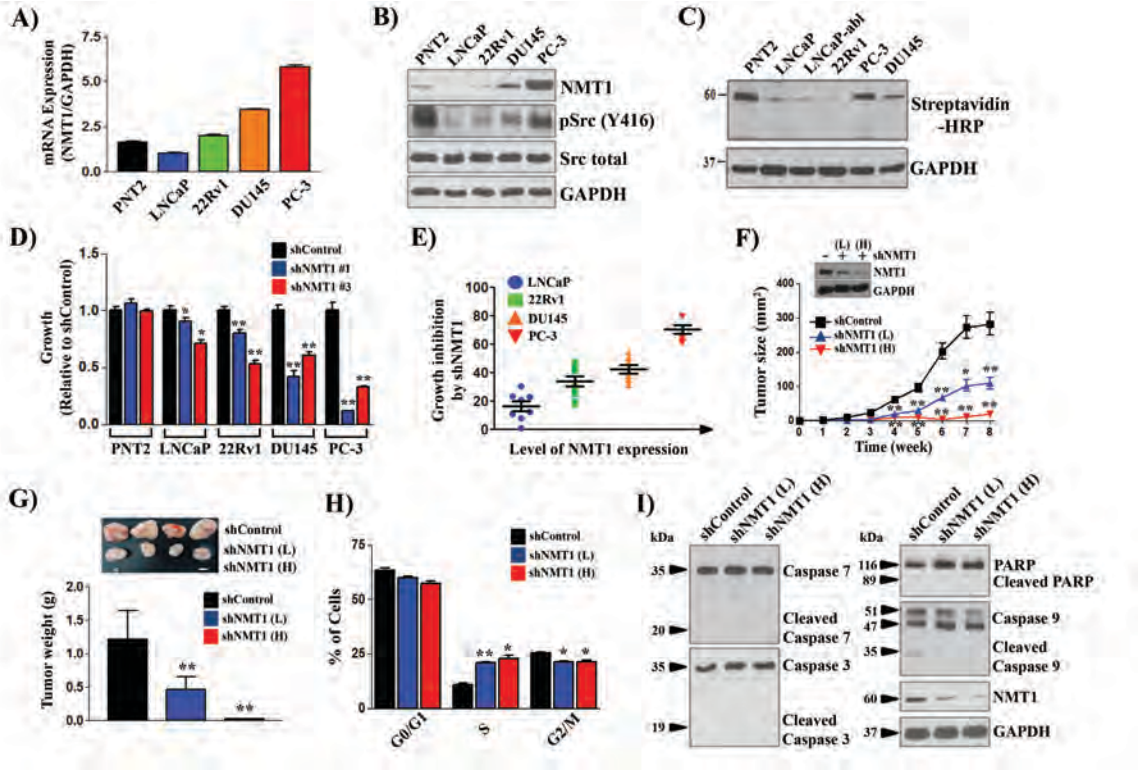

Figure 3.1. NMT1 regulates the proliferation of prostate cancer cells and xenograft tumors. **(A-C)** PNT2 (normal prostate cells) and prostate cancer cells were grown with 60 μM myristic acid-azide. Cell lysates were subjected to Click chemistry for detecting myristoylated proteins. Expression levels of NMT1 mRNA (A), protein (B), and myristoylated proteins (C) were analyzed. Note: PNT2 cells are immortalized by the large T-antigen, which usually leads to the activation of Src kinase. **(D)** NMT1 was knocked down by two independent shRNA-NMT1 by lentiviral infection and proliferation measured after 5 d. Data are relative to the control (set as 1). Also see Supplemental Figure S1 for the growth curve. **(E)** The correlation of NMT1 expression levels with growth inhibitory rate of shRNA-NMT1. **(F-G)** PC-3 cancer cells infected with control shRNA or shRNA-NMT1 of low titer (L, MOI=10) and high titer (H, MOI=50) were implanted subcutaneously in SCID mice (n=6 per group). Tumor size was measured weekly and tumor weight measured at week 8. **(H-I)** PC-3 cancer cells infected with control shRNA or shRNA-NMT1 (L,

MOI=10; H, MOI=50) were cultured for 3 d followed by cell cycle analysis. The percentage of the cells in G0/G1, S, and G2/M phases is relative to the control shRNA (H). Levels of the indicated apoptosis-related proteins were detected by immunoblotting (I). *: $p<0.05$; **: $p<0.01$.

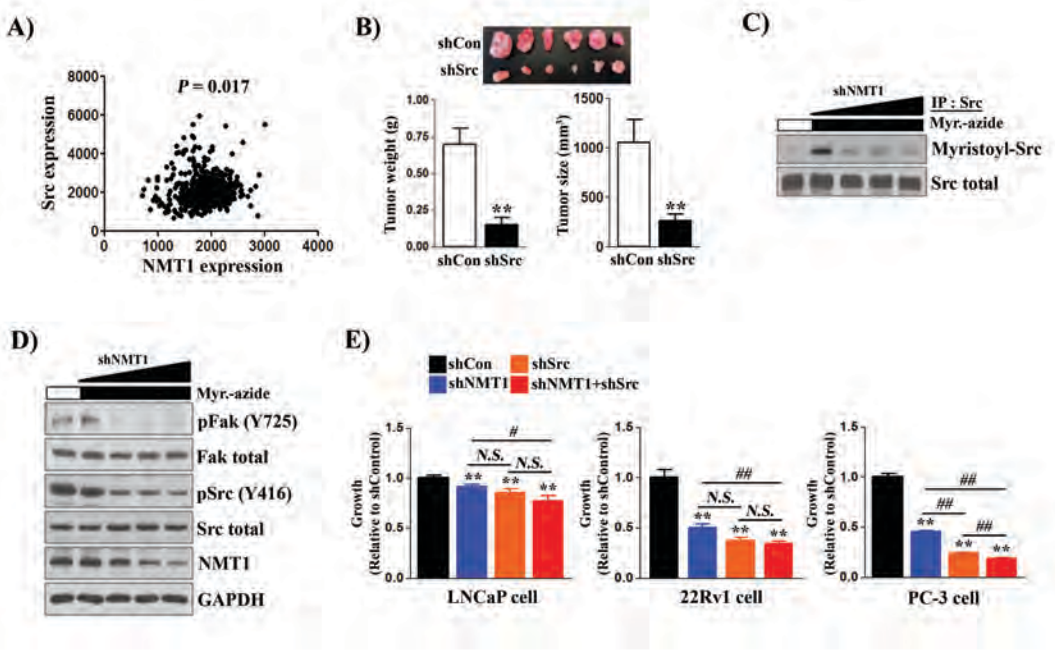

Figure 3.2. NMT1 knockdown causes tumor suppression by down-regulation of Src kinase myristoylation and tyrosine phosphorylation**. (A)** Correlation of Src and NMT1 expression (copy number from the TCGA database (n = 498 tumors). **(B)** PC-3 cancer cells infected with control shRNA or shRNA-Src were implanted subcutaneously in SCID mice (n=6 per group). The size and weight of xenograft tumors were measured at week 8. **(C-D)** PC-3 cancer cells were transduced with shRNA-NMT1 (MOI= 0, 10, 30, 50) by lentiviral infection. The transduced cells were grown with/without myristic acid-azide and myristoylated Src was detected by Click chemistry and immunoblotting with streptavidin-HRP **(C).** The expression levels of the indicated proteins from the protein lysates were measured by immunoblotting (D). **(E)** LNCaP, 22Rv1, and PC-3 cancer cells were transduced with control, shRNA-NMT1, shRNA-Src, or both and proliferation was measured by the MTT assay after 5 d. Data are relative to the control (set as 1). **: $p<0.01$ (each treatment group was compared with the control group). #: $p<0.05$; ##: $p<0.01$ (the compared groups were indicated in the figure).

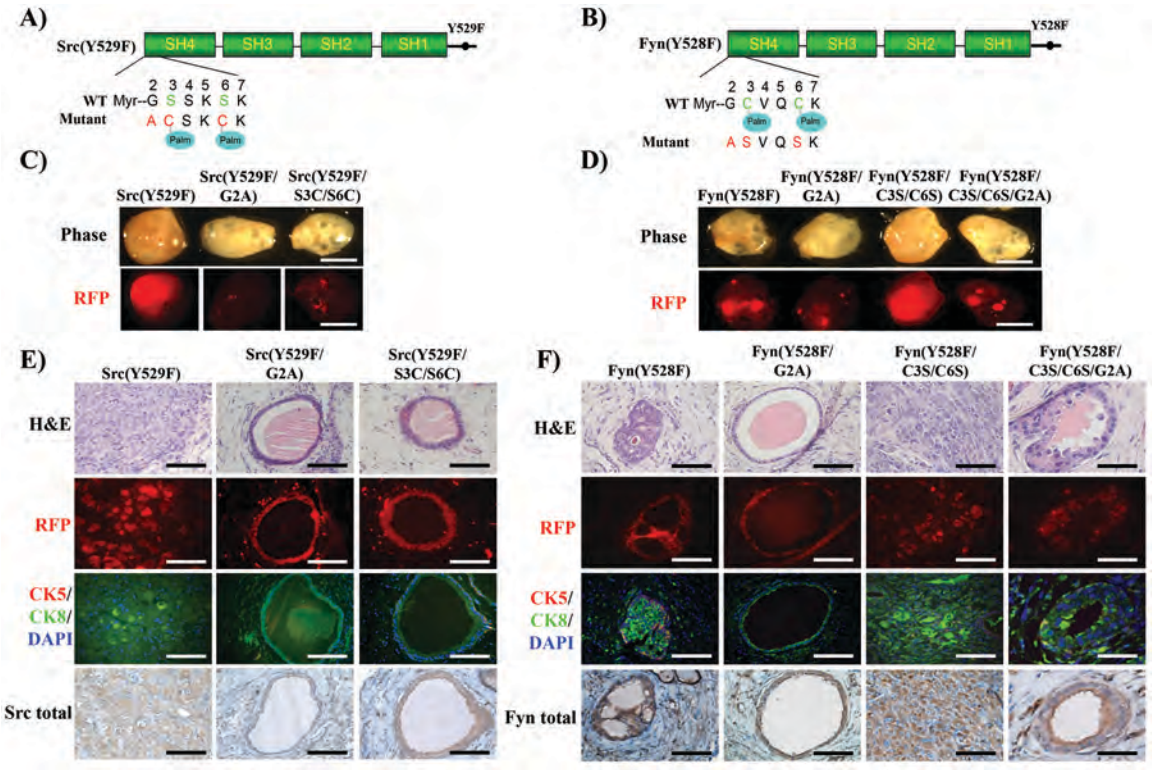

Figure 3.3. Loss of myristoylation inhibits SFK mediated tumorigenesis. (A-B) Schematic of constitutively active Src(Y529F) and Fyn(Y528F) mutations resulting in loss of myristoylation and gain or loss of palmitoylation sites. Gly2 was mutated to Ala (loss of myristoylation site) in constitutively active Src(Y529F) or Fyn(Y528F) kinases. Ser3 and Ser6 sites of Src(Y529F) were mutated to Cys (gain of palmitoylation sites), and the Cys3 and Cys6 sites of Fyn(Y528F) were mutated to Ser (loss of palmitoylation sites). **(C-D)** The *in vivo* prostate regeneration assay was performed with the Src(Y529F) or Fyn(Y528F) and acylation mutants (RFP marker). Representative images of regenerated prostate tissue and RFP detection. Scale bar, 2 mm. **(E-F)** Representative H&E, RFP fluorescence, and IHC staining of CK5 (basal mark, red)/CK8(luminal mark, green)/DAPI (nucleus staining), and Src kinase or Fyn kinase in the regenerated tissues. Scale bar, 100 μm.

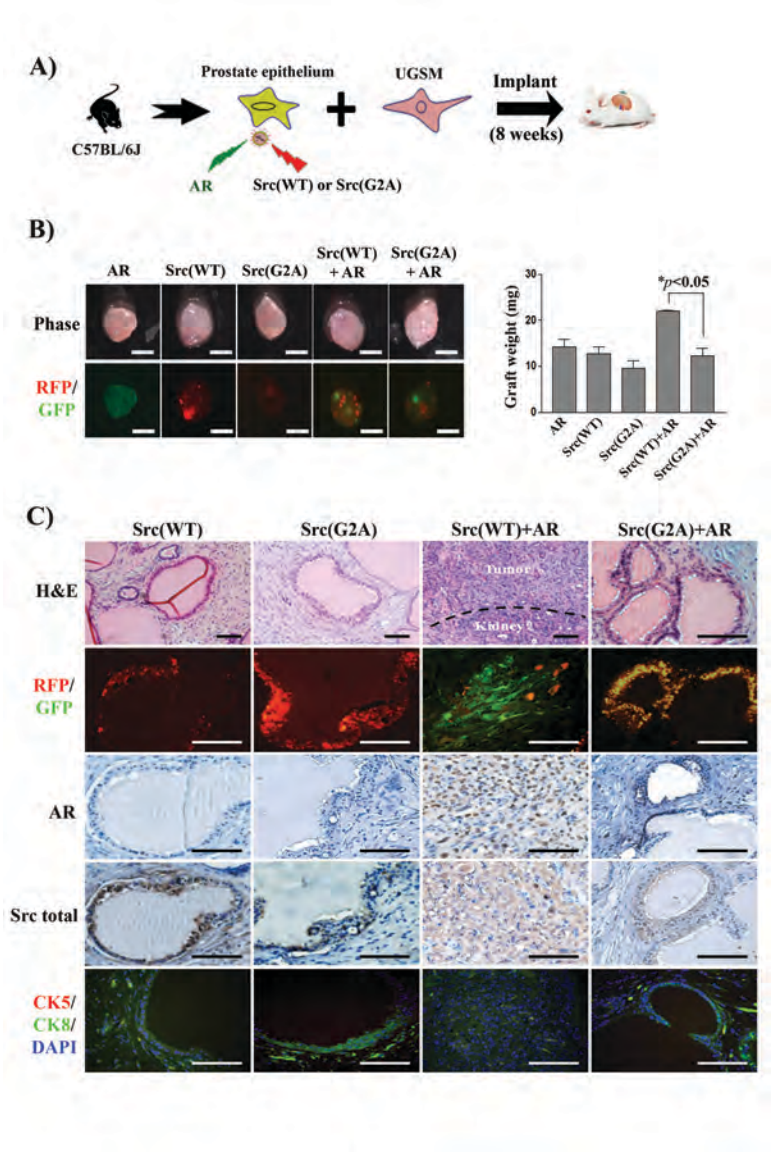

Figure 3.4. Loss of myristoylation in Src kinase inhibits the synergy of Src(WT) with androgen receptor (AR) in prostate tumorigenesis. (A) Schematic for examining the synergy of Src and AR in prostate tumorigenesis. Primary prostate epithelial cells were transduced with AR (GFP marker), Src(WT) (RFP marker), Src(G2A) (RFP marker), or co-transduced with Src(WT)/Src(G2A) and AR and the infected cells were combined with UGSM, and implanted under the renal capsule of SCID mice. Regenerated prostate tissue was isolated after 8 weeks. **(B)**

Representative images of regenerated prostate tissue and RFP/GFP detection (scale bar, 2 mm). The weight of prostate tissues was compared in the bar graph. The * indicates an unpaired, two-tailed t test. **(C)** H&E, RFP/GFP, and IHC staining of AR and total Src, and co-staining of CK8, CK5 and DAPI in regenerated tissue. Scale bar, 100 μm.

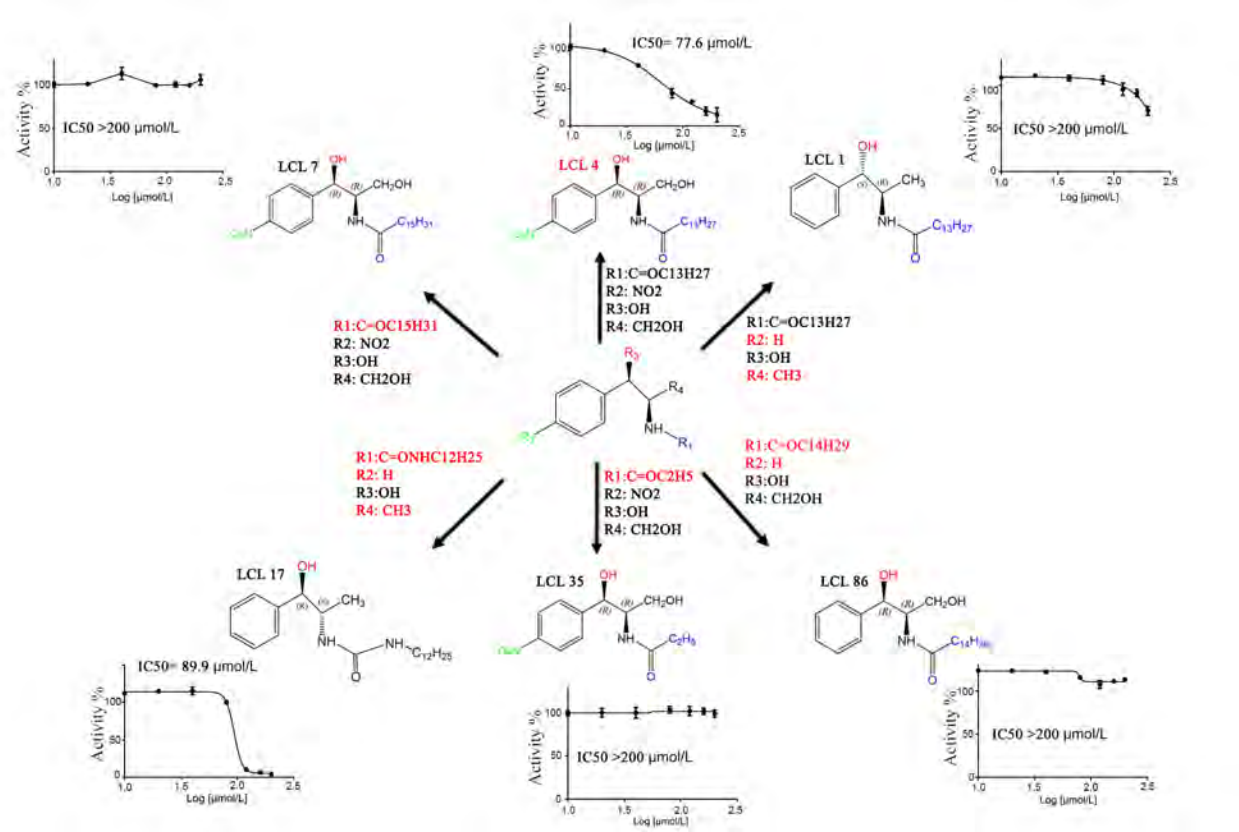

Figure 3.5. Chemical structures and IC_{50} values of LCL compounds targeting NMT1 enzymatic activity. The IC_{50} of LCL compounds on NMT1 enzymatic activity was measured. LCL7 and LCL35 represent a compound with a longer and shorter acyl-chain (R1 group in Figure 5A) than LCL4/B13, respectively. LCL17 represents a compound with NH group in the acyl-chain, which enhances inhibitory effect. LCL86 represents a compound with longer acyl-chain and without nitro group (R2 group). LCL1 represents a compound without both nitro and hydroxyl group (R4 group). The bold highlights the chemical groups different to LCL4/B13 compound.

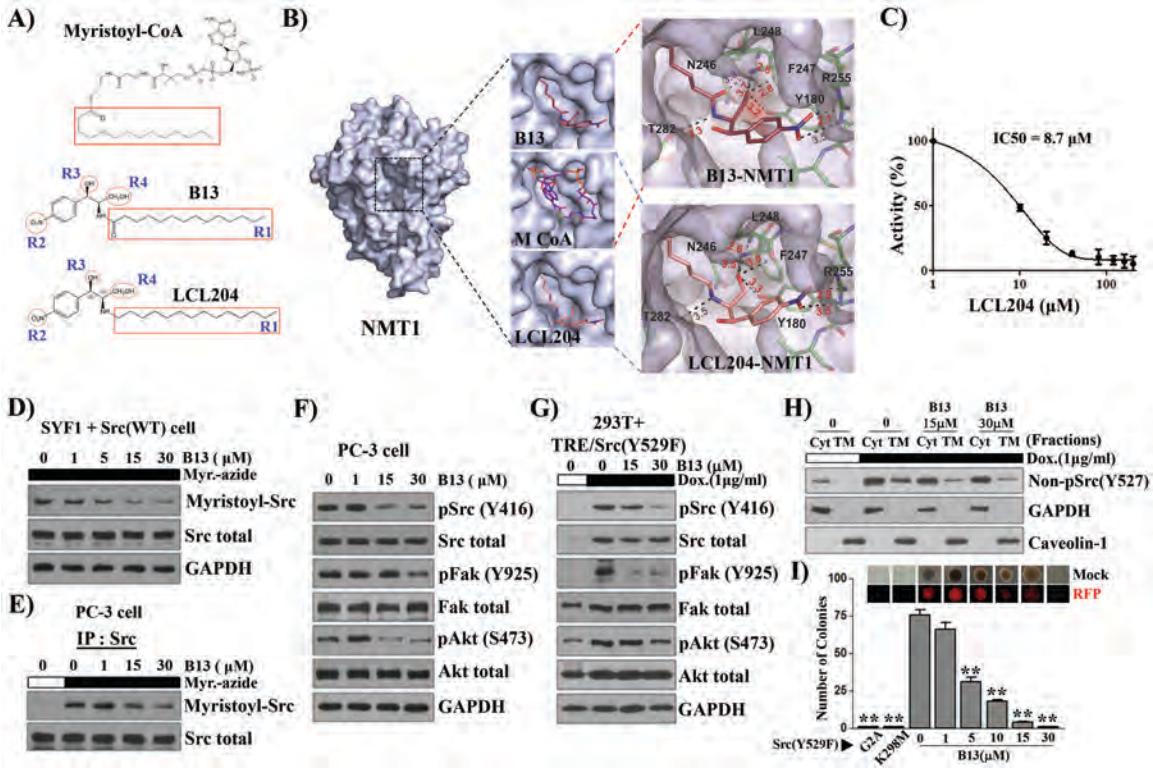

Figure 3.6. Myristoyl-CoA analog, B13, inhibits NMT1 enzymatic activity and suppresses Src kinase mediated cell transformation. (A) Comparison of the myristoyl-CoA structure with B13 and LCL204. The C14 acyl-group (R1) highlighted with a red square in B13 is identical with that in myristoyl-CoA. R2 (nitro group), R3 (hydroxyl group), and R4 (hydroxymethyl group) are important for the inhibitory effect based on structure-activity relationship (SAR) analysis in the Supplemental Figure S9. **(B)** The analysis of the NMT1 protein structure with B13 and LCL204 inhibitor. The binding site of myristoyl-CoA with the NMT1 crystal structure was replaced with B13. The upper right panel shows B13 interactions with neighboring side chains. Myristoyl-CoA and LCL204 were modeled in the NMT1 binding pocket. The bottom right panel shows that LCL204 interactions with the neighboring side chains. According to the structure replacement, the replacement of the methoxide group in B13 with -CH_2 led to a B13 derivative, LCL204, which favors the interactions of the functional groups with amino acids in the binding pocket of NMT1. **(C)** The inhibitory effect of LCL204 on NMT1 enzymatic activity. The IC_{50} of LCL204 on NMT1

enzymatic activity was 8.7 μM, which increased about 9-fold in comparison with that of B13. **(D-E)** SYF1 cells were transduced with Src(WT) and the transduced cells, SYF1+Src(WT) (D) or PC-3, (E) were cultured with B13 overnight followed by myristic acid-azide (60 μM) for 8 h. The lysates from SYF1+Src(WT) cells (D) and Src immunoprecipitates from PC-3 cells (E) were subjected to Click chemistry. The expression levels of myristoyl-Src detected by streptavidin-HRP, total Src, and GAPDH were analyzed by immunoblotting. **(F)** The expression levels of the indicated proteins in the total lysates from (E) were measured by immunoblotting. **(G)** 293T cells expressing doxycycline inducible Src(Y529F) were treated with/without doxycycline (Dox, 1μg/ml) and with DMSO (C), 15, and 30 μM of B13 for 24 h. The levels of the indicated proteins were determined by immunoblotting. **(H)** The lysate from (G) was fractionated. Caveolin-1 and GAPDH were used as markers for total cytoplasmic membrane (TM) and cytosolic fraction (Cyt), respectively. Immunoblot detection using the non-pSrc(Y527F) antibody represented the *de novo* synthesized Src kinase. **(I)** SYF1 cells were transduced with Src (Y529F), Src (Y529F/G2A), or Src (Y529F/K298M) and subjected to the soft agar assay. SYF1-Src(Y529F) cells were treated with B13 and the number of resulting colonies was counted. Representative phase and RFP images of colonies in the soft agar assay are displayed. **: $P<0.01$.

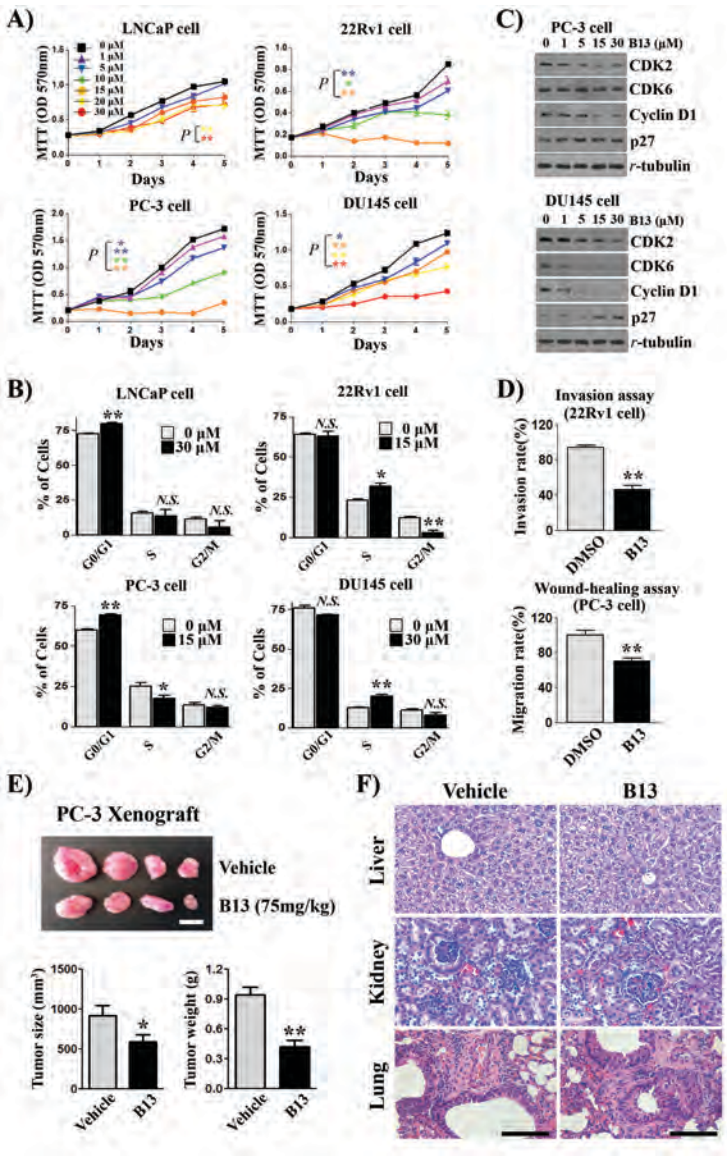

Figure 3.7. The myristoyl-CoA analog B13 inhibits cell cycle progression and growth of xenograft tumors. (A) Prostate cancer cell lines were cultured with B13 for 5 d and cell proliferation was measured. The value is expressed as the mean ± SEM (n=6 wells). The statistical analysis is indicated by the color representing the labeled concentration of B13 treatment. **(B)** Cell cycle analysis of LNCaP, 22Rv1, PC-3, and DU145 cells cultured with B13 for 3 d. The percentage of cells in G0/G1, S, and G2/M phases was compared between the control and B13 treatment. **(C)** PC-3 and DU-145 cells treated with/without different concentrations of B13 were analyzed for the

expression levels of CDK2, CDK6, cyclin D1, p27, and tubulin by immunoblotting. **(D)** 22Rv1 and PC-3 cancer cells grown with/without 15 μM B13 were examined in the Transwell invasion assay and the wound-healing assay, respectively. **(E)** PC-3 prostate cancer cells were subcutaneously injected into both flank sides of SCID mice (3 months-old, n=6 per group). Vehicle or B13 (75mg/kg/mouse) were administered intravenously twice a week for 6 weeks. Representative images of the xenograft tumors are shown (upper panel; scale bar, 10 mm). The size and weight of xenograft tumors were measured as mean ± SEM (bottom panel). *: $P<0.05$, **: $P<0.01$. **(F)** Histology analysis of B13 on major organs. H&E staining of liver, kidney, and lung tissues derived from (E) were evaluated. Scale bar, 400 μm.

Supplemental Materials and Methods

Expression and Purification of NMT1

A modified NMT1 gene containing a His_6-tag at the N-terminus and the catalytic domain of NMT1 (excluding 108 amino acids of the N-terminus of the full length NMT1) was synthesized by GenScript (Fig. S6A-B). The gene was cloned in the pET-11a vector and transformed into Rosetta 2 competent cells by heat shock. Cells were grown at 37 ^oC in LB broth, supplemented with 100 μg/ml ampicillin and 35 μg/ml chloramphenicol, to OD_{600} 0.6-0.8. Cultures were induced with 1 mM IPTG and grown overnight at 18 ^oC. The cells were harvested by centrifugation at 5000 xg for 10 min. The cells were suspended in a buffer containing 20 mM Tris (pH 7.5), 500 mM NaCl, 10 mM imidazole, 1 mM $MgCl_2$, and 0.1% (v/v) Triton X-100 and lysed by four 1 min rounds of sonication, 5 s on 5 s off, at 50% amplitude, on ice. The lysate was cleared by centrifugation at 48,000 xg for 20 min at 4 ^oC. Cleared lysate was applied to high-density nickel agarose beads (Gold Biotechnology, Olivette, MO) equilibrated with 20 mM Tris (pH 7.5), 500 mM NaCl and 10 mM imidazole. Protein was eluted with the equilibration buffer containing 250 mM imidazole. This elution was diluted 20 fold in Buffer A (20 mM Tris pH 8.9 and 1 mM DTT) and loaded onto a Mono Q anion-exchange column (GE Healthcare, Pittsburgh, PA). NMT1 was eluted in a 0-50% NaCl gradient over 20 column volumes of Buffer A and Buffer B (20 mM Tris pH 8.9, 1 mM DTT, and 1 M NaCl) (1). The His_6-tag was cleaved using HRV 3C protease. The remaining free His-tag, His-tagged NMT1, and HRV 3C protease were separated from cleaved NMT1 by nickel affinity chromatography.

Characterization of NMT1 kinetics

Purified NMT1 catalyzes the incorporation of the myristoyl group of myristoyl-CoA into the N-terminus of glycine in the peptide of Gly-Ser-Asn-Lys-Ser-Lys-Pro-Lys (derived from the N-

terminus of human pp60Src tyrosine kinase) releasing CoA. The amount of released CoA could be measured by 7-diethylamino-3-(4'-maleimidylphenyl)-4-methylcoumarin (CMP). The assay was performed in 96-well black microplates (Greiner Bio-One, Germany) and the reaction mixture contained 33.6 μL of 2X reaction buffer (100 mM HEPES and 1 mM EDTA), 4 μL of 5.6 μM of the purified hNMT1 stock, 30.4 μL of ddH_2O, and 4 μL of 70, 100, 200, and 400 μM stock concentration of the above synthetic peptide, respectively. At each peptide concentration of the above mixture, 8 μL of the myristoyl-CoA stock solution was added to reach a final concentration of 0, 10, 20, 40, 80, 160 μM, respectively, and react time was 1, 2.5, 5, 10 minutes, respectively. Reactions were stopped by adding 80 μL of 30 μM of CMP, and incubated in the dark for 12 minutes. The fluorescence intensity was measured by a Flex Station 3, microplate reader (excitation at 390 nm; emission at 479 nm). The reciprocal values of the velocity and the myristoyl-CoA concentration were plotted on Lineweaver-Burk plots.

LCL and GRU compounds and molecular docking

LCL compounds were synthesized by the Synthetic Unit of Lipidomics Shared Resource at the Medical University of South Carolina as previously described (2-4). GRU compounds were synthesized by Dr. Iryna Lebedyeva's lab. Molecular docking was performed using Autodock Vina against compound structures outlined in Figure 6 and S9 by using the binding pocket of the X-ray structure of NMT1 (4C2Y) (1).

Chemical synthesis of B13 and LCL204

For the chemical synthesis of B13, (2*R*,3*R*)-2-amino-1-(4-nitrophenyl)-1,3-propanediol (0.1 mmol, 212 mg) was dissolved in dry THF (50 mL) and cooled to 4 ^oC, EDCI (156 mg, 1 mol) and HOBt (135 mg, 1 mmol) were added to the solution followed by the addition of tetradecanoic acid (228 mg, 1 mmol). The mixture was kept under N_2 at room temperature overnight. After the

reaction mixture was taken to dryness, the product was extracted with ethyl acetate and using sodium carbonate and 3M hydrochloric acid solutions for the extraction to give B13. Product B13 (5) was then purified by column chromatography using ethyl acetate:hexane 1:10 as eluent.

For the chemical synthesis of LCL204, (2*R*,3*R*)-2-amino-1-(4-nitrophenyl)-1,3-propanediol (1 mmol, 212 mg) was reacted with tetradecanal (255 mg, 1.2 mmol) in methanol/0.05 N acetic acid, 9:1 for 15 min and sodium cyanoborohydride ($NaCNBH_3$, 130 mg, 2 mmol) was added in portions during 1 h. The mixture was stirred overnight at room temperature, evaporated to dryness and the residue dissolved in DCM/MeOH, 2:1. The product was purified by recrystallization using DCM/Pentane 1:3 to give LCL204 (6) as white solid in 72 % yield.

Quantitative RT-PCR analysis

Total RNA was isolated from human prostate cell lines using an RNeasy kit (Qiagen). cDNA was prepared from 2 μg of total RNA using the High-Capacity cDNA Kit (Applied Biosystem). Each cDNA sample was diluted 10-fold, and a 5 μL aliquot was used in a 20 μL PCR reaction (PerfeCTa SYBR Green FastMix, Quantabio) containing primers at concentrations of 10 pM each. The primers are listed in Table S1. PCR reactions were run in triplicate and quantitated using StepOne Software v2.1 (Applied Biosystem). The results were expressed as a fold change of mRNA compared with control group. Expression data were normalized to GAPDH.

Immunoprecipitation for the analysis of Src-AR interaction

For the protein interactions between AR and Src(WT) or Src(WT/G2A), LNCaP and 22Rv1 cells were transduced with Src(WT) or Src(WT/G2A) genes by lentiviral infection. The transduced cells were grown in 100 mm dishes, and the protein lysates were extracted with the immunoprecipitation (IP) lysis buffer (25 mM Hepes pH 7.5, 50 mM NaCl, 5 mM EDTA, 10% glycerol, 1% Triton X-100) supplemented with protease inhibitor cocktail (Calbiochem) and phosphatase inhibitor

cocktail 1 and 2 (P5726 and P2850, Sigma). 500 µg protein was incubated with specific antibodies for 16 h at 4 °C. Protein A agarose beads were added, and the mixtures were incubated for 1 h at 4 °C. After washing five times with IP lysis buffer, an equal volume of 2X SDS sample buffer was added to the immuoprecipitated proteins and boiled for 10 min. AR and Src proteins were analyzed by immunoblotting with specific antibodies.

Immunohistochemistry

Formalin-fixed/paraffin-embedded grafts and tissues were sectioned at 4 µm thickness and mounted on positively charged microscope slides. Sections were analyzed by hematoxylin and eosin (H&E), and immunohistochemistry (IHC) staining. The primary antibodies and dilutions used for detection of Src, Fyn, CK5, CK8, and AR expression were described previously (7). Phase or fluorescent images were taken under a fluorescence microscope.

Antibodies

Antibodies against Src, phospho-Src family (Tyr416), phospho-Erk1/2 (Thr202/Tyr204), Fak, phospho-Fak (Tyr925), Akt, phospho-Akt (Ser473), Fyn, GAPDH and Caveolin-1 were purchased from Cell Signaling Technology (Beverly, MA). Antibodies against Androgen receptor (AR) and Erk2 were obtained from Santa Cruz Biotechnology (Santa Cruz, CA). The anti-NMT1 and γ-tubulin antibody and all other reagents were purchased from Sigma Chemical Co. (St. Louis, MO) and Calbiochem (San Diego, CA). These antibodies were used for immunoblotting.

Supplemental References

1. Thinon E, Serwa RA, Broncel M, Brannigan JA, Brassat U, Wright MH, et al. Global profiling of co- and post-translationally N-myristoylated proteomes in human cells. Nature communications. **2014**;5:4919.
2. Bielawska A, Linardic CM, Hannun YA. Ceramide-mediated biology. Determination of structural and stereospecific requirements through the use of N-acyl-phenylaminoalcohol analogs. The Journal of biological chemistry. **1992**;267:18493-7.
3. Szulc ZM, Mayroo N, Bai A, Bielawski J, Liu X, Norris JS, et al. Novel analogs of D-e-MAPP and B13. Part 1: synthesis and evaluation as potential anticancer agents. Bioorganic & medicinal chemistry. **2008**;16:1015-31.
4. Bielawska A, Bielawski J, Szulc ZM, Mayroo N, Liu X, Bai A, et al. Novel analogs of D-e-MAPP and B13. Part 2: signature effects on bioactive sphingolipids. Bioorganic & medicinal chemistry. **2008**;16:1032-45.
5. Bhabak KP, Kleuser B, Huwiler A, Arenz C. Effective inhibition of acid and neutral ceramidases by novel B-13 and LCL-464 analogues. Bioorganic & medicinal chemistry. **2013**;21:874-82.
6. Dagan A, Wang C, Fibach E, Gatt S. Synthetic, non-natural sphingolipid analogs inhibit the biosynthesis of cellular sphingolipids, elevate ceramide and induce apoptotic cell death. Biochimica et biophysica acta. **2003**;1633:161-9.
7. Cai H, Babic I, Wei X, Huang J, Witte ON. Invasive Prostate Carcinoma Driven by c-Src and Androgen Receptor Synergy. Cancer Res. **2011**;71:862-72.
8. Kumar S, Sharma RK. N-terminal region of the catalytic domain of human N-myristoyltransferase 1 acts as an inhibitory module. PloS one. **2015**;10:e0127661.

Supplemental figures

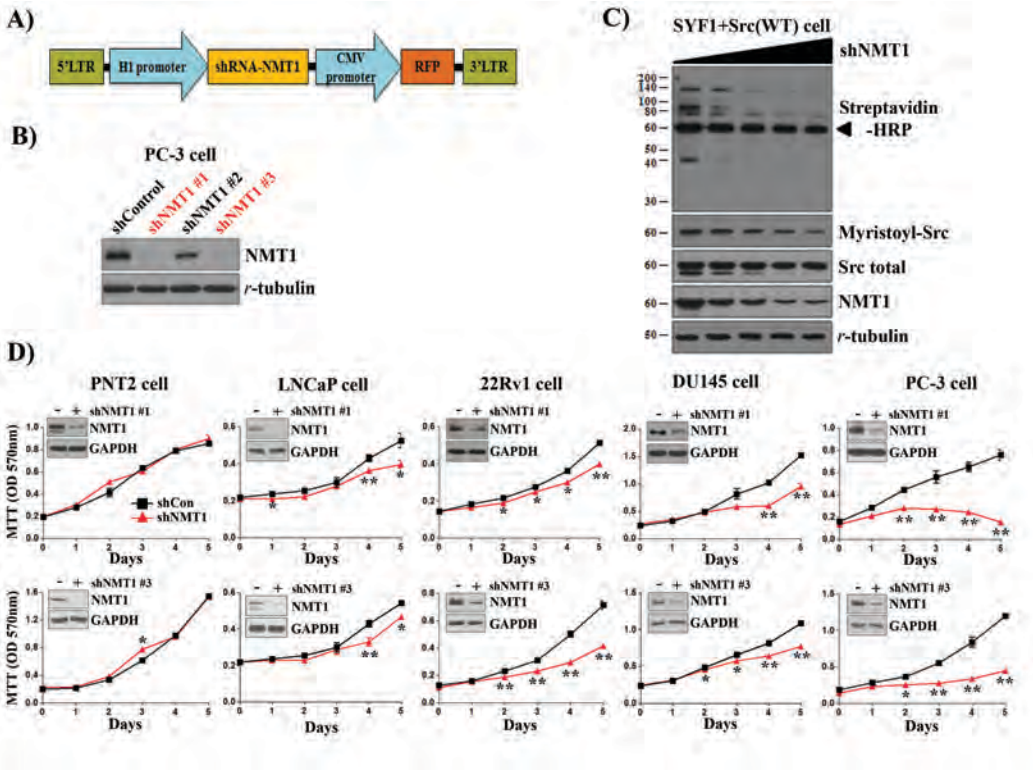

Figure S3.1. Knockdown of NMT1 by shRNA-NMT1 inhibits Src myristoylation and proliferation of prostate cancer cells.

(A) Diagram of the lentiviral vector expressing the shRNA targeting NMT1. **(B)** shRNA-NMT1 inhibited the expression of NMT1 in PC-3 cells. PC-3 cells were transfected with control vector or three different shRNAs (#1-3) by lentiviral infection. shNMT1#1 showed the highest efficacy and was used for further studies. **(C)** SYF1 ($Src^{-/-}Yes^{-/-}Fyn^{-/-}$) cells expressing Src(WT) were transduced with shRNA-NMT1 (MOI of 0, 1, 5, 10, and 20) by lentiviral infection. The infected cells were grown with 60 μM myristic acid azide for 24 h. The total myristoylated proteins or myristoyl-Src were detected by streptavidin-HRP via Click chemistry. The protein expression levels of NMT1, Src, and the tubulin loading control were detected by Western blot analysis. **D)** NMT1 was knocked down by two independent shRNA-NMT1 (#1 and #3) in PNT2, LNCaP,

22Rv1, PC-3, and DU145 cells by lentiviral infection. The growth curve was measured by the MTT assay from day 0 to day 5. Also see Figure 1.

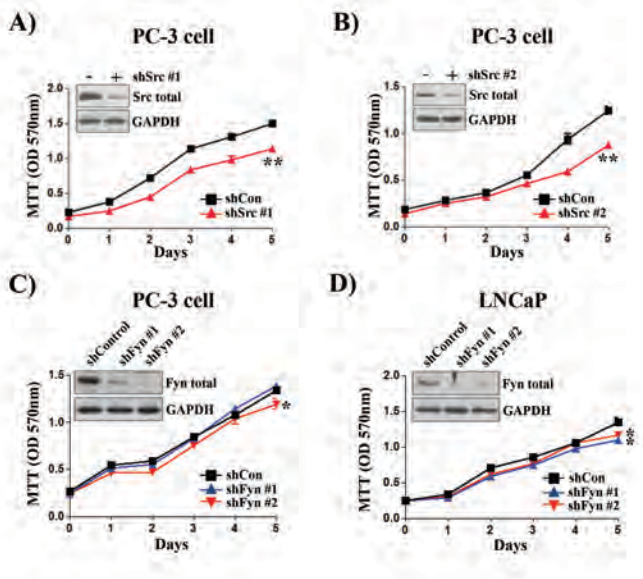

Figure S3.2. Knockdown of Src and Fyn kinase inhibits the growth of prostate cancer cells. **(A-B)** PC-3 cancer cells were transduced with shRNA-control or two independent shRNA-Src. **(C-D)** PC-3 or LNCaP were transduced with shRNA-control or shRNA-Fyn by lentiviral infection. The proliferation of the transduced cells was measured by the MTT assay. The efficiency of knockdown was confirmed by Western blot analysis (inserted panel). **P*<0.05;***P*<0.01.

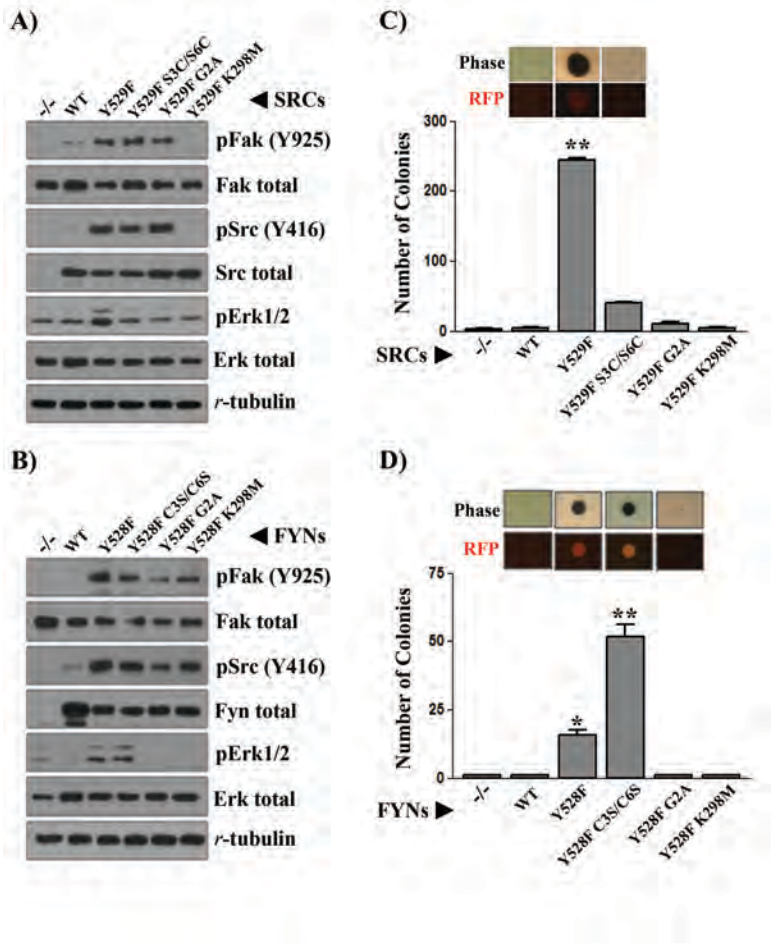

Figure S3.3. The contribution of myristoylation and palmitoylation to the activity of SFKs. **(A)** SYF1 ($Src^{-/-}Fyn^{-/-}Yes^{-/-}$) cells were transfected with Src(Y529F) (constitutively active mutant), Src(Y529F/S3C/S6C) (gain of palmitoylation sites mutant), Src(Y529F/G2A) (loss of myristoylation site mutant), or Src(Y529F/K298M) (kinase dead mutant) by lentiviral infection. The levels of total Src, pSrc(Y416), total Erk, pErk, total Fak, pFak(Y925), and tubulin were determined by immunoblotting. **(B)** SYF1 cells were transfected with Fyn(Y528F) (constitutively active mutant), Fyn(Y528F/C3S/C6S) (loss of palmitoylation sites mutant), Fyn(Y528F/G2A)

(loss of myristoylation site mutant), or Fyn(Y528F/K298M) (kinase dead mutant) by lentiviral infection. The levels of total Fyn, pSrc(Y416) (which detects the activation of Fyn), total Erk, pErk1/2, total Fak, and pFak(Y925) were determined by immunoblotting. **(C)** The Src kinase mutants mediated transformation potential. The SYF1 cells and SYF1 cells stably expressing Src(WT), Src(Y529F), Src(Y529F/S3C/S6C), Src(Y529F/G2A), or Src(Y529F/K298M) were subjected to the soft agar assay. The number of colonies is reported as the mean ± SEM. The expression levels of Src kinase were confirmed before the assay (not shown). **(D)** The SYF1 cells and SYF1 cells stably expressing Fyn(WT), Fyn(Y528F), Fyn(Y528F/C3S/C6S), Fyn(Y528F/G2A), or Fyn(Y528F/K298M) were subjected to the soft agar assay. The number of colonies is reported as the mean ± SEM. Representative phase and RFP images of colonies generated from the soft agar assay of the above were displayed. *P<0.05, **P<0.01.

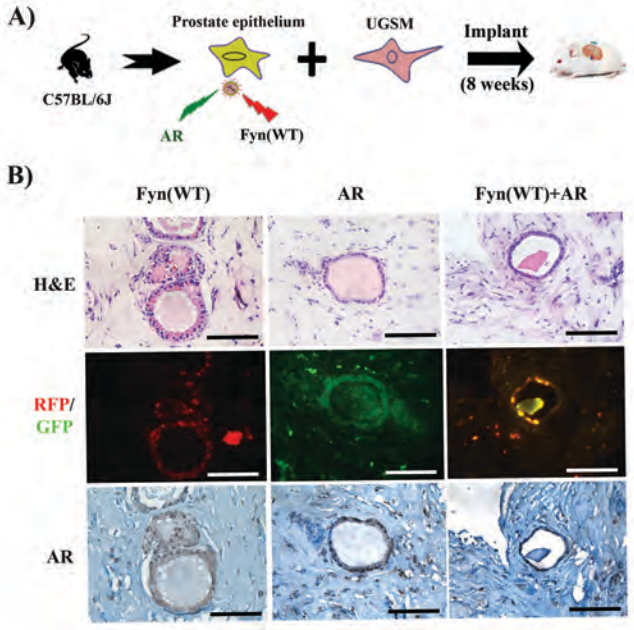

Figure S3.4. Fyn kinase has no synergistic effect with androgen receptor (AR). (A) Schematic for examining the synergy of Fyn and AR in prostate tumorigenesis. Primary prostate epithelial cells (from Bl6 mice) were transduced with AR (GFP marker), Fyn(WT) (RFP marker), or co-transduced with Fyn(WT) and AR by lentiviral infection. The infected cells were combined with UGSM, and implanted under the renal capsule of SCID mice. Regenerated prostate tissue was isolated after 8 weeks. **(B)** H&E, RFP/GFP, and IHC staining of AR in regenerated tissue. Scale

bar, 100 μm. No pathological phenotype was observed in Fyn(WT)+AR regenerated tissues, suggesting no synergistic effect of Fyn(WT) and AR in tumor progression.

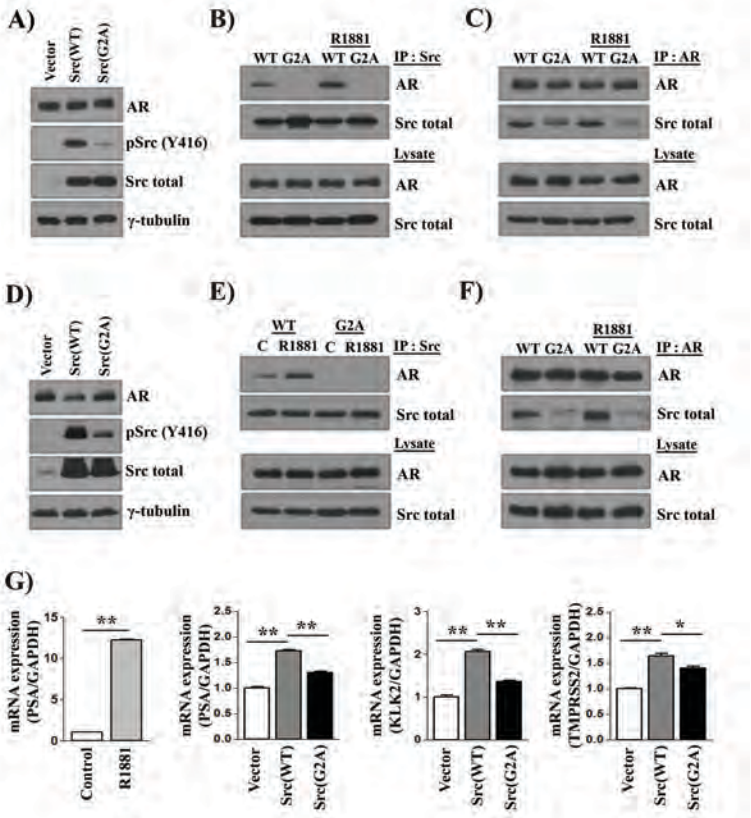

Figure S3.5. Loss of myristoylation in Src kinase inhibits its interaction with androgen receptor (AR) and activation of AR down-stream signaling. (A and D) 22Rv1 and LNCaP prostate cancer cells were transduced with Src(WT), Src(G2A), or control by lentiviral infection. The expression of total Src, pSrc(Y416), and AR in 22Rv1 (A) and LNCaP (D) cells were confirmed by Western blot analysis. **(B-C and E-F)** Protein-protein interactions between endogenous AR and overexpressed Src(WT) or Src(G2A). Src and AR were detected by immunoprecipitation (IP) from 22Rv1 cells (B and C) and LNCaP (E and F) in the presence or

absence of the AR agonist R1881 (5 nM). **(G)** The mRNA levels of PSA, KLK2, and TMPRSS2 genes by synergy of exogenously expressed Src(WT)/Src(G2A) in LNCaP cells. The addition of R1881 on the regulation of PSA in LNCaP cells was a positive control. *P<0.05, **P<0.01.

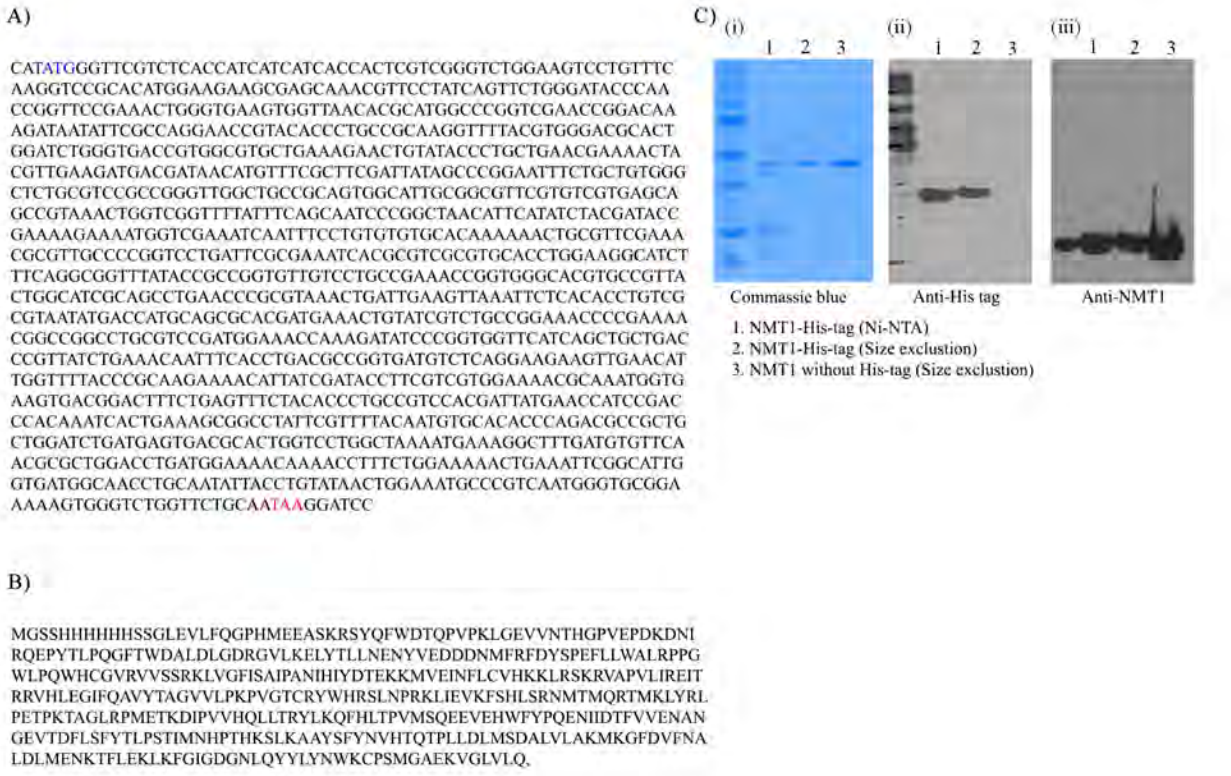

Figure S3.6. Expression and purification of NMT1. (A) The human NMT1 DNA sequence (with an exclusion of the 108 amino acids DNA sequence in the N-terminus) was optimized for bacterial expression and synthesized by GenScript. **(B)** Comparison of protein sequences between the full-length NMT1 protein (upper panel) and the purified NMT1 (lower panel). The N-terminus of NMT1 possesses an inhibitory function of the NMT1 enzymatic activity (8). To increase the enzymatic activity of NMT1 for inhibitor screening, the un-highlighted N-terminal region in NMT1 protein was excluded and an N-terminal His_6-tag was added for the protein purification (Lower panel). **(C)** The NMT1 gene was expressed in *Escherichia coli*. The protein was purified by Ni-NTA affinity chromatography (Lane 1). The purified protein was further purified by anion exchange chromatography (Lane 2). The His_6-tag was removed by HRV 3C protease by enzymatic

digestion (Lane 3). The processed protein was used for enzymatic assays and crystallization. Protein was detected by Coomassie blue staining (i), Western blot analysis using anti-His_6-tag (ii), and human NMT1 antibody (iii).

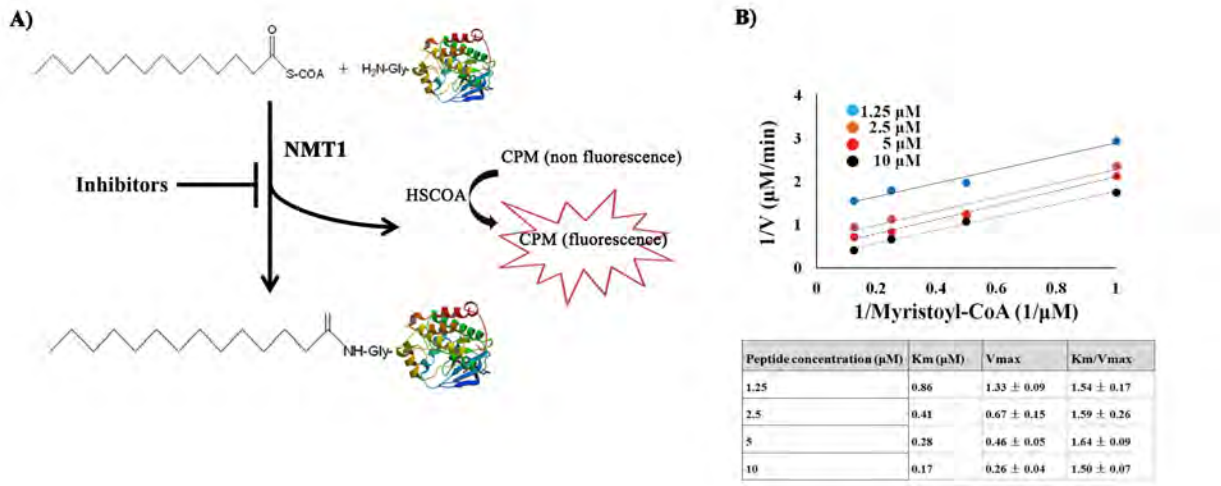

Peptide concentration (µM)	Km (µM)	Vmax	Km/Vmax
1.25	0.86	1.33 ± 0.09	1.54 ± 0.17
2.5	0.41	0.67 ± 0.15	1.59 ± 0.26
5	0.28	0.46 ± 0.05	1.64 ± 0.09
10	0.17	0.26 ± 0.04	1.50 ± 0.07

Figure S3.7. Kinetic analysis of purified NMT1. **(A)** NMT1 catalyzes the attachment of the myristoyl- group from myristoyl-CoA to the N-terminal Gly of a peptide or protein, and releases HSCoA. The reaction of HSCoA with 7-diethylamino-3-(4'-maleimidylphenyl)-4-methylcoumarin (CMP), is detected by fluorescence (excitation 390 nm and emission at 479 nm). Inhibitors were examined for their ability to reduce fluorescence. **(B)** Kinetic characterization of the purified NMT1. Lineweaver–Burk plots of hNMT1 with different concentrations of myristoyl-CoA (1, 2, 4, or 8 µM) in the presence of 1.25, 2.5, 5, or 10 µM of the peptide. Km and Vmax are reported and the Km/Vmax remained the same.

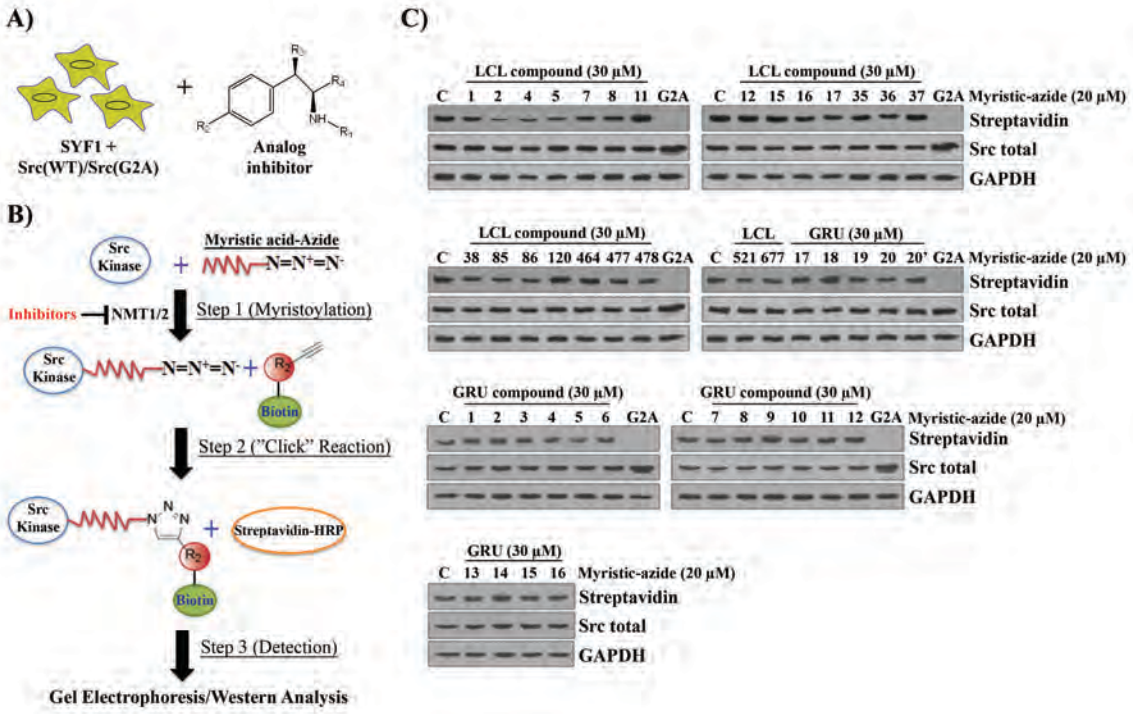

Figure S3.8. Identifying compounds inhibiting Src myristoylation by Click chemistry. (A) Schematic of the experimental design to examine the inhibitory effect of a compound on the myristoylation of Src kinase at the cellular level. SYF1 cells expressing Src(WT) or Src(G2A), a positive control of un-myristoylated-Src were cultured in a DMEM medium with 2% BSA and 30 μM of a compound for 24 h,followed by addition of myristic acid-azide to the medium. Cells were harvested for the detection of myristoylated-Src by Click chemistry. **(B)** Schematic of the Click reaction to detect the myristoylation of Src kinase. The incorporation of myristic acid-azide to Src kinase is catalyzed by NMT enzymes, which will be reduced by an inhibitor. The myristoylated-Src in protein lysate is labeled by biotin-alkyne via the Click chemistry reaction. The labeled myristoylated-Src is detected by streptavidin-HRP in Western analysis. **(C)** The expression of myristoylated Src was detected by streptavidin-HRP, and the expression of total Src and GAPDH under treatment of LCL and GRU compounds was also measured by Western blot analysis.

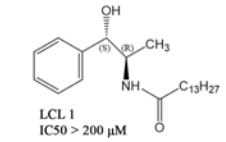

LCL 1
IC50 > 200 μM

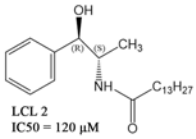

LCL 2
IC50 = 120 μM

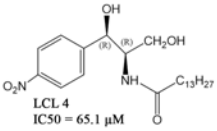

LCL 4
IC50 = 65.1 μM

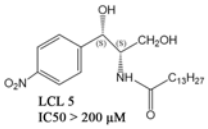

LCL 5
IC50 > 200 μM

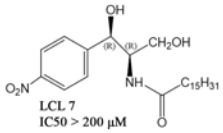

LCL 7
IC50 > 200 μM

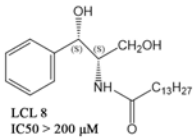

LCL 8
IC50 > 200 μM

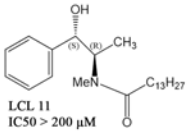

LCL 11
IC50 > 200 μM

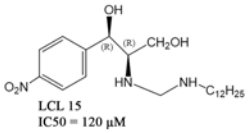

LCL 15
IC50 = 120 μM

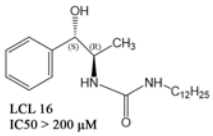

LCL 16
IC50 > 200 μM

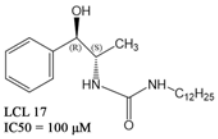

LCL 17
IC50 = 100 μM

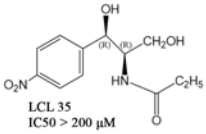

LCL 35
IC50 > 200 μM

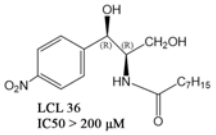

LCL 36
IC50 > 200 μM

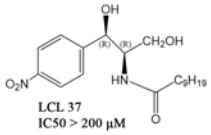

LCL 37
IC50 > 200 μM

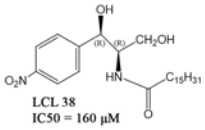

LCL 38
IC50 = 160 μM

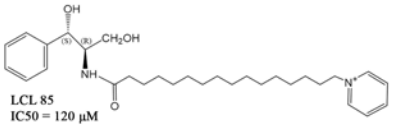

LCL 85
IC50 = 120 μM

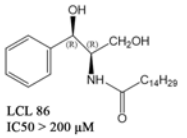

LCL 86
IC50 > 200 μM

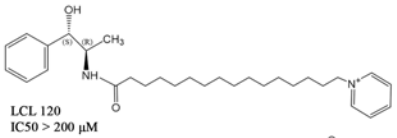

LCL 120
IC50 > 200 μM

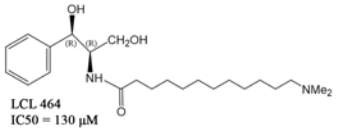

LCL 464
IC50 = 130 μM

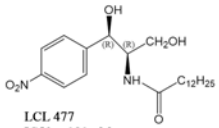

LCL 477
IC50 = 181 μM

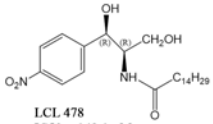

LCL 478
IC50 = 149.1 μM

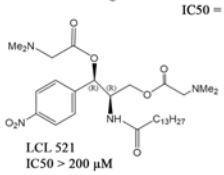

LCL 521
IC50 > 200 μM

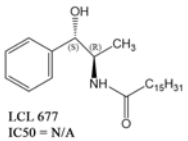

LCL 677
IC50 = N/A

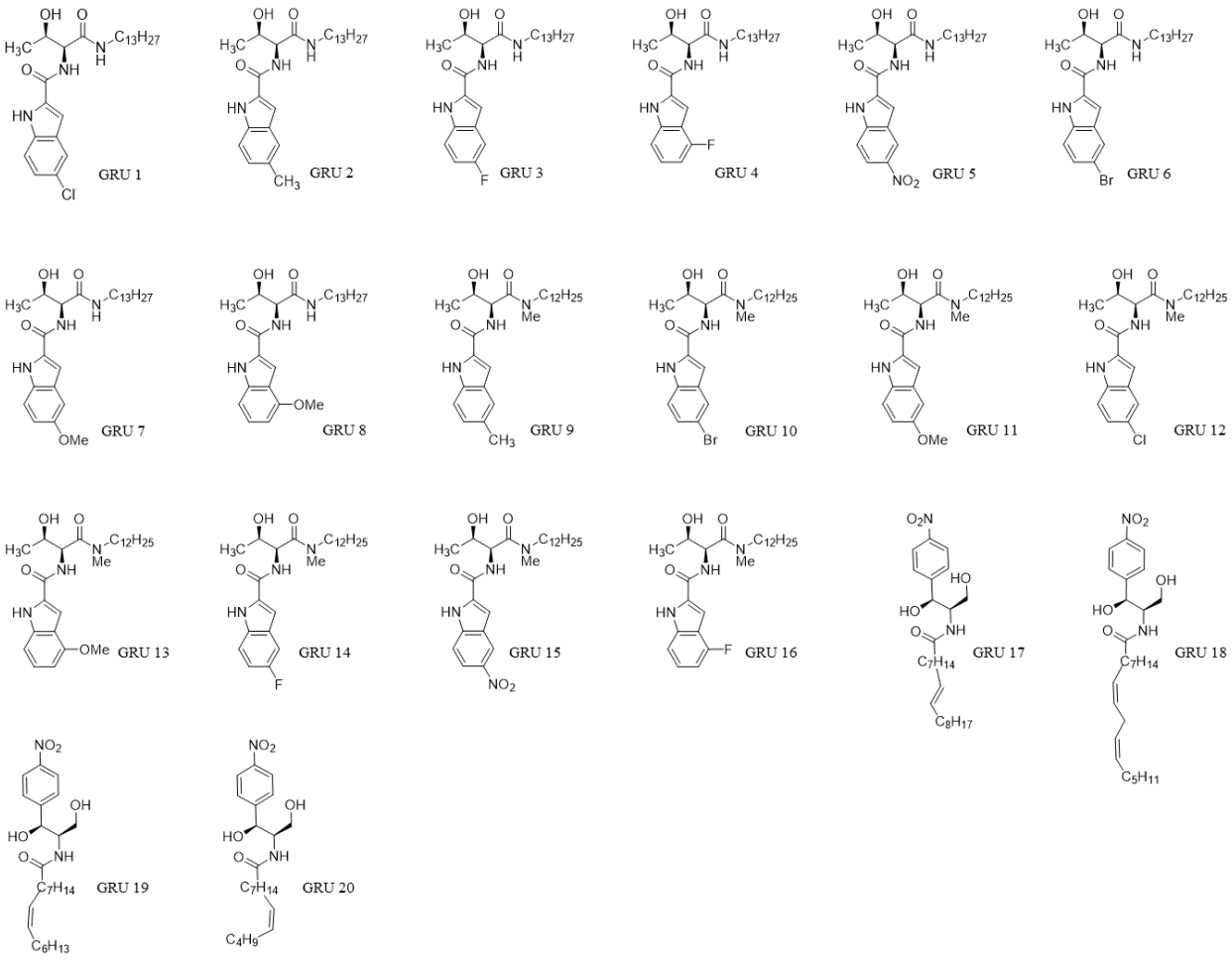

Figure S3.9. Structures and/or IC_{50} values of LCL and GRU compounds. The LCL compounds were previously synthesized by Dr. Bielawska Alicja's lab. The compounds GRU1-20 were synthesized by Dr. Iryna Lebedyeva's lab. The IC_{50} of LCL compounds were measured by the fluorescence-based assay as described in the Figure S7A. GRU compounds were not further studied due to no activity in inhibition of Src myristoylation shown in Figure S8C.

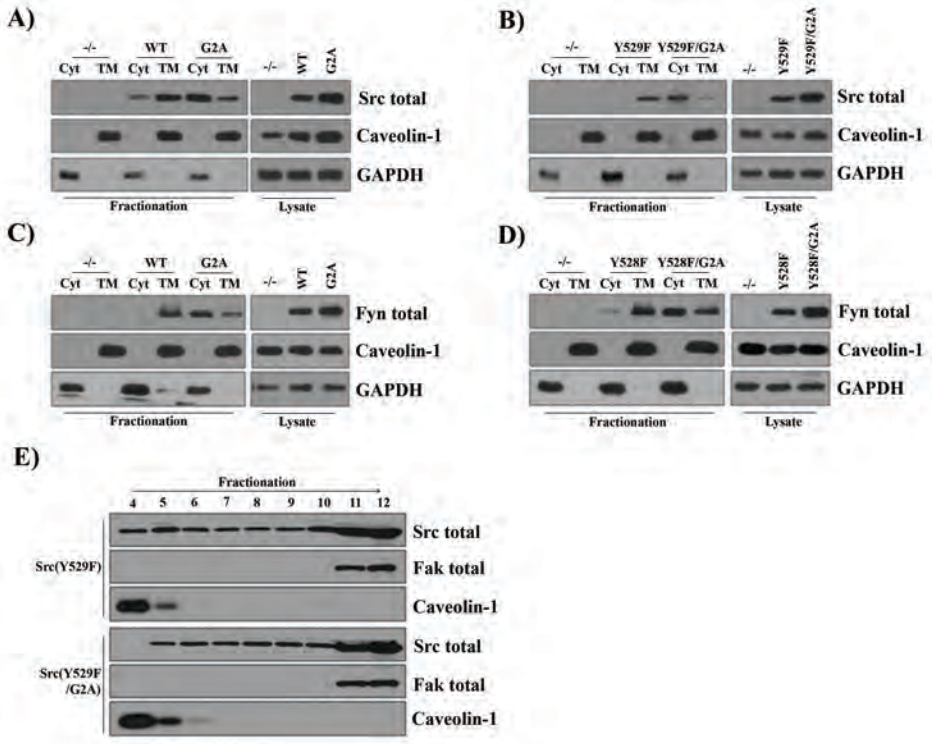

Figure S3.10. Loss of myristoylation inhibits the localization of Src kinase at the cytoplasmic membrane. (A-D) Expression levels of Src kinase in the cytosol (Cyt) and total membrane (TM) fractions were determined by immunoblotting. SYF1 ($Src^{-/-}Yes^{-/-}Fyn^{-/-}$) cells stably expressed **(A)** Src(WT)/Src(G2A), **(B)** Src(Y529F)/Src(Y529F/G2A), control vector (-/-), **(C)** Fyn(WT)/Fyn (G2A), or **(D)** Fyn(Y528F)/Fyn(Y528F/G2A). Cell lysates were fractionated into cytosolic and membrane fractions. Caveolin-1 and GAPDH were used as markers for TM and Cyt fractions, respectively. The ratio of Src or Fyn in the membrane versus the cytosol fraction was much higher in Src(WT)/Src(Y529F) compared with Src(G2A)/Src(Y529F/G2A), or in Fyn(WT)/Fyn(Y528F) compared with Fyn(G2A)/Fyn(Y528F/G2A). **(E)** Localization of Src(Y529F) and Src(Y529F/G2A) in lipid rafts by sucrose gradient centrifugation and immunoblotting. Following centrifugation, twelve fractions were collected starting from the top (#4) to bottom (#12). Src

kinase, Fak, and Caveolin-1 (lipid raft marker) were detected in equal aliquots of each fraction by immunoblotting. Src kinase could not be detected in fractions 1-3 (not shown).

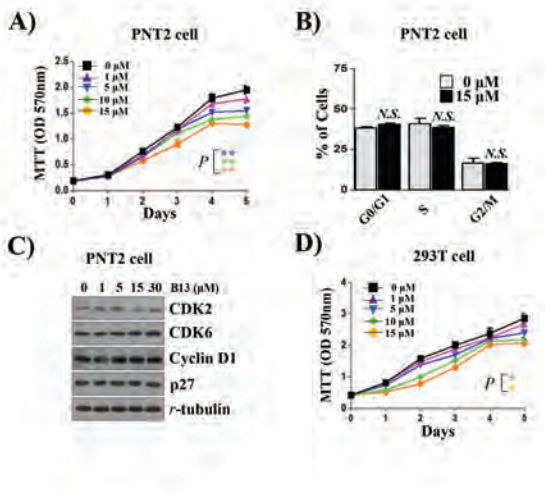

Figure S3.11. The myristoyl-CoA analog, B13 has limited effect in PNT2 normal prostate cells and 293T cells. (A) PNT2 cells were cultured in the medium with 0, 1, 5, 10, or 15 μM B13. The media with compound were replaced daily and cell viability was determined by the MTT assay. **(B)** PNT2 cells were cultured in the medium with 0 or 15 μM B13 for 3 days. The cells were collected and stained with propidium iodide for cell cycle analysis. The percentage of cells in G0/G1, S, and G2/M phases were recorded by flow cytometry. **(C)** PNT2 cells treated with 0, 1, 5, 10, or 15 μM B13 were analyzed for the expression of CDK2, CDK6, cyclin D1, p27, and tubulin. **(D)** 293T cells were cultured with 0, 1, 5, 10, 15 μM B13 for 5 days. Cell viability was determined by the MTT assay. B13 showed limited inhibition on 293T cells. N.S. no significant; *: $p<0.05$; **:$p<0.01$.

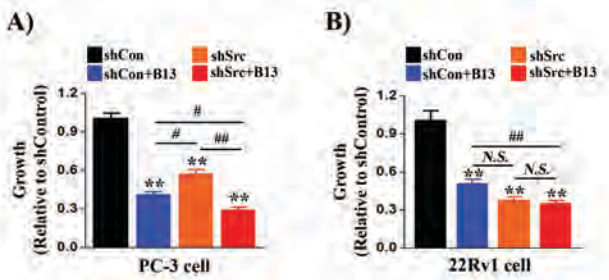

Figure S3.12. The additive effect of B13 with knockdown of Src kinase in regulating proliferation of 22Rv1 and PC-3 cells. 22Rv1 and PC-3 cancer cells were transduced with control or shRNA-Src, and treated with or without B13. Proliferation was measured by the MTT assay. **(A)** The inhibition of the proliferation of PC-3 cells in B13+shRNA-Src group were lower than shRNA-Src or B13 group, suggesting B13 had additive effect with shRNA-Src, but was largely over-lapped. **(B)** The inhibition on the proliferation of 22Rv1 cells in B13+shRNA-Src group had no significant difference in comparison with shRNA-Src group, suggesting B13 had no additive effect with shRNA-Src in 22Rv1 cells. Collectively, consistent with genetic knockout presented in Figure 2E, inhibition by B13 on NMT activity largely overlapped with shRNA-Src. **: $p<0.01$ (each treatment group was compared with the control group). #: $p<0.05$; ##:$p<0.01$ (the compared groups were indicated in the figure).

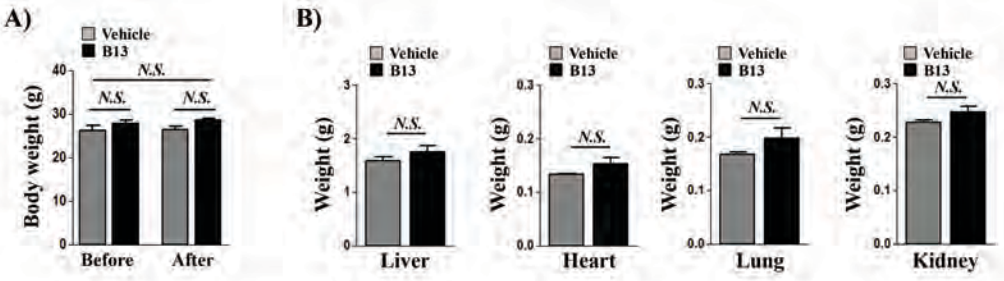

Figure S3.13. Effects of B13 in host mice. (A-B) PC-3 prostate cancer cells were subcutaneously injected into both flank sides of SCID mice (3 months-old, n=6 per group). Vehicle or B13 (75mg/kg/mouse) was administered intravenously twice a week for 6 weeks. The body weight before and after B13 treatment (A) and the weight of major organs (the liver, heart, lung, and kidney) with/without B13 treatment (B) were measured as mean $\pm$ SEM. N.S.: no significant difference.

CHAPTER 4

N-MYRISTOYLTRANSFERASE 1 REGULATES DEGRADATION OF ANDROGEN RECEPTOR PROTEIN IN PROSTATE CANCER CELLS

Omar Awad Alsaidan, Emmanuel Onobun, Lei Lou, Zanna beharry, Zhong-Ru Xie, Iryna Lebedyeva, David Crich, Houjian Cai

Submitted to Cell Chemical Biology- Brief Communication journal

Graphical abstract

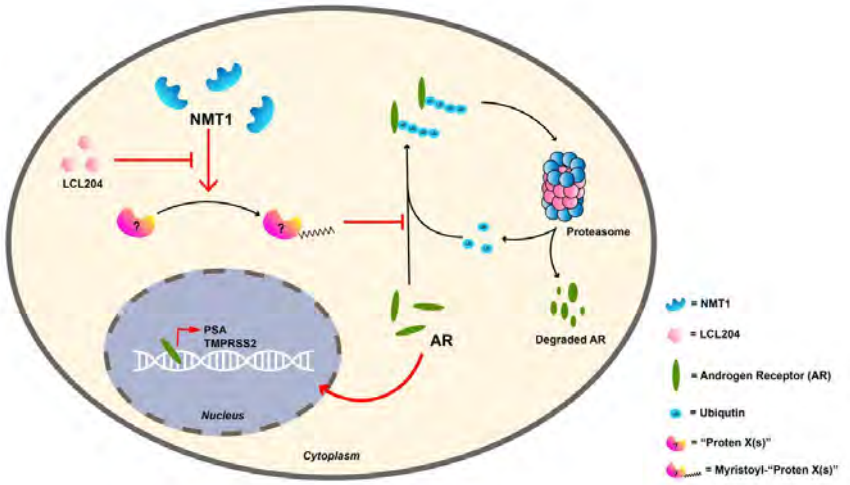

In Brief:

NMT1 regulates functions of a set of proteins by facilitating its myristoylation. NMT1-mediated protein myristoylation inhibits AR ubiquitination and degradation and enhances its transcriptional activity in prostate cancer cells. Inhibition of NMT1 levels genetically or NMT1 activity pharmacologically by LCL204 suppress myristoylation of unknown protein(s), thereby enhancing AR-ubiquitination and degradation through the proteasome pathway.

Highlights:

- Inhibitory efficacy on N-myristoyltransferase activity by D-NMAPPD is stereospecific.
- (1*R*,2*R*)-LCL204 reduced global N-myristoylation and androgen receptor protein levels at low micromolar concentrations.
- (1*R*,2*R*)-LCL204 reduced AR full-length or variant protein levels and their transcriptional activity in prostate cancer cells.
- Genetic and pharmacological inhibition of NMT1 enhances ubiquitin-mediated proteasome degradation of AR.

Summary:

Even though prostate cancer patients initially respond to androgen deprivation therapy, some will eventually develop castration resistant prostate cancer (CRPC). However, androgen receptor (AR) signaling still remains a major driver in the progression of CRPC. In this study, we demonstrate that AR protein levels were regulated by N-myristoyltransferase 1 expression levels and activity in prostate cancer cells. A small molecule compound (1*R*,2*R*)-D-NMAPPD, but not its enantiomer(1*S*,2*S*)-D-NMAPPD, inhibited NMT1 activity and reduced AR protein levels. (1*R*,2*R*)-LCL204, a derivative of (1*R*,2*R*)-D-NMAPPD, inhibited global protein myristoylation. Additionally, genetic regulation of NMT1 levels and pharmacological inhibition of NMT activity suppressed protein levels, nuclear translocation, and transcriptional activity of AR full-length or variants in prostate cancer cells. This was due in-part to enhanced ubiquitin and proteasome-mediated degradation of AR. Overexpression of NMT1 promoted prostate cancer progression by synergizing with AR, and knockdown of NMT1 inhibited growth of castration resistant prostate xenograft tumors. This study illustrates a novel function of protein myristoylation and provides a strategy for treatment of CRPC.

Introduction

Prostate cancer is the second leading cause of cancer-related deaths in men in developed countries (1). Androgen receptor (AR) signaling is crucial in prostate development and cancer progression (2, 3). Medical or surgical androgen deprivation therapy (ADT) is usually a standard treatment for prostate cancer patients (4). Tremendous effort has been made in developing effective treatments by targeting androgen synthesis and/or AR signaling, however patients usually develop ADT resistance and progress to castration resistance prostate cancer (CRPC) (5-7). Multiple molecular mechanisms have merged in CRPC cells including an increase of AR expression, AR mutations, intratumoral androgen synthesis, and AR splice variants, and others (8, 9). As a result, AR signaling remains active (3, 10), and targeting AR signaling still remains as an effective treatment approach for CRPC (11, 12).

While current treatment approaches mainly rely on inhibition of circulated androgen and blockade of androgen/AR interaction, direct degradation of AR levels has been considered as another effective strategy to inhibit AR-pathway mediated cancer progression (13). Post-translational modifications (PTMs) including phosphorylation, methylation, acylation, SUMOylation, and ubiquitination, regulate AR stability and activity (14). Particularly, AR ubiquitination regulates AR protein turnover and transcriptional activity (14-16). Although numerous E3 ligases have been reported to associate with the AR ubiquitination process (15)(17)(18)(19)(20)(21), pharmacological inhibition leading to increased ubiquitination-mediated AR degradation has not been well established.

N-Myristoylation is a co/post-translational lipid modification process where myristic acid, a 14 carbon saturated fatty acid, is attached to an N-terminal glycine (22). In humans, two enzymes facilitate modification by N-myristoylation; NMT1 and NMT2, which share 77% sequence

similarity (23). A panel of proteins possess the modification in mammalian cells (24). For example, oncogenic proteins including Src, PKA, and AMPK require myristoylation for their functions (31-34). N-myristoylation promotes stability and association with the cytoplasmic membrane, and facilitates protein-protein interaction (32, 35, 36). As a result, NMT1 regulates molecular functions of these downstream proteins (25-28), subsequently controlling cancer cell proliferation (29, 30).

An inhibitory role for NMT in cancer progression makes it an attractive therapeutic target for anticancer drug development (37). Several small molecule compounds have been discovered that inhibit NMT activity. We have previously reported that genetic ablation of NMT1 or the small molecule compound D-NMAPPD (B13) inhibited prostate cancer proliferation through suppression of Src kinase activity (38). However, controversy regarding this compound targeting NMT activity has arisen (42). In this study, we discovered that the absolute stereochemical configuration of D-NMAPPD is important in inhibition of NMT1 activity. More importantly, we demonstrated that NMT1 regulated AR protein levels, nuclear translocation, and AR transcriptional activity in prostate cancer cells. Genetic and pharmacological inhibition of NMT1 promoted AR degradation through the ubiquitin proteasome pathway. Given the important role of NMT1 in mediating prostate cancer progression, our study demonstrates a novel function of NMT1 and provides a potential strategy for treatment of CRPC through AR degradation.

Materials and Methods:

Cell culture and reagents

The human prostate cancer cell lines LNCaP, 22RV1, C4-2B, and VCaP were purchased from the American Type Culture Collection (ATCC). All the cell lines were cultured using the ATCC recommended medium of RPMI-1640 with 10% fatal bovine serum (FBS) (Corning) and 1% streptomycin/penicillin (Thermo Fischer Scientific). Cells were maintained in a 37 °C incubator with 5% carbon dioxide (CO_2). All the cell lines purchased from the ATCC had a certificate indicating they are mycoplasma-free.

Plasmid construction and lentiviral production

The open reading frame of human NMT1 (#25274, Addgene) and human AR (43) were cloned into FUCRW or FUCGW lentiviral vectors as described (44, 45). The expression was under the control of the human ubiquitin promoter. To knockdown human NMT1, shRNA target sequences were inserted into psiRNA-W [H1.4] vector at the BbsI site. The H1 promoter together with shRNA was further sub-cloned into FUCRW or FUCGW at the PacI site. The primers used for cloning are listed in Table S1. Lentivirus was generated in HEK293T cells by co-transfecting the lentiviral packaging vectors including MDL, REV, and VSV and a lentiviral vector expressing the gene of interest such as NMT1, AR, or shRNA-NMT1. Virus infection was performed as described previously (46). All lentivirus procedures followed the guidelines and regulations of the University of Georgia.

Western blot and antibodies

Cells were lysed in by incubation in RIPA buffer [20 mM Tris-HCl (pH 7.4), 137 mM NaCl, 1% Triton X-100, 0.5% sodium deoxycholate, 10% glycerol, 0.1% SDS, and EDTA-free protease inhibitor cocktail set V (Millipore, 539137)] on ice for 20 minutes. After short sonication, cell lysates were centrifuged at 12,000 rpm for 20 minutes, and supernatants were collected for downstream analysis. Twenty micrograms of proteins were subjected to SDS-polyacrylamide gels before being transferred onto nitrocellulose membranes (Bio-Rad). Membranes were blocked with 5% milk powder (Lab1 Scientific) in 1X TBS containing 1% Tween-20 (TBST) for 1 h, washed with TBST, and incubated with the specific antibodies overnight at 4 ^{o}C. After washing membranes 3 times with TBST, they were incubated with the appropriate secondary antibody for 1 h at room temperature.

AR antibody (1:1000) was purchased from Santa Cruz Biotechnology (Dallas, TX) (#441) or Millipore Sigma (Burlington, MA) (#06-680). Antibodies against ubiquitin (#3933), HDAC-1 (#5356) (1:1000), and GAPDH (#2118) (1:2500) were purchased from Cell Signaling Technology (Beverly, MA). The anti-NMT1 (#HPA022949) and γ-tubulin (#T6557) antibody were purchased from Sigma Chemical Co. (St. Louis, MO) and Calbiochem (San Diego, CA).

Quantitative RT-PCR analysis

Total RNA was extracted from cultured cells using TRIzol reagent according to the manufacturer's instructions. One μg of total RNA was reverse transcribed using the High-Capacity cDNA Kit (Applied Biosystem). The cDNA samples were used for quantitative RT-PCR reactions. Each PCR reaction contained the synthesized cDNA, SYBR Green (PerfeCTa SYBR Green FastMix, Quantabio), and primers at concentrations of 10 pM each. The primers are listed in Table S1. StepOne Software v2.1 (Applied Biosystem) was used to quantify PCR reactions and expression

levels of a target gene was normalized to GAPDH levels in the corresponding samples. Each PCR reaction was done in triplicate.

Isolation of the cytoplasmic and nuclear protein fractions

Isolation of nuclear and cytoplasmic fractions were prepared using NE-PER Nuclear and Cytoplasmic extraction kit (Cat# 78833, ThermoFischer Scientific) according to manufacturer's protocol. Briefly, cell pellets were washed with cold PBS and centrifuged at 600 g for 5 min. The cell pellet was resuspended with 200 µL cytoplasmic extraction reagent containing protease inhibitor. The cell lysates were vortexed for 15 sec followed by incubation on ice for 10 min. The cytoplasmic extraction reagent II (11 µL) was added to the sample and vortexed for 5 sec. After incubation on ice for 5 min, the lysates were centrifuged at 15,000 g for 5 min. The cytoplasmic fraction (supernatant) was transferred to a new tube. Nuclear extraction reagent (100 µl) was added to the insoluble pellet and incubated on ice for 40 min with vortexing for 15 sec at 10 min intervals. After samples were centrifuged at 15,000 g for 10 min, the supernatant (nuclear fraction) was collected and transferred to a new tube.

Quantitative analysis of AR fluorescence

Subcellular localization of androgen receptor protein and its fluorescence intensity were determined by fluorescence microscopy using a Zeiss Axio observer A1 microscopy with a 40x objective lens (Carl Zeiss Microimaging Inc., Germany). LNCaP cells were treated with 5 µM LCL204 for 48 h. Cells were fixed for 10 min with 4% paraformaldehyde/PBS (Affymetrix, USA), washed with PBS and permeabilized with 0.5% Triton-X100 in PBS for 5 min. Cells were blocked with 5% goat serum and incubated with AR antibody overnight. Cells were washed with PBS and

incubated with Alexa Fluor 488 Goat Anti-Rabbit IgG (Invitrogen, USA) secondary antibody (1:700). Cells were mounted with PBS/DAPI. To evaluate AR intensity, samples were imaged and analyzed using ZEN software. In brief, channels of images were split using ZEN image channels split tool and the threshold values of fluorescence signals by the ZEN threshold tool were used to determine the fluorescence signal intensity values.

Protein stability and degradation

To assess the effect of shRNA-NMT1 on AR protein stability, LNCaP and 22Rv1 cells were treated with LCL204 for 24 h. One day after the treatment, 10 μM cycloheximide (Cayman Chemicals; 14126) was added to the media of LNCaP and 22Rv1 cells for 2, 4, 6 h. Cell lysates were prepared and protein levels of AR, NMT1, and GAPDH were determined by Western blotting. AR protein degradation was also examined in LNCaP and 22Rv1 cells treated with 10 μM Bortezomib for 9 hrs (Cayman Chemical; 10008822) after one day of treatment with LCL204. Similarly, protein levels of AR, NMT1, and GAPDH were determined by Western blotting.

Immunoprecipitation for the analysis of AR ubiquitination

For the detection of AR ubiquitination, LNCaP cells were transduced with shRNA-NMT1 by lentiviral infection, or LNCaP and 22Rv1 cells were treated with 5 μM LCL204 for 48 hrs. The transduced or LCL204-treated cells were grown in 10 cm dishes, and cell lysates were extracted with the immunoprecipitation (IP) lysis buffer (20 mM HEPES, pH 7.5, 150 mM NaCl, 1 mM EGTA, 10% glycerol, 1% Triton X-100, 1.5 mM $MgCl_2$) containing protease inhibitor and phosphatase inhibitor. One mg of protein was incubated with androgen receptor (AR) (#441)

antibody for 16 h at 4 ℃. Protein A agarose beads (30 μl) were added to the lysate, and the mixtures were incubated for 2 h at 4 ℃. After the incubation, the beads were washed three times with IP lysis buffer followed by addition of 2X SDS sample buffer and heated at 98 ℃ for 10 min. Ubiquitinated AR was detected by the ubiquitin antibody and AR antibody (Santa Cruz Biotechnology, Inc., SC-7305).

Xenograft tumors

To examine the effect of NMT1 knockdown on AR protein expression and tumor growth *in vivo*, 22Rv1 (5×10^5) and C4-2B (2×10^6) cells transduced with shRNA-NMT1 or control by lentiviral infection were subcutaneously inoculated in the flank side of SCID male mice. Body weight and tumor size were measured (length × width × width/2) weekly. 22Rv1 and C4-2B xenograft tumors were harvested after 8 weeks or when the humane endpoint was reached. Grafts were subjected for hematoxylin and eosin (H&E) and immunohistochemistry (IHC) analysis. All animals were maintained according to the surgical and experimental procedures of the protocol A2013 03-008 approved by the institutional animal use and care committee at the University of Georgia.

Immunohistochemistry

Formalin-fixed/paraffin-embedded grafts were sectioned at 5 μm thickness and mounted to positively charged microscopic slides. H&E and immunohistochemistry (IHC) staining analysis were performed as described previously (45). The following primary antibodies and dilutions were used for immunohistochemistry analysis: AR (Santa Cruz Biotechnology, Inc., SC-7305; 1:400), NMT1 (Sigma Aldrich, HPA022963; 1:200), Ki67 (Novus Biologicals, NB500-170; 1:400), and cleaved Caspase-3 (Cell Signaling Technology, 9661; 1:200).

Synthesis of (1*R*, 2*R*)-D-NMAPPD (LCL4) and (1*R*,2*R*)-LCL204

For (1*R*,2*R*)-D-NMAPPD (LCL4) synthesis, (2*R*,3*R*)-2-amino-1-(4-nitrophenyl)-1,3-propanediol (0,1 mmol, 212 mg) was dissolved in dry THF (50 mL) and cooled to 4 ^{o}C followed by addition of EDCI (156 mg, 1 mol), HOBt (135 mg, 1 mmol), and tetradecanoic acid (228 mg, 1 mmol). The mixture was kept under N_2 at room temperature overnight. After the reaction mixture was taken to dryness, the product was extracted with ethyl acetate. The extracts were washed with aqueous sodium carbonate and then 3 M hydrochloric acid, dried and evaporated to give crude (1*R*,2*R*)-D-NMAPPD. Product (1*R*,2*R*)-D-NMAPPD (47) was then purified by column chromatography over silica gel using ethyl acetate:hexane 1:10 as eluent.

For (1*R*,2*R*)-LCL204 synthesis, (2*R*,3*R*)-2-amino-1-(4-nitrophenyl)-1,3-propanediol (1 mmol, 212 mg) was reacted with tetradecanal (255 mg, 1.2 mmol) in methanol/0.05 N acetic acid, 9:1 for 15 min and sodium cyanoborohydride ($NaCNBH_3$, 130 mg, 2 mmol) was added in portions over 1 h. The mixture was stirred overnight at room temperature, evaporated to dryness and the residue dissolved in DCM/MeOH, 2:1. The product was purified by recrystallization from DCM/pentane 1:3 to give (1*R*,2*R*)-LCL204 (48) as white solid in 72 % yield.

Characterization of synthetic and commercial D-NMAPPD by NMR spectroscopy and polarimetry

(1*R*, 2*R*)-D-NMAPPD was synthesized in-house as described above, and D-NMAPPD [also called (1*R*, 2*R*)-B13] was purchased from Cayman Chemical (Item No. 10006305; CAS No. 35922-06-6). Due to different biological efficacies in inhibition of global protein myristoylation reported by two different labs (38, 42), we examined the chemical differences of these two compounds. After various measurements, it was established that the D-NMAPPD from Cayman Chemical is the

enantiomer of the in-house synthesized (1*R*,2*R*)-D-NMAPPD. Identical NMR spectra were obtained for the two samples, indicating them to have the same relative configuration (additional measurements also in the Supplemental Materials and Methods):

NMR spectra were recorded in methanol-d_4 using a 500 MHz instrument. The (1*S*,2*S*)-D-NMAPPD was characterized as follows: ^{1}H NMR (500 MHz, CD_3OD) δ 8.15 (d, *J* = 8.8 Hz, 2H, 2Ar), 7.61 (d, *J* = 8.7 Hz, 2H, 2Ar), 5.11 (d, *J* = 2.8 Hz, 1H, benzylic), 4.16 (ddd, *J* = 7.5, 5.8, 2.8 Hz, 1H), 3.74 (dd, *J* = 10.8, 7.5 Hz, 1H, CH_2'), 3.54 (dd, *J* = 10.7, 5.9 Hz, 1H, CH_2''), 2.06 (t, *J* = 7.3 Hz, 2H, $2CH_2$), 1.43 – 0.98 (m, 22H, $11CH_2$), 0.88 (t, *J* = 6.9 Hz, 3H, CH_3). The (1*R*, 2*R*)-D-NMAPPD was characterized as follows: ^{1}H NMR (500 MHz, CD_3OD) δ 8.15 (d, *J* = 8.8 Hz, 2H, 2Ar), 7.61 (d, *J* = 8.7 Hz, 2H, 2Ar), 5.11 (d, *J* = 2.8 Hz, 1H, benzylic), 4.16 (ddd, *J* = 7.5, 5.8, 2.8 Hz, 1H), 3.74 (dd, *J* = 10.8, 7.5 Hz, 1H, CH_2'), 3.54 (dd, *J* = 10.7, 5.9 Hz, 1H, CH_2''), 2.06 (t, *J* = 7.3 Hz, 2H, $2CH_2$), 1.43 – 0.98 (m, 22H, $11CH_2$), 0.88 (t, *J* = 6.9 Hz, 3H, CH_3).

Specific rotations for the two samples were measured in methanol on an automatic polarimeter with a path length of 10 cm, and were found to be equal within experimental error but opposite in sign pointing to their enantiomeric nature: (1*S*,2*S*)-D-NMAPPD had $[\alpha]^{20}_D$ + 4.2 (c = 0.19, CH_3CH_2OH), while (1*R*, 2*R*)-D-NMAPPD had $[\alpha]^{20}_D$ -3.6 (c = 0.21, CH_3CH_2OH).

Molecular docking of two D-NMAPPD stereoisomers

The crystal structure of NMT1 used in this study was retrieved from the RCSB PDB database (PDB file ID: 5UUT) (38). Models of the enantiomers of (1*R*,2*R*)-D-NMAPPD and (1*S*,2*S*)-D-NMAPPD were prepared by Ligprep module of Schrodinger Maestro, and the process includes converting 2D structures of ligands to 3D ones, adding hydrogens, calculating partial charges, and optimizing the structures. The protein structure preparation process which includes adding all

hydrogens and missing side chains/loops, deleting useless water molecules, and correcting bond information, were applied to NMT1 structure by Protein Preparation Wizard. Water beyond 5.00 Å from het groups (i.e. ligand atoms) were deleted and generated het status's pH = 7.0 +/- 2.0. An optimization of H-bonds assignment was performed. The PROPKA was kept at 7.0. The system was minimized to cover heavy atoms to RMSD 0.30 Å using force field OPLS3e. For ligands preparation, the same features mentioned above were applied to keep pH = 7.0 +/- 2.0. Enantiomers of the stereoisomers of D-NMAPPD were generated. Finally, XP (extra-precision) docking was applied for identifying the binding interactions. As for Van der Waals radii scaling, the scaling factor was set to 0.80 and partial charge cutoff was set to 0.15 to soften the potential for non-polar parts of the ligands.

Statistical analysis

Statistical analysis was performed using GraphPad prism (GraphPad Inc., La Jolla, CA). The data are presented as mean ± S.E. and analyzed using Student's t-test for experiments containing two groups and one-way analysis of variance (ANOVA) followed by Tukey post-hoc test for experiments containing more than two groups. All t tests were performed at the two-sided 0.05 level for significance. *, $p < 0.05$; **, $p < 0.01$.

RESULTS:

(1*S*,2*S*)-D-NMAPPD, the enantiomer of (1*R*,2*R*)-D-NMAPPD (LCL4) lost its inhibitory efficacy on global protein myristoylation.

N-myristoyltransferases are involved in numerous essential cellular functions (22). Loss of NMT1 results is embryonic lethal (49) and inhibits proliferation of cancer calls (29, 38, 50). We have previously reported that an NMT1 inhibitor, (1*R*,2*R*)-D-NMAPPD (LCL4), which was synthesized in-house, inhibits protein myristoylation with IC_{50} = 77.6 μM (38). However, a recent study showed that commercial D-NMAPPD (from Cayman Chemical, Cat#10006305) has a limited inhibitory effect on protein myristoylation (42). Seeking to ro resolve this discrepancy, we have determined that the two compounds from different sources are enantiomers. Both compounds have identical ^{1}H and ^{13}C NMR spectra (Fig. 4.1A and Fig. S4.1), molecular weight, elution times in UHPLC (Fig. S4.2), and melting point ranges [(1*S*,2*S*)-D-NMAPPD: 79 – 80 ºC; (1*R*,2*R*)-D-NMAPPD (LCL4): 78 – 80 ºC]. However, the circular dichroism spectra of both compounds showed an enantiomeric relationship, with approximately equal but opposite traces (Fig. 4.1B). The enantiomeric relationship was further confirmed by polarimetry: (1*S*,2*S*)-D-NMAPPD, $[\alpha]^{20}_{D}$ +4.2; (1*R*,2*R*)-D-NMAPPD, $[\alpha]^{20}_{D}$ -3.6) (Fig. 4.1C). The absolute configuration of (1*R*,2*R*)-D-NMAPPD was confimred by hydrolysis of the parent amide to the corresponding amine. Thus, treatment of (1*R*,2*R*)-D-NMAPPD with 10% HCl in methanol generated a (-)-base with identical properties to those previously reported by Rebstock *et al*. (51) (Fig. S4.3). The (-)-base is a precursor of the antibiotic chloramphenicol, a known inhibitor of *Shigella paradysenteriae* (51, 52), whose configuration has been confirmed by optical rotation data (51), optical rotatory dispersion and circular dichroism measurements (53-55).

To examine if the two enantiomers function differently in inhibition of NMT1 activity, both compounds were docked with the crystal structure of NMT1 (38). (1*R*,2*R*)-D-NMAPPD exhibited

lower binding free energy in comparison to (1*S*,2*S*)-D-NMAPPD (Fig. 4.1C). Several favorable interactions between (1*R*,2*R*)-D-NMAPPD and the myristoyl-CoA binding pocket of NMT1 were revealed. These interactions include 1) the hydroxy group of (1*R*,2*R*)- D-NMAPPD with Tyr180 or Leu248 of NMT1; 2) the hydroxymethyl of (1*R*,2*R*)- D-NMAPPD with Thr282 or Ile245; and 3) the amide group with Thr282 (Fig. S4.4A-B). In contrast, only two favorable interactions were observed between (1*S*,2*S*)-D-NMAPPD and the NMT1 binding pocket (Fig. S4.4C-D).

(1*R*,2*R*)-LCL204 is a derivative of (1*R*,2*R*)-D-NMAPPD (Fig. S4.5), which we previously reported inhibits NMT1 activity with IC_{50} = 8.7 μM using purified recombinant NMT1 without the N-terminal inhibitory motif (38, 56). (1*R*,2*R*)-LCL204 inhibited full-length NMT1 activity (Fig. S4.6) with IC_{50} of 2.3 μM (Fig. 4.1D), indicating that loss of the N-terminal motif indeed enhances NMT1 activity (56). The inhibition of three different compounds on global protein myristoylation was further investigated using click chemistry. (1*R*,2*R*)-D-NMAPPD and (1*R*,2*R*)-LCL204, but not (1*S*,2*S*)-D-NMAPPD inhibited global protein myristoylation at 20-30 μM and 5 μM, respectively. More importantly, (1*R*,2*R*)-D-NMAPPD and (1*R*,2*R*)-LCL204 also significantly inhibited AR protein levels (Fig. 4.1E). For simplicity, (1*R*,2*R*)-LCL204 will be called LCL204 from this point of the manuscript.

LCL204 inhibited AR protein levels in the nucleus and its transcriptional activity.

AR activity requires its translocation to the nucleus to activate its downstream genes (3). Therefore, we further investigated if LCL204 inhibits AR levels in the nucleus and its transcriptional activity in prostate cancer cells. LCL204 inhibited both total and nuclear AR protein levels in C4-2B (Fig. 4.2A) and 22Rv1 cells (Fig. 4.2B). Of note, LCL204 inhibited levels of both AR full length (FL) (110 kDa) and AR variant (V7) in 22Rv1 (Fig. 4.2B). Additionally, LCL204

inhibited nuclear translocation of AR-FL protein (110 kDa) in the presence or absence of AR agonist (R1881) and AR-V7 variant in 22Rv1 cells in the absence of R1881 (Fig. 4.2B). This result was further confirmed with immuno-fluorescence analysis. As expected, AR nuclear levels (green fluorescence) were significantly elevated under the induction of R1881 but were inhibited by LCL204 in the presence or absence of R1881 stimulation (Fig. 4.2C). In addition, as expected, R1881 increased mRNA levels of PSA and KLK2 in C4-2B cells (Fig. 4.2D). LCL204 did not change AR mRNA levels in C4-2B and 22Rv1 cells (Fig. 4.2D), but inhibited PSA and KLK2 gene expression with or without R1881 (Fig. 4.2D). Taken together, the data suggest that LCL204 reduces AR protein levels and transcription of its regulated downstream genes, but reduced protein levels is not due to reduced AR transcription.

Knockdown of NMT1 inhibited AR protein levels and its transcriptional activity in prostate cancer cells.

We further investigated if similar to LCL204, knockdown of NMT1 suppressed AR levels and its transcriptional activity. AR^+ prostate cancer cell lines including VCaP, 22Rv1, C4-2B, and LNCaP cells were transduced with shRNA-NMT1 by lentiviral infection. shRNA-NMT1 efficiently suppressed expression levels of NMT1 protein and mRNA in VCaP (Fig.S4.7A-B) and 22Rv1 cells (Fig. S4.7C-D), and significantly inhibited AR proteins levels (Fig. S4.7A and S7C) with no change of AR mRNA in LNCaP and C4-2B cells or a mild change in VCaP and 22Rv1 cells (Fig. S4.8). Corresponding to a decrease of AR protein levels, shRNA-NMT1 inhibited expression levels of AR-regulated down-stream genes such as PSA gene and TMPRSS2 (Fig. S4.7B and S4.7D). Additionally, ablation of NMT1 protein (Fig. S4.7E and S4.7G) and mRNA (Fig. S4.7F and S7H) also inhibited both total AR protein levels (Fig. S4.7E and S4.7G) and nuclear AR levels

(Fig. S4.7E and S4.7G) as well as PSA gene and TMPRSS2 mRNA levels (Fig. S4.7F and S4.7H) in C4-2B and LNCaP cells. Finally, as expected, PSA and TMPRSS2 expression levels were significantly elevated under the induction of R1881. Knockdown of NMT1 inhibited expression levels of PSA gene and TMPRSS2 in the absence or presence of R1881 (Fig. S4.7I). Taken together, the data suggest that similar to the inhibition of NMT1 activity by LCL204, down-regulation of NMT1 expression levels inhibits AR protein levels and its transcriptional activity and suppresses agonist-induced AR transcriptional activity in prostate cancer cells.

Overexpression of NMT1 upregulates AR levels, nuclear localization, and its transcriptional activity in prostate cancer cells.

We further examined if overexpression of NMT1 up-regulated endogenous AR levels in LNCaP and C4-2B cells. Ectopic expression of NMT1 led to an increase of AR protein levels in LNCaP (Fig. S4.9A) and C4-2B cells (Fig. S4.9C). In addition, ectopic expression of NMT1 increased AR in the nuclear fraction (Fig. S4.9A and S4.9C). Correspondingly, increased NMT1 levels significantly increased gene expression of AR-regulated down-stream genes such as PSA and TMPRSS2 (Fig. S4.9B and S4.9D), however AR mRNA levels remained unchanged (Fig. S4.9B and S9D), suggesting that NMT1-regulated AR levels do not occur at the transcriptional level.

Next, we further examined if the increase of AR nuclear localization by overexpression of NMT1 required the binding of a ligand to AR. As expected, nuclear AR protein levels were significantly increased in the presence of R1881 in LNCaP cells. Similar to the R1881 induction, over-expression of NMT1 significantly increased nuclear AR levels in the absence or presence of R1881 (Fig. S4.9E). Similar to R1881 induction, overexpression of NMT1 up-regulated AR down-stream genes such as PSA and TMPRSS2 mRNA levels in the absence or presence of R1881 (Fig. S4.9F).

The data further suggest that similar to androgen induction, overexpression of NMT1 enhances AR nuclear localization in prostate cancer cells.

Targeting NMT1 activity promotes AR ubiquitination and degradation.

AR can be poly-ubiquitinated and subsequently degraded (20). We examined if NMT1 regulation of AR protein levels was associated with the ubiquitination-proteasome degradation pathway. Down-regulation of AR protein levels by LCL204 was rescued by treatment with bortezomib, a proteasome inhibitor, in LNCaP and 22Rv1 cells (Fig. 4.3A-B). Additionally, de novo protein synthesis was blocked by cycloheximide (CHX) and AR degradation was observed over time with and without LCL204 (Fig. 4.3C-D). Next, treatment with LCL204 or shRNA-NMT1 increased the levels of ubiquitinated AR in both LNCaP and 22Rv1 cells (Fig. 4.3E). The data indicate that a decrease of AR protein levels by down-regulation of NMT1 levels or activity is mediated through ubiquitination-proteasome degradation pathway.

NMT1 synergized with AR in prostate tumorigenesis

Overexpression of NMT1 has been reported in colon, brain, and gallbladder cancers (57-59). NMT1 is expressed in all prostate cancer cells and inhibition of NMT1 suppressed prostate tumor progression (36, 38). To further investigate how NMT1 regulates AR in prostate cancer progression, we examined simultaneous overexpression of NMT1 and AR using the prostate tissue regeneration assay *in vivo*. Ectopic expression of NMT1 and AR was confirmed *in vitro* (Fig. S4,10A-B). In the prostate regeneration assay, prostate primary cells isolated from C57BL/6J mice prostate tissue were transduced with NMT1 and/or AR by lentiviral infection (Fig. S4.10C). RFP and/or GFP fluorescence indicated successful transduction of NMT1 and/or AR in regenerated

prostate tissues (Fig. S4,10D). Regenerated prostate tissue overexpressing NMT1 alone were comprised of prostate tubules with one single layer of luminal and basal cells (Fig. S4.10E). Regenerated tissues overexpressing AR alone showed atrophic tubules with limited prostatic secretion. The majority of prostate tubules contained epithelial cells with luminal and basal cells, while some tubules had limited luminal cells. However, simultaneous overexpression of NMT1 and AR led to solid tumors, which showed a lack of glandular structure and proliferation of luminal cells (Fig. S4.10E). Collectively, the data suggest that overexpression of NMT1 synergizes with AR in prostate tumor progression.

Knockdown of NMT1 inhibits AR levels and growth of prostate xenograft tumors.

We further investigated if knockdown of NMT1 led to inhibition of AR levels and suppressed growth of prostate xenograft tumors. C4-2B and 22Rv1 cells were transduced with shRNA-NMT1 by lentiviral infection (Fig. 4.4A and Fig. S4.11A). The size and weight of xenograft tumors were significantly inhibited in cells expressing shRNA-NMT1 in comparison with the control (Fig. 4.4B-D and Fig. S4.11B-D). As expected, expression levels of NMT1 were suppressed in the xenograft tumors expressing shRNA-NMT1 (Fig. 4.4F and Fig. S4.11E). Expression levels of AR and Ki67 were significantly inhibited as well (Fig. 4.4F and Fig. S4,11E). The data suggest that down-regulation of NMT1 inhibits growth of prostate xenograft tumors and is associated with a decrease of AR levels.

Discussion:

Stereochemistry plays an important role in determining selectivity, affinity, and efficacy of inhibitors (60). Our study demonstrates that inhibitor absolute configuration dictates the efficacy of inhibiting NMT1 enzymatic activity. Recently, numerous small molecule compounds targeting NMT activity have been developed for tumor treatment including COPP24, IMP-366, and (1*R*,2*R*)-D-NMAPPD (LCL4) (30, 38, 39). By comparing our previously reported compound (1*R*,2*R*)-D-NMAPPD (LCL4) (35) with the commercial similar compound (1*S*,2*S*)-D-NMAPPD (42), we clearly showed that this enantiomer of (1*R*,2*R*)-D-NMAPPD (LCL4) was less effective at inhibiting global protein myristoylation in prostate cancer cells. In contrast to (1*R*,2*R*)-D-NMAPPD (LCL4), (1*S*,2*S*)-D-NMAPPD was also predicted to bind poorly within the myristoyl-CoA binding site of NMT1 by docking analysis. We further demonstrated that LCL204, a derivative of (1*R*,2*R*)-D-NMAPPD, improved inhibition of global protein myristoylation and induced AR degradation in prostate cancer cells. Other compounds, such as IMP-366, bind to the peptide substrate binding pocket which also effectively inhibits NMT1 function (38), which could inhibit tumor growth through induction of ER-stress and cell cycle arrest in cancer cells, leading to cell apoptosis (30, 50). Our study provides an example that stereochemistry regulates the efficacy of an inhibitor in drug design.

More importantly, this study has revealed a novel molecular function of NMT1 in regulating AR protein levels in prostate cancer cells. Overexpression of NMT1 increased total or nuclear AR protein levels. Conversely, knockdown of NMT1 or pharmacological inhibition of NMT1 activity led to a decrease of AR protein levels and its transcriptional activity. Interestingly, inhibition of NMT levels and activity decreased both AR full-length and variants by an increase

of AR ubiquitination-proteasome degradation. AR ubiquitination plays a role in the regulation of AR stability and its activity (14). There are three major AR ubiquitination sites: K311, K845, and K847 (15, 16). Since the AR-variant, which lacks the AR ligand binding domain at the C-terminus, is also regulated by NMT1, we reasoned that NMT1 regulation of AR-ubiquitination likely take place at the AR N-terminus. Since K845 and K847 are located within the AR ligand binding sites, NMT1 regulation of AR ubiquitination might potentially take place at K311, which is in the AR transcriptional activation function domain (AF-1) (16, 61), or at other unknown sites. Identification of AR ubiquitination site(s) regulated by NMT1 will further provide mechanistic understanding of this degradation pathway.

It is not clear which E3 ligase is involved in NMT1 regulation of AR ubiquitination and degradation. Different E3 ligases have been reported to be involved in AR ubiquitination, which could either promote AR transcriptional activity or lead to degradation of AR (16). For instance, RNF6 is reported to be an E3 ligase for AR ubiquitination leading to an increase of AR transcriptional activity (15). On the other hand, Mdm2 is reported to bind with AR in a phosphorylation-dependent manner to promote its ubiquitination and degradation (17). Other E3 ligases including CHIP (c-terminus of Hsp-70-interacting protein), SKP2, and Siah2 could also potentially be involved in ubiquitination and degradation of AR (18, 20, 21). Future studies should focus on identification of which E3 ligase that mediates AR ubiquitination is regulated by protein myristoylation. This knowledge will be very valuable for development of a novel AR degradation strategy.

Directly targeting AR for degradation remains an effective therapeutic strategy for treatment of castration resistant prostate cancer (CRPC). Numerous selective androgen receptor degraders (SARDs) such as UT-69 and SARD033 or Proteolysis Targeting Chimeric molecules

(PROTACs) such as ARCC-4 and ARV-330 have been developed for targeting full length of AR (62-68). However, the efficacy of these compounds relies on interaction with the ligand binding domain of AR. AR splice variants such as AR-V1 and AR-V7 which lack the ligand binding domain could frequently occur in tumors after androgen deprivation therapy (69). As a result, ARV-330 and ARCC-4 usually lose their efficacy in targeting AR-V7 for degradation. Currently other AR degraders such as ASC-J9 (a curcumin derivative) and 17-allylamino-17-demethoxygeldanamycin (17-AAG) are reported to enhance AR degradation and inhibit growth of CRPC cells (70, 71). However, the biological mechanisms of ASC-J9 are still unknown, and 17-AAG induced AR degradation via inhibition of Hsp90 function might be non-specific for AR degradation since it could also down-regulate a subset of cellular proteins such as HER2, HER3, and Akt (72). In this study, LCL204 pharmacologically inhibits NMT1 activity which leads to the degradation of full-length AR as well as its variant at low micromolar concentrations. In comparison with other AR degraders, our study provides an alternative approach for treatment of androgen sensitive and CRPC by inhibiting both AR-FL and AR-V7 levels in prostate cancer cells.

Our study shows the functional role of NMT1 in prostate tumor progression. While knockdown of NMT1 inhibited growth of prostate xenograft tumors, overexpression of NMT synergized with AR in prostate tumorigenesis. This is consistent with other studies regarding NMT1 in cancer progression of various cancer types (29, 35, 37, 38, 50). Overexpression of NMT1 stabilizes AR protein levels and might promote AR nuclear translocation and its transcriptional activity. In addition, NMT1 also promotes myristoylation of a set of its downstream proteins such as AMPKA, Src kinase, and PKA (32, 38, 73, 74). These proteins require myristoylation modification to carry out their molecular functions, and further synergize with AR in tumor progression. For example, Src kinase requires myristoylation for its kinase activity and oncogenic

potential to synergize with AR in prostate tumorigenesis (38). The catalytic subunit of cAMP-dependent protein kinase (PKA) is another protein that requires myristoylation for its molecular function (74-76). PKA regulates AR protein levels, nuclear translocation, and its transcriptional activity (33, 77). Elevation of PKA expression is associated with the progression of CRPC (78, 79). Further studies will be required to illustrate the cross-talk between NMT1 and AR in prostate cancer progression.

Acknowledgements:

The work was supported by the NIH (R01CA172495) and by DOD (W81XWH-14-PCRP-IDA).

Author contribution:

O. A. A. and H. C. designed the experiments; O. A. A. executed the experiments; E. O. and D. C. provided chemical analysis; L. L. and Z. R. X. provided docking analysis; Z. B. participated in the preparation of the manuscript; I. L. synthesized LCL compounds; O. A. A. and H. C. wrote the paper.

References

1. F. Bray *et al.*, Global cancer statistics 2018: GLOBOCAN estimates of incidence and mortality worldwide for 36 cancers in 185 countries. *CA Cancer J Clin* **68**, 394-424 (2018).
2. H. Huang, D. J. Tindall, The role of the androgen receptor in prostate cancer. *Crit Rev Eukaryot Gene Expr* **12**, 193-207 (2002).
3. M. H. Tan, J. Li, H. E. Xu, K. Melcher, E. L. Yong, Androgen receptor: structure, role in prostate cancer and drug discovery. *Acta Pharmacol Sin* **36**, 3-23 (2015).
4. P. Dell'oglio *et al.*, Treatment trends and Medicare reimbursements for localized prostate cancer in elderly patients. *Can Urol Assoc J* **12**, E338-E344 (2018).
5. J. Holzbeierlein *et al.*, Gene expression analysis of human prostate carcinoma during hormonal therapy identifies androgen-responsive genes and mechanisms of therapy resistance. *Am J Pathol* **164**, 217-227 (2004).
6. W. P. Harris, E. A. Mostaghel, P. S. Nelson, B. Montgomery, Androgen deprivation therapy: progress in understanding mechanisms of resistance and optimizing androgen depletion. *Nat Clin Pract Urol* **6**, 76-85 (2009).
7. M. A. Rice, S. V. Malhotra, T. Stoyanova, Second-Generation Antiandrogens: From Discovery to Standard of Care in Castration Resistant Prostate Cancer. *Front Oncol* **9**, 801 (2019).
8. T. Chandrasekar, J. C. Yang, A. C. Gao, C. P. Evans, Mechanisms of resistance in castration-resistant prostate cancer (CRPC). *Transl Androl Urol* **4**, 365-380 (2015).
9. M. Nakazawa, C. Paller, N. Kyprianou, Mechanisms of Therapeutic Resistance in Prostate Cancer. *Curr Oncol Rep* **19**, 13 (2017).
10. C. Abate-Shen, M. M. Shen, Molecular genetics of prostate cancer. *Genes Dev* **14**, 2410-2434 (2000).
11. H. I. Scher, G. Buchanan, W. Gerald, L. M. Butler, W. D. Tilley, Targeting the androgen receptor: improving outcomes for castration-resistant prostate cancer. *Endocr Relat Cancer* **11**, 459-476 (2004).
12. J. Schalken, J. M. Fitzpatrick, Enzalutamide: targeting the androgen signalling pathway in metastatic castration-resistant prostate cancer. *BJU Int* **117**, 215-225 (2016).
13. R. Ge *et al.*, Degradation of Androgen Receptor through Small Molecules for Prostate Cancer. *Curr Cancer Drug Targets* **18**, 652-667 (2018).
14. D. Gioeli, B. M. Paschal, Post-translational modification of the androgen receptor. *Mol Cell Endocrinol* **352**, 70-78 (2012).
15. K. Xu *et al.*, Regulation of androgen receptor transcriptional activity and specificity by RNF6-induced ubiquitination. *Cancer Cell* **15**, 270-282 (2009).
16. U. L. McClurg *et al.*, Identification of a novel K311 ubiquitination site critical for androgen receptor transcriptional activity. *Nucleic Acids Res* **45**, 1793-1804 (2017).
17. H. K. Lin, L. Wang, Y. C. Hu, S. Altuwaijri, C. Chang, Phosphorylation-dependent ubiquitylation and degradation of androgen receptor by Akt require Mdm2 E3 ligase. *EMBO J* **21**, 4037-4048 (2002).
18. S. Sarkar, D. L. Brautigan, S. J. Parsons, J. M. Larner, Androgen receptor degradation by the E3 ligase CHIP modulates mitotic arrest in prostate cancer cells. *Oncogene* **33**, 26-33 (2014).

19. J. An, C. Wang, Y. Deng, L. Yu, H. Huang, Destruction of full-length androgen receptor by wild-type SPOP, but not prostate-cancer-associated mutants. *Cell Rep* **6**, 657-669 (2014).
20. J. Qi *et al.*, The E3 ubiquitin ligase Siah2 contributes to castration-resistant prostate cancer by regulation of androgen receptor transcriptional activity. *Cancer Cell* **23**, 332-346 (2013).
21. B. Li *et al.*, Skp2 regulates androgen receptor through ubiquitin-mediated degradation independent of Akt/mTOR pathways in prostate cancer. *Prostate* **74**, 421-432 (2014).
22. J. A. Boutin, Myristoylation. *Cell Signal* **9**, 15-35 (1997).
23. T. A. Farazi, G. Waksman, J. I. Gordon, The biology and enzymology of protein N-myristoylation. *J Biol Chem* **276**, 39501-39504 (2001).
24. E. Thinon *et al.*, Global profiling of co- and post-translationally N-myristoylated proteomes in human cells. *Nat Commun* **5**, 4919 (2014).
25. J. I. Gordon, R. J. Duronio, D. A. Rudnick, S. P. Adams, G. W. Gokel, Protein N-myristoylation. *J Biol Chem* **266**, 8647-8650 (1991).
26. M. D. Resh, Trafficking and signaling by fatty-acylated and prenylated proteins. *Nat Chem Biol* **2**, 584-590 (2006).
27. J. Zha, S. Weiler, K. J. Oh, M. C. Wei, S. J. Korsmeyer, Posttranslational N-myristoylation of BID as a molecular switch for targeting mitochondria and apoptosis. *Science* **290**, 1761-1765 (2000).
28. H. Li, J. Dou, L. Ding, P. Spearman, Myristoylation is required for human immunodeficiency virus type 1 Gag-Gag multimerization in mammalian cells. *J Virol* **81**, 12899-12910 (2007).
29. C. E. Ducker, J. J. Upson, K. J. French, C. D. Smith, Two N-myristoyltransferase isozymes play unique roles in protein myristoylation, proliferation, and apoptosis. *Mol Cancer Res* **3**, 463-476 (2005).
30. E. Thinon, J. Morales-Sanfrutos, D. J. Mann, E. W. Tate, N-Myristoyltransferase Inhibition Induces ER-Stress, Cell Cycle Arrest, and Apoptosis in Cancer Cells. *ACS Chem Biol* **11**, 2165-2176 (2016).
31. A. Varkaris, A. D. Katsiampoura, J. C. Araujo, G. E. Gallick, P. G. Corn, Src signaling pathways in prostate cancer. *Cancer Metastasis Rev* **33**, 595-606 (2014).
32. P. Patwardhan, M. D. Resh, Myristoylation and membrane binding regulate c-Src stability and kinase activity. *Mol Cell Biol* **30**, 4094-4107 (2010).
33. M. Sarwar, S. Sandberg, P. A. Abrahamsson, J. L. Persson, Protein kinase A (PKA) pathway is functionally linked to androgen receptor (AR) in the progression of prostate cancer. *Urol Oncol* **32**, 25 e21-12 (2014).
34. A. S. Khan, D. E. Frigo, A spatiotemporal hypothesis for the regulation, role, and targeting of AMPK in prostate cancer. *Nat Rev Urol* **14**, 164-180 (2017).
35. Q. Li *et al.*, Pharmacologically targeting the myristoylation of the scaffold protein FRS2alpha inhibits FGF/FGFR-mediated oncogenic signaling and tumor progression. *J Biol Chem* **293**, 6434-6448 (2018).
36. S. Kim *et al.*, Myristoylation of Src kinase mediates Src-induced and high-fat diet-accelerated prostate tumor progression in mice. *J Biol Chem* **292**, 18422-18433 (2017).
37. U. Das, S. Kumar, J. R. Dimmock, R. K. Sharma, Inhibition of protein N-myristoylation: a therapeutic protocol in developing anticancer agents. *Curr Cancer Drug Targets* **12**, 667-692 (2012).

38. S. Kim *et al.*, Blocking Myristoylation of Src Inhibits Its Kinase Activity and Suppresses Prostate Cancer Progression. *Cancer Res* **77**, 6950-6962 (2017).
39. K. J. French *et al.*, Cyclohexyl-octahydro-pyrrolo[1,2-a]pyrazine-based inhibitors of human N-myristoyltransferase-1. *J Pharmacol Exp Ther* **309**, 340-347 (2004).
40. G. L. Vilas *et al.*, Posttranslational myristoylation of caspase-activated p21-activated protein kinase 2 (PAK2) potentiates late apoptotic events. *Proc Natl Acad Sci U S A* **103**, 6542-6547 (2006).
41. S. S. Bhandarkar *et al.*, Tris (dibenzylideneacetone) dipalladium, a N-myristoyltransferase-1 inhibitor, is effective against melanoma growth in vitro and in vivo. *Clin Cancer Res* **14**, 5743-5748 (2008).
42. W. W. Kallemeijn *et al.*, Validation and Invalidation of Chemical Probes for the Human N-myristoyltransferases. *Cell Chem Biol* **26**, 892-900 e894 (2019).
43. S. Memarzadeh *et al.*, Role of autonomous androgen receptor signaling in prostate cancer initiation is dichotomous and depends on the oncogenic signal. *Proceedings of the National Academy of Sciences of the United States of America* **108**, 7962-7967 (2011).
44. L. Xin *et al.*, Progression of prostate cancer by synergy of AKT with genotropic and nongenotropic actions of the androgen receptor. *Proc Natl Acad Sci U S A* **103**, 7789-7794 (2006).
45. H. Cai *et al.*, Differential transformation capacity of Src family kinases during the initiation of prostate cancer. *Proceedings of the National Academy of Sciences of the United States of America* **108**, 6579-6584 (2011).
46. L. Xin, H. Ide, Y. Kim, P. Dubey, O. N. Witte, In vivo regeneration of murine prostate from dissociated cell populations of postnatal epithelia and urogenital sinus mesenchyme. *Proceedings of the National Academy of Sciences of the United States of America* **100 Suppl 1**, 11896-11903 (2003).
47. K. P. Bhabak, B. Kleuser, A. Huwiler, C. Arenz, Effective inhibition of acid and neutral ceramidases by novel B-13 and LCL-464 analogues. *Bioorg Med Chem* **21**, 874-882 (2013).
48. A. Dagan, C. B. Wang, E. Fibach, S. Gatt, Synthetic, non-natural sphingolipid analogs inhibit the biosynthesis of cellular sphingolipids, elevate ceramide and induce apoptotic cell death. *Bba-Mol Cell Biol L* **1633**, 161-169 (2003).
49. S. H. Yang *et al.*, N-myristoyltransferase 1 is essential in early mouse development. *The Journal of biological chemistry* **280**, 18990-18995 (2005).
50. L. Deng *et al.*, NMT1 inhibition modulates breast cancer progression through stress-triggered JNK pathway. *Cell Death Dis* **9**, 1143 (2018).
51. M. C. Rebstock, H. M. Crooks, J. Controulis, Q. R. Bartz, Chloramphenicol (Chloromycetin) .4. Chemical Studies. *Journal of the American Chemical Society* **71**, 2458-2462 (1949).
52. J. Controulis, M. C. Rebstock, H. M. Crooks, Chloramphenicol (Chloromycetin) .5. Synthesis. *Journal of the American Chemical Society* **71**, 2463-2468 (1949).
53. L. A. Mitscher, F. Kautz, J. Lapidus, Optical Rotatory Dispersion and Circular Dichroism of Diastereoisomers .I. Ephedrines and Chloramphenicols. *Can J Chemistry* **47**, 1957-& (1969).
54. J. Dillon, K. Nakanishi, Absolute Configurational Studies of Vicinal Glycols and Amino Alcohols .2. With Pr(Dpm)3. *Journal of the American Chemical Society* **97**, 5417-5422 (1975).

55. J. Dillon, K. Nakanishi, Absolute Configurational Studies of Vicinal Glycols and Amino Alcohols .1. With Ni(Acac)2. *Journal of the American Chemical Society* **97**, 5409-5417 (1975).
56. S. Kumar, R. K. Sharma, N-terminal region of the catalytic domain of human N-myristoyltransferase 1 acts as an inhibitory module. *PLoS One* **10**, e0127661 (2015).
57. A. Shrivastav *et al.*, Elevated N-myristoyltransferase activity and expression in oral squamous cell carcinoma. *Oncol Rep* **18**, 93-97 (2007).
58. Y. Lu *et al.*, Expression of N-myristoyltransferase in human brain tumors. *Neurochem Res* **30**, 9-13 (2005).
59. R. V. Rajala, J. M. Radhi, R. Kakkar, R. S. Datla, R. K. Sharma, Increased expression of N-myristoyltransferase in gallbladder carcinomas. *Cancer* **88**, 1992-1999 (2000).
60. J. McConathy, M. J. Owens, Stereochemistry in Drug Action. *Prim Care Companion J Clin Psychiatry* **5**, 70-73 (2003).
61. W. Gao, C. E. Bohl, J. T. Dalton, Chemistry and structural biology of androgen receptor. *Chem Rev* **105**, 3352-3370 (2005).
62. S. Ponnusamy *et al.*, Novel Selective Agents for the Degradation of Androgen Receptor Variants to Treat Castration-Resistant Prostate Cancer. *Cancer Res* **77**, 6282-6298 (2017).
63. J. L. Gustafson *et al.*, Small-Molecule-Mediated Degradation of the Androgen Receptor through Hydrophobic Tagging. *Angew Chem Int Ed Engl* **54**, 9659-9662 (2015).
64. X. Han *et al.*, Discovery of ARD-69 as a Highly Potent Proteolysis Targeting Chimera (PROTAC) Degrader of Androgen Receptor (AR) for the Treatment of Prostate Cancer. *J Med Chem* **62**, 941-964 (2019).
65. J. Salami *et al.*, Androgen receptor degradation by the proteolysis-targeting chimera ARCC-4 outperforms enzalutamide in cellular models of prostate cancer drug resistance. *Commun Biol* **1**, 100 (2018).
66. B. A. Teply, E. S. Antonarakis, Novel mechanism-based therapeutics for androgen axis blockade in castration-resistant prostate cancer. *Curr Opin Endocrinol Diabetes Obes* **23**, 279-290 (2016).
67. T. K. Neklesa *et al.*, ARV-330: Androgen receptor PROTAC degrader for prostate cancer. *Journal of Clinical Oncology* **34**, 267-267 (2016).
68. T. Neklesa *et al.*, ARV-110: An oral androgen receptor PROTAC degrader for prostate cancer. *Journal of Clinical Oncology* **37**, 259-259 (2019).
69. A. Sharp *et al.*, Androgen receptor splice variant-7 expression emerges with castration resistance in prostate cancer. *J Clin Invest* **129**, 192-208 (2019).
70. S. Yamashita *et al.*, ASC-J9 suppresses castration-resistant prostate cancer growth through degradation of full-length and splice variant androgen receptors. *Neoplasia* **14**, 74-83 (2012).
71. R. Wang *et al.*, ASC-J9((R)) suppresses castration resistant prostate cancer progression via degrading the enzalutamide-induced androgen receptor mutant AR-F876L. *Cancer Lett* **379**, 154-160 (2016).
72. D. B. Solit *et al.*, 17-Allylamino-17-demethoxygeldanamycin induces the degradation of androgen receptor and HER-2/neu and inhibits the growth of prostate cancer xenografts. *Clinical cancer research : an official journal of the American Association for Cancer Research* **8**, 986-993 (2002).
73. K. I. Mitchelhill *et al.*, Posttranslational modifications of the 5'-AMP-activated protein kinase beta1 subunit. *The Journal of biological chemistry* **272**, 24475-24479 (1997).

74. S. E. Tillo *et al.*, Liberated PKA Catalytic Subunits Associate with the Membrane via Myristoylation to Preferentially Phosphorylate Membrane Substrates. *Cell Rep* **19**, 617-629 (2017).
75. A. C. Bastidas *et al.*, Role of N-terminal myristylation in the structure and regulation of cAMP-dependent protein kinase. *J Mol Biol* **422**, 215-229 (2012).
76. E. C. Gaffarogullari *et al.*, A myristoyl/phosphoserine switch controls cAMP-dependent protein kinase association to membranes. *J Mol Biol* **411**, 823-836 (2011).
77. A. H. Tien, M. D. Sadar, Keys to unlock androgen receptor translocation. *The Journal of biological chemistry* **294**, 8711-8712 (2019).
78. A. Pollack *et al.*, The importance of protein kinase A in prostate cancer: relationship to patient outcome in Radiation Therapy Oncology Group trial 92-02. *Clinical cancer research : an official journal of the American Association for Cancer Research* **15**, 5478-5484 (2009).
79. M. Dagar, J. P. Singh, G. Dagar, R. K. Tyagi, G. Bagchi, Phosphorylation of HSP90 by protein kinase A is essential for the nuclear translocation of androgen receptor. *The Journal of biological chemistry* **294**, 8699-8710 (2019).
80. T. Gao, C. Yang, Y. G. Zheng, Comparative studies of thiol-sensitive fluorogenic probes for HAT assays. *Analytical and bioanalytical chemistry* **405**, 1361-1371 (2013).

Figure legends

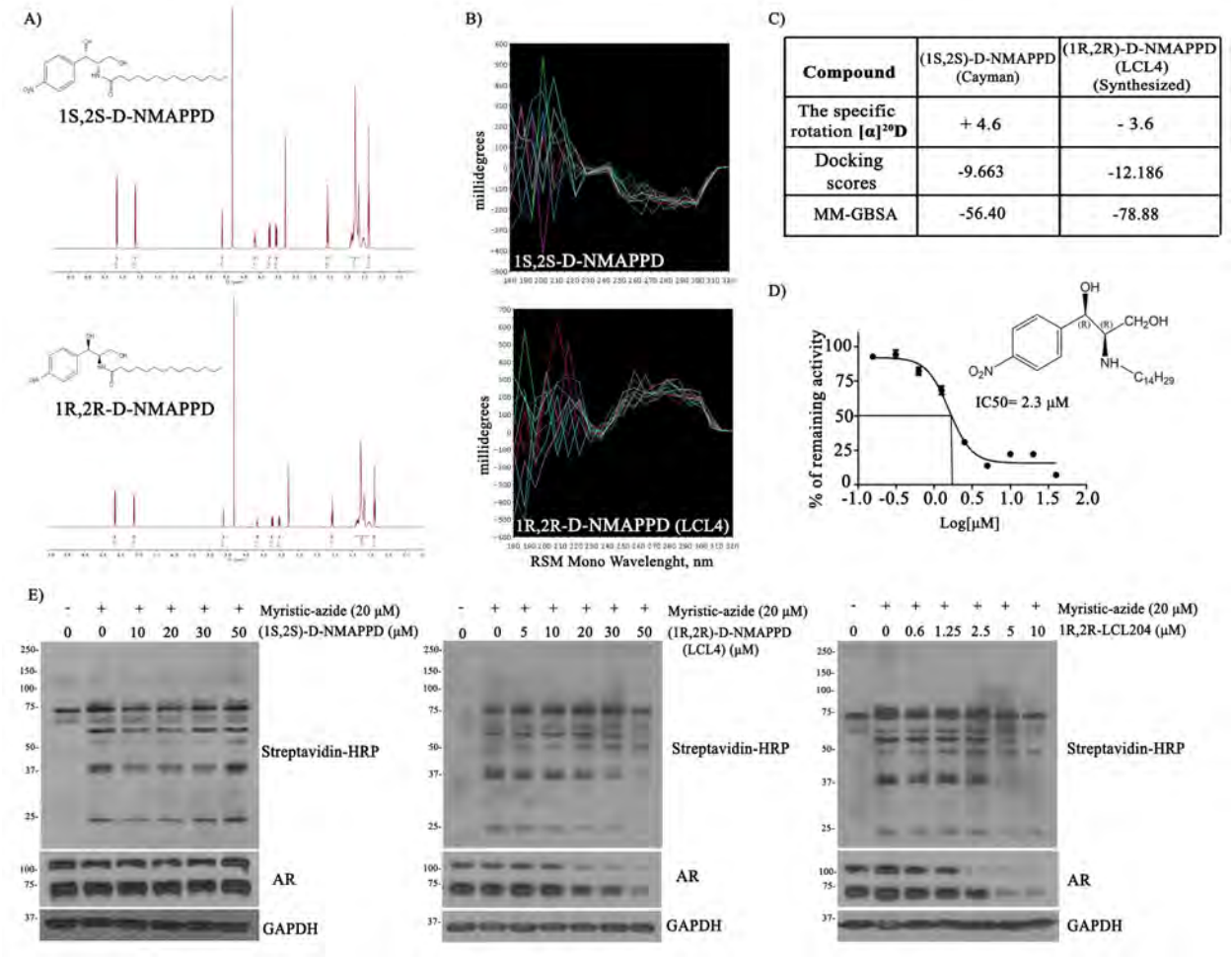

Compound	(1S,2S)-D-NMAPPD (Cayman)	(1R,2R)-D-NMAPPD (LCL4) (Synthesized)
The specific rotation $[\alpha]^{20}D$	+ 4.6	- 3.6
Docking scores	-9.663	-12.186
MM-GBSA	-56.40	-78.88

Fig. 4.1 Characterization and biological inhibitory activities of (1*R*,2*R*)-D-NMAPPD, (1*S*,2*S*)-D-NMAPPD, and 1*R*,2*R*-LCL204. A-B) Characterization of (1*S*,2*S*)-D-NMAPPD (top panel) and (1*R*,2*R*)-D-NMAPPD (lower panel) by ^{1}H NMR and circular dichroism. NMR spectra of both stereoisomers were recorded in methanol-d_4 using a 500 MHz instrument. The ^{1}H NMR spectrum of (1*S*,2*S*)-D-NMAPPD (top panel) and (1*R*,2*R*)-D-NMAPPD (bottom panel) were identical (A). Both (1*S*,2*S*)-D-NMAPPD and (1*R*,2*R*)-D-NMAPPD were dissolved in CH_3OH and circular dichroism spectra recorded from 180 nm to 320 nm for 200 scans (0.2 sec integration time) (B). **C)** Specific rotation ($[\alpha]^{20}D$) of (1*S*,2*S*)-D-NMAPPD and (1*R*,2*R*)-D-NMAPPD and their

docking energy with NMT1. The docking scores and MM-GBSA values for two stereoisomers were generated by using the XP (extra-precision) docking. **D)** Determination of IC_{50} of (1*R*,2*R*)-LCL204 on the full length NMT1 enzyme. The full length of NMT1 gene was expressed in *E. coli*, and NMT1 protein was purified by affinity chromatography. NMT1 catalyzes the incorporation of myristoyl group to the N-terminus of glycine of the Gly-Ser-Asn-Lys-Ser-Lys-Pro-Lys peptide and releases CoA. The amount of the released CoA could be measured by its reaction with 7-diethylamino-3-(4'-maleimidylphenyl)-4-methylcoumarin (80). The IC_{50} of (1*R*,2*R*)-LCL204 on NMT1 enzymatic activity was 2.3 μM. Each data point represents three repeats. **E)** 22Rv1 cells were grown with DMSO or various concentrations of (1*S*,2*S*)-D-NMAPPD, (1*R*,2*R*)-D-NMAPPD, or (1*R*,2*R*)-LCL204 for 3 h, and cells were furthered treated with/without 20 μM myristic acid-azide for 24 h. Expression levels of AR, GAPDH, and myristoylated proteins were measured by Western blot or in combination with Click chemistry.

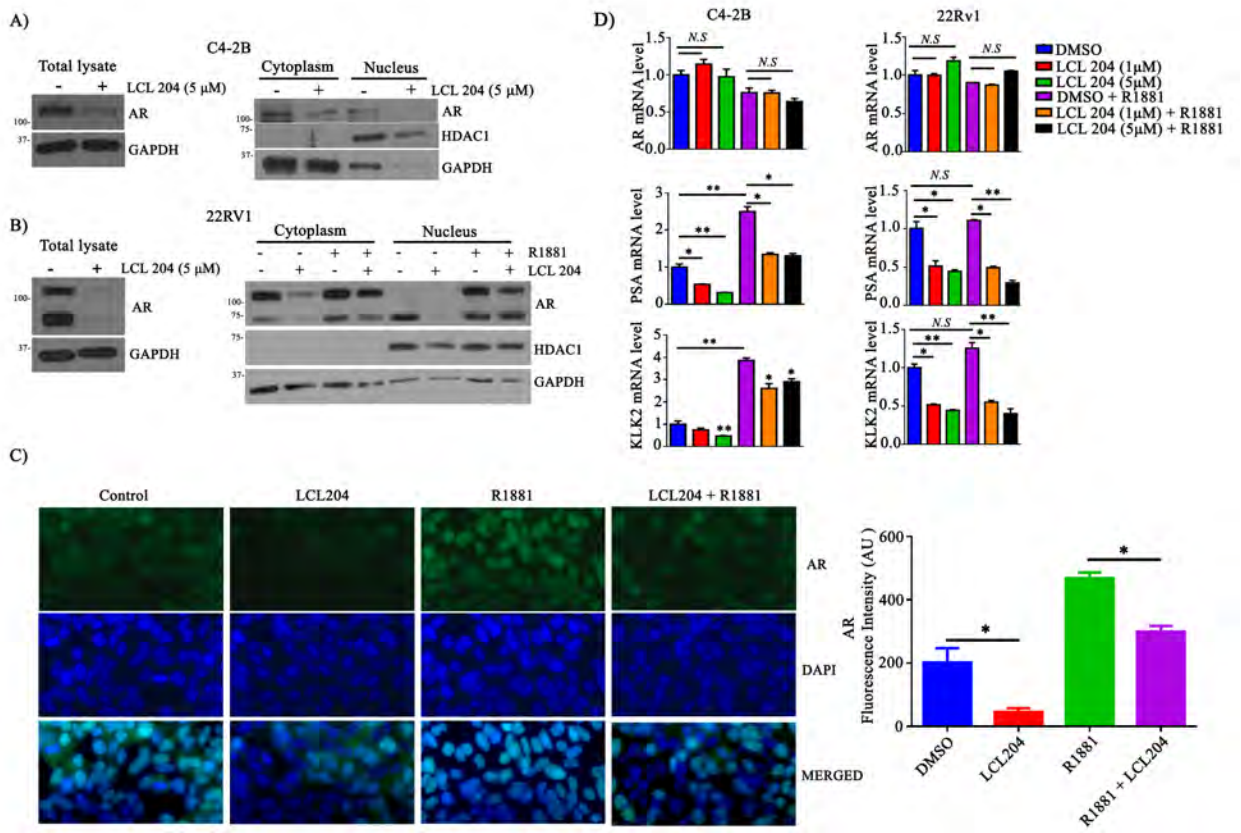

Fig. 4.2 (1*R*,2*R*)-LCL204 reduces total AR protein levels, and its nuclear translocation and transcriptional activity. A-B) C4-2B cells were grown in the medium with DMSO or 5 μM LCL204 for 48 h (A). 22Rv1 cells were grown with charcoal stripped FBS for 2 days and then treated with/without 10 nM R1881 and 5 μM LCL204 for 48 h (B). AR expression levels were measured in total cell lysate, the cytoplasmic and nuclear protein fractions. GAPDH and HDAC1 were used as the cytoplasmic and nuclear protein loading controls, respectively. **C)** LNCaP cells were grown with charcoal stripped FBS for 1 day, then treated with/without 10 nM R1881 and 5 μM LCL204 for 24 h. Immunofluorescence staining for AR (green) was followed by counterstaining with DAPI (blue). The merged images are also shown. **D)** C4-2B and 22Rv1 cells were grown with DMSO, 1, or 5 μM LCL 204 in the presence or absence of 10 nM R1881 for 48

h. Expression levels of AR and its downstream genes, PSA and KLK2 in C4-2B and 22Rv1 cells were measured by qRT-PCR. Expression levels of AR, PSA, or KLK2 in cells grown without LCL 204 and R1881 were normalized to 1. Data are shown as mean ± SEM. N.S.: not significance; *p < 0.05; **p < 0.01.

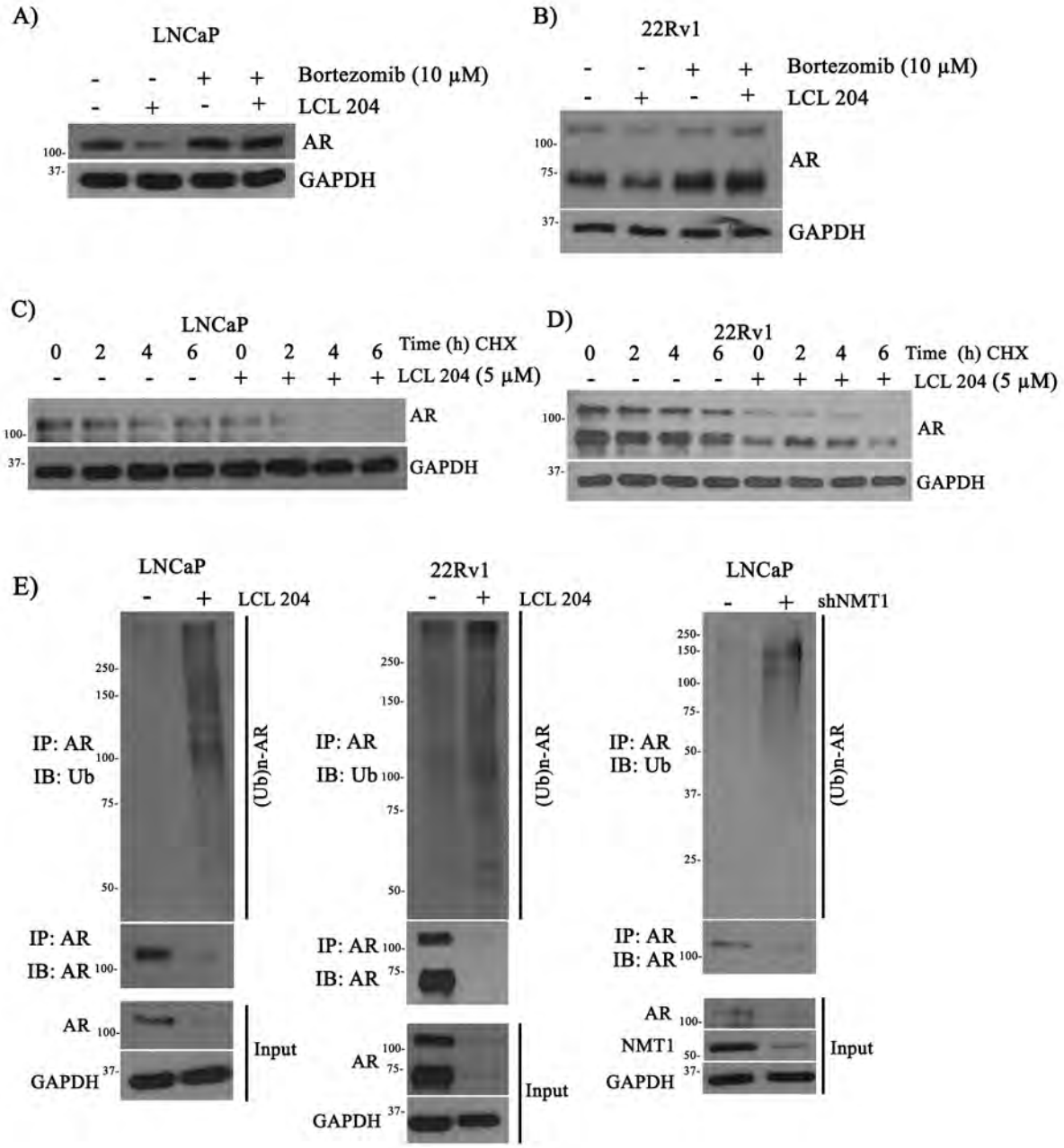

Fig. 4.3 NMT1 suppresses AR degradation through protein ubiquitination. A-D) LNCaP and 22Rv1 cells were grown with/without 5 μM LCL204 and 10 μM Bortezomib, a small molecule proteasome inhibitor, for 24 h (A-B). Additionally, LNCaP and 22Rv1 cells were grown in charcoal-stripped medium with/without 5 μM LCL 204 for 18 h and further treated with 50 μM

cycloheximide for 0, 2, 4, 6 h (C-D). Expression levels of AR and GAPDH protein was measured by Western blot. **E)** LNCaP and 22Rv1 cells were treated with DMSO or 5 μM LCL204 for 24 h. LNCaP cells were also transduced with shRNA-NMT1 or control by lentiviral infection. Protein levels of AR, NMT1, and GAPDH were measured in total cell lysates. Additionally, cell lysates were immunoprecipitated with AR antibody and AR and AR-ubiquitin levels were determined by Western blotting with anti-AR or anti-ubiquitin antibodies.

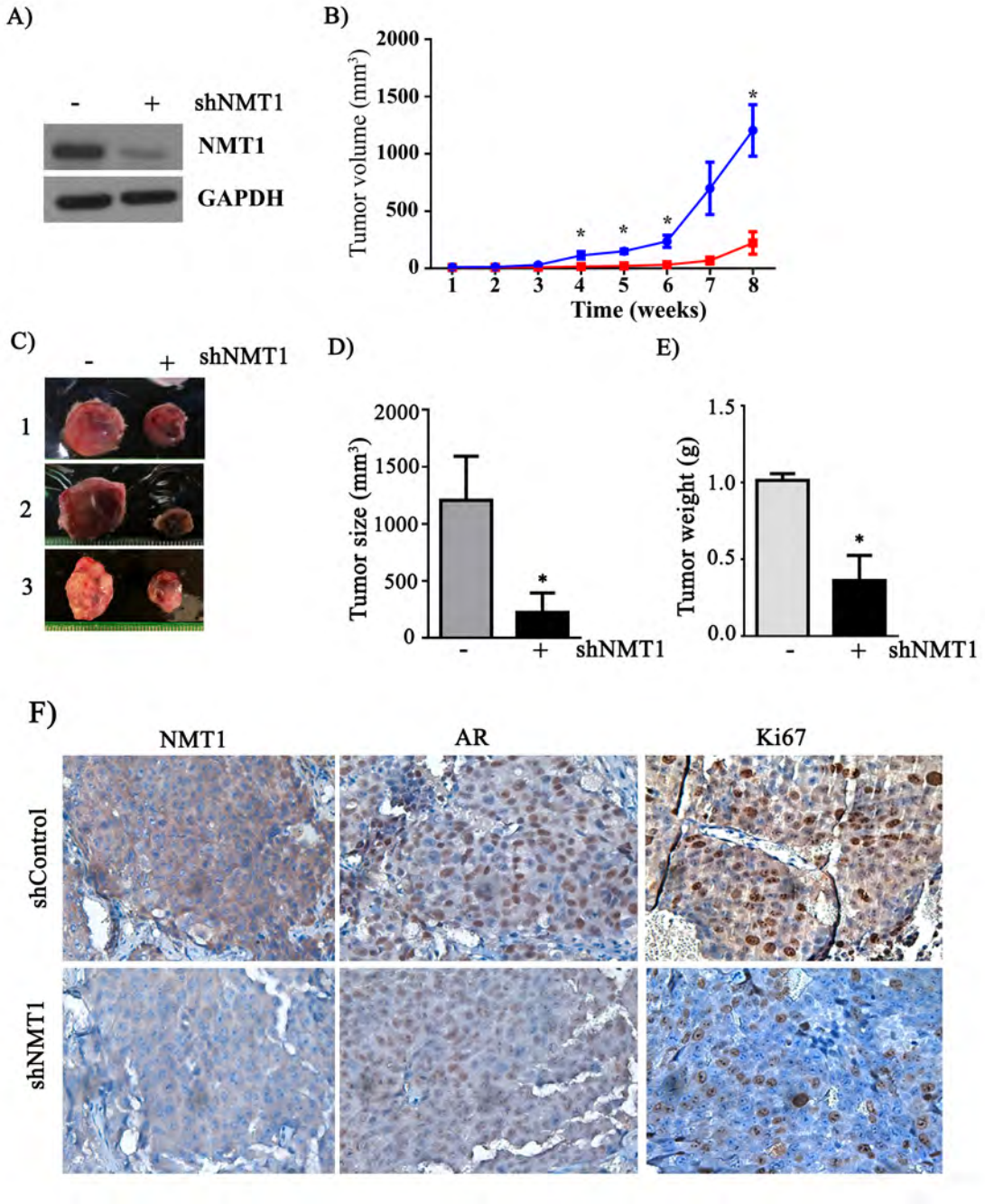

Fig. 4.4 Knockdown of NMT1 inhibits prostate cancer xenograft tumors. C4-2B cells were transduced with shRNA-NMT1 or control by lentiviral infection and inoculated subcutaneously in SCID mice. **A)** To confirm the knockdown of NMT1, total lysate was harvested from the transduced cells before the cells were inoculated and subjected to Western blotting. **B-D)** The size

of xenograft tumors were examined weekly, and the weights were measured after tumors were harvested (mean ± SEM). *, $p < 0.05$. **E)** Expression levels of NMT1, AR, Ki-67 and cleaved caspase-3 in the xenograft tumors were analyzed by IHC staining. Scale bar, 100 μm.

Supplemental Materials and Methods

Characterization of two different sources of D-NMAPPD by high resolution mass spectrometry (HRMS) and UHPLC

All reactions were carried out under argon. Solvents used for column chromatography were analytical grade. Thin-layer chromatography was carried out with 250 μm glass backed silica (XHL) plates. Plates were visualized under UV light (254 nm) and stained with ninhydrin in *n*-butanol/AcOH. Purification of crude residues was performed over silica gel chromatography using 230–400 mesh grade 60 silica unless otherwise stated.

High-resolution mass spectrometry (HRMS) was performed in the electrospray mode using an orbitrap mass analyzer (ESI-Orbtrap). The m/z for D-NMAPPD (from Cayman Chemical) was calculated for $C_{23}H_{39}N_2O_5$ [M + H] to be 423.2859 and found to be 423.2845. Similarly, the m/z of (1*R*,2*R*)-D-NMAPPD (LCL4) was calculated for $C_{23}H_{39}N_2O_5$ [M + H] to be 423.2859 and found to be 423.2847.

UHPLC analysis was performed with an Acclaim™ 120 C18 5μm (4.6 x 50) equipped with mass and a UV detector. D-NMAPPD (from Cayman Chemical) and (1*R*,2*R*)-D-NMAPPD (LCL4) were characterized with a UHPLC retention time of 5.55 min (flow rate: 0.4 mL/min; initial: H_2O 30/CH_3CN 70: 2 min; H_2O 5/CH_3CN 95: 4 min).

Characterization of two different sources of D-NMAPPD by NMR spectroscopy

NMR spectra were recorded in methanol-d_4 using a 500 MHz instrument. The D-NMAPPD (from Cayman Chemical) was characterized with the following parameters including ^{13}C NMR (500 MHz, CD_3OD) δ 174.9, 150.9, 147.1, 127.0, 122.7, 70.2, 61.3, 56.2, 35.6, 31.7, 29.4, 29.4, 29.3, 29.2, 29.1, 28.7, 25.6, 22.4, 13.1. Similarly, (1*R*,2*R*)-D-NMAPPD (LCL4) was characterized with

the following parameters including ^{13}C NMR (500 MHz, CD_3OD) δ 174.9, 150.9, 147.1, 127.0, 122.7, 70.2, 61.3, 56.2, 35.6, 31.7, 29.4, 29.4, 29.3, 29.2, 29.1, 28.7, 25.6, 22.4, 13.1.

The melting point range for (1*S*,2*S*)-D-NMAPPD and (1*R*,2*R*)-D-NMAPPD was 79 – 80 ºC.

Formation of (1*R*,2*R*)-2-Amino-1-(4-nitrophenyl)-1,3-propanediol (Chloramphenicol D base)

(1*R*,2*R*)-D-NMAPPD (LCL4) (12 mg) was heated with 10 % HCl in CH_3OH (0. 95 ml) at 80 ºC for 18 h. The reaction mixture was concentrated in *vacuo*. The residue was dissolved in saturated $NaHCO_3$ (1 ml) and extracted 5 times with ethyl acetate (2 ml). The combined organic layer was dried over Na_2SO_4, filtered and concentrated. The crude product was purified by column chromatography (CH_2Cl_2/ CH_3OH/ NH_3OH 90 : 9 : 1 to 60 : 30 : 10) to yield chloramphenicol D base (3.67 mg, 61%) as white solid.

Characterization of (1*R*,2*R*)-2-Amino-1-(4-nitrophenyl)-1,3-propanediol (Chloramphenicol D base) by NMR, high resolution mass spectrometry (HRMS), and UHPLC

The melting point range for (1*R*,2*R*)-2-Amino-1-(4-nitrophenyl)-1,3-propanediol was 160-161 ºC (literature m.p. 162-163 ºC) (52). Specific rotations were measured in methanol on an automatic polarimeter with a path length of 10 cm. (1*R*,2*R*)-2-Amino-1-(4-nitrophenyl)-1,3-propanediol rotation was $[\alpha]^{21}_D$ -22.9 (c = 0.07 , CH_3OH) (literature $[\alpha]^{27}_D$ -23.1 (c = 1.58 , CH_3OH)) (52).

NMR spectra were recorded in methanol-d_4 using a 500 MHz instrument. The (1*R*,2*R*)-2-Amino-1-(4-nitrophenyl)-1,3-propanediol was characterized as follows: ^1H NMR (500 MHz, CD_3OD) δ 8.20 (d, *J* = 8.8 Hz, 2H, 2Ar), 7.61 (d, *J* = 8.6 Hz, 2H, 2Ar), 4.77 (d, *J* = 5.7 Hz, 1H), 3.52 (dd, *J*

= 10.9, 5.1 Hz, 1H, CH_2'), 3.37 (dd, *J* = 10.9, 5.9 Hz, 1H, CH_2''), 2.91 (q, *J* = 5.6 Hz, 1H); ^{13}C NMR (500 MHz, CD_3OD) δ 150.8, 127.3, 123.0, 72.5, 62.4, 58.4.

High-resolution mass spectra (HRMS) were recorded in the electrospray mode using an orbitrap mass analyzer (ESI-Orbtrap). The (1*R*,2*R*)-2-Amino-1-(4-nitrophenyl)-1,3-propanediol was characterized as follows: ESI-HRMS m/z calculated for $C_9H_{13}O_4N_2$ [M + H] 213.0870 found 213.0867.

NMT1 gene expression and protein purification

A modified full length NMT1 genetic sequence containing a His_6-tag at the N-terminus was synthesized by GenScript. The gene was cloned in the pET-11a vector and transformed into Rosetta 2 competent cells by heat shock. Cells were grown at 37 ºC in LB broth, supplemented with 100 μg/ml ampicillin and 35 μg/ml chloramphenicol, to OD_{600} 0.6-0.8. Cultures were induced with 1 mM IPTG and grown overnight at 18 ºC. The cells were harvested by centrifugation at 5000 x g for 10 min. The cells were suspended in a buffer containing 20 mM Tris (pH 7.5), 500 mM NaCl, 10 mM imidazole, 1 mM $MgCl_2$, and 0.1% (v/v) Triton X-100 and lysed by four 1 min rounds of sonication, 5 sec on 5 sec off, at 50% amplitude, on ice. The lysate was cleared by centrifugation at 48,000 x g for 20 min at 4 ºC. Cleared lysate was applied to high-density nickel agarose beads (Gold Biotechnology, Olivette, MO) equilibrated with 20 mM Tris (pH 7.5), 500 mM NaCl and 10 mM imidazole. Protein was eluted with the equilibration buffer containing 250 mM imidazole. This elution was diluted 20-fold in Buffer A (20 mM Tris pH 8.9 and 1 mM DTT) and loaded onto a Mono Q anion-exchange column (GE Healthcare, Pittsburgh, PA). NMT1 was eluted in a 0-50% NaCl gradient over 20 column volumes of Buffer A and Buffer B (20 mM Tris pH 8.9, 1 mM DTT, and 1 M NaCl). The His_6-tag was cleaved using HRV 3C protease. The

remaining free His-tag, His-tagged NMT1, and HRV 3C protease were separated from cleaved NMT1 by nickel affinity chromatography.

Prostate regeneration assay

Primary prostate cells were isolated from 8–12-week-old male C57BL/6J mice and were transduced with NMT1, AR, or co-transduced with NMT1 and AR by lentiviral infection (2-3 x 10^5 cells/graft). The infected cells were mixed with urogenital sinus mesenchymal (UGSM) cells at a ratio 1:1. The cell mixture was resuspended in 20 μl of collagen type I (pH 7.0) (BD Biosciences). After overnight incubation at 37 ℃, grafts were implanted under the kidney capsule of SCID male mice. Grafts were harvested after 8-week incubation. Phase or fluorescent images of grafts were taken under a fluorescence microscope. C57BL/6J and CB.17$^{SCID/SCID}$ (SCID) mice were purchased from Taconic (Hudson, NY) and maintained in the lab.

Table S4.1. Primer sequences used for cloning NMT1, shRNAs, and RT-PCR

Gene	Direction	Sequence (5'-3')
NMT1	Forward	ATATACTAGTGCCGCCACCATGGCGGACGAGAGTGA GACAG
NMT1	Reverse	GGCTACTAGTCTACTTGTCGTCATCGTCTTTGTAGTCT TGTAGCACCAGTCCAACCTTC
NMT1 shRNA 1	Forward	TCCCGGAGGCTTCAACTCCTCGGACACCGTCACTTCA AGAGAGTGACGGTGTCCGAGGAGTTGAAGCCTCC
	Reverse	AAAAATGCAGCGCACCATGAAGCTCTACCGACTTCT CTTGAAAGTCGGTAGAGCTTCATGGTGCGCTGCAT
NMT1 shRNA 2	Forward	TCCCTTACCAAACCGCCAGCGAACTTGACAATTTTCA AGAGAAATTGTCAAGTTCGCTGGCGGTTTGGTAA
	Reverse	AAAATTACCAAACCGCCAGCGAACTTGACAATTTCT CTTGAAAATTGTCAAGTTCGCTGGCGGTTTGGTAA
NMT1 shRNA 3	Forward	TCCCGATCCAGGAAATACAGAAGGCCATTGAGCTTC AAGAGAGCTCAATGGCCTTCTGTATTTCCTGGATC
	Reverse	AAAAGATCCAGGAAATACAGAAGGCCATTGAGCTCT CTTGAAGCTCAATGGCCTTCTGTATTTCCTGGATC
NMT1	Forward	TTTTATACGCTGCCCTCCAC
	Reverse	TCCCCTATGCCAAACTTGAG
PSA	Forward	ACGCTGGACAGGGGGCAAAAG
	Reverse	GGGCAGGGCACATGGTTCACT
KLK2	Forward	CAGCATCGAACCAGAGGAGT
	Reverse	ACTAGAGGTAGGGGTGGGAC
NOV	Forward	ACCGTCAATGTGAGATGCTG
	Reverse	TCTTGAACTGCAGGTGGATG
TMPRSS2	Forward	CAGGAGTGTACGGGAATGTGATGGT
	Reverse	GATTAGCCGTCTGCCCTCATTTGT

Supplemental Figure legends

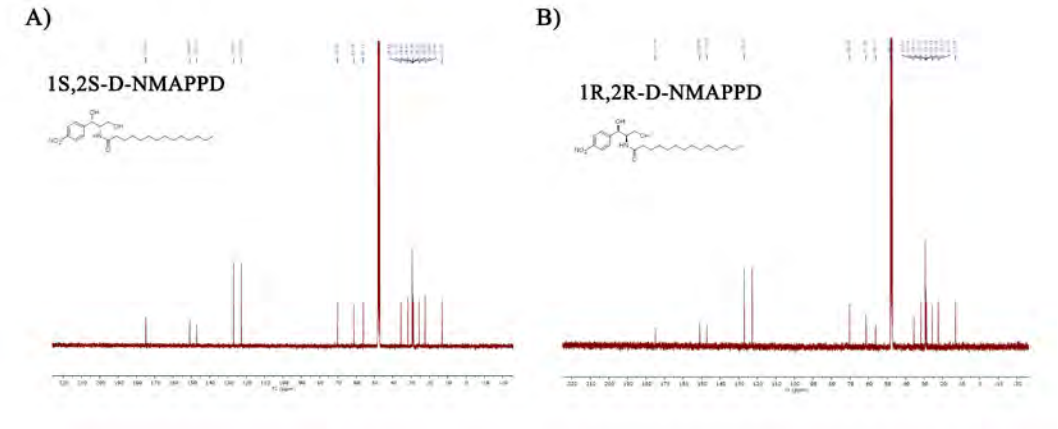

Figure S4.1. Two different sources of D-NMAPPD have identical ^{13}C NMR spectra.

Two different sources of the D-NMAPPD compounds, D-NMAPPD from the Cayman Chemical (Cat #10006305) **A)** and D-NMAPPD (synthesized in-house) **B)** were characterized by ^{13}C NMR. NMR spectra were recorded in methanol-d_4 using a 500 MHz instrument. Signals were observed at δ 174.9, 150.9, 147.1, 127.0, 122.7, 70.2, 61.3, 56.2, 35.6, 31.7, 29.4, 29.4, 29.3, 29.2, 29.1, 28.7, 25.6, 22.4, 13.1.

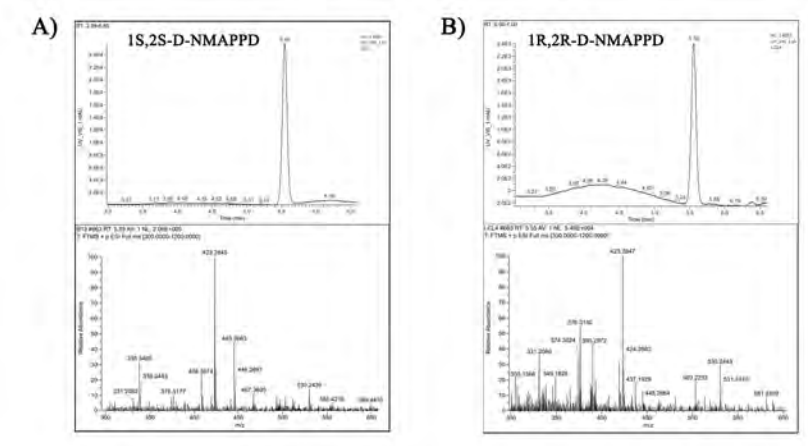

Figure S4.2. Two different sources of D-NMAPPD have identical UHPLC chromatograms and high-resolution mass spectra (HRMS). Two different sources of the D-NMAPPD compounds, D-NMAPPD from the Cayman Chemical (Cat #10006305) **A)** and D-NMAPPD (synthesized in-house) **B)** were subjected to UHPLC analysis (top panel) and mass spectrometry (lower panel). UHPLC analysis was performed with an Acclaim™ 120 C18 5 µm (4.6 x 50) equipped with mass and UV detectors. High-resolution mass spectra (HRMS) were recorded in the electrospray mode using an orbitrap mass analyzer (ESI-Orbtrap).

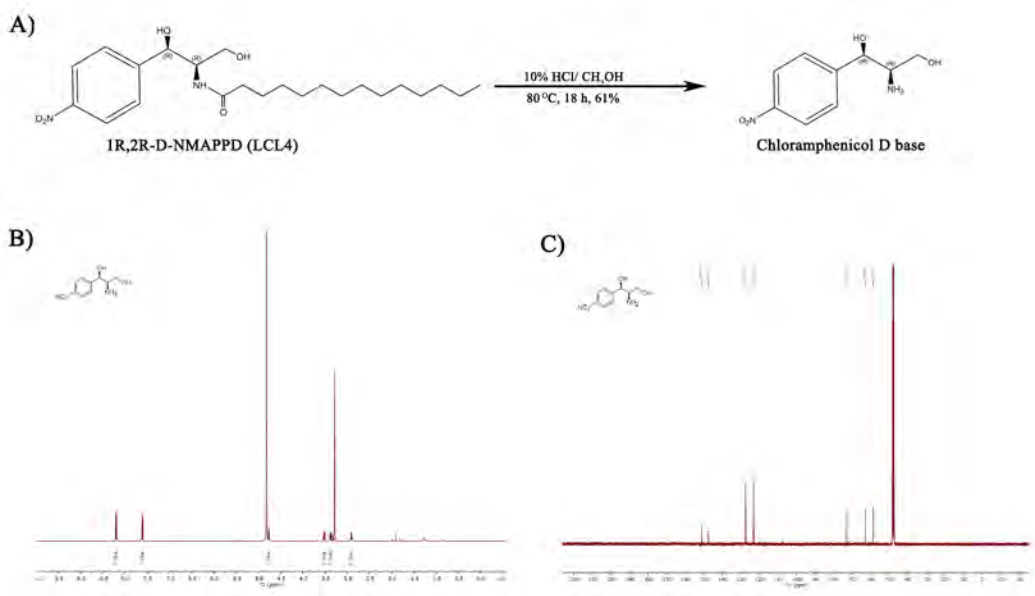

Figure S4.3. Synthesis and characterization of (1*R*,2*R*)-2-Amino-1-(4-nitrophenyl)-1,3-propanediol (Chloramphenicol D base) by NMR. A) Hydrolysis of the parent amide of (1*R*,2*R*)-D-NMAPPD (in-house synthesized) with 10% HCl in methanol to generate (1*R*,2*R*)-2-Amino-1-(4-nitrophenyl)-1,3-propanediol. The reaction was carried out at 80 °C for 18 h. **B-C)** The ^{1}H NMR and ^{13}C NMR spectra of (1*R*,2*R*)-2-Amino-1-(4-nitrophenyl)-1,3-propanediol. NMR spectra of (1*R*,2*R*)-2-Amino-1-(4-nitrophenyl)-1,3-propanediol were recorded in methanol-d_4 using a 500 MHz instrument.

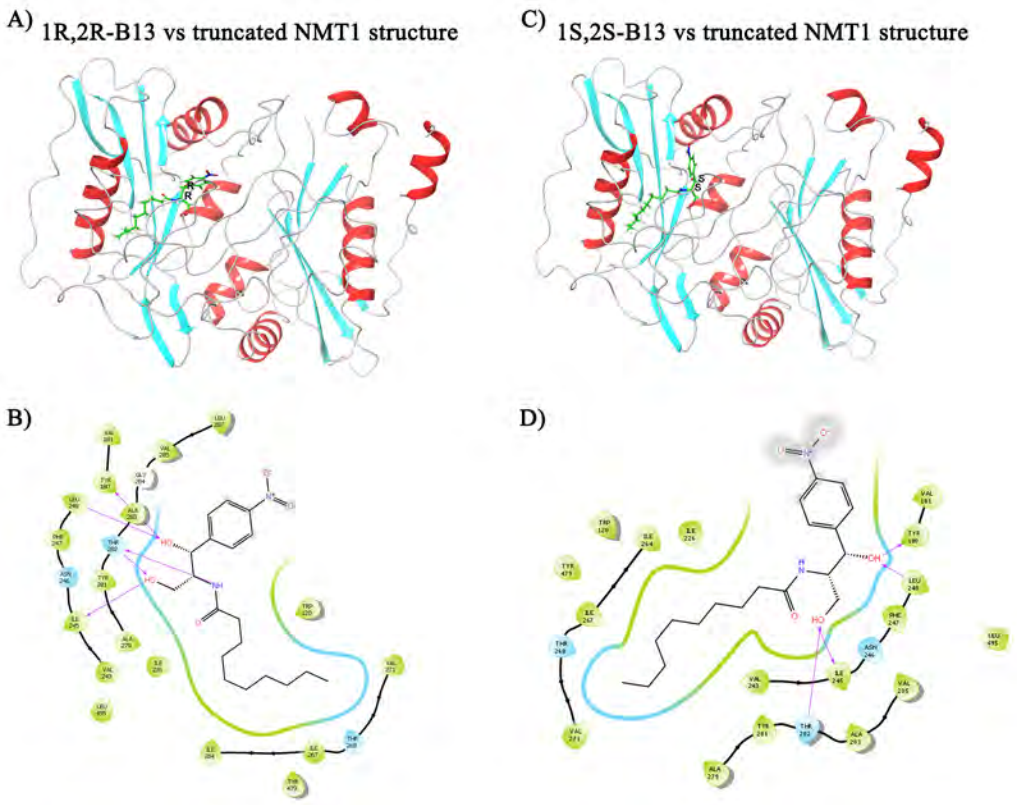

Figure S4.4. Docking analysis of two stereoisomers, (1*R*,2*R*)-D-NMAPPD and (1*S*,2*S*)-D-NMAPPD, to the myristoyl-CoA binding site of NMT1 protein. The crystal structure of NMT1 protein (truncated form) has been resolved in previous studies (38) . The structure was retrieved from the RCSB PDB database (PDB ID: 5UUT). The structures of (1*R*,2*R*)-D-NMAPPD and (1*S*,2*S*)-D-NMAPPD were prepared by Ligprep. The interaction of the compounds with the surrounding functional groups of amino acids in NMT1 was revealed for (1*R*,2*R*)-D-NMAPPD (A) or (1*S*,2*S*)-D-NMAPPD (C). The binding site of myristoyl-CoA in the NMT1 structure was replaced with (1*R*,2*R*)-D-NMAPPD (B) or (1*S*,2*S*)-D-NMAPPD (D) in the docking analysis.

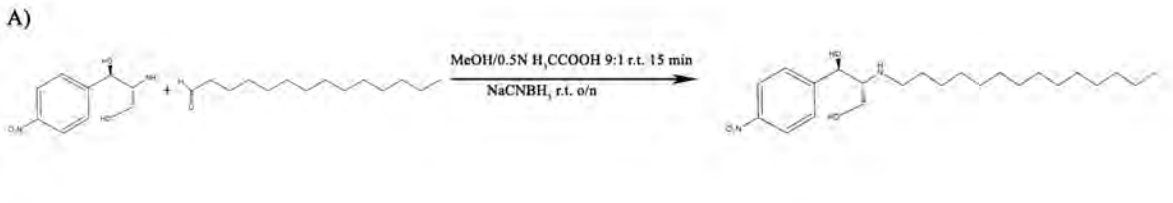

Figure S4.5. Synthesis of 1*R*,2*R*-LCL204. The reaction of (2*R*,3*R*)-2-amino-1-(4-nitrophenyl)-1,3-propanediol with tetradecanal in methanol/0.05 N acetic acid and sodium cyanoborohydride. The final product was purified by recrystallization using DCM/pentane.

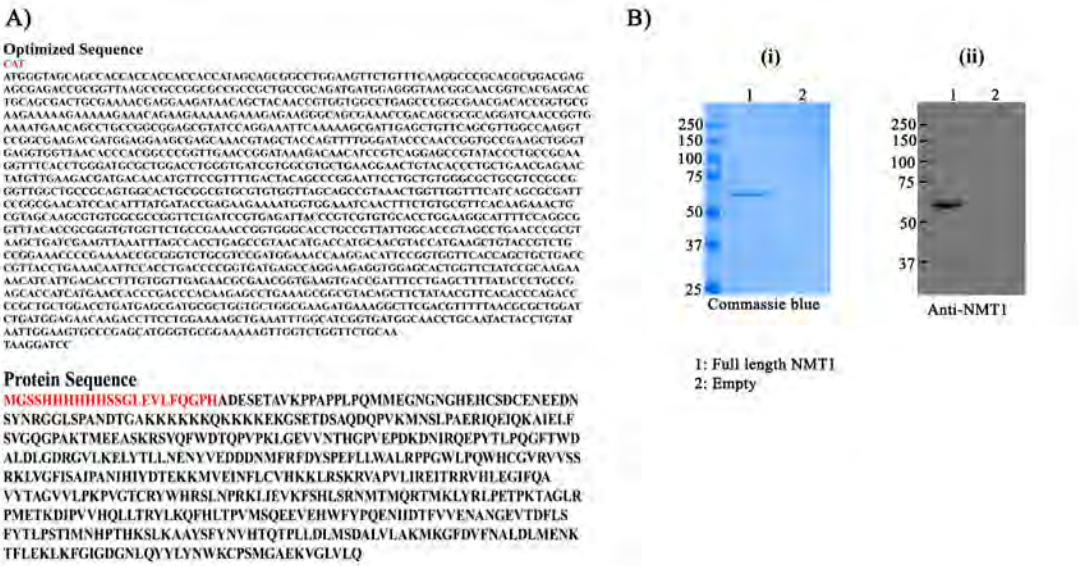

Figure S4.6. NMT1 sequence, expression and purification. A) The human NMT1 DNA sequence was optimized for bacterial expression and synthesized by GenScript. **B)** The NMT1 protein was His_6-tagged and expressed in *E. coli*. The protein was purified by Ni-NTA affinity chromatography, anion exchange chromatography, and the His_6-tag was removed by digestion with HRV 3C protease. The purified NMT1 protein was detected by Coomassie blue staining (i) and Western blot analysis using anti-human NMT1 antibody (ii).

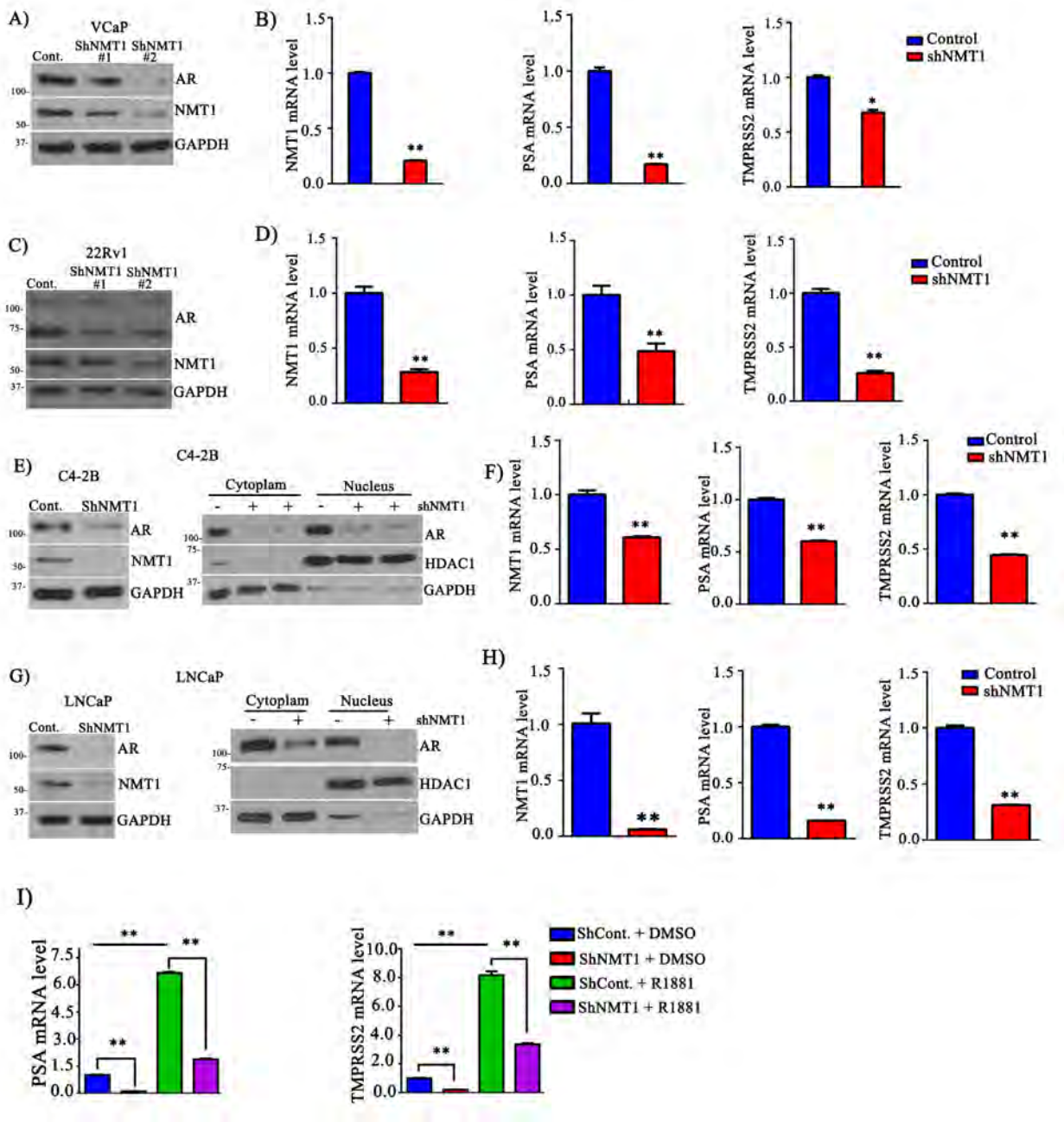

Figure S4.7. NMT1 knockdown decreases AR protein levels, its nuclear translocation and transcriptional activity. A-D) VCaP or 22Rv1 cells were transduced with shRNA-NMT1 (shNMT1-1# or shRNA-NMT1-2#) or control by lentiviral infection. Expression levels of AR, NMT1, and GAPDH in total cell lysates of VCaP (A) and 22Rv1 (C) were measured by Western

blotting. Additionally, mRNA expression levels of NMT1, PSA, and TMPRSS2 in VCaP (B) or 22Rv1 (D) cells were measured by qRT-PCR, and expression levels were normalized to GAPDH. Expression levels of NMT1, PSA, TMPRSS2 in cells expressing control vector were normalized to 1. **E-H)** C4-2B (E) or LNCaP (G) cells were transduced with shRNA-NMT1 or control by lentiviral infection. Expression levels of AR, NMT1, and GAPDH in total cell lysate of C4-2B (E) or LNCaP (G) were measured by Western blotting. Additionally, protein lysate was further fractionated into the nuclear and cytoplasmic fractions. Expression levels of AR in these two fractions were analyzed. GAPDH and HDAC1 levels were used as the cytoplasmic and nuclear loading controls, respectively. Next, expression levels of NMT1 and AR downstream genes (PSA and TMPRSS2) in C4-2B (F) or LNCaP (H) cells expressing shRNA-NMT1 or control were analyzed by qRT-PCR. **I)** LNCaP cells expressing shRNA-NMT1 or control were grown with charcoal stripped FBS for 24 h, then treated with DMSO or 10 nM R1881 for 24 h. Expression levels of PSA and TMPRSS2 were analyzed by qRT-PCR. Expression levels in the cells expressing control vector treated with DMSO were normalized to 1. Data are shown as mean ± SEM. $^{**}p < 0.01$.

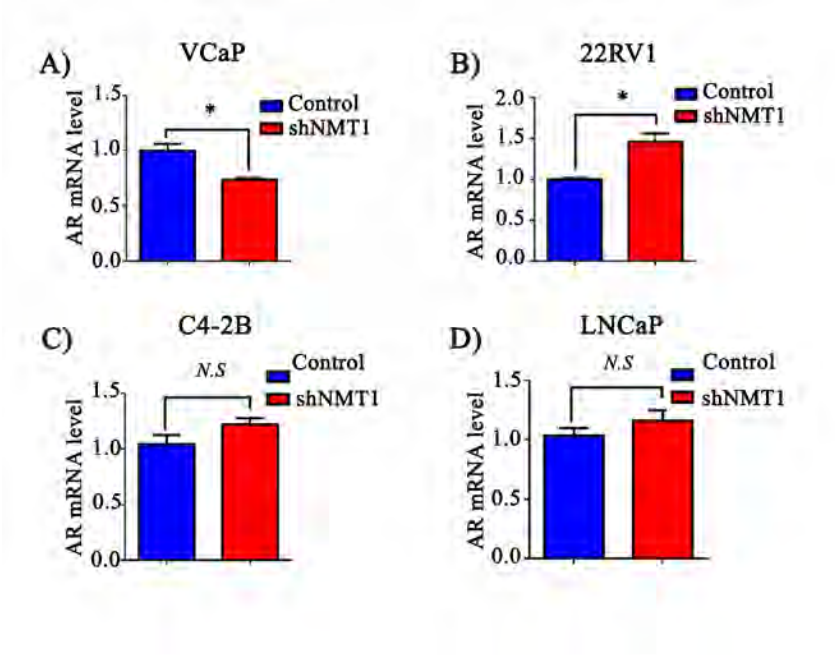

Figure S4.8. Knockdown of NMT1 has no effect or a mild effect on AR mRNA levels in prostate cancer cells. A-D) VCaP (A), 22Rv1 (B), C4-2B (C)**,** or LNCaP (D) cells were transduced with shRNA-NMT1 or control by lentiviral infection. Expression levels of AR mRNA were measured by qRT-PCR, and expression levels were normalized to GAPDH. Expression levels in the cells expressing control vector were normalized to 1. Data are shown as mean ± SEM. **$p < 0.01$.

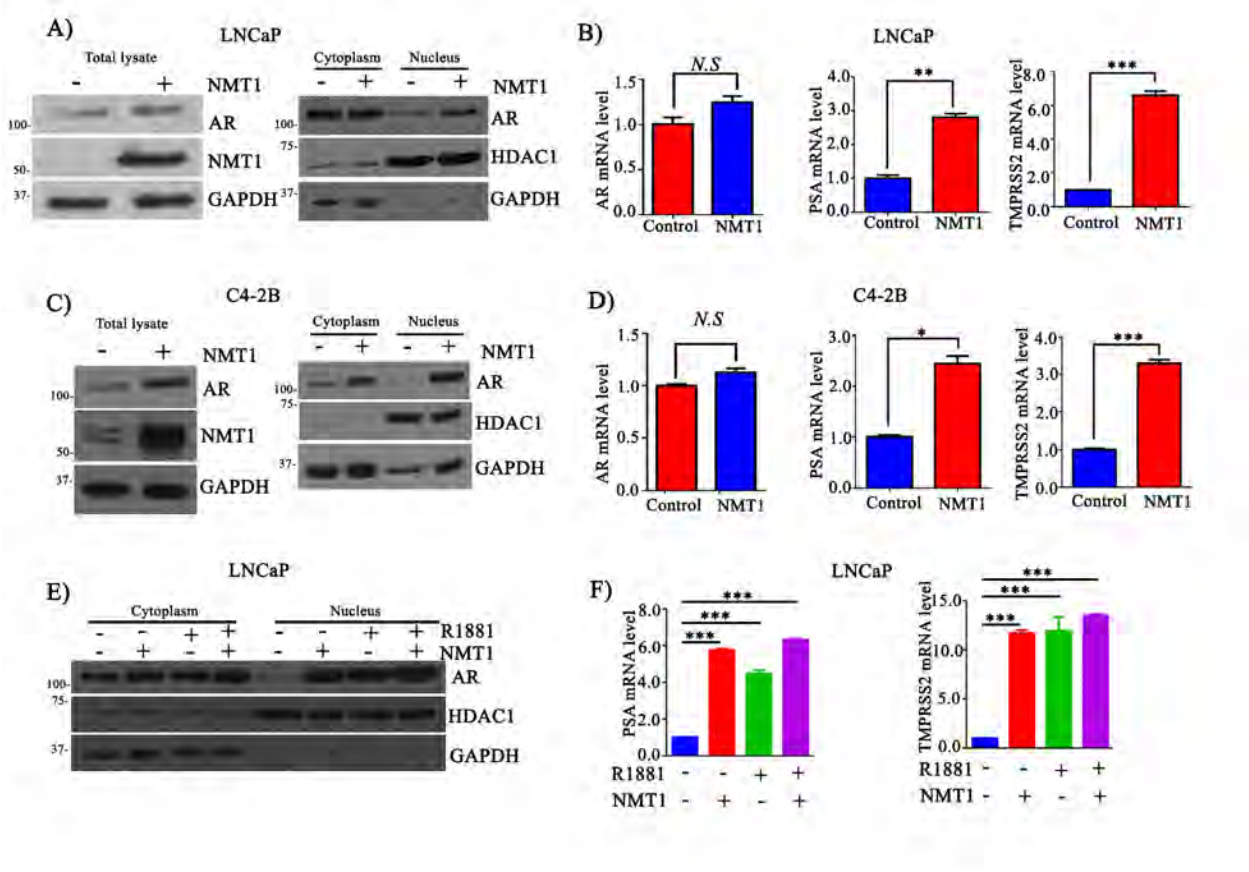

Figure S4.9. Ectopic expression of NMT1 enhances expression levels, nuclear translocation, and transcriptional activity of AR in prostate cancer cells. LNCaP and C4-2B cells were transduced with control vector or NMT1 by lentiviral infection. **A-D)** Expression levels of AR, NMT1, and GAPDH of total cell lysate were analyzed in the transduced LNCaP (A) or C4-2B cells (C). Levels of AR, HDAC1, and GAPDH were determined in cytoplasmic and nuclear fractions. GAPDH and HDAC1 were used as the loading controls of the cytoplasmic and nuclear fractions, respectively. Additionally, mRNA expression levels of AR, PSA, and TMPRSS2 in LNCaP (B) or C4-2B cells (D) expressing control vector or NMT1 were measured by qRT-PCR. Expression levels were normalized to GAPDH, and expression levels in cells expressing control

vector was normalized to 1. **E-F)** LNCaP cells expressing control vector or NMT1 were grown with charcoal-stripped FBS for 24 h, then treated with DMSO or 10 nM R1881 for 24 h. The cells were lysed and fractionated into cytoplasmic and nuclear fractions and levels of AR, HDAC1, and GAPDH were measured. GAPDH and HDAC1 were used as the cytoplasmic and nuclear protein loading controls, respectively (E). Expression levels of AR downstream genes, PSA and TMPRSS2 were analyzed by qRT-PCR. PSA and TMPRSS2 levels were normalized to GAPDH, and expression levels in LNCaP cells expressing vector control and DMSO treatment was normalized as 1. Data are shown as mean ± SEM. *$p < 0.05$; **$p < 0.01$; ***$p < 0.001$.

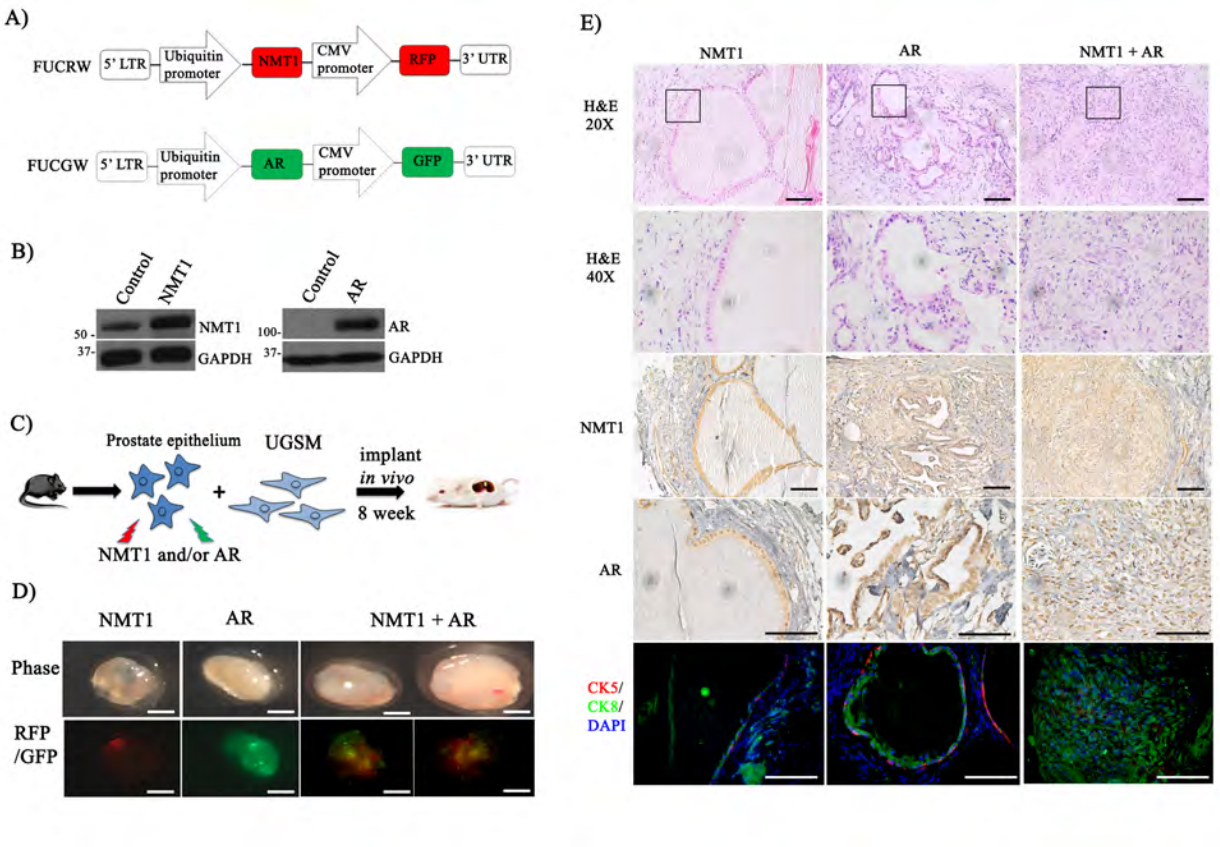

Figure S4.10. Synergy of NMT1 with AR promotes prostate cancer progression. A) NMT1 and AR were cloned into a bi-cistronic lentiviral vector. NMT1 or AR was regulated by the ubiquitin promoter, and RFP or GFP was regulated by the CMV promoter. **B)** 293T and PC-3 cells were transduced with NMT1 and AR by lentiviral infection, respectively. The overexpression of NMT1 or AR was confirmed. **C)** Schematic outline of the *in vivo* prostate tissue regeneration. Prostate epithelial cells (PrECs) were isolated from C57BL/6J and transduced with NMT1, AR, or NMT1/AR by lentiviral infection. The transduced PrECs were mixed with UGSM cells. The cell mixture was implanted under the renal capsule of SCID mice, and incubated for 8 weeks before the regenerated tissues were harvested. **D)** The regenerated prostate tissues were harvested after 8 weeks incubation from panel A. Phase, RFP, and GFP fluorescence images of the regenerated

tissues were taken. Scale bar: 2 mm**. E)** H&E and IHC staining of NMT1, AR, and CK5(red)/CK8(green) were examined in regenerated tissues derived from NMT1, AR, or NMT1 + AR groups. Scale bar: 100 μm.

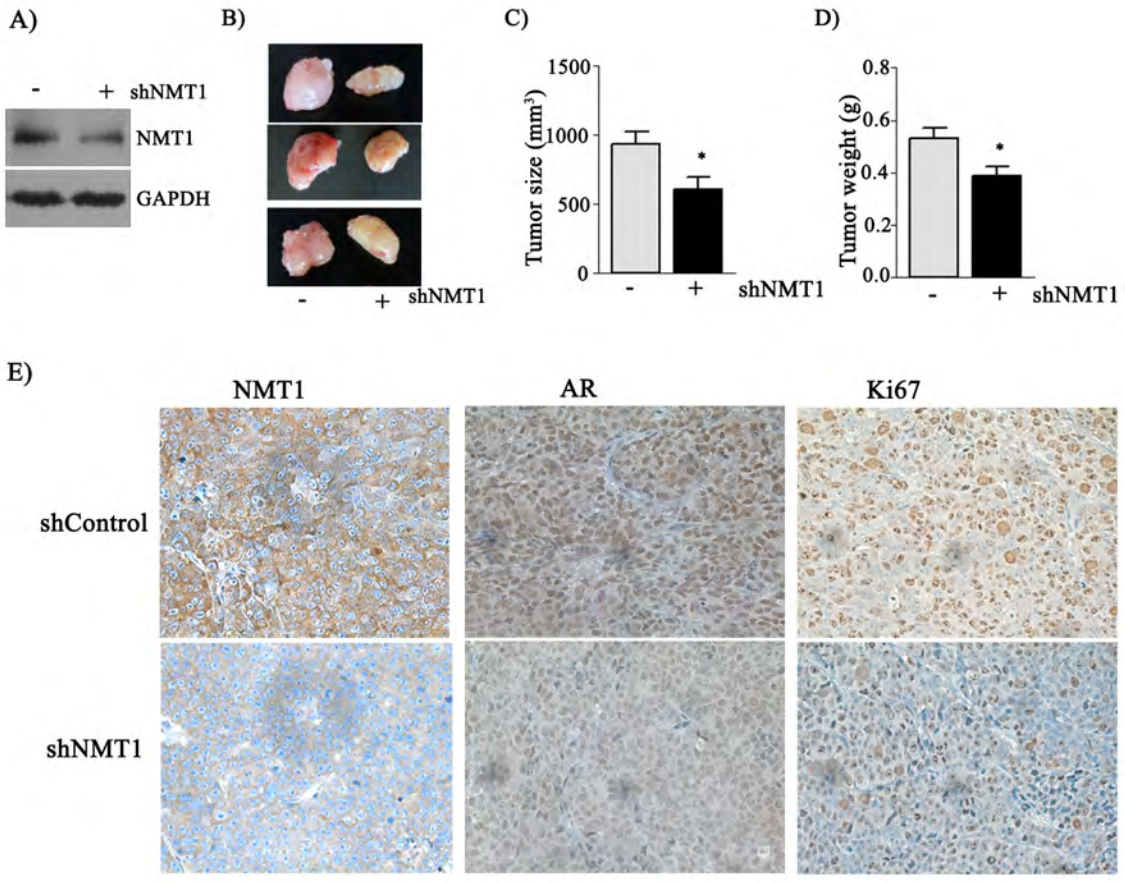

Figure S4.11. Knockdown of NMT1 inhibits growth of prostate cancer xenograft tumors. 22Rv1 cells were transduced with shRNA-NMT1 or control by lentiviral infection. The transduced cells were inoculated subcutaneously in SCID mice. **A-C)** The size and weight of xenograft tumors were recorded and measured (mean ± SEM). *, $p < 0.05$. **D)** Expression levels of NMT1, AR, Ki-67 and cleaved caspase-3 in xenograft tumors expressing shRNA-NMT1 or control were analyzed by IHC staining. Scale bar, 100 μm.

CHAPTER 5

SUMMARY AND FUTURE WORK

This chapter discusses and concludes the major findings of our work on understanding the role of protein myristoylation and N-myristoyltransferase 1 (NMT1) in prostate cancer tumorigenesis. In addition, in this chapter, we proposed potential future studies for this work.

Advanced prostate cancer comes as a second leading cause of deaths in men in the US. The high mortality rate of castration-resistant prostate cancer (CRPC) arises from the poor understanding of the underlying molecular mechanisms and lacks the proper therapeutic target. The emerging role of fatty acid metabolism in prostate cancer directs the current focus to understand the role of fatty acylated protein modifications on the activity of oncoproteins in prostate cancer tumorigenesis. In particular, protein myristoylation, which is a post-translational covalent attachment of myristic acid to a set of proteins, including some well-known oncoproteins.

The chief purpose of this dissertation is to identify any potential role of NMT1 in prostate cancer tumorigenesis. To achieve this purpose, we first determined the mRNA and protein expression levels of NMT1 in different prostate cancer cells (LNCaP, 22Rv1, DU145, and PC3) compared to normal prostate cells (PNT2). Second, we decided to see if the expression levels and activity of NMT1 promote prostate cancer progression using in vitro and in vivo systems. Third, we performed a drug screening to identifies candidate inhibitors for NMT1. Finally, we discovered a novel regulatory role of NMT1 on androgen receptor (AR) protein levels and its mediated transcriptional activity in prostate cancer.

The first aim of this study was to identify the role of N-myristoyltransferase 1 in the progression of prostate cancer. Previous reports have demonstrated that myristoylation of Src kinase is essential for its activity and Src kinase-mediated high-fat diet-accelerated prostate tumorigenesis (1). In this study, we demonstrated that mRNA and protein expression levels of NMT1 are elevated in prostate cancer cells compared to normal prostate cells. Additionally, the expression levels were correlated with the activity of NMT1 in prostate cancer cells. We showed that NMT1 knockdown inhibited growth of prostate cancer cells in vitro and in vivo through inducing cell cycle arrest at the S-phase with no effect on the apoptosis signaling pathway. The inhibition of prostate cancer cell proliferation is due to the inhibition of the NMT1-Src kinase axis. We further identified small molecule compounds that inhibit NMT1 activity at enzymatic and cellular levels. LCL4 (1R,2R-DMNAPPD) was identified as a novel NMT inhibitor that targets myristoyl-CoA binding site with IC50= 77.6 μM. Additionally, LCL204, a derivative of LCL4, was more potent than LCL4 with IC50= 8.7 μM. We illustrated that LCL4 inhibited the growth of prostate cancer cells by inducing cell cycle arrest. The compound inhibited growth of prostate cancer cells in vivo with no observed pathological toxicity.

Given the fact that NMT1 was aberrantly expressed in prostate cancer cells, future studies should focus on identifying the NMT1 downstream substrates, which their myristoylation might highly up-regulated in highly expressed NMT1 cancer cells, and study oncogenic properties of these downstream proteins. Further, the role of myristoylation modification and how this modification influences their oncogenic properties should be assessed. Next, by conducting chemical modification on LCL4 (1R,2R-DMNAPPD), we developed a more potent compound (LCL204) on targeting NMT1 activity. Future studies should investigate other chemical modifications to increase its potency and bioavailability in vivo. Since protein myristoylation is

essential for the activity of several proteins in normal tissues, developing an efficient and selective drug delivery method would be considered in future studies.

The second aim of this study was to investigate regulatory role of protein myristoylation on AR protein expression levels and its mediated activity in prostate cancer. It has been reported that AR expression and activity are regulated by some of the myristoylated proteins such as cAMP-dependent protein kinase (PKA) and Src kinase (2) (3) (4). Here, we demonstrated that NMT1 regulated AR protein levels in prostate cancer cells. Genetic knockdown of NMT1 expression levels and pharmacological inhibition of NMT1 activity inhibited AR protein levels post-transitionally. The reduction of AR protein levels was coupled with a decrease of AR nuclear levels and its transcriptional activity. Next, we investigated ectopic expression of NMT1 in regulating endogenous levels of AR in prostate cancer cells. The data showed that over-expression of NMT1 increased AR protein levels, nuclear translocation, and its transcriptional activity. Additionally, over-expression of NMT1 synergized with AR in prostate tumor progression. The molecular mechanism of NMT1 regulating AR protein levels is mediated through the ubiquitination-proteasome degradation pathway. It is known that NMT1 is highly expressed in several cancers, such as the brain and colon (5) (6). We showed that NMT1 genetic knockdown inhibited growth of prostate tumors *in vivo*. This inhibition might partially depend on AR-signaling. As shown previously, knockdown of NMT1 could lead to inhibit growth of PC3 (AR-) xenografts.

Finally, future studies should understand how NMT1 cross talks with AR in prostate cancer progression. NMT1 controls activity and localization of different downstream proteins by myristoylation, including proteins involved in ubiquitination and proteasome pathways. Therefore, investigate and identify protein/proteins interaction that are involved in this NMT1-AR crosstalk would help to identify new therapeutic targets for prostate cancer. Alternatively, a future study can

investigate the role of myristoylation on proteins which have previously reported to control AR activity, such as PKA. Although androgen is very important for the activity of AR, androgen independent AR activation is considered as one of molecular mechanisms in CRPC. My studies support a hypothesis that NMT1 contributes to the activation AR in the absence of androgen in vivo. Approval of this hypothesis in future studies will provide a novel approach for treatment of CRPC.

In conclusion, this work has provided fundamental knowledge about the functional role of NMT1 in prostate cancer and discovered a novel function of NMT1 in regulation of AR protein levels and its transcriptional activity in prostate cancer cells. Our studies are clinically relevant with pharmacological inhibition of NMT1. We have revealed a new regulation pathway of AR in prostate cancer for targeting CRPC.

1. S. Kim *et al.*, Myristoylation of Src kinase mediates Src-induced and high-fat diet-accelerated prostate tumor progression in mice. *J Biol Chem* **292**, 18422-18433 (2017).
2. I. Chattopadhyay *et al.*, Src promotes castration-recurrent prostate cancer through androgen receptor-dependent canonical and non-canonical transcriptional signatures. *Oncotarget* **8**, 10324-10347 (2017).
3. I. H. Gelman, Androgen receptor activation in castration-recurrent prostate cancer: the role of Src-family and Ack1 tyrosine kinases. *Int J Biol Sci* **10**, 620-626 (2014).
4. M. Sarwar, S. Sandberg, P. A. Abrahamsson, J. L. Persson, Protein kinase A (PKA) pathway is functionally linked to androgen receptor (AR) in the progression of prostate cancer. *Urol Oncol* **32**, 25 e21-12 (2014).
5. A. Shrivastav, S. Varma, A. Saxena, J. DeCoteau, R. K. Sharma, N-myristoyltransferase: a potential novel diagnostic marker for colon cancer. *J Transl Med* **5**, 58 (2007).
6. Y. Lu *et al.*, Expression of N-myristoyltransferase in human brain tumors. *Neurochem Res* **30**, 9-13 (2005).

Appendix

Face pages of accepted/published articles

Therapeutics, Targets, and Chemical Biology

Cancer Research

Blocking Myristoylation of Src Inhibits Its Kinase Activity and Suppresses Prostate Cancer Progression

Sungjin Kim[1], Omar Awad Alsaidan[1], Octavia Goodwin[1], Qianjin Li[1], Essilvo Sulejmani[1], Zhen Han[1], Aiping Bai[2], Thomas Albers[3], Zanna Beharry[4], Y. George Zheng[1], James S. Norris[5], Zdzislaw M. Szulc[2], Alicja Bielawska[2], Iryna Lebedyeva[3], Scott D. Pegan[1], and Houjian Cai[1]

Abstract

Protein *N*-myristoylation enables localization to membranes and helps maintain protein conformation and function. *N*-myristoyltransferases (NMT) catalyze co- or posttranslational myristoylation of Src family kinases and other oncogenic proteins, thereby regulating their function. In this study, we provide genetic and pharmacologic evidence that inhibiting the *N*-myristoyltransferase NMT1 suppresses cell-cycle progression, proliferation, and malignant growth of prostate cancer cells. Loss of myristoylation abolished the tumorigenic potential of Src and its synergy with androgen receptor in mediating tumor invasion. We identified the myristoyl-CoA analogue B13 as a small-molecule inhibitor of NMT1 enzymatic activity. B13 exposure blocked Src myristoylation and Src localization to the cytoplasmic membrane, attenuating Src-mediated oncogenic signaling. B13 exerted its anti-invasive and antitumor effects against prostate cancer cells, with minimal toxic side-effects *in vivo*. Structural optimization based on structure–activity relationships enabled the chemical synthesis of LCL204, with enhanced inhibitory potency against NMT1. Collectively, our results offer a preclinical proof of concept for the use of protein myristoylation inhibitors as a strategy to block prostate cancer progression. *Cancer Res; 77(24); 6950–62. ©2017 AACR.*

Introduction

N-myristoylation is a co- and posttranslational modification that results in the covalent attachment of the 14-carbon saturated myristic acid to the N-terminus of a target protein (1). *N*-myristoyltransferase (NMT) catalyzes this transfer of the myristoyl-group of myristoyl-CoA to a glycine in the N-terminus. *N*-myristoylation is ubiquitously found in eukaryotes, and two mammalian NMT isoforms, NMT1 and NMT2, have been identified that share 77% identity (2). NMTs have been considered as promising targets for the development of antifungal, antiparasitic, and antitumor progression therapeutics (3).

One set of proteins where myristoylation has been observed to play an important role is Src family kinases (SFK). Myristoylation together with other modifications allow SFKs to attach to the cytoplasmic membrane and mediate their kinase activity and cellular functions (4, 5). SFKs are pleiotropic activators in signal transduction pathways and numerous studies have documented their role as oncogenic driver genes in a variety of cancers (6). SFKs interact with a variety of cellular receptors, and are downstream effectors of G protein–coupled receptors, integrins, and many receptor tyrosine kinases (RTK; refs. 7, 8). Activation of SFKs also activates a variety of downstream signaling to facilitate tumor growth, angiogenesis, and metastatic invasion (6, 9, 10). Particularly, aberrant expression of Src kinase facilitates the phosphorylation of androgen receptor (AR) and bypasses ligand dependent AR activation in castration-resistant prostate cancer (9, 11). Our previous study showed that co-overexpression of Src and AR promotes invasive prostate adenocarcinoma (11, 12).

In vitro studies have indicated that NMT1 regulates Src kinase myristoylation and phosphorylation or kinase activity in COS-1 cells (5) or HT-29 cells (13). Here we further study if genetic and pharmacologic inhibitions of NMT1 regulate proliferation of prostate cancer cells and growth of prostate tumor *in vivo*. We demonstrate that knockdown of NMT1 suppressed proliferation of prostate cancer cells by blocking cell-cycle progression, and inhibited the myristoylation and tyrosine phosphorylation of Src kinase. The inhibitory effect increased with increasing expression levels of NMT1. Myristoylation was shown to facilitate SFKs-mediated prostate tumorigenesis, and mediate the interaction of Src kinase with AR, with the synergistic effect of promoting prostate tumor progression. Screening a panel of small-molecule compounds based on the myristoyl-CoA scaffold identified a compound that blocked the enzymatic activity of NMT1 and

[1]Department of Pharmaceutical and Biomedical Sciences, College of Pharmacy, University of Georgia Athens, Athens, Georgia. [2]Department of Biochemistry and Molecular Biology, Medical University of South Carolina, Charleston, South Carolina. [3]Department of Chemistry and Physics, Augusta University, Augusta, Georgia. [4]Department of Chemistry and Physics, Florida Gulf Coast University, Fort Myers, Florida. [5]Department of Microbiology and Immunology, Medical University of South Carolina, Charleston, South Carolina.

Note: Supplementary data for this article are available at Cancer Research Online (http://cancerres.aacrjournals.org/).

S. Kim and O.A. Alsaidan are the co-first authors of this article.

Corresponding Author: Houjian Cai, University of Georgia, Athens, 240 West Green Street, Athens, GA 30602. Phone: 706-542-1079; Fax: 706-542-5358; E-mail: caihj@uga.edu

doi: 10.1158/0008-5472.CAN-17-0981

JBC ARTICLE

Stromal Gli signaling regulates the activity and differentiation of prostate stem and progenitor cells

Received for publication, April 1, 2018, and in revised form, May 5, 2018 Published, Papers in Press, May 17, 2018, DOI 10.1074/jbc.RA118.003255

Qianjin Li[‡1], Omar A. Alsaidan[‡1], Sumit Rai[§1], Meng Wu[‡], Huifeng Shen[‡], Zanna Beharry[¶], Luciana L. Almada[‖], Martin E. Fernandez-Zapico[‖], Lianchun Wang[§], and Houjian Cai[‡2]

From the [‡]Department of Pharmaceutical and Biomedical Sciences, College of Pharmacy, University of Georgia, Athens, Georgia 30602, the [§]Carbohydrate Research Center and Department of Biochemistry and Molecular Biology, University of Georgia, Athens, Georgia 30602, the [¶]Department of Chemistry and Physics, Florida Gulf Coast University, Fort Myers, Florida 33965, and the [‖]Schulze Center for Novel Therapeutics, Division of Oncology Research, Mayo Clinic, Rochester, Minnesota 55905

Edited by Eric R. Fearon

Interactions between cells in the stroma and epithelium facilitate prostate stem cell activity and tissue regeneration capacity. Numerous molecular signal transduction pathways, including the induction of sonic hedgehog (Shh) to activate the Gli transcription factors, are known to mediate the cross-talk of these two cellular compartments. However, the details of how these signaling pathways regulate prostate stem and progenitor cell activity remain elusive. Here we demonstrate that, although cell-autonomous epithelial Shh-Gli signaling is essential to determine the expression levels of basal cell markers and the renewal potential of epithelial stem and progenitor cells, stromal Gli signaling regulates prostate stem and progenitor cell activity by increasing the number and size of prostate spheroids *in vitro*. Blockade of stromal Gli signaling also inhibited prostate tissue regeneration *in vivo*. The inhibition of stromal Gli signaling suppressed the differentiation of basal and progenitor cells to luminal cells and limited prostate tubule secretory capability. Additionally, stromal cells were able to compensate for the deficiency of epithelial Shh signaling in prostate tissue regeneration. Mechanistically, suppression of Gli signaling increased the signaling factor transforming growth factor β (TGFβ) in stromal cells. Elevation of exogenous TGFβ1 levels inhibited prostate spheroid formation, suggesting that a stromal Gli–TGFβ signaling axis regulates the activity of epithelial progenitor cells. Our study illustrates that Gli signaling regulates epithelial stem cell activity and renewal potential in both epithelial and stromal compartments.

Stromal– epithelial cell interactions are essential for prostate development and adult prostate tissue regeneration (1). The prostate gland is composed of numerous connected tubules and the surrounding stromal microenvironment. Each tubule consists of three types of prostate epithelial cells (PrECs),[3] including secretory luminal cells, basal cells, and neuroendocrine cells (2, 3). Luminal cells typically expressing cytokeratin (CK) 8 or 18 locate at the apical region of the epithelium, are sensitive to androgen stimulation, and produce secretory proteins. Basal cells expressing CK5 or p63 reside underneath the luminal cells and attach to the basement lamina (4). Both luminal and basal cells in the epithelial compartment contain stem/progenitor cells, which are capable of self-sustentation in tissue regeneration (5).

PrECs are surrounded by the stromal microenvironment, providing an important niche to nurse epithelial progenitor cells (6). The stromal compartment comprises a variety of cell types, including smooth muscle cells, subepithelial cells, wrapping cells, interstitial fibroblasts, and others (3, 7). Stromal cells secrete important signaling factors to stimulate prostate development and adult prostate tissue regeneration (1, 8). These paracrine signaling factors include stromal androgen, fibroblast growth factor (FGF), TGFβ, bone morphogenetic protein (BMP), Sonic hedgehog (Shh), and others; they induce prostatic secretion in luminal cells and maintain the self-renewal capacity of prostate stem/progenitor cells (9–12). Shh–Gli signaling exists in both prostate basal cells and stromal cells (7). However, how this signaling pathway controls the renewal capacity of stem/progenitor cells through the stromal– epithelial interaction remains elusive.

Shh–Gli signaling is an important signal transduction pathway in regulating the normal development of multiple organs, including growth of prostatic tissues and differentiation of prostate epithelia (13, 14). It has been reported that Shh–Gli signaling facilitates prostate branching morphogenesis through regulation of hepatocyte growth factor (15). In mammalian cells, the Gli family consists of three members (Gli1, Gli2, and Gli3). Although both Gli2 and Gli3 have C-terminal transcrip-

This work was supported by National Institutes of Health Grants R01CA172495 (to H. C.) and HL-09339 and GM103390 (to L. W.) and Department of Defense Grant W81XWH-15-1-0507 (to H. C.). The authors declare that they have no conflicts of interest with the contents of this article. The content is solely the responsibility of the authors and does not necessarily represent the official views of the National Institutes of Health.
This article contains Figs. S1–S7 and Table S1.
[1] These authors contributed equally to this work.
[2] To whom correspondence should be addressed. Fax: 706-542-5358; E-mail: caihj@uga.edu.

[3] The abbreviations used are: PrEC, prostate epithelial cell; CK, cytokeratin; Shh, sonic hedgehog; AR, androgen receptor; shRNA, short hairpin RNA; PEB, prostate epithelial basal; UGSM, urogenital sinus mesenchyme; RFP, red fluorescent protein; H&E, hematoxylin and eosin; DMEM, Dulbecco's modified Eagle's medium; PE, phycoerythrin; FBS, fetal bovine serum; SCID, severe combined immunodeficiency; IHC, immunohistochemistry; GAPDH, glyceraldehyde-3-phosphate dehydrogenase; E18.5, embryonic day 18.5; PrEGM, prostate epithelial cell growth medium; APC, allophycocyanin; TAMRA, tetramethylrhodamine; BTTP, bis(*tert*-butyl)-tris(triazolylmethyl)amine-propanol.

JBC ARTICLE

Pharmacologically targeting the myristoylation of the scaffold protein FRS2α inhibits FGF/FGFR-mediated oncogenic signaling and tumor progression

Received for publication, November 13, 2017, and in revised form, March 2, 2018 Published, Papers in Press, March 14, 2018, DOI 10.1074/jbc.RA117.000940

Qianjin Li[‡], Omar Awad Alsaidan[‡], Yongjie Ma[‡], Sungjin Kim[‡], Junchen Liu[§], Thomas Albers[¶], Kebin Liu[‖], Zanna Beharry[**], Shaying Zhao[‡‡], Fen Wang[§], Iryna Lebedyeva[¶], and Houjian Cai[‡1]

From the [‡]Department of Pharmaceutical and Biomedical Sciences, College of Pharmacy, and the [‡‡]Department of Biochemistry and Molecular Biology, University of Georgia, Athens, Georgia 30602, the [§]Center for Cancer and Stem Cell Biology, Institute of Biosciences and Technology, Texas A&M University Health Science Center, Houston, Texas 77030, the Departments of [¶]Chemistry and Physics and [‖]Biochemistry and Molecular Biology, Augusta University, Augusta, Georgia 30912, and the [**]Department of Chemistry and Physics, Florida Gulf Coast University, Fort Myers, Florida 33965

Edited by Henrik G. Dohlman

Fibroblast growth factor (FGF)/FGF receptor (FGFR) signaling facilitates tumor initiation and progression. Although currently approved inhibitors of FGFR kinase have shown therapeutic benefit in clinical trials, overexpression or mutations of FGFRs eventually confer drug resistance and thereby abrogate the desired activity of kinase inhibitors in many cancer types. In this study, we report that loss of myristoylation of fibroblast growth factor receptor substrate 2 (FRS2α), a scaffold protein essential for FGFR signaling, inhibits FGF/FGFR-mediated oncogenic signaling and FGF10-induced tumorigenesis. Moreover, a previously synthesized myristoyl-CoA analog, B13, which targets the activity of *N*-myristoyltransferases, suppressed FRS2α myristoylation and decreased the phosphorylation with mild alteration of FRS2α localization at the cell membrane. B13 inhibited oncogenic signaling induced by WT FGFRs or their drug-resistant mutants (FGFRs^{DRM}). B13 alone or in combination with an FGFR inhibitor suppressed FGF-induced WT FGFR- or FGFR^{DRM}-initiated phosphoinositide 3-kinase (PI3K) activity or MAPK signaling, inducing cell cycle arrest and thereby inhibiting cell proliferation and migration in several cancer cell types. Finally, B13 significantly inhibited the growth of xenograft tumors without pathological toxicity to the liver, kidney, or lung *in vivo*. In summary, our study suggests a possible therapeutic approach for inhibiting FGF/FGFR-mediated cancer progression and drug-resistant FGF/FGFR mutants.

Fibroblast growth factor (FGF)[2]/FGF receptor (FGFR) signaling regulates the fundamental development of multiple organs (1). However, a large body of research has demonstrated that this signaling axis is highly deregulated in numerous cancers, including amplification of FGFs in epithelial or stromal cells and/or aberrant expression or activation of FGFRs resulting from genetic translocation, mutation, or amplification in tumorigenic cells (2). Pathological FGF/FGFR signaling promotes cross-talk of tumorigenic cells with their microenvironment, which drives tumor proliferation, angiogenesis, and metastasis in cancer progression (3–8).

FGF/FGFR signaling requires recruiting a scaffold protein called the fibroblast growth factor receptor substrate 2 (FRS2) to initiate downstream signaling. The FRS2 family is composed of two members, FRS2α and FRS2β. Both proteins contain the phosphotyrosine-binding domain and multiple tyrosine phosphorylation sites (9, 10). FRS2α mainly associates with FGF/FGFR signaling. It binds to the juxtamembrane region of FGFRs through its phosphotyrosine-binding domain (10, 11), and the activation of FGFRs phosphorylates several tyrosine sites of FRS2α. Whereas four sites mediate the binding with Grb2, which activates phosphatidylinositol 3-kinase/AKT signaling and to a lesser extent Ras/ERK signaling, the other two sites facilitate binding with SHP2, which activates mainly the Ras/ERK pathway (10). Therefore, FRS2α is essential for FGF/FGFR-induced signaling and facilitates cancer cell proliferation and migration (12). The aberrant expression of FRS2α is also observed in some cancers (13). Therefore, targeting FRS2α is considered an important therapeutic approach in the inhibition of FGF/FGFR-mediated tumorigenesis (14).

Myristoylation of FRS2α is essential for its anchoring to the plasmatic membrane. FRS2α contains the MG*XXX*(S/T) consensus sequence at the N terminus for *N*-myristoylation modification (10). *N*-Myristoyltransferase (NMT) catalyzes the myristoylation modification process by transferring the myristoyl group from myristoyl-CoA to the glycine at the N terminus of a protein (15). In this study, we investigated a therapeutic approach to inhibit FGF/FGFR-mediated oncogenic signaling and proliferation of cancer cells by blocking myristoylation of

This work was supported by National Institutes of Health Grant R01CA172495 and Department of Defense Grant W81XWH-15-1-0507 (to H.C.). The authors declare that they have no conflicts of interest with the contents of this article. The content is solely the responsibility of the authors and does not necessarily represent the official views of the National Institutes of Health.

This article contains Table S1, Figs. S1–S9, and supporting Materials and Methods.

[1] To whom correspondence should be addressed. Fax: 706-542-5358; E-mail: caihj@uga.edu.

[2] The abbreviations used are: FGF, fibroblast growth factor; FGFR, FGF receptor; ERK, extracellular signal–regulated kinase; NMT, *N*-myristoyltransferase; MAPK, mitogen-activated kinase; p-, phosphorylated; PLCγ, phospholipase Cγ; IHC, immunohistochemistry; gRNA, guide RNA; MTT, 3-(4,5-dimethylthiazol-2-yl)-2,5-diphenyltetrazolium bromide; UGSM, urogenital sinus mesenchyme; H&E, hematoxylin and eosin.